

UNIVERSITY OF OKLAHOMA
GRADUATE COLLEGE

AN INTEGRATED ANALYSIS OF SEQUENCE STRATIGRAPHY, PETROLEUM
GEOCHEMISTRY, AND DEVONIAN MASS EXTINCTION EVENTS IN THE
WOODFORD SHALE, SOUTHERN OKLAHOMA

A THESIS
SUBMITTED TO THE GRADUATE FACULTY
in partial fulfillment of the requirements for the
Degree of
MASTER OF SCIENCE

By
LYDIA CATHERINE JONES
Norman, Oklahoma
2017

AN INTEGRATED ANALYSIS OF SEQUENCE STRATIGRAPHY, PETROLEUM
GEOCHEMISTRY, AND DEVONIAN MASS EXTINCTION EVENTS IN THE
WOODFORD SHALE, SOUTHERN OKLAHOMA

A THESIS APPROVED FOR THE
CONOCOPHILLIPS SCHOOL OF GEOLOGY AND GEOPHYSICS

BY

Dr. Roger Slatt, Chair

Dr. R. Paul Philp

Dr. Michael Engel

© Copyright by LYDIA CATHERINE JONES 2017
All Rights Reserved.

Dedicated to my mother, who has given me strength, taught me to think for myself, and instilled the confidence in me to keep moving forward ...and to my father, for his love, support, and inspiration to keep working hard. Thank you both for all you have sacrificed for me.

Acknowledgements

Many people helped me through this project the past two years and without them, it would not have been possible to complete. I would like to thank my advisor, Dr. Paul Philp, for research support over the past two years, as well as the unique opportunity to study petroleum geochemistry. I have enjoyed the challenging material and hands-on experience, which most geology students would not have the chance to participate in. I would like to express my gratitude to Dr. Roger Slatt for agreeing to act as chair of my thesis committee, his helpful feedback, as well as the encouragement he has given me while attending University of Oklahoma. I especially appreciate the opportunity to participate and present my work with the Institute for Reservoir Characterization. I am also thankful to Dr. Michael Engel for his careful feedback and support as a committee member and graduate liaison- I have enjoyed our classes and talks.

Thank you to those who took the time to help me both in and out of lab; I think of you as mentors: Jonathan Allen, Larry Hyde, Tomasz Kuder, Silvana Barbanti, Ann Sullivan Ojeda, and Richard Brito. I also am thankful to the Organic Geochemistry Group, especially Cecilia Lopez-Gamundi, Andreina Liborius Parada, Yağmur Sümer Görenekli, and Emilio Torres-Parada. Thank you for the support and friendship. In addition, I need to thank the members of IRC for welcoming me in, particularly Daniella Becerra and Henry Galvis for the meticulous work collecting samples and data. I really appreciate the time you took to discuss our research.

I still have many people at OU to thank who made my time here special. I am sincerely grateful to Dr. John Pigott for the guidance and mentorship through the past

couple years. I would also like to express thanks to my IBA teammates: Joseph Snyder, Jennifer Roberts, Rae Jacobsen, and Gabriel Machado- you were one of the best groups I've worked with. Also, I need to thank the rest of the ConocoPhillips School of Geology and Geophysics, especially my dear friends who supported me through this process- you know who you are.

Finally and most importantly, I cannot express enough thanks to my family for their love and support. To my mother, who has been my best friend and main support system through all of this- thank you for encouraging me. To my father, the best coach/teacher/mentor I could hope for- thank you for sharing your interests and inspiring me to work hard. I am indebted to you for introducing me to geology and geochemistry, and the endless support you've given along the way. Mom and dad, you are my role models. To Audrey- thank you for being so caring, compassionate, and patient with me. To Allison- thank you for being my friend; you are inspiring and wise beyond your age. To Megan- you are like a sister to me, and I have been lucky to have you in my life and to lean on through this. Indeed, I could not have done it without my family, and I love you all.

Table of Contents

Acknowledgements.....	iv
Table of Contents.....	vi
List of Tables	ix
List of Figures	xii
Abstract.....	xix
I. INTRODUCTION.....	1
1.1. Significance of Woodford Shale Analysis.....	1
1.1.1. Sequence Stratigraphy and Geochemistry of the Woodford Shale.....	1
1.1.2. The Kellwasser Event and the Hangenburg Crisis in the Woodford Shale.....	7
1.2. Objective and Scope of Thesis.....	11
II. GEOLOGIC SETTING.....	13
2.1. Regional Geology	13
2.2. Local Geology and Previous Work.....	15
2.2.1. Ardmore Basin.....	15
2.2.2. Woodford Shale	15
2.2.3. The I-35 Woodford Outcrop	19
III. METHODOLOGY	27
3.1. Study Area	27
3.2. Experimental.....	31
3.2.1 Sample Handling and Preparation	31
3.2.2. Rock Eval Pyrolysis and TOC	31

3.2.3. Extraction and Precipitation.....	32
3.2.4. Bitumen Fractionation	32
3.2.5. Maltene Fractionation: Liquid Column Chromatography	33
3.2.5. Gas Chromatography	35
3.2.7. Quantification and Identification	36
3.2.8. Gas Chromatography-Mass Spectrometry-Mass Spectrometry.....	36
IV. RESULTS AND DISCUSSION.....	38
4.1. Bulk Data Analysis	38
4.1.1. Total Organic Carbon (TOC).....	38
4.1.2. Kerogen Type.....	41
4.1.3. Maturity.....	48
4.1.4. Fractionation Weights.....	49
4.2. Saturate Biomarkers.....	52
4.2.1. n-Alkanes and Isoprenoids.....	52
4.2.2. Steranes	55
4.2.3. Hopanes.....	64
4.2.4. Tricyclic Terpanes	67
4.2.5. Tetracyclic Polyprenoids	72
4.3. Aromatic Biomarkers.....	74
4.3.1. Identifying Photic Zone Euxinia: Carotenoids and Aryl Isoprenoids.....	74
4.4. Polycyclic Aromatic Hydrocarbons.....	85
4.4.1. Terrestrial Plant Biomarkers	85
4.4.2. Diagenesis vs. Combustion Derived PAHs	96

4.4.3. Perylene and Alteration Products.....	101
4.4.4. Maturity and Biodegradation: Phenanthrenes.....	107
4.4.5. Sulfate Reduction: Dibenzothiophenes.....	108
4.5. Evidence of Kellwasser and Hangenberg Events from PZE and Organic Input	113
V. CONCLUSIONS.....	122
References.....	125
Appendix A: Compound Structures.....	142
Appendix B: Gas Chromatography Results.....	151
Appendix C: GCMS Results.....	166
Appendix D: Selected GC/MS/MS Identifications.....	196
Appendix E: Conodont Biostratigraphy Information (Over, 1992).....	198

List of Tables

Table 1. Rock Eval Pyrolysis and TOC values, based on height from the base of the I-35 outcrop. (TOC = total organic carbon; HI= hydrogen index; OI= oxygen index; PI= production index; NOC = normalized oil content). S ₁ and S ₂ measured in mg HC/g rock. S ₃ mg CO ₂ /g rock. Calculated R ₀ = (0.0180)(Tmax) – 7.16.....	39
Table 2. Generative potential (quantity) of immature source rocks (from Peters and Cassa, 1994). Bitumen= extractable fraction of organic matter in rock. Hydrocarbons= extractable portion of compounds comprised of only hydrogen and carbon.....	40
Table 3. Inferred maceral type, depositional conditions, and hydrogen index for each kerogen type (modified after Peters and Cassa, 1994).	42
Table 4. Sample weights used to extract, deasphaltene, and fractionate, and the resulting yields from each step. (Soxhlet= grams of powderized rock extracted in soxhlet; Extract= weight of extract; Centifuge= recoverable extract after centrifuging; Maltene= maltene weight recovered; asphaltene= asphaltene weight recovered; Fractionated= mg of sample fractionated; Aliphatic, Aromatic, and Polar refer to final yields of each fraction).....	51
Table 5. Sterane identities of numbered GC/MS/MS peaks. Names in parentheses refer to abbreviations used in Figure 25 and Table 6.	58
Table 6. Integrated areas and calculated values for steranes calculated for the various parameters used to interpret sterane distributions. (C ₂₇ SI= C ₂₇ sterane ratio = C ₂₇ ααα/[C ₂₇ ααα +C ₂₈ ααα +C ₂₉ ααα]; C ₂₈ SI = C ₂₈ sterane ratio = C ₂₈ ααα/[C ₂₇ ααα +C ₂₈ ααα +C ₂₉ ααα]; C ₂₉ SI = C ₂₉ sterane ratio = C ₂₉ ααα/[C ₂₇ ααα +C ₂₈ ααα +C ₂₉ ααα]; C ₃₀	

SI= C₃₀ Sterane Index= C₃₀ααα/[C₂₇ααα +C₂₈ααα +C₂₉ααα+C₃₀ααα]; C₂₇ DR = Diasterane ratio= C₂₇βα diasteranes/[C₂₇βα diasteranes + C₂₇ααα steranes]. Ratios calculated adding R and S isomers together 63

Table 7. Hopane and tricyclic terpane ratios used. (Gammacerane Index = 10* gammacerane / [gammacerane + C₃₀ hopane]; C₂₆/C₂₅ TT = C₂₆/C₂₅ tricyclic terpanes; C₃₁R/ C₃₀ = C₃₁R/ C₃₀ hopanes; TT/Hop = [C₂₈ + C₂₉ tricyclic terpanes] / [C₂₉ -C₃₃ hopanes] ; 22S/[22S+22R] ratio calculated for C₃₁ hopane). 73

Table 8. Ratios and concentrations expressed in µg / g TOC, calculated for aryl isoprenoids and carotenoids. (Paleo=paleorenieratane; Iso=isorenieratane; Ren=renieratane; RPur=renierapurpurane; AIR=(C₁₃₋₁₇/C_{18-c22}); 3,4,5-TMB= Σ[3,4,5 trimethylated aryl isoprenoids]; 2,3,6-TMB= Σ[2,3,6 trimethylated aryl isoprenoids]). 84

Table 9. Concentrations of various PAHs in extracts, expressed in µg / g TOC. (biP= biphenyl; Cad= cadalene; DBF= dibenzofuran; Py= pyrene; Fl= fluoranthene; BFl= benzofluoranthene). 95

Table 10. Chrysene and Benzo(a)anthracene concentrations expressed in µg / g TOC. (BaA Ratio = BaA/ (BaA +Triphenylene+Chrysene). 100

Table 11. Concentrations (µg / g TOC) and relative amounts of perylene and derivatives. (BeP= benzo(e)pyrene; BaP=benzo(a)pyrene; P= perylene; BghiP= benzo(g,h,i)perylene) 106

Table 12. Concentrations (µg / g TOC) and ratios of dibenzothiophenes (DBT), methyl-dibenzothiophenes (MDBT), phenanthrenes (P), and calculated vitrinite reflectance.

(DBT ratio = $DBT/(DBT+MDBT)$); MPI=methylphenanthrene index= $1.5*[2-MP + 3-MP]/[P + 1-MP + 9-MP]$; Rc= calculated vitrinite reflectance= $0.6[MPI] + 0.4$)...... 112

List of Figures

Figure 1. Schematic representing the three primary systems tracts in stratigraphy as a function of sea level (Slatt and Rodriguez, 2012). Sea level and sedimentation behavior defined for each systems tract..... 2

Figure 2. Anticipated sea level, marine circulation, oxic conditions, and TOC preservation as sea level rises, modified from Slatt (2013) interpretation of Woodford sedimentation. 5

Figure 3. Model demonstrating the relationship between increased nutrient input and expansion of the OMZ (oxygen minimum zone) during the EPME (end-Permian mass extinction), thus causing onset of PZE. (Zhou et al., 2016)..... 10

Figure 4. Major Geologic Provinces of Oklahoma (Johnson, 2008). 14

Figure 5. Chronostratigraphy of the Woodford Shale in the Anadarko, Ardmore and Arkoma Basins (Comer, 2008). In the Arbuckle Mountains, the Woodford is just above the Hunton Group, and overlain by the Sycamore Limestone..... 16

Figure 6. Stratigraphic Column for Woodford Shale in Southern Oklahoma. Red star indicates Kellwasser Event; blue star indicates Hangenberg Event. (U= upper, M=middle, L= lower). 17

Figure 7. North America at 360 Ma, i.e. approximately the Devonian-Carboniferous transition (Blakey, 2011). 18

Figure 8. Map of study area in Oklahoma. Yellow star denotes outcrop location; red line indicates strike (Galvis-Portilla et al., 2016). 20

Figure 9. Gamma ray, TOC, sample location, hardness, and lithology for the I-35 Woodford outcrop. Images demonstrate typical rock samples for ‘soft siliceous shale’ and ‘hard chert beds’ (Modified from Becerra-Rondon, 2017). 22

Figure 10. Gamma ray, chemofacies (Becerra-Rondon, 2017), and approximate stratigraphic location of Over (1990) conodont biostratigraphy of the Interstate 35 outcrop based on best estimate from 1990 report (blue) and lithology (red). Last occurrence of praesulcata (Devonian) and first occurrence of duplicata (Carboniferous) identified, along with approximate D-C boundary. 23

Figure 11. Distant image of the I-35 outcrop, exposing relatively softer, eroded Woodford Shale, along with Sycamore, and Hunton units (Galvis-Portilla et al., 2017). Red circle indicates study location. 28

Figure 12. Image of I-35 outcrop study location, overlain by gamma ray profile (Galvis-Portilla et al., 2016). 28

Figure 13. Well-to-outcrop correlation using digitized log from Speake-1 and Jud Little 4-6 wells from Northern Carter County, OK, as well as the Speake Ranch, Henry House, OHMEGCO, and I-35 outcrop gamma ray profiles (Becerra-Rondon, 2017). The I-35 outcrop demonstrates middle and upper Woodford gamma ray signature. 29

Figure 14. Map indicating location of wells and outcrops used to make a correlation (Cardott, 2012; Becerra-Rondon, 2017). 30

Figure 15. Workflow for geochemical analysis of samples- including extraction and separation of sample fractions. 34

Figure 16. Conversions for biomarker quantification. B = biomarker; Stnd = standard; PA = peak area; Wt = weight; f_n = normalization factor for maltenes fractionated; Mal = maltenes; Ext = extract.	37
Figure 17. Schematic of temperature ramp and peaks in Rock-Eval pyrogram. Figure provided by R. P. Philp (Slatt, 2013).	43
Figure 18. Modified Van Krevelen Plot using OI and HI. Green arrow denotes trend of increasing weathering. (Red = samples used in biomarker analysis; blue = samples only analyzed by Rock Eval pyrolysis and TOC.) Most samples for the I-35 Woodford outcrop plot between HI=450-650, OI<30.	44
Figure 19. S ₂ vs. TOC, provided by GeoMark. (red = samples used in biomarker analysis; blue = samples only analyzed by Rock Eval pyrolysis and TOC.) Samples for this study plot primarily as a Type II, oil prone kerogen.	45
Figure 20. Modified from Langford and Blanc-Valleron's model for adsorbed carbon (%) and HI.	47
Figure 21. T _{max} (°C) versus HI. Graph provided by GeoMark. (red = samples used in biomarker analysis; blue = samples only analyzed by Rock Eval pyrolysis and TOC.) T _{max} values range from 426° to 439°; HI ranges from 76 to 657.	49
Figure 22. Chromatograms of aliphatic fractions, selected to demonstrate variable weathering up the outcrop. (Pr = pristane ; Ph = phytane). MFS = maximum flooding surface. Sequence stratigraphic interpretation based on interpretations of Galvis, 2017 and Becerra, 2017.	53
Figure 23. GCMS m/z 217.3 fragmentogram identifying C ₂₇ -C ₃₀ steranes and diasteranes. Peak identities in Table 5.	57

Figure 24. GC/MS/MS Identifications of C ₂₇ -C ₃₀ sterane and diasterane isomers.....	58
Figure 25. Ternary plot showing the relative proportions of the C ₂₇ :C ₂₈ :C ₂₉ steranes compared to distributions originally proposed by Moldowan (1985) for source rocks of varying ages.	59
Figure 26. Sterane Index and diasterane ratio versus lithostratigraphic column, gamma ray (Becerra-Rondon, 2017) and interpreted sequence stratigraphy and sea level. (Sterane Index = C ₃₀ ααα/ (C ₂₇ ααα-C ₃₀ ααα) steranes; Diasterane Index = C ₂₇ βα diasteranes / (C ₂₇ βα diasteranes + C ₂₇ ααα steranes).	61
Figure 27. Tricyclic terpane and hopane identification using m/z 191.3 plot of sample 43.....	65
Figure 28. Gammacerane concentration up the outcrop, and gamma ray curve.....	66
Figure 29. Comparison of tricyclic terpane/hopane abundance, as compared to lithofacies. (Tricyclic terpane / hopane ratio = [C ₂₈ -C ₂₉ tricyclic terpanes / C ₂₉ -C ₃₃ hopanes]).	69
Figure 30. C ₂₆ /C ₂₅ Cheilanthanes vs. C ₃₁ R Hopanes/C ₃₀ Hopanes. (Blue = samples designated as dolomitic mudstone by Becerra-Rondon, 2017).	71
Figure 31. Sample 13 aromatics, with apparent contamination.	71
Figure 32. Generalized model for photic zone euxinia, after Connock, 2015. Colors indicate relative positions of sulfur bacteria species, with brown GSB existing deeper than GSB, which inhabits deeper position than PSB.	75
Figure 33. Identification of aryl isoprenoids using added mass fragments (m/z 133 +134).	77

Figure 34. Identification of beta-carotane, C ₃₂ and C ₃₃ aryl isoprenoids, and C ₄₀ Carotenoids using m/z 133 + 134.	77
Figure 35. Aryl isoprenoid sum (3,4,5- + 2,3,6- trimethyl-substituted aryl isoprenoids); total 3,4,5-trimethyl substituted aryl isoprenoids; total 2,3,6-trimethyl substituted aryl isoprenoids; and C ₁₈ AIR = 3,4,5- / 2,3,6- trimethyl-substituted aryl isoprenoids.	78
Figure 36. Gammacerane concentration versus AIR. (AIR= C ₁₃₋₁₇ aryl isoprenoids / C _{18-C22} aryl isoprenoids. Green= intermittent PZE, blue=transitional conditions, purple= persistent PZE; Orange zone demonstrating gammacerane and AIR correlation.).....	80
Figure 37. C ₄₀ carotenoid concentrations and aryl isoprenoid sum (µg / g TOC). Blue = elevated carotenoids, persistent euxinia, yellow = elevated aryl isoprenoids.....	82
Figure 38. GC/MS identification of biphenyl, dibenzofuran, and fluorene by comparing previously identified peaks for the coal tar standard with peaks in the aromatic fraction of sample 14 and 16. Peak numbers defined in table on the right.	89
Figure 39. GC/MS identification of fluoranthene, pyrene, benzofluoranthenes, benzopyrenes, and perylene, by comparing previously identified peaks for the coal tar standard with peaks in the aromatic fraction of sample 14.....	90
Figure 40. Zoomed in m/z 252 of Standard Ref. Mat #1597 and Woodford Aromatic #4.....	91
Figure 41. m/z 183 from aromatic fraction of Woodford sample #4 before and after coinjection with cadalene standard. Increased peak height in bottom fragmentogram demonstrates coelution with cadalene in the standard and cadalene in the sample.....	92

Figure 42. Concentrations of dibenzofuran, biphenyl, and cadalene by height from outcrop base.	93
Figure 43. Concentrations of fluoranthene, pyrene, and benzofluoranthenes by height from base of outcrop.	94
Figure 44. Comparison of benzoanthracene and chrysene/triphenylene between the Woodford #32 sample and the coal standard.	98
Figure 45. Concentrations of benzo(a)anthracene, chrysene, and BaA ratio from the base of the outcrop compared with interpreted gamma ray, PZE conditions and interpreted sequence stratigraphy. BaA ratio = benzo(a)anthracene / (benzo(a)anthracene + chrysene + triphenylene). Blue = PZE onset, yellow = diminishing PZE conditions.	99
Figure 46. Identification of perylene, benzo(e)pyrene, benzo(a)pyrene, and benzo(g,h,i)perylene using m/z 252 and 276.	102
Figure 47. Artificial maturation of perylene (from Marynowski et al., 2015).	103
Figure 48. Quantity of perylene, benzo(e)pyrene, benzo(a)pyrene, and benzo(g,h,i)perylene in $\mu\text{g} / \text{g TOC}$	105
Figure 49. Identification of phenanthrene, methyl-phenanthrenes, dimethylphenanthrenes, trimethylphenanthrenes, and tetramethylphenanthrenes using and mass fragments (m/z 178 + 192 + 206+ 220 + 234). (a= 3-methylphenanthrene; b= 2-methylphenanthrene; c= 9-methylphenanthrene; d=1-methylphenanthrene).	107
Figure 50. Identification of DBT, MDBT, and DMDBT (m/z 184+198+202). (a= 4-MDBT; b= 2- + 3-MDBT; c= 1-MDBT)	110

Figure 51. Concentration of DBT, MDBT by height from the base of the outcrop, as well as DBT/ P ratio. (DBT/P = dibenzothiophenes/phenanthrenes). 111

Figure 52. Inferred onset of euxinic conditions using DBT, sum of aryl isoprenoids, and paleorenieratane. Yellow= onset PZE, blue = diminishing PZE. 118

Figure 53. Comparison of interpreted Woodford PZE, higher-plant proxies, conifer proxy, water column stratification and combustion proxy. 121

Abstract

Geochemical analyses of the Late Devonian-Early Mississippian Woodford Shale have revealed a more dynamic history than previously considered, reflecting discrete changes in the conditions surrounding its depositional history. Biomarkers, pyrolysis, and chemostratigraphy provide evidence for paleoenvironmental variations in setting, water chemistry, and organofacies. Dominated by an overall transgressive sequence, the Oklahoma Woodford Shale demonstrates alternating circulation patterns with fluctuating marine and continental organic input, and intermittent events of photic zone euxinia (PZE), resulting in heterogenic distributions regionally and sequentially.

Furthermore, biomarker studies have indicated two Late-Devonian biotic crises including the Frasnian-Famennian (F-F) Kellwasser Event and the Devonian-Carboniferous (D-C) Hangenberg Event. Cumulatively, the two events contribute to one of five of the most devastating mass extinctions in Earth's history. These boundaries, located in the middle and upper Woodford respectively, have also been closely studied in time-equivalent shales worldwide. Biomarkers from Devonian land plants and their combusted derivatives highlight an influx of continental organic matter into the Late Devonian-Early Mississippian Woodford Sea. Increased soil runoff and nutrient flux from newly evolved vascular plants and massive forest fires could have contributed to the widespread eutrophication and anoxia, which resulted in the high organic matter preservation of this important source rock.

A well-preserved, 80-foot Interstate-35 outcrop in Carter County, Oklahoma provides a unique opportunity to investigate detailed geochemical and stratigraphic trends across the middle and upper Woodford. A biomarker study was conducted to

assess complexities of the Woodford's deposition, with a particular focus on the relationship between sequence stratigraphy, organic input, euxinic episodes, and the two Late Devonian mass extinctions. For the first time, the geochemical evidence of the Hangenberg Crisis is defined for the Woodford Shale. Analysis of biomarkers, including carotenoids, aryl isoprenoids, and polycyclic aromatic hydrocarbons demonstrated cyclic patterns in depositional history, leading to better prediction of hydrocarbon-rich intervals.

This study found aryl isoprenoids and carotenoids, indicators of PZE, to be higher in abundance than previously seen in the upper Woodford, signifying regional differences in circulation and oxic conditions, and possibly greater preservation within the Ardmore Basin. In addition, terrestrially-sourced biomarkers and their pyrogenic derivatives were identified, demonstrating a link between basinal input from land plants and euxinic conditions in the Woodford Sea.

I. INTRODUCTION

1.1. Significance of Woodford Shale Analysis

The Woodford Shale of Oklahoma has proven to be a prolific oil and gas source for decades, and thus attracts much attention in the world of petroleum exploration. For example, between the years of 2004 and 2011, over 2,000 horizontal and vertical wells were completed in the Woodford Shale, producing gas, oil, and condensate (Cardott, 2012). By July 2010, the Woodford alone had produced 932 Bcf gas and 3.7 Mbbl of oil (Cardott, 2012). Furthermore, the 2014 Annual Energy Outlook from the EIA reported that there was as much as 610 Tcf of shale gas and 59 billion barrels of recoverable tight oil in proven reserves in the United States. As one of the most substantial petroleum resources in the continental US, the Woodford Shale can lend insight into exploration and production potential of other shale plays. Thanks to the widespread availability of Woodford Shale outcrops throughout Southern Oklahoma, this resource is readily accessible for both academic and industrial research.

1.1.1. Sequence Stratigraphy and Geochemistry of the Woodford Shale

In recent years, geochemical studies of the Woodford Shale have highlighted the fact that seemingly subtle differences in lithology can represent a wide range of depositional conditions (e.g. Miceli-Romero and Philp, 2012; Connock, 2015; Infante et al., 2016; Turner, 2016; Villalba, 2016). Such revelations have ultimately improved characterization of the Woodford Shale as a source and reservoir rock, thus contributing to its increased production, especially through unconventional means (e.g. Comer,

2008; Cardott, 2012; Slatt et al., 2012; McCullough, 2014; DeGarmo, 2015). Organic geochemistry, elemental analysis, vitrinite and maceral studies are continuously revealing a more dynamic story of the Woodford's sequence stratigraphy in ways seismic or petrophysical data never could.

Sequence stratigraphy is founded on the principle that through geologic time, changes in sea level and deposition occur in a cyclic and predictable manner (Slatt et al., 2012). These cycles can be identified by regionally correlative boundaries, which indicate transgressive, regressive, and high-stand periods within a basin's history (van Wagoner, 1988; Slatt and Rodriguez, 2012; Figure 1). Discerning the geologic and chronostratigraphic patterns holds great significance to understanding a reservoir or basin, as well as economic implications when it comes to efficiently exploring and exploiting a reservoir of interest.

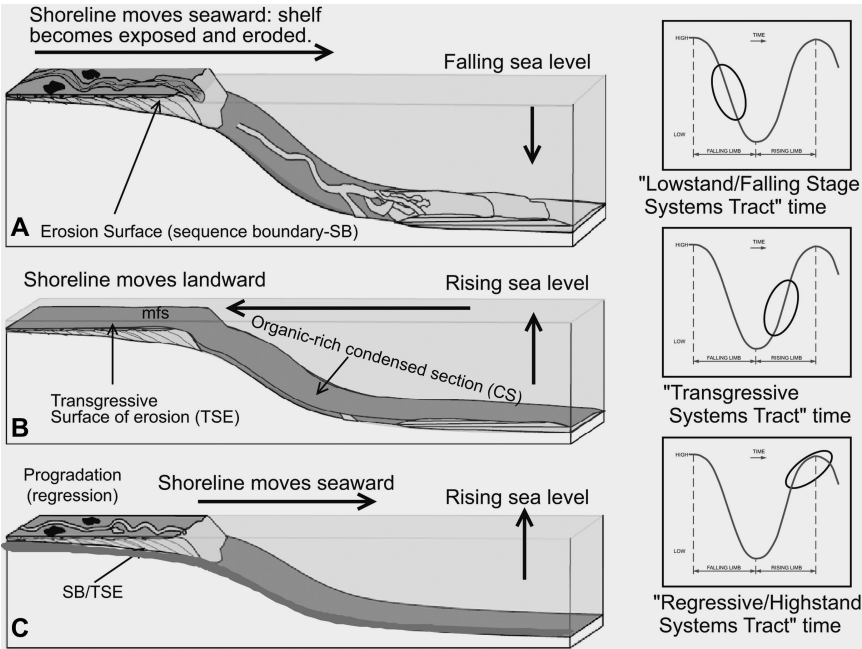


Figure 1. Schematic representing the three primary systems tracts in stratigraphy as a function of sea level (Slatt and Rodriguez, 2012). Sea level and sedimentation behavior defined for each systems tract.

Extensive research has been conducted in order to better understand the Woodford's stratigraphy, and novel methods have contributed to more precise models. For example, Serna-Bernal (2013) identified the Woodford Shale as a 2nd order sequence, with 14 3rd order parasequences throughout the interval. By utilizing a Devonian sea level curve, total organic carbon (TOC) and carbonate content, Serna-Bernal (2013) was able to correlate the intercalated brittle/ductile beds with parasequences, and infer that minor changes in sea level were responsible for the alternating rock mechanics between the differing lithologies. Another example of novel tools used for stratigraphic interpretation in the Woodford includes the utilization of elemental proxies from handheld XRF by Turner (2016). The study used concentrations of certain elemental assemblages to make interpretations of high-frequency sequence cycles (i.e. highstand systems tract= high Ti, Zr, Al, and K, low Mo and V). Turner (2016) found that chemostratigraphic cyclicity in the Woodford was regionally correlative across the basin, and could be connected with global sea level trends described by Johnson et al. (1985).

In terms of geochemical applications to sequence stratigraphy, variations in total organic carbon can give insight where an interval fits in a sequence stratigraphic framework. Lowstand systems tracts (LST) are identified for their low organic content (2% or less), and are distinguishable from transgressive system tracts (TST), which have significantly higher amounts of organic input (up to 10% TOC; Isaksen and Bohacs, 1995). Generally, condensed sections (CS), which occur between the late transgressive systems tracts (TST) and the maximum flooding surface (MFS) at the beginning of highstand systems tract (HST) deposition, are characterized as having the highest TOC

and best source rock potential (Slatt et al., 2012). These condensed sections are caused by slow sedimentation rates, resulting in organic matter being packed more densely in marine shales (Vail et al., 1984). Furthermore, the flooding of a continental shelf promotes formation of high quality source rocks because of the increased potential for bioproductivity on previously exposed soil horizons, and the increased tendency for anoxia related to water column stratification (Katz, 1995). Because of this generalization, assumptions are frequently made in exploration when identifying CS shale units via petrophysical and seismic methods. In fact, condensed sections do not always occur exactly below the maximum flooding surface, and not every shale unit found at the TST/HST boundary will result in a good source rock (Curiale et al., 1992). For example, in the case of the Woodford Shale, this generalization proves to be misleading as the middle Woodford, which is characterized by an overall transgressive pattern, is known to have significantly higher average TOC than its upper or lower counterparts. There are also many high TOC, ‘frackable’ zones other than the supposed condensed section (Hester et al., 1988; DeGarmo, 2015). Ultimately, using a sequence stratigraphic framework in conjunction with the geochemistry can clear up pitfalls associating Woodford stratigraphy with its potential productivity.

When it comes to the Woodford, high organic productivity seems to be reliant on restriction in marine circulation. The interpreted changes in environmental conditions from early to late Woodford deposition are demonstrated in Figure 2. Variable topography underlying the Woodford resulted in pockets of restricted marine circulation, accompanied by organic-rich shale deposition (falling and early stage Woodford; i.e., lower Woodford). As sea level rose, the increased circulation caused

oxygenation and decreased organic preservation. Parasequences demonstrating increasing oxygenation are reflected in the middle Woodford (continued sea level rise). Toward the end of Woodford Sea transgression, open circulation dominated, resulting in a relatively organic-lean upper Woodford.

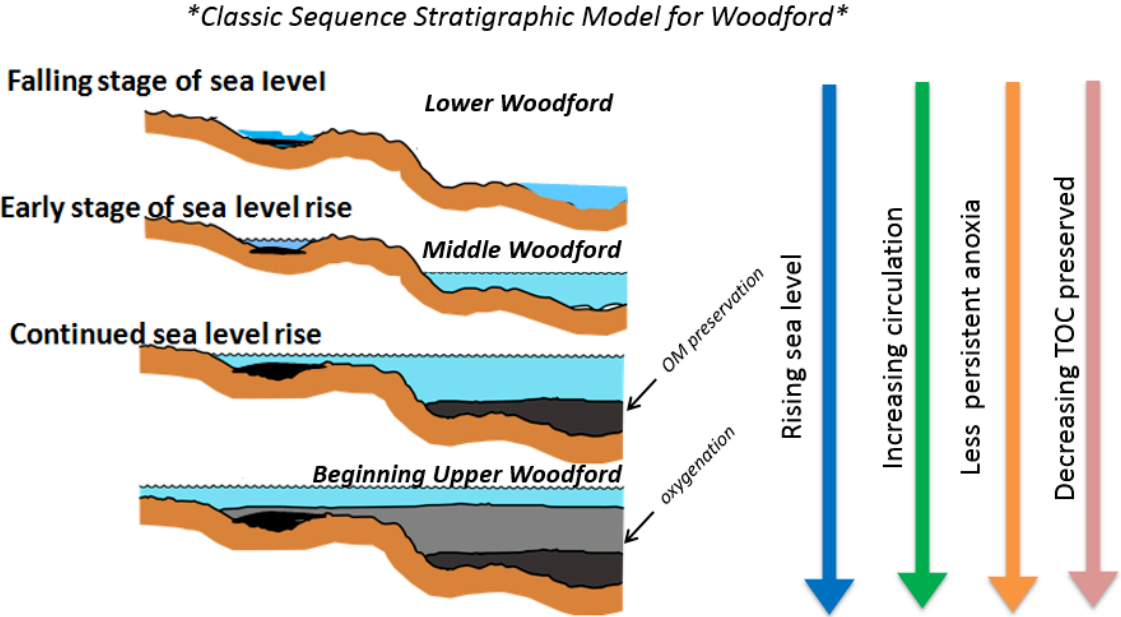


Figure 2. Anticipated sea level, marine circulation, oxic conditions, and TOC preservation as sea level rises, modified from Slatt (2013) interpretation of Woodford sedimentation.

Further examination of hydrocarbons using gas chromatography and mass spectrometry allows for the measurement of relative proportions of biomarkers. These compounds act as “molecular fossils”, which can then be linked back to a parent species from which they are derived (Eglinton and Calvin, 1967). Because biomarker assemblages vary based on the organisms they are derived from (algal, bacterial, higher

plant, etc.), the geochemical signature of a particular unit of interest has implications for the depositional environment when building a sequence stratigraphic framework in a basin. In the case of the Woodford, where lithology can appear relatively homogenous in certain zones, biomarkers may even be necessary for full interpretation of stratigraphy and depositional history. Of the hundreds of thousands of compounds that could potentially be found in petroleum samples, only a couple thousand have been identified, and fewer are used on a regular basis (commercially or otherwise). That being said, their distribution and abundance provides potential means to correlate samples, identifying source rocks and their lithology, understanding the depositional environment and burial history (diagenesis), and determining thermal maturity and age (Peters et al., 2005). For example, previous studies of the Woodford shale have been able to display predominantly marine distributions of alkanes, steranes, hopanes, and terpanes, with some indication of terrestrial organic input interspersed (Miceli-Romero and Philp, 2012; Degarmo, 2015).

One tool to demonstrate the utility of geochemistry to sequence stratigraphic interpretations is the occurrence of episodic PZE within the Woodford. The ability to better predict such events with biomarkers is of great importance for oil and gas exploration, as anoxic events tend to provide better organic preservation (Turner and Slatt, 2012). The use of C₄₀ carotenoid and aryl isoprenoid biomarkers is becoming increasingly popular as a proxy for episodic PZE, which is often found to coincide with high TOC values (Summons and Powell, 1987; Requejo et al., 1992; Miceli-Romero and Philp, 2012; and French et al., 2014). Carotenoids are derived from phototrophic, anaerobic green sulfur bacteria (GSB) that rely on PZE conditions in order to survive,

and aryl isoprenoids are the diagenetic products of carotenoids. While aryl isoprenoids are less source-specific and can be derived from β -carotane, the presence of both carotenoids and aryl isoprenoids provides proxies for minimum depth of PZE, water stratification, basin restriction and organic input (Summons and Powell, 1987; Connock, 2015). Therefore, the presence of such biomarkers is indicative of PZE, and potentially, a rich source rock. This brief example demonstrates the wide array of information available using two compound classes. Thus, the integration of data from many biomarker classes can provide volumes of information that can enhance sequence stratigraphy models.

1.1.2. The Kellwasser Event and the Hangenburg Crisis in the Woodford Shale

The deposition of the Woodford Shale coincides with a late Devonian globally-correlative biotic crisis, which resulted in one of the five largest mass extinction events in Earth's history (e.g. McGhee, 1981; Nowaczewski, 2011). Much debate surrounds the event's boundary definitions – most significantly, whether there was only one event, or a culmination of several smaller extinctions. The general consensus involves two extinctions: the Kellwasser Event, which occurred at the Frasnian-Famennian transition (~372 Ma), and the Hangenberg Crisis at the Devonian-Carboniferous boundary (~359 Ma) (e.g. McGhee, 1996; Sepkoski, 1996). Paleontological data indicates a marked decrease in growth of Devonian reef biota after the mid-Frasnian (Sandberg et al., 1988). Such behavior is evinced by the extinction of stromatoporiid and metazoan reefs, as well as the significant negative impact in brachiopod, ammonoid, ostracod, and trilobite diversity (Becker et al., 2012; Kaiser et al., 2015). The occurrence of varying

conodont biota before, during, and after the Kellwasser Event is evidence of shifting environmental conditions and extinctions during this time, and is reflected in biodiversity changes across all life forms (Over, 1992).

It has long been speculated that the cause of the Kellwasser Event is related to the widespread anoxic events within epeiric seas of the time period (e.g. Marynowski et al., 2011). Recent research has uncovered an increase in biomarker signatures from land plants and massive forest fires to Devonian basins coinciding with the biotic crisis (Marynowski and Filipiak, 2007; Grice et al., 2009; Kaiho et al., 2013; DeGarmo, 2015). While the Devonian saw desecration of marine fauna, it coincided with the era in which vascular plants evolved and the first forests came into existence (e.g. McGhee, 1996; Sepkoski, 1996). Continued research into these terrestrial land plant biomarkers has led many to connect the Late Devonian extinction with the increased runoff of soil and nutrients from the Devonian forests, causing anoxia and eutrophication of reef systems (Kaiho et al., 2013; Mizukami et al., 2013; Zhou et al., 2016). For example, dibenzothiophene (DBT) and dibenzofuran (DBF) have been measured and linked to the runoff that may have contributed to the mass extinction (DeGarmo, 2015). Dibenzothiophene can be derived from several pathways, but is likely the result of early diagenesis of functionalized organic molecules with inorganic sulfur at the sediment surface (Hughes et al., 1995). Methylated dibenzothiophene indicates sulfur reduction and organic degradation in anoxic environments (Hughes et al., 1995). Mizukami et al. (2013) found DBT in high abundance with indicators of euxinia, such as aryl isoprenoids, and proposed that the rapid input of terrestrial matter was responsible for the consumption of oxygen, which would cause the reducing conditions to produce

dibenzothiophene. As for dibenzofuran, the exact diagenetic pathway to its formation is unclear, but it is likely a derivative of compounds from lichens (Radke et al., 2000) or lignin in woody plants (Fenton et al., 2007). Therefore, both of these biomarkers can work as terrestrial input proxies; dibenzofuran for plant input, and dibenzothiophene for anoxic conditions purportedly caused by terrestrial input. In fact, DeGarmo (2015), identified both DBT and DBF in the Woodford and found that their abundances tracked with other known plant markers, such as cadalene and perylene. Such observations have been made at different intervals such as the Permian-Triassic Boundary (PTB), where the concentrations of DBT and DBF closely follow other compounds from plant sources, such as biphenyl (Fenton et al., 2007). In the cases of the Famennian-Frasnian and Permian-Triassic boundaries, DBT and DBF abundances are found to be high leading up to the extinction event, and then die down soon after (Fenton et al., 2007; Kaiho et al., 2013). This covariation between DBT and DBF provides further evidence of the hypothesis that terrestrial input may have contributed to the biotic crises. A model for terrestrial nutrient influx causing the expansion of photic zone euxinia has been suggested for the end-Permian extinction (Figure 3; Zhou et al., 2016). Based on this model, increased soil erosion can result in elevated nutrients supplied to the marine environment, which triggers eutrophication, thereby consuming available oxygen and expanding the oxygen minimum zone (Sephton et al., 2005; Fenton et al., 2007; Xie et al., 2007; Zhou et al., 2016). As a result, further studies into the environmental conditions surrounding the Kellwasser and Hangenberg crises can contribute to 1) understanding the history of the Woodford's sequence stratigraphy, and 2) the prediction of episodic high organic preservation, as seen in the Woodford Shale.

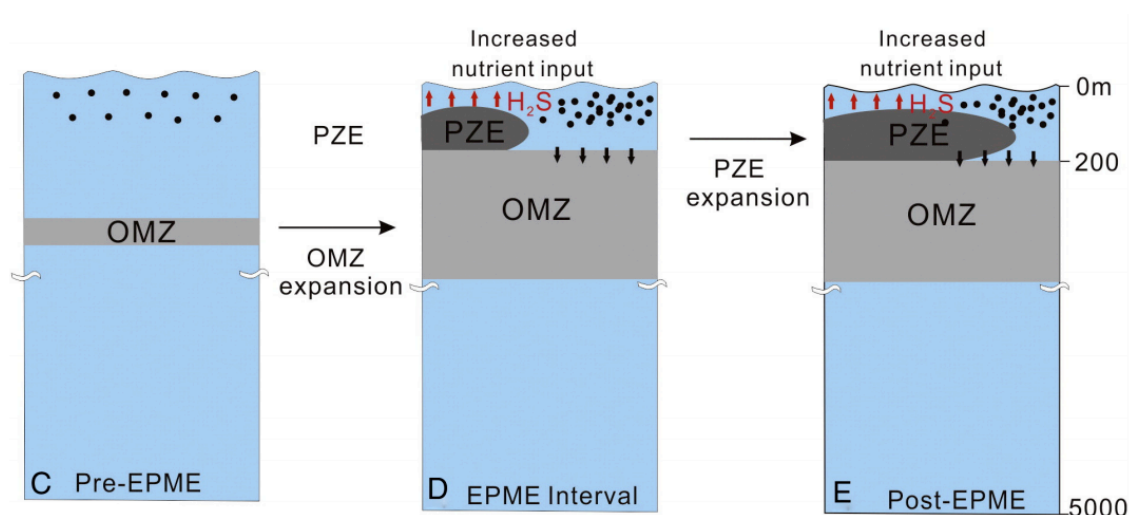


Figure 3. Model demonstrating the relationship between increased nutrient input and expansion of the OMZ (oxygen minimum zone) during the EPME (end-Permian mass extinction), thus causing onset of PZE. (Zhou et al., 2016)

Pyrogenic aromatic biomarkers provide a unique opportunity to identify influx of terrigenous material to the basin, and thus have major implications for sequence stratigraphic interpretation (Marynowski and Filipiak, 2007). The origin of such compounds is well understood because they are long studied carcinogens from industrial combustion of fossil fuels, although they have now also been linked to ancient forest fires in the rock record (Stout et al., 2015). Some biomarkers are thought to have multiple diagenetic and kinetic aromatization pathways, and thus do not make great source indicators, but in the case of pyrogenic biomarkers, the necessity for combustion to reach their final form requires terrestrial sourcing. Thus, these trace compounds serve as indicators of both terrestrial input and ancient forest fires.

A prominent example of pyrogenic biomarker analysis is the use of perylene and its combusted derivatives. As an indicator of wood-degrading fungi, perylene is a

marker for terrestrial organic input (Marynowski et al., 2015). Induced thermal maturation of perylene by heating the compound up to 500 °C has confirmed the alteration of the compound to benzo(e)pyrene and benzo(ghi)perylene, which have been previously identified in the Woodford Shale (Marynowski et al., 2015; DeGarmo, 2015). Other important pyrogenic compounds include coronene, chrysene, fluoranthene, and anthracene, which are markers for combusted land plants. (Jiang et al., 1998; Arinobu et al., 1999; Li et al., 2012; Marynowski et al., 2014). Incorporation of these biomarkers associated with terrestrial organic input and fires will ultimately contribute to current understanding of the Woodford and mass extinction events.

1.2. Objective and Scope of Thesis

The objective of this thesis is to build on previous interpretations of Woodford sequence stratigraphy and depositional history, with a specific focus on the middle and upper Woodford and the extinction boundaries of the Devonian period. In terms of laboratory analysis, bulk geochemical parameters, such as the relative extraction yields, TOC, Rock Eval pyrolysis, and biomarker data were quantified and analyzed to characterize the I-35 outcrop. In particular, biomarker analysis aims to:

- Assess biomarkers that pertain to Devonian terrestrial biota, and their combusted derivatives that may indicate the occurrence of forest fires.
- Recognize patterns or cycles in organic matter input, how they relate to productivity, preservation, and episodic euxinic events.

- Propose a relationship between sequence stratigraphy, organic input, and anoxic events.
- Relate geochemical parameters to conditions at the Frasnian-Famennian Boundary and the onset and aftermath of the Devonian-Carboniferous Boundary.

II. GEOLOGIC SETTING

2.1. Regional Geology

The geologic history of Oklahoma involves a dynamic sequence of marine transgression, sedimentation, rifting, and tectonically induced uplift, folding, and basin subsidence. These processes that occurred in the shelf-like region resulted in the deposition of interbedded shallow marine carbonates and shales, many of which are organic-rich, thus are targets for exploration (Johnson, 2008).

Deposition of Oklahoma's sedimentary layers began in the Late Cambrian, when the igneous and metamorphic basement was intruded by shallow seas from the southwest. The Arbuckle Group (Cambrian-Early Ordovician) was deposited throughout most of the state, made up of interbedded shallow marine carbonates, thin-bedded marls, and sandstones (Johnson et al., 1989; Johnson, 2008). Marine sediments accumulated extensively in the Southern Oklahoma Aulacogen, a remnant from the breakup of Rodinia (Ham et al., 1964). From the Late Cambrian to the Early Ordovician, the Oklahoma Basin accumulated between 1,000 – 10,000 feet of carbonates, with the thickest layers occurring in the Ouachita Trough (Johnson and Cardott, 1992).

From the Ordovician through the Mississippian, the aulacogen continued to subside, accumulating more strata into the basin (Amsden, 1975). Ordovician-aged Simpson sandstone, Viola limestone, and Sylvan shale covered a great portion of Oklahoma, particularly in the Ardmore Basin and Arkoma Basin (Johnson, 2008). Carbonate strata of the Hunton group were deposited in the Silurian and later eroded,

causing an unconformity between it and the Devonian Woodford shale above it. Shallow seas of the Early Mississippian caused the formation of the Sycamore and Mississippian limestones. Increased sedimentation in the Late Mississippian resulted in more significant subsidence and deposition of about 10,000 feet of black shale, limestone, sandstone, and flysch, known as the Caney Shale, Goddard Formation, and Springer Formation (Craig et al., 1979). Pennsylvanian tectonic activity resulted in deformation and thrusting of the Ouachita foldbelt, leading to the development and subdivision of the uplifts, mountain belts, and sub-basins (Anadarko, Ardmore, Arkoma, Marietta, and Hollis) that we see today (Ham and Wilson, 1967; Johnson, 2008; Figure 4.). Transgressions throughout the Triassic, Jurassic, and Cretaceous further deposited and buried strata, leading to hydrocarbon generation from the important petroleum systems that exist today, including the Woodford Shale, the Sooner Trend of the Anadarko Basin in Canadian and Kingfisher counties (STACK) and the South Central Oklahoma Oil Province (SCOOP).

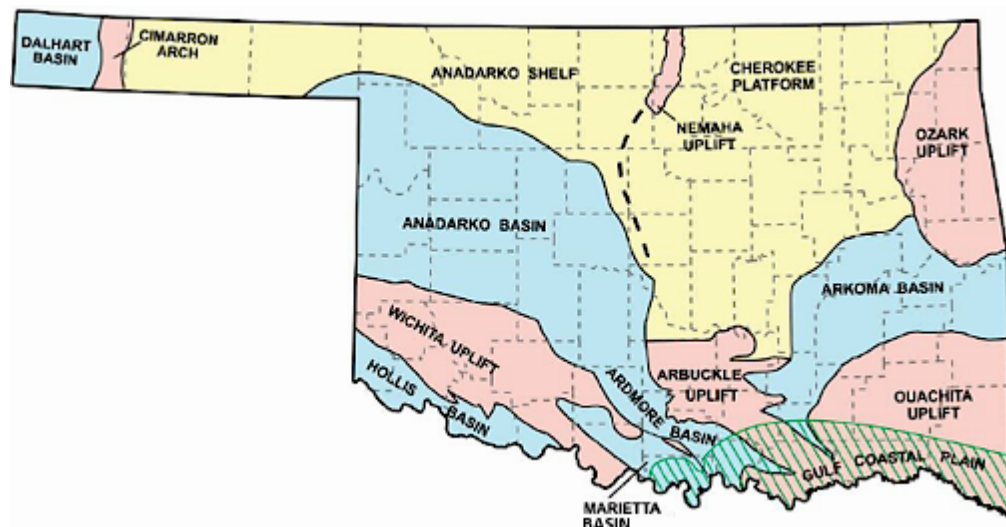


Figure 4. Major Geologic Provinces of Oklahoma (Johnson, 2008).

2.2. Local Geology and Previous Work

2.2.1. Ardmore Basin

Pennsylvanian foreland subsidence resulted in the elongated Ardmore Basin (Ham and Wilson, 1967). The Arbuckle Mountains provide the upper boundary to the northern flank of the basin, where numerous outcrops of the Woodford shale have been studied. A chronostratigraphic representation of the Arbuckle Mountains is seen juxtaposed with other Oklahoma basins in Figure 5, demonstrating the fact that the surrounding Anadarko and Arkoma subbasins have slightly different underlying and overlying lithologies (Comer, 2008). It is from an outcrop in the Arbuckle Mountains that the samples for this study were taken.

2.2.2. Woodford Shale

The Woodford formation is informally subdivided into three distinct units: the lower, middle, and upper Woodford (Figure 6; Ellison, 1950; Hester et al., 1988; Hester et al., 1990). As mentioned previously, the Woodford Shale unconformably overlies the Hunton Group (Turner et al., 2015). Due to the differential weathering and subaerial karstification of the Hunton limestones, the lower Woodford displays a range of thicknesses as it tended to preferentially fill topographic lows (Comer, 2008; Infante et al., 2016; Turner and Slatt, 2016). As the Devonian sea continued its transgression, covering the majority of the North American continent (Figure 7), the middle Woodford was deposited. The maximum flooding surface (MFS) for this sequence lies approximately just under the middle/upper Woodford boundary (Slatt et al., 2014).

Highstand and falling stage facies dominate the upper Woodford, which is overlain by the Mississippian Sycamore group.

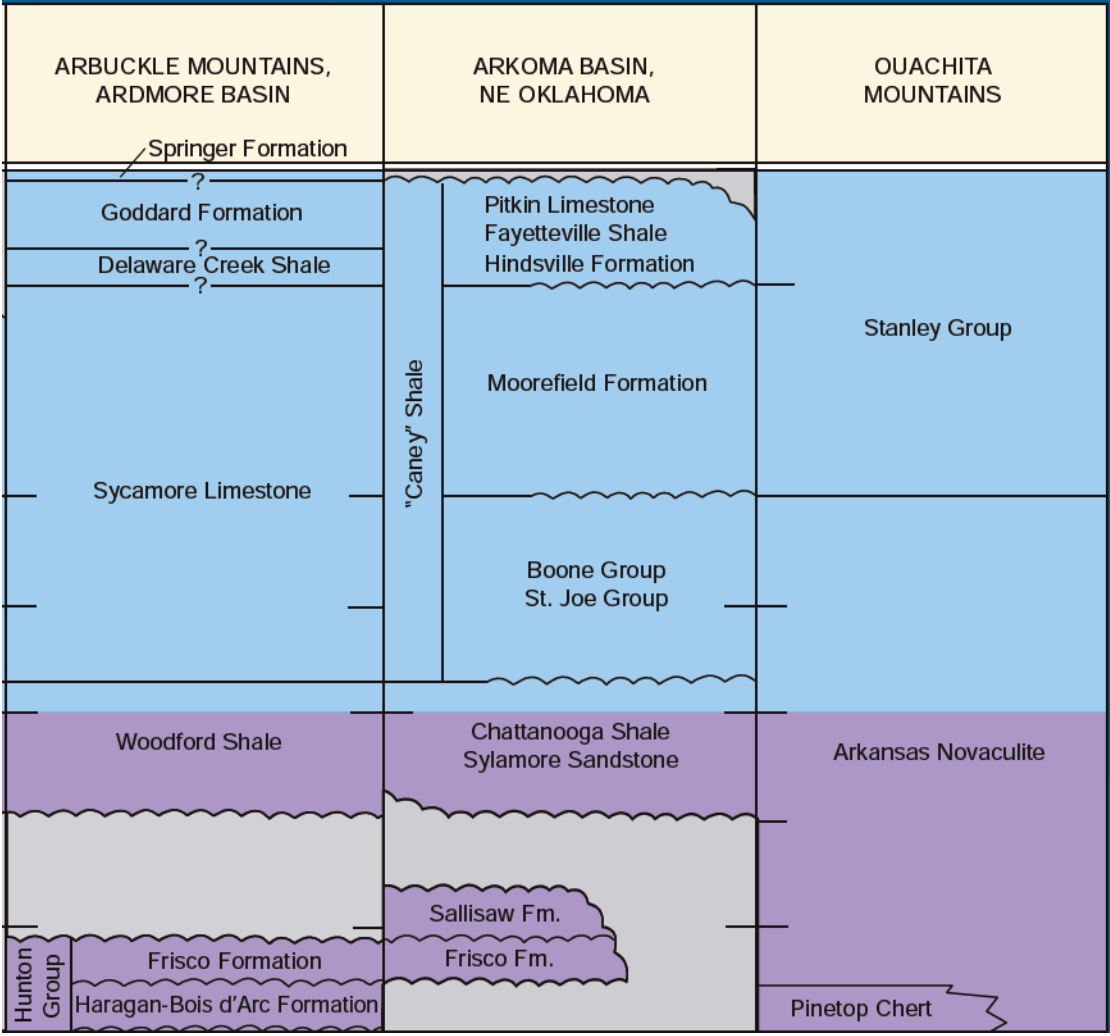
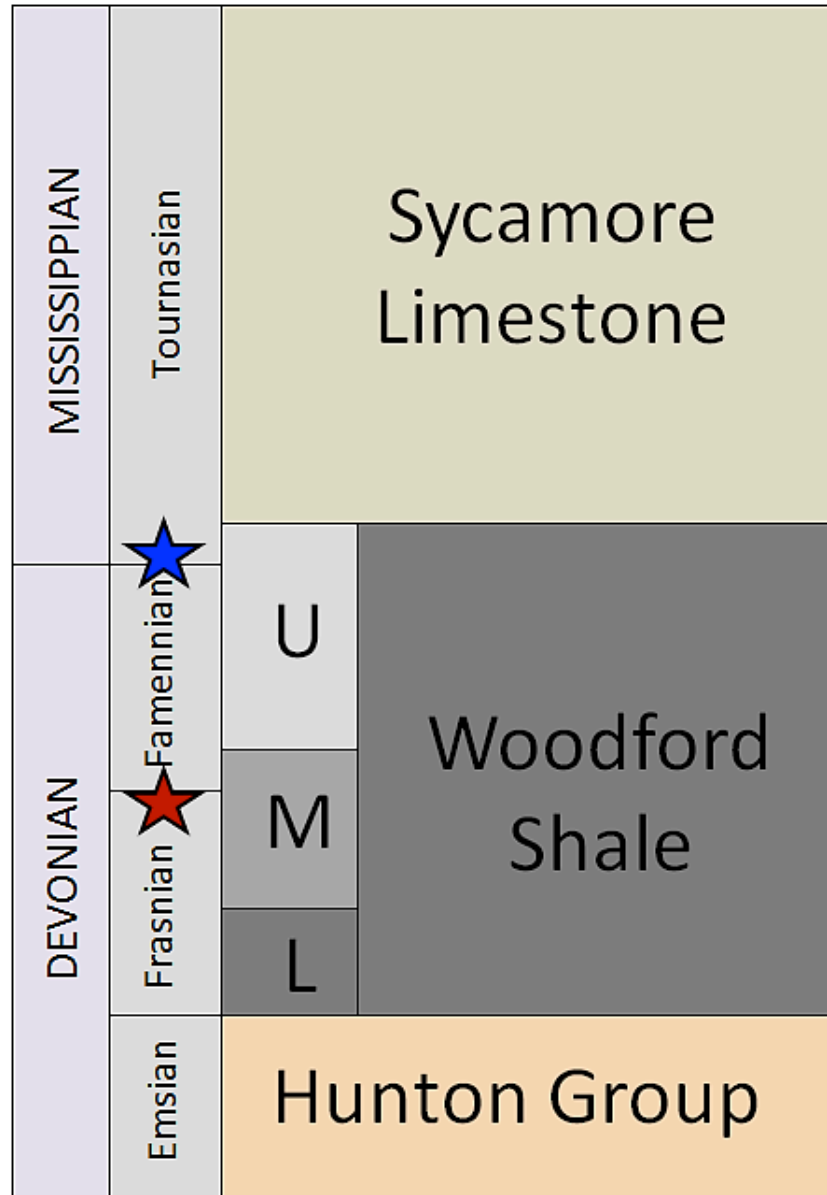


Figure 5. Chronostratigraphy of the Woodford Shale in the Anadarko, Ardmore and Arkoma Basins (Comer, 2008). In the Arbuckle Mountains, the Woodford is just above the Hunton Group, and overlain by the Sycamore Limestone.





-  Devonian-Carboniferous “Hangenberg” mass extinction.
-  Frasnian-Famennian “Kellwasser” mass extinction.

Figure 6. Stratigraphic Column for Woodford Shale in Southern Oklahoma. Red star indicates Kellwasser Event; blue star indicates Hangenberg Event. (U= upper, M= middle, L= lower).



Figure 7. North America at 360 Ma, i.e. approximately the Devonian-Carboniferous transition (Blakey, 2011).

Based on previous studies, the Woodford is primarily a Type II and/or mixed II/III kerogen, with TOC values ranging from 3-28% (Miceli-Romero and Philp, 2012; Slatt and Rodriguez, 2012). Classic sedimentary patterns in the Woodford include intercalation of brittle, biogenic shale beds and ductile, detrital beds (Slatt and Abousleiman, 2011). Increased periods of bioproductivity and planktonic blooms resulted in brittleness of the more biogenic beds. The crystalline skeletons of the microorganisms accompanied by the lack of clay input resulted in high organic concentration in fractureable beds between more ductile, TOC-rich beds (Slatt and Rodriguez, 2012). This type of pattern has been heavily studied for fracking and horizontal drilling purposes (Slatt, 2013). The Woodford Shale also has distinct clastic marine characteristics in its mineral content. The upper Woodford was deposited at a time when water circulation was mostly unrestricted, and upwellings and/or increased terrestrial input occurred providing more oxic conditions (Slatt and Abousleiman,

2011). As a result, the upper Woodford is easily identified by its prevalent phosphate nodules and pyrite concretions (Becerra-Rondon, 2017).

2.2.3. The I-35 Woodford Outcrop

The I-35 outcrop in Carter County has long been a source of interest due to its accessibility and location on the Arbuckle Uplift (Figure 8). This section dips 40° to the south on the west side of the interstate on the southern limb of the Arbuckle Anticline (NW1/4, SE1/4, Se. 25, T2S, R2E, Springer Quadrangle; Over, 1990). Over (1990) noted the predominance of chert and siliceous shale lithofacies for the uppermost portion of the Woodford as seen in outcrops throughout Southern Oklahoma. Because the Woodford Shale is situated on the southern margin of North America and demonstrates transgressive onlap, a marine, offshore setting is interpreted. The inferred depositional environment is used to describe the decrease in fine clays and increase in silica-rich biogenic shales in the uppermost portion of the Woodford. The presence of the black, organic-rich portions is attributed to dysoxic/anoxic conditions in the shallow marine setting.

Lewan (1983) used samples from the I-35 outcrop as classic examples of Woodford shale lithofacies in order to perform hydrous pyrolysis and delineate hydrocarbon generation phases between kerogen and oil. Based on the changing ¹³C isotope values with maturity, the results of this early study concluded that solid bitumen is an intermediate between kerogen and oil (Hackley and Cardott, 2016). Furthermore, it was found that the formation of continuous water-saturated bitumen networks, as seen in the Woodford, accounts for increased oil migration and expulsion- a phenomenon

that has also been used to explain the petroleum generation in the Williston Basin (Meissner, 1978; Lewan, 1992).

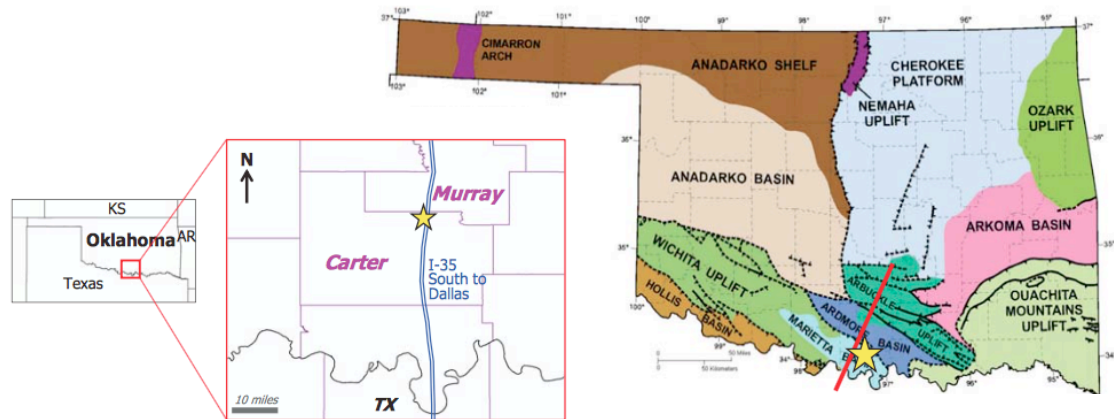


Figure 8. Map of study area in Oklahoma. Yellow star denotes outcrop location; red line indicates strike of beds (Galvis-Portilla et al., 2016).

Comer and Hinch (1987) used various outcrops and cores throughout Oklahoma to understand expulsion efficiency of the Woodford. Among these sample sites, the I-35 outcrop was studied in thin section. Based on petrographic evidence such as the presence of flattened *Tasmanites*, higher concentrations of amorphous organic matter, and lack of chert, it was recognized that the black siliceous shale beds within the outcrop had undergone significant compaction and remained mostly uncemented and unsealed while generating oil. This observation was used to point out the likelihood of high rates of expulsion from these units.

Galvis-Portilla et al. (2016), who collected the samples for this study, also performed several forms of mineralogical and lithological tests, including gamma ray, XRD, XRF, brittleness, thin section and fracture analysis. Becerra-Rondon (2017)

subdivided the outcrop into three lithofacies: chert, siliceous shale, and dolomitic mudstone (Figure 9). The ratio of chert/siliceous shale increases up section, reflecting increased upwellings in the Woodford Sea. The cherty units were dominated by radiolarian while the siliceous shale units demonstrated higher abundances in *Tasmanites*. The lithofacies also showed differentiation in terms of TOC and brittleness: chert units were more brittle with lower TOC, while siliceous shales demonstrated higher TOC and ductile behavior (Figure 9; Becerra-Rondon, 2017). Given the direct relationship between organic content and lithology, potential correlations between biomarkers and the fine scale parasequences were investigated.

The XRD analysis provided by Becerra-Rondon (2017) allows for fine-scale mineralogic interpretation of the outcrop. Chemostratigraphy (XRF) was also utilized, which refers to the application of elemental proxies in order to resolve high frequency cycles within a sequence stratigraphic framework (Turner, 2016). Turner (2016) defined chemofacies for various locations within a sequence stratigraphic framework. High values of silica, aluminum, potassium, and titanium are associated with continental input. Calcium, strontium, and magnesium provide proxies for carbonate lithology. Restricted circulation within a basin is denoted by high abundance of molybdenum and vanadium, which precipitate out of solution under anoxic/euxinic events (Algeo and Rowe, 2012; Turner et al., 2015).

Assessing elemental abundances in the I-35 outcrop reveals mineralogical intercalation of cherts and siliceous shale beds (Figure 10). High Si and low Al values present throughout the siliceous beds of the section, which are indicative of biogenic input from radiolarian and sponge spicules (Turner, 2016). The interbedded siliceous

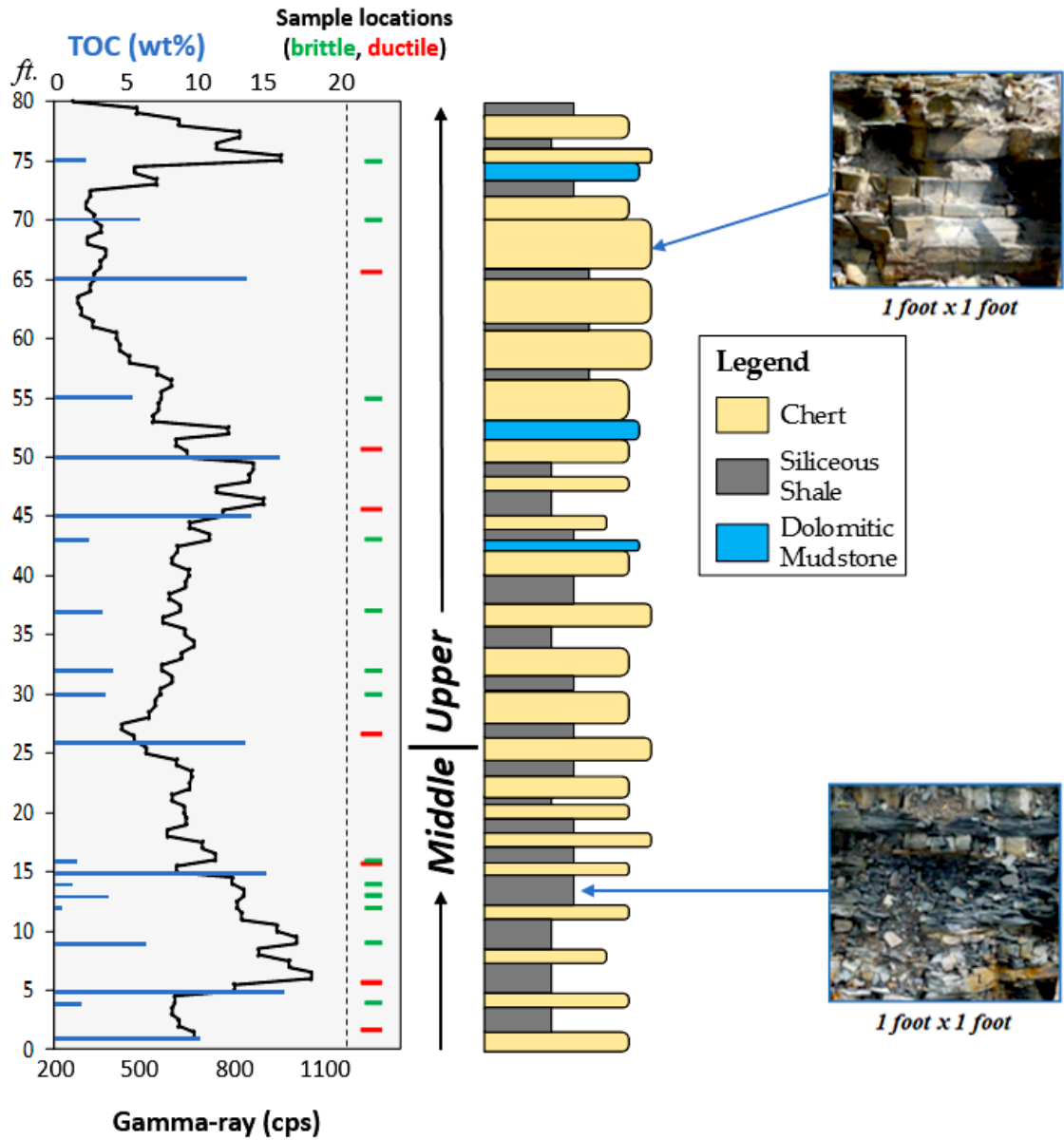


Figure 9. Gamma ray, TOC, sample location, hardness, and lithology for the I-35 Woodford outcrop. Middle and upper Woodford boundary indicated. Images demonstrate typical rock samples for ‘soft siliceous shale’ and ‘hard chert beds’ (Modified from Becerra-Rondon, 2017).

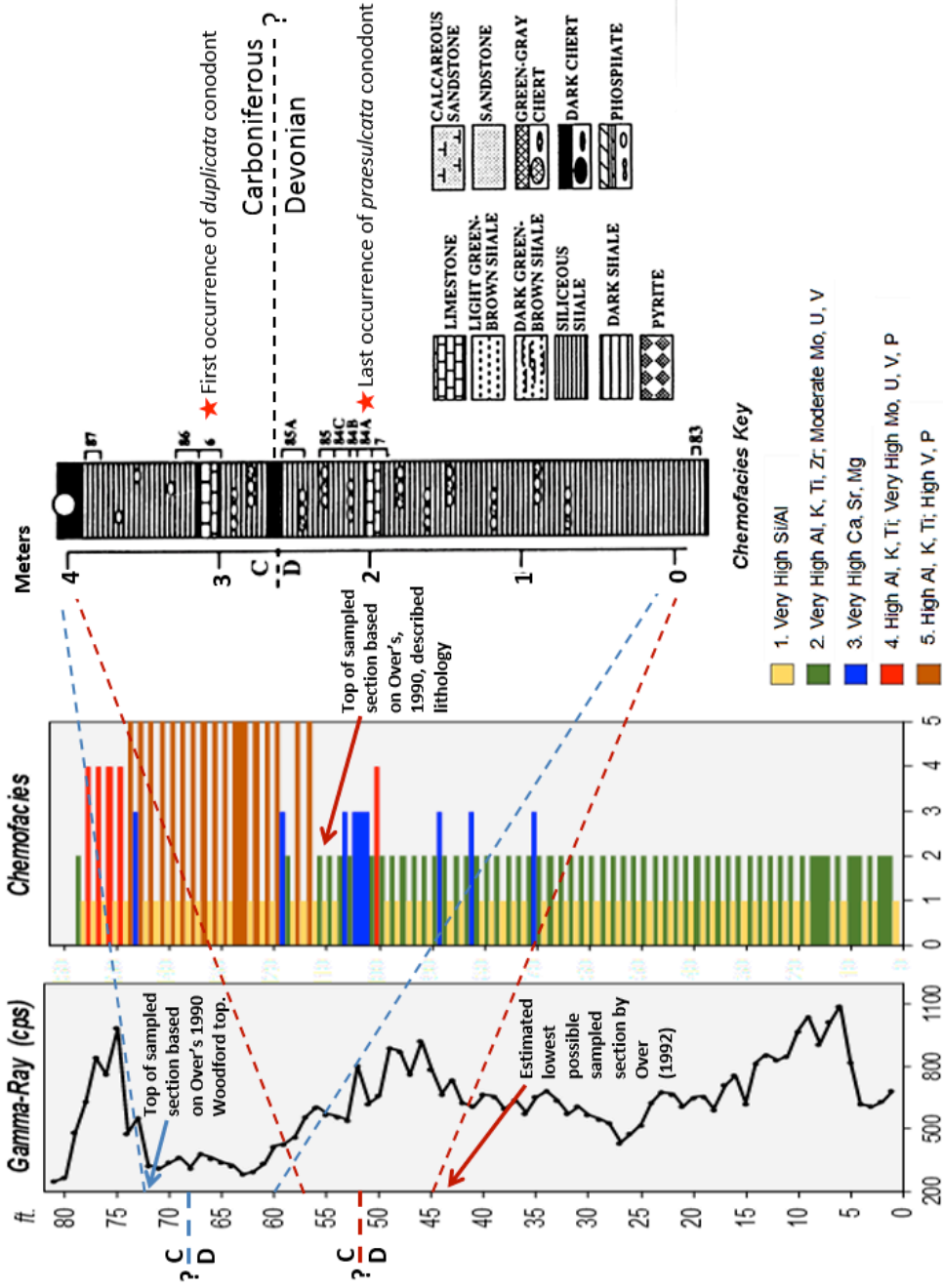


Figure 10. Gamma ray, chemofacies (Becerra-Rondon, 2017), and approximate stratigraphic location of Over (1990) conodont biostratigraphy of the Interstate 35 outcrop based on best estimate from 1990 report (blue) and lithology (red). Last occurrence of *praesulcata* (Devonian) and first occurrence of *duplicata* (Carboniferous) identified, along with approximate D-C boundary.

shales are increasingly clay-rich moving up the outcrop, which is related to increased terrigenous input. The elemental proxies demonstrated are consistent with highstand sedimentation coming primarily from biogenic sources rather than detrital sources. The combination of increased molybdenum, vanadium, and clay proxies indicates potential falling stage systems tract in the upper 20 feet of the section (Turner, 2016). Furthermore, the increasing molybdenum (Mo) and vanadium (V) values, ranging from moderate to very high at the top of the section, imply increasing bottom water anoxia. This observation is an important detail, considering that the location of anoxic events in the upper Woodford has proven to be problematic. Connock (2015) demonstrated a lack of euxinia in the upper Woodford section of the Wyche quarry using biomarker parameters, while Turner (2016) showed high levels of Mo and V for that section. Despite the lack of organic geochemical indications of anoxia in the upper Woodford section of the Wyche Quarry, Degarmo (2015) found an episode of photic zone euxinia in the upper Woodford, and identified it as the maximum flooding surface. These examples demonstrate the discrepancy in the literature in trying to identify anoxia in the upper Woodford, thus, a combination of the lithologic and geochemical parameters must help in this assessment.

Over (1990) used conodont biostratigraphy of outcrops and cores to date the boundaries and extinctions within the Woodford. The Frasnian-Famennian Boundary is defined by “the extinction of *Ancryodella* and *Palmatolepis linguliformis*, the occurrence of *Ancryognathus ubiquitous* and *Pa. praetriangularis*... and the appearance of *Palmatolepis triangularis*” (Over, 1990). At the I-35 outcrop, Over (1990) only studied the upper Woodford portion, and did not include the Frasnian-Famennian

boundary. The Devonian-Carboniferous boundary is identified where *Siphondella praesulcata* ends and where *Siphondella sulcata* appears. Over (1990) found the last occurrence of *Siphondella praesulcata* biota, but was unable to find the *sulcata* species. Instead, he discovered *Siphondella duplicata* in the biostratigraphy, which evolved after *Siphondella sulcata*. For this reason, he was unable to identify the exact location of the Devonian-Carboniferous boundary, but rather the interval in which it is expected to occur. In Figure 10, the approximate location of Over's 4-meter interval is tentatively identified within this study's measured section. Limited information provided by Over (1992) makes comparison between his interval and this study's stratigraphic section difficult. Over did not provide a scale for where his 4 meters of detailed section fell within the outcrop (Appendix E), thus making its placement within the context of the entire outcrop strata challenging. Based on his diagram, Over's section could be located between 60 and 72 feet from the base of the outcrop, as he did not take samples all the way up to the top of the Woodford (blue dotted lines, Figure 10). However, based on elemental analysis (Becerra-Rondon, 2017) and lithofacies described by Over (1990), it would make more sense if Over's section ranged from 43 to 55 feet from the base of the outcrop, as he described the section as consisting almost entirely of siliceous shale (red dotted lines, Figure 10). The limestone lithofacies identified by Over would fit better with the section of the outcrop with high calcium, strontium, and magnesium, as well as dolomitic mudstone intervals identified by Becerra-Rondon (2017). Moreover, it is highly possible that Over's interpretation of the top of the Woodford was hindered by brush or soil covering sections that are exposed today.

Despite the significant error associated with placing the Devonian-Carboniferous (D-C) boundary based on previous work, conodont biofacies for the I-35 outcrop show a portion of the section with strictly Devonian fossils, and a section with distinctly Carboniferous species. Thus, the D-C boundary does definitively fall within this outcrop. The upper and lowermost potential boundary provides a context for where the D-C boundary may occur in today's section, and a framework to explore the geochemical parameters associated with this mass extinction.

III. METHODOLOGY

3.1. Study Area

The primary data available for this thesis came from 20 samples taken from the I-35 Woodford outcrop along the Ardmore Basin, Carter County, Oklahoma. Although this thesis will focus on geochemical analyses, additional data including XRF, gamma ray and brittleness data collected by Galvis-Portilla (2016) and Becerra-Rondon (2016) have been made available to provide the opportunity to compare geochemical and chemostratigraphic interpretations.

In Figure 11, an image taken a distance from the outcrop is provided, indicating the Sycamore, Woodford, and Hunton contacts. Most of the relatively softer middle Woodford has been eroded to a greater extent, causing a topographic low at the center of the image. Adjacent to the eroded section, the only exposure that remains intact at the surface is circled in red, demonstrating why this study is limited to the uppermost middle Woodford and upper Woodford. The correlation of this outcrop to the middle and upper Woodford has been verified by comparing the gamma ray of the I-35 outcrop with logs and outcrops from Carter County near the study site (Becerra-Rondon, 2017). The gamma ray profile, measured by a handheld scintillometer, is overlain on the image of the outcrop (Figure 12). Correlations between the gamma ray profile of the I-35 outcrop were made with nearby gamma ray logs from the Speake-1 and Jud Little 4-6 wells, as well as the Speake Ranch, Henry House, and OHMEGCO Quarry outcrops (Figure 13; maps of outcrop and well locations in Figure 14).

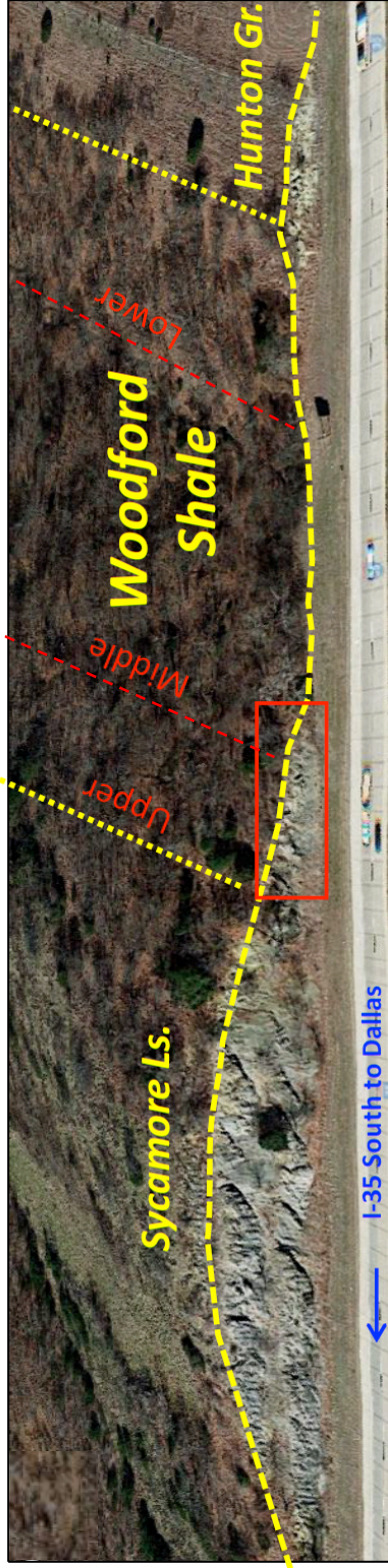


Figure 10. Distant image of the I-35 outcrop, exposing relatively softer, eroded Woodford Shale, along with Sycamore, and Hunton units (Becerra, 2017). Red circle indicates upper Woodford study location.

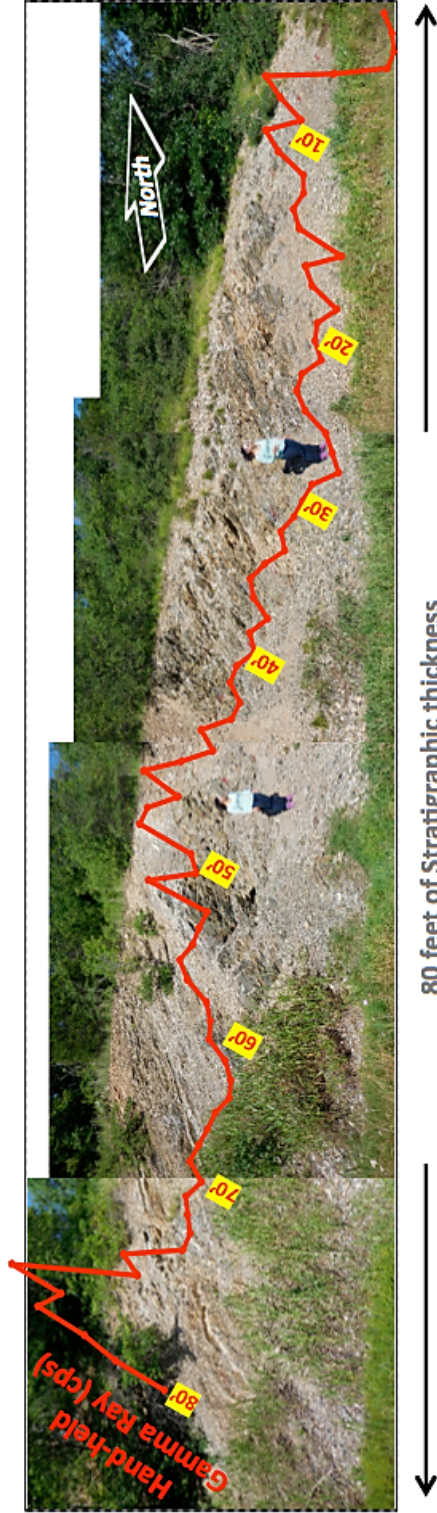


Figure 12. Image of I-35 outcrop study location, overlain by gamma ray profile (Galvis-Portilla et al., 2016).

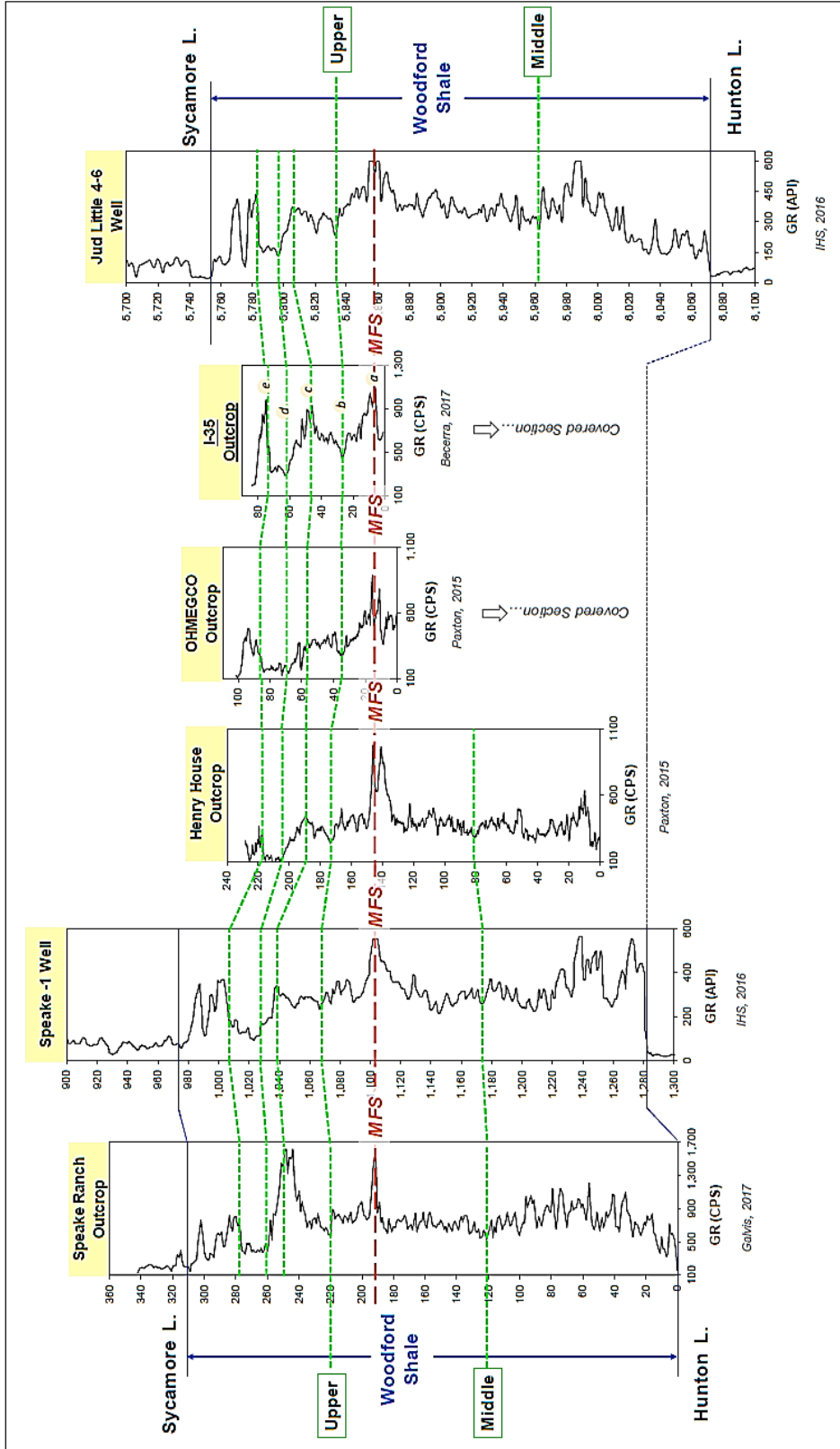


Figure 13. Well-to-outcrop correlation using digitized log from Speake-1 and Jud Little 4-6 wells from Northern Carter County, OK, as well as the Speake Ranch, Henry House, OHMEGCO, and I-35 outcrop gamma ray profiles (Becerra-Rondon, 2017). The I-35 outcrop demonstrates middle and upper Woodford gamma ray signature.

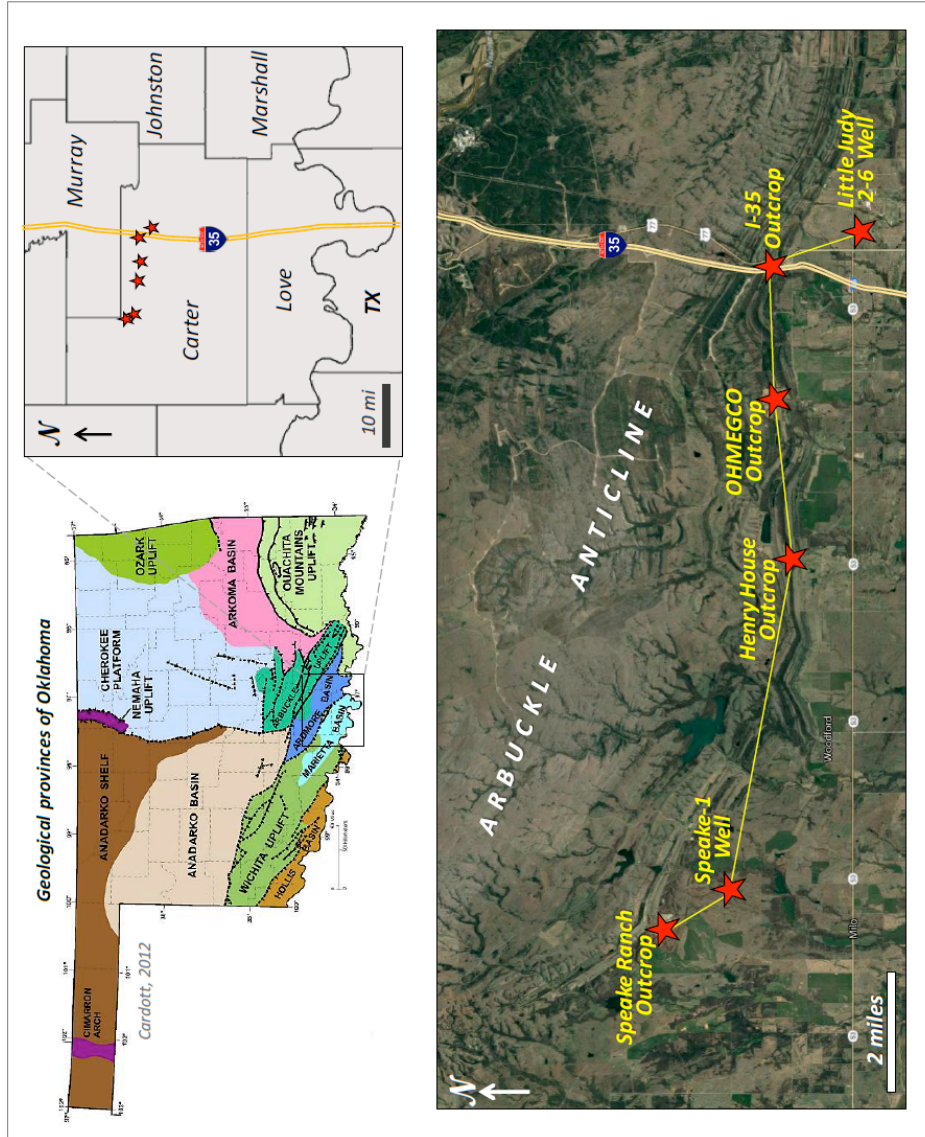


Figure 14. Map indicating location of wells and outcrops used to make a correlation (Cardott, 2012; Becerra-Rondon, 2017).

3.2. Experimental

3.2.1 *Sample Handling and Preparation*

Twenty outcrop samples were taken from the I-35 roadcut. Between 50 and 100 grams of rock were taken for each sample at approximately 1 foot below the surface of the outcrop. Samples were scrubbed and rinsed in deionized water to remove dirt or contamination from the surface. With sterilized metal tongs, each sample was dipped into methanol 3 times, and left to dry for several hours. Then, the same procedure was repeated with dichloromethane. Samples were left to dry for 24 hours in a vent hood. Approximately 50 grams of each sample were weighed out and crushed using a mortar and pestle until each sample was fine enough to be sieved through a US Standard Mesh No. 40 (0.425 mm).

3.2.2. *Rock Eval Pyrolysis and TOC*

One gram of each of the 20 crushed samples was sent to GeoMark™ (Houston, TX) for Rock Eval Pyrolysis and TOC measurements. To determine TOC, ground rock is acidified in HCl to remove carbonate material, then combusted in a Leco Carbon Analyzer at 1000 °C. The CO₂ released from the combustion is detected by infrared detectors and used to calculate TOC. For the pyrolysis measurements, the samples are heated at 25 °C per minute, and the released hydrocarbons are measured by a flame ionization detector. As a part of this commercial service, many bulk data measurements were made: percent carbonate (wt%); Leco TOC (wt%); Rock-Eval S1 (mg HC/g), S2 (mg HC/g), S3 (mg CO₂/g), and T_{max} (°C). From these measurements, certain

calculations are undertaken to obtain other meaningful values: calculated vitrinite reflectance (%Ro); hydrogen index (HI; $S2*100/TOC$); oxygen index (OI; $S3*100/TOC$); S2/S3 concentration (mg HC/mg CO₂); S1/TOC normal oil content; and production index ($S1/[S1+S2]$).

3.2.3. Extraction and Precipitation

Using the Rock Eval results, 15 samples were selected for biomarker analysis. To remove soluble bitumen from each sample, Soxhlet extraction was utilized. The glass apparatus, thimble, glass wool and boiling chips were pre-extracted for 24 hours with approximately 400 mL of a 1:1 mixture of dichloromethane and methanol before the start of each extraction. The Soxhlet was allowed to cool, solvent was removed and replaced, keeping the boiling chips in place. The 50 grams of ground sample was poured into each thimble and recovered with the pre-extracted wool. The apparatus was placed back on the Soxhlet and cycled on medium heat for 24 more hours, or until the solvent in the thimble was clear.

3.2.4. Bitumen Fractionation

The extracts from above were concentrated using a rotary evaporator until they were nearly dry. Using dichloromethane, the extracts were removed from the flask and placed in a pre-weighed 20 mL vial, evaporated back down and reweighed.

At this stage, the asphaltene fraction was removed from the bitumen samples prior to column chromatography. In order to do this, the bitumen was transferred into 40 mL centrifuge tubes, taking care to transfer as much bitumen as possible, since much of

the sample tended to adhere to the side of the container. Using a nitrogen dryer, the excess solvent was blown off from each sample. Approximately 1 milliliter of DCM was added to each centrifuge tube before it was placed in the sonicator. This ensured maximum dissolution into the n-pentane. Next, the sonicator was turned on for 10 minutes while n-pentane was added dropwise to the centrifuge tube to break up the organic material until the tube was filled. Tubes were placed standing up overnight in a freezer set to -2 °C. After 24 hours, the samples were centrifuged for 10 minutes so the asphaltenes collected at the bottom of the tube. The solvent was decanted and filtered through 1 inch of packed glass wool in a glass pipette, while making sure not to disturb the asphaltene pellet at the bottom. The product was collected in a 100 mL round bottom flask and dried via rotary evaporation, then transferred with 2 mL of dichloromethane into a pre-weighed 4 mL vial, dried under nitrogen, and reweighed to assess maltene weight. The remaining asphaltene was also removed from the centrifuge tube and weighed.

3.2.5. Maltene Fractionation: Liquid Column Chromatography

In a new 4 mL vial, 15-20 mg of the maltene fraction were weighed out and diluted with 200 microliters of hexane. For samples that had limited extract, as little as 10 mg of sample were used for fractionation. The final weight of sample #12 was only 3.72 mg so it was analyzed straight from its maltene fraction. In a glass pipette, a half centimeter of glass wool was packed into the bottom and 3.8 grams of powdered AlSiO_2 was measured on aluminum foil, and poured into the pipette. The pipettes were tapped until the powder was settled and leveled. Using air to pack the column further,

approximately 40 mL of hexane was pushed through the column. By doing this while avoiding drying out the column, the alumina forms a continuous substrate on which the various compound classes could be fractionated. Next, the 200 microliter maltene/hexane solution was introduced to the column. The aliphatic fraction was collected using 8.5 mL of hexane; the aromatic fraction with 25 mL of a 3:7 mix dichloromethane and methanol; the remaining polar fraction with 100% dichloromethane. Each of these products were collected in separate heated 100 mL round bottom flasks, and dried via rotary evaporation. The dried fractions were diluted with approximately 1 mL of their respective solvents, and transferred to pre-weighed 4 mL vials. The final weight of each fraction was recorded. A summary of the entire laboratory workflow used to analyze samples is illustrated in Figure 15.

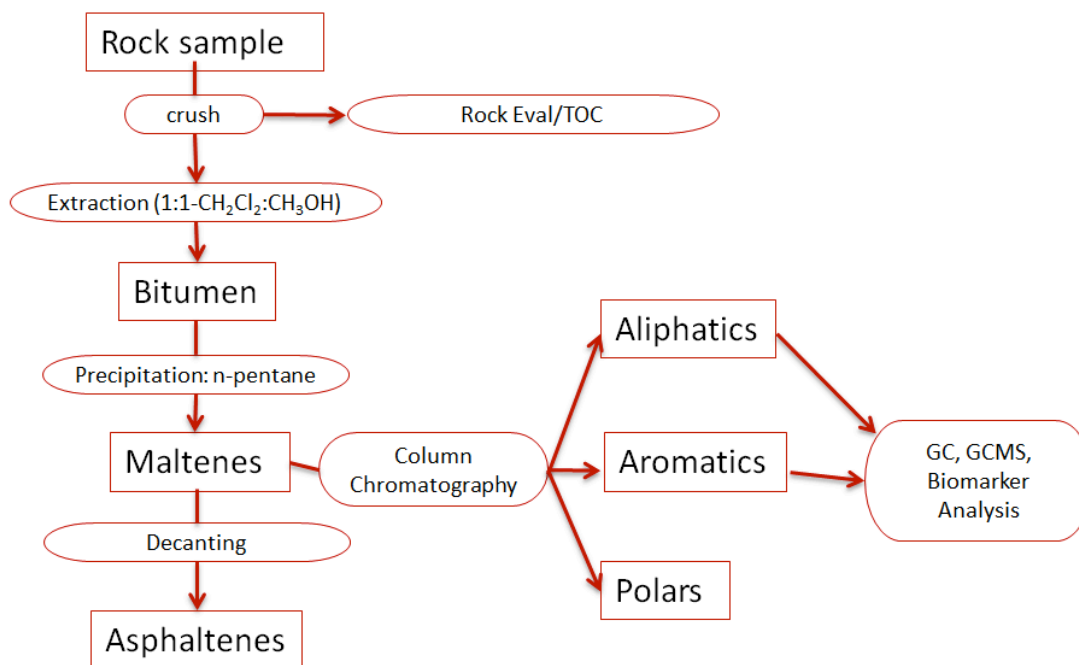


Figure 15. Workflow for geochemical analysis of samples- including extraction and separation of sample fractions.

3.2.5. Gas Chromatography

An Agilent Technologies 6890 Gas Chromatograph was used to analyze each aliphatic and aromatic fraction, which were diluted 3:1 with hexane. One microliter of each dilution was injected into a splitless capillary injection system equipped with a 60 m J&W Scientific DB-1 122-0162 fused silica column using helium as the carrier gas (1.4 mL/min). The oven was programmed such that each run began with a 1.5 minute hold at 40°C, followed by a 4 °C per minute ramp, until it reached 310 °C, where the oven was held isothermally for 24 minutes. In doing this, the quality of each run was checked i.e. no obvious contaminants, alkanes completely in the aliphatic fraction, etc.

3.2.6. Gas Chromatography-Mass Spectrometry (GCMS)

Fifteen saturate, aromatic and maltene fractions were diluted to 3mg/mL in hexane and spiked with deuterated tetrocosane ($C_{24}D_{50}$). The spiked dilutions were analyzed on an Agilent Technologies 7890A Gas Chromatograph with a splitless injector coupled to Agilent Technologies 5975XL Mass Selective Detector. The GC was equipped with a 60 m J&W Scientific DB-5MS 122-5562 fused silica column and helium was used for the carrier gas (1.4 mL/min). The saturate fractions were run using a temperature program such that the oven was held at 40 °C for 1.5 minutes, ramped at 4 °C per minute to 315 °C, then held isothermally for 50 minutes. For aromatic and polar fractions, the programs were run longer and ramped to a higher temperature in order to elute the C_{40+} carotenoids (Romero and Philp, 2012). More specifically, they began with a 1.5 minute hold at 40 °C, ramped at 4 °C per minute to 320 °C, where the oven was held isothermally until the end of the 120 minute program. For all analyses,

the ion source was held at 250 °C, while the quadrupole analyzer was held at 200°C. Mass spectrometry analysis utilized 70 eV ionization energy while in single ion monitoring (SIM) acquisition mode with multiple ion detection (MID).

3.2.7. Quantification and Identification

Agilent Technologies MSD Productivity ChemStation ver. E.02.XX. was used to identify and quantify each sample. The peak identities were determined by their retention time, relative position to the standard and by comparison to the literature. Mass spectra were also used and compared to literature in order to verify compound identities. For samples quantified, the standard of known concentration was used to calculate concentrations in micrograms/gram TOC. Details for various conversions for quantification of biomarkers are provided in Figure 16.

3.2.8. Gas Chromatography-Mass Spectrometry-Mass Spectrometry

Selected samples were analyzed using Thermo Scientific TRACE 1310 GC coupled with an 8000 triple stage quadrupole (TSQ) operating in splitless injection mode. For more detailed analyses, the GC/MS/MS was equipped with a 60 m by 0.25 mm J&W scientific DB-5MS fused silica capillary column coated with a 0.25 micrometer liquid film. Using helium as the carrier gas (1.4 mL/min), the oven was programmed with a 1.5 minute hold at 40 °C, with a 4 °C per minute ramp to 300 °C, where it was held isothermally for 34 minutes. The identities of the compounds were determined by utilizing parent → daughter ion relationships and literature comparisons.

$$\left\{ \frac{\text{Std}_{\text{wt}\%}}{\text{PA}_{\text{Std}}} \right\} \times \left\{ \text{PA}_B \right\} = B_{\text{wt}\%}$$

$$\left\{ \frac{\text{Rock}_{\text{wt (g)}} \times \text{TOC}_{\text{wt}\%}}{100} \right\} = \text{TOC wt (g)}$$

$$\left\{ \frac{\text{Mal}_{\text{fractionated}}}{\text{Mal}_{\text{total}}} \right\} = f_n$$

$$\left\{ \frac{B_{\text{wt}\%} \times \text{Ext}_{\text{wt (mg)}} \times f_n}{100} \right\} = B_{\text{wt (mg)}}$$

$$\left\{ \frac{B_{\text{wt (mg)}}}{\text{TOC}_{\text{wt (g)}}} \right\} \times \frac{1000 \mu\text{g}}{\text{mg}} = B_{(\mu\text{g/g TOC})}$$

Figure 16. Conversions for biomarker quantification. B = biomarker; Std = standard; PA = peak area; Wt = weight; f_n = normalization factor for maltenes fractionated; Mal = maltenes; Ext = extract.

IV. RESULTS AND DISCUSSION

4.1. Bulk Data Analysis

4.1.1. Total Organic Carbon (TOC)

Total Organic Carbon (TOC) is utilized to determine the amount of organic matter in a given rock/sediment relative to the weight of the sample. Although it does not indicate the solubility or volatility of the organic components in a measured sample, there are general assumptions that can be made about the quality of a source rock using the total organic carbon measurement (Jones, 1987). The results for Rock Eval pyrolysis and TOC for 20 samples are included in Table 1. For this set of samples, the TOCs ranged from 0.45 to 15.7 wt%, giving them source rock potential in the ‘poor’ through ‘excellent’ categories according to Peters and Cassa’s classification (1994), indicating the likelihood of high extraction weights for some samples (Table 2). Becerra (2017) found that the TOC tended to correlate with the lithology, such that brittle beds averaged lower TOC values (3.19 wt%) than the ductile beds (13.60 wt%). The lowest TOC value reported, 0.45 wt%, is less than minimum TOC values usually reported in the Woodford (~3%), which is likely due to biodegradation or weathering since this study was done using outcrop samples. The ability to accurately assess TOC in a resource shale remains valuable for assessing source rock potential because the analysis is done quickly, and the results can be easily communicated to professionals in the petroleum industry - even those with minimal background in geochemistry. While TOC

Table 1. Lithofacies, Rock Eval Pyrolysis and TOC values, based on height from the base of the I-35 outcrop. (TOC = total organic carbon; HI= hydrogen index= (S2x100/TOC); OI= oxygen index= (S3x100/TOC); PI= production index= (S1/S1+S2); NOC = normalized oil content= (S1/TOC)). S₁ and S₂ measured in mg HC/g rock. S₃ mg CO₂/g rock. Calculated R₀ = (0.0180)(Tmax) – 7.16.

Sample ID	Lithofacies	Height (ft.)	TOC (wt%)	S ₁	S ₂	S ₃	T _{max} (°C)	Calc. R ₀	HI	OI	PI	NOC	S ₂ /S ₃ Conc.
WDFD I35-75-143	Dolomitic Mudstone	75	2.16	1	12	0.39	435	0.67	576	18	0.05	28	32
WDFD I35-70-139	Chert	70	5.88	2	36	0.77	438	0.72	620	13	0.05	33	47
WDFD I35-65-135	Siliceous Shale	65	13.1	5	81	1.24	438	0.72	620	9	0.06	41	66
WDFD I35-55-123	Chert	55	5.35	1	32	0.65	428	0.54	604	12	0.02	15	50
WDFD I35-50-111	Siliceous Shale	50	15.4	2	92	2.75	431	0.6	595	18	0.02	11	33
WDFD I35-45-96	Siliceous Shale	45	13.5	2	78	1.62	428	0.54	577	12	0.02	12	48
WDFD I35-43-100	Dolomitic Mudstone	43	2.32	0	14	0.55	437	0.71	601	24	0.02	15	25
WDFD I35-37-76	Dolomitic Mudstone	37	3.3	0	9	1.61	428	0.54	285	49	0.03	8	6
WDFD I35-32-64	Chert	32	4.01	1	26	0.39	436	0.69	657	10	0.03	17	68
WDFD I35-30-59	Chert	30	3.43	1	19	0.55	430	0.58	558	16	0.03	18	35
WDFD I35-26-46	Siliceous Shale	26	13	3	80	1.32	431	0.6	618	10	0.03	22	61
WDFD I35-16-29d	Chert	16	1.55	0	3	0.96	431	0.6	166	62	0.05	9	3
WDFD I35-15-28	Siliceous Shale	15	14.5	1	76	2.57	430	0.58	522	18	0.02	10	29
WDFD I35-14-26	Chert	14	1.25	0	3	0.57	432	0.62	241	46	0.03	8	5
WDFD I35-13-22	Chert	13	3.71	0	17	0.79	431	0.6	461	21	0.02	9	22
WDFD I35-12-20	Chert	12	0.45	0	0	0.43	426	0.51	75	95	0.11	9	1
WDFD I35-9-14	Chert	9	6.26	1	20	2.14	427	0.53	316	34	0.03	10	9
WDFD I35-5-8	Siliceous Shale	5	15.7	2	87	2.37	429	0.56	551	15	0.02	12	36
WDFD I35-4-7c	Chert	4	1.84	0	8	0.31	435	0.67	443	17	0.03	11	26
WDFD I35-1-2	Siliceous Shale	1	9.97	1	48	1.53	426	0.51	480	15	0.03	15	31

Table 2. Generative potential (quantity) of immature source rocks (from Peters and Cassa, 1994). Bitumen= extractable fraction of organic matter in rock. Hydrocarbons= extractable portion of compounds comprised of only hydrogen and carbon.

Potential (quantity)	TOC (wt%)	S1 (mg HC/g rock)	S2 (mg HC/g rock)	Bitumen (ppm)	Hydrocarbons (ppm)
Poor	<0.5	<0.5	<2.5	<500	<300
Fair	0.5-1	0.5-1	2.5-5	500-1000	300-600
Good	1-2	1-2	5-10	1000-2000	600-1200
Very Good	2-4	2-4	10-20	2000-4000	1200-2400
Excellent	>4	>4	>20	>4000	>2400

is subject to alteration via oxidation and contamination in an outcrop setting, it is important to note that these values are not necessarily less valuable than those taken from a core study. As noted by Rodriguez and Katz (2017), Rock Eval, TOC, and biomarker parameters are affected by oil-based drilling fluid. They found that the introduction of drilling fluids results in a reduction of the S2 value, as well as the total organic carbon itself, lowering the estimated source rock generation potential. They suggested that oil-based drilling muds acted on the rock cuttings in a similar fashion as a solvent extraction (Rodriguez and Katz, 2017).

Furthermore, the prolific use of oil-based drilling muds leads to a contaminated biomarker signature and anomalously high S1 values for core samples, rendering the data almost useless. For this reason, comparison of outcrop and core samples may be used in order to check for extent of drilling contamination in cores. With that being said, the issue of weathering and biodegradation in an outcrop remains, and biomarker parameters that are more resistant to biodegradation can provide a basis for improved source rock interpretations.

4.1.2. Kerogen Type

Kerogen is defined as the organic matter in rocks and coals that is both insoluble in solvents, and resistant to acid digestion of the mineral matrix (Durand, 1980). The basis for kerogen classification comes from petrographic and geochemical analysis of the macerals, or individual organic particles within the kerogen (Peters et al., 2005). Kerogen types are broadly classified to include liptinites, vitrinites, and inertinites. Liptinites are further divided into two subcategories: alginite (derived from algae), and exinite (plant spores, pollen, cuticles, and resins). Kerogen derived from such sources is characterized as oil-prone, whereas vitrinite is linked to more gas-prone source rocks, and inertinite tends to be largely incapable of generating hydrocarbons. Because the basis for kerogen typing relies on variable organic input, the nature of depositional conditions is implied with certain kerogen types (Table 3). For example, alginite is linked to lacustrine settings due to the abundance of algae in such a setting.

The kerogen type of a given sample of organic matter can be approximated using the H/C and O/C atomic ratios measured by elemental analysis (van Krevelen, 1961). When H/C versus O/C is plotted against each other, each type of kerogen (Type I-IV) follows its own distinct path of hydrogen and oxygen depletion during thermal maturation. Thus, a plot known as a van Krevelen diagram can be used to discern the kerogen type for analyzed samples. A modified van Krevelen diagram is made from Rock Eval pyrolysis data, whereby the H/C ratio is replaced with the hydrogen index (mg HC/g TOC) and the O/C is replaced with the oxygen index (mg HC/g TOC). The hydrogen index (HI) can be determined using the $(S2/TOC)*100$ and the oxygen index (OI) can be determined using $(S3/TOC)*100$, and are used to classify kerogen type

(Peters, 1986). The characteristic maceral make up and Rock-Eval signatures for each type of kerogen is shown in Table 3.

Kerogen Types				
	Type I	Type II	Type III	Type IV
Maceral type	Alginite, with some vitrinite and exinite	Exinite	Vitrinite and inertinite	Inertinite
Inferred depositional conditions	Lacustrine or restricted marine	Marine	High terrigenous input	Reworked and oxidized organic matter
Hydrogen Index (HC/g TOC)	> 600	300-600	50-200	<50

Table 3. Inferred maceral type, depositional conditions, and hydrogen index for each kerogen type (modified after Peters and Cassa, 1994).

The parameters, S1, S2, and S3, are obtained from Rock Eval pyrolysis and the integration of peaks, as per the pyrogram shown in Figure 17. The S1 peak of the pyrogram represents remaining extractable hydrocarbons in a sample, while the S2 peak represents the thermal degradation products of kerogen that remain to be cracked by increased maturation (temperature). The S3 peak measures CO₂ released during the temperature ramp. The HI is calculated using the S2 value ($S2 \cdot 100 / \text{TOC}$) and the OI value is calculated using the measured CO₂ from the sample ($S3 \cdot 100 / \text{TOC}$).

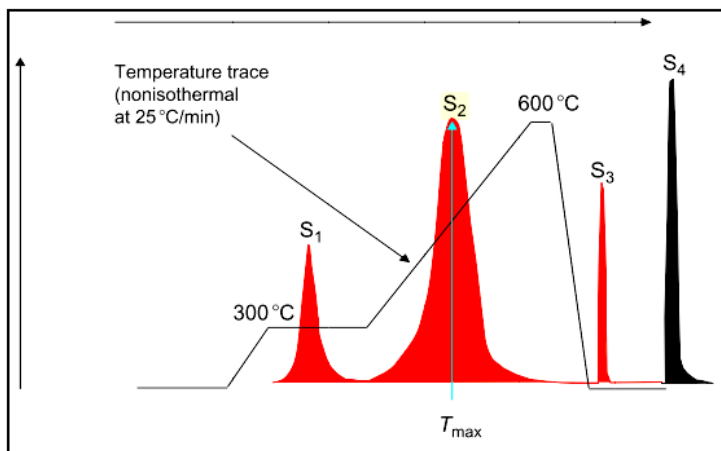


Figure 17. Schematic of temperature ramp and peaks in Rock-Eval pyrogram. Figure provided by R. P. Philp (Slatt, 2013).

Results from the Rock Eval of the 20 I-35 outcrop samples in Table 1 are plotted on a modified van Krevelen diagram, revealing a range of results characteristic of Type I to Type III kerogens (Figure 18). The Woodford is usually designated as a Type II source, and given the depositional history mainly in a marine setting, that would be expected. Therefore, this widespread distribution is most likely an artifact of the high hydrogen index values for the Type I samples, or weathering history of the samples plotting as Type III, especially since variable maturity should not occur within the 80 foot interval of this outcrop. A relatively high HI value is expected for Type II samples, corresponding with high generative potential, yet oxidative weathering in the outcrop can lower the hydrogen content and enrich oxygen content in a sample. These tendencies have been well documented both for this formation, as well as other source rocks that have been compared between outcrop and core (Lo and Cardott, 1995). Specifically, samples from 9, 12, 14, 16, and 37 feet appear to have undergone more

degradation of HI by weathering, as highlighted in Figure 18. Samples from 12, 14, and 16 feet also have the lowest TOC values (<1.55 wt%). Conversely, samples with low OI and high HI values correlate with the highest TOC values. Another possible factor affecting the van Krevelen interpretation is the high clay content of the Woodford Shale. Because HI is based on S₂, hydrocarbons adsorbed onto clay are released at a higher temperature, therefore making HI and S₂ values appear smaller (Langford and Blanc-Valleron, 1990). Therefore, the range of interpreted kerogen types raises some questions as to 1) degree of variable sourcing; 2) effects of weathering; 3) the extent of organic adsorption into the clay matrix; and 4) variable depositional environment.

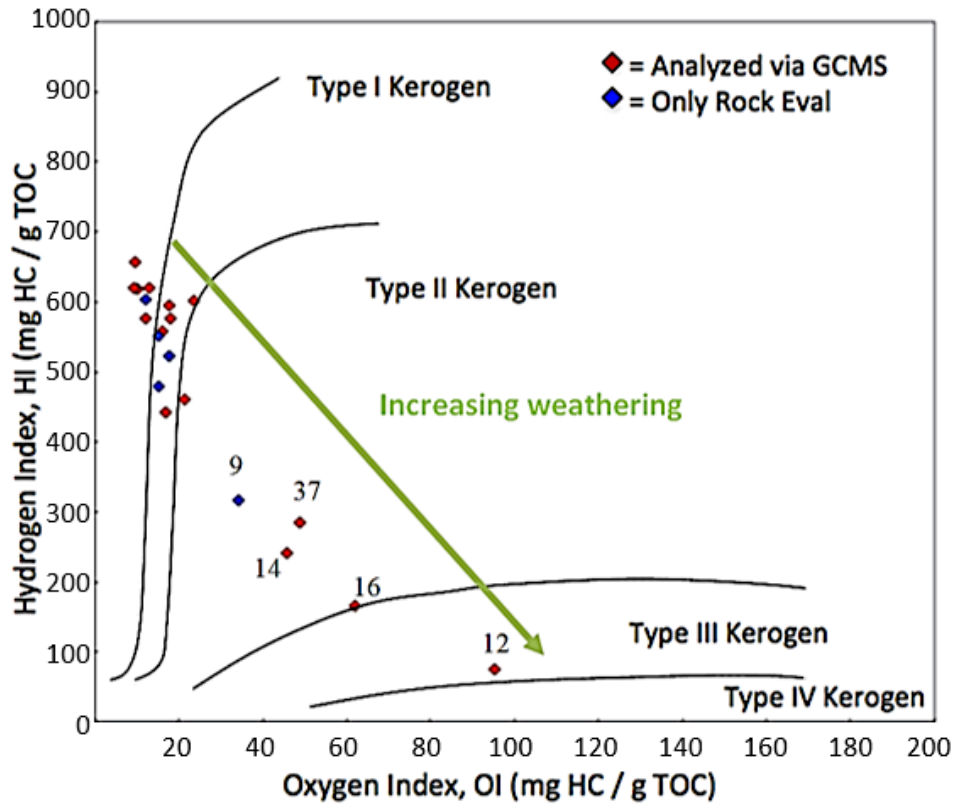


Figure 18. Modified Van Krevelen Plot using OI and HI. Green arrow denotes trend of increasing weathering. (Red = samples used in biomarker analysis; blue = samples only analyzed by Rock Eval pyrolysis and TOC.) Most samples for the I-35 Woodford outcrop plot between HI=450-650, OI<30.

To check for effects of weathering and clay adsorption in the outcrop, an S2 vs. TOC plot can be used as a more reliable method of characterizing kerogen type (Langford and Blanc-Valleron, 1990). When S2 and TOC are plotted against each other, the sample set mostly plot in the region interpreted as being characteristic of oil-prone marine source rocks (Figure 19).

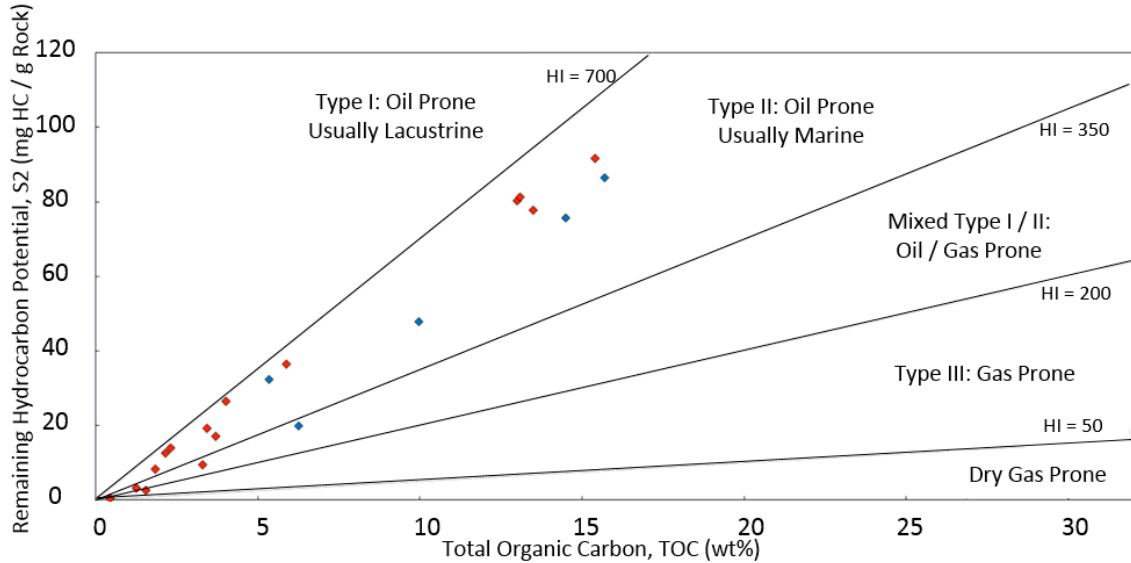


Figure 19. S2 vs. TOC, provided by GeoMark™. (red = samples used in biomarker analysis; blue = samples only analyzed by Rock Eval pyrolysis and TOC.) Samples for this study plot primarily as a Type II, oil prone kerogen.

Langford and Blanc-Valleron (1990) also proposed that the S2 vs. TOC plot could be used to model the degree of clay adsorption in order to interpret a more characteristic HI for a sample set. The linear regression line of these two values tends to demonstrate a high degree of correlation and coherency among the data group (Langford and Blanc-Valleron, 1990). In this type of plot, the difference between the x-intercept value can be used to approximate the percent of adsorbed carbon in a sample (i.e., x-intercept = 1 = 1% carbon adsorbed). The linear regression line of the S2 vs.

TOC data was plotted (black, solid line), along with 4 trend lines originating from the x-axis that modeled 0%, 1%, 2%, and 3.25% adsorbed carbon (Figure 20), where the 0% trend line was drawn to capture the highest S2 values. The remaining 3 trend lines were plotted using the same slope, but modeled to show varying amounts of adsorbed carbon. The x-intercept of the linear regression occurred at 0.5 wt% TOC, indicating that as much as 0.5 wt% total organic carbon could be adsorbed by clay matrix for samples in this outcrop. Individual points deviated variably; 14 of the samples fell into the category of <1% adsorbed carbon, 3 into the <2% adsorbed carbon, and 3 in the <3.25% adsorbed carbon. Samples that were modeled to have significantly higher amounts of adsorbed TOC (i.e. >1.0) than the linear regression demonstrate relatively lower S2 to TOC values and less remaining hydrocarbon yield, which would indicate increased kerogen reworking and inert kerogen relative to those that fell on the line (Peters, 1986).

For samples that fell on the 0% adsorbed carbon line, the mode of HI values was 620. Based on this model, samples demonstrating 0% adsorption should provide more representative HI values. Therefore, a hydrogen index of 620 may reflect actual kerogen signature without the effects of adsorption and kerogen reworking. If this is the case, it would be consistent with the Type II marine kerogen as anticipated for the Woodford, despite some samples appearing to be I, II/III, and III as per the van Krevelen diagram (Figure 18). If samples reflect sourcing that is not consistent with type II marine, it should be reflected moving forward in the biomarker data by assemblages of lacustrine (Type I) or predominantly land plant (Type III) biomarkers. Alternatively, if the biomarkers reflect a marine setting, then using this method with an S2 vs. TOC plot can

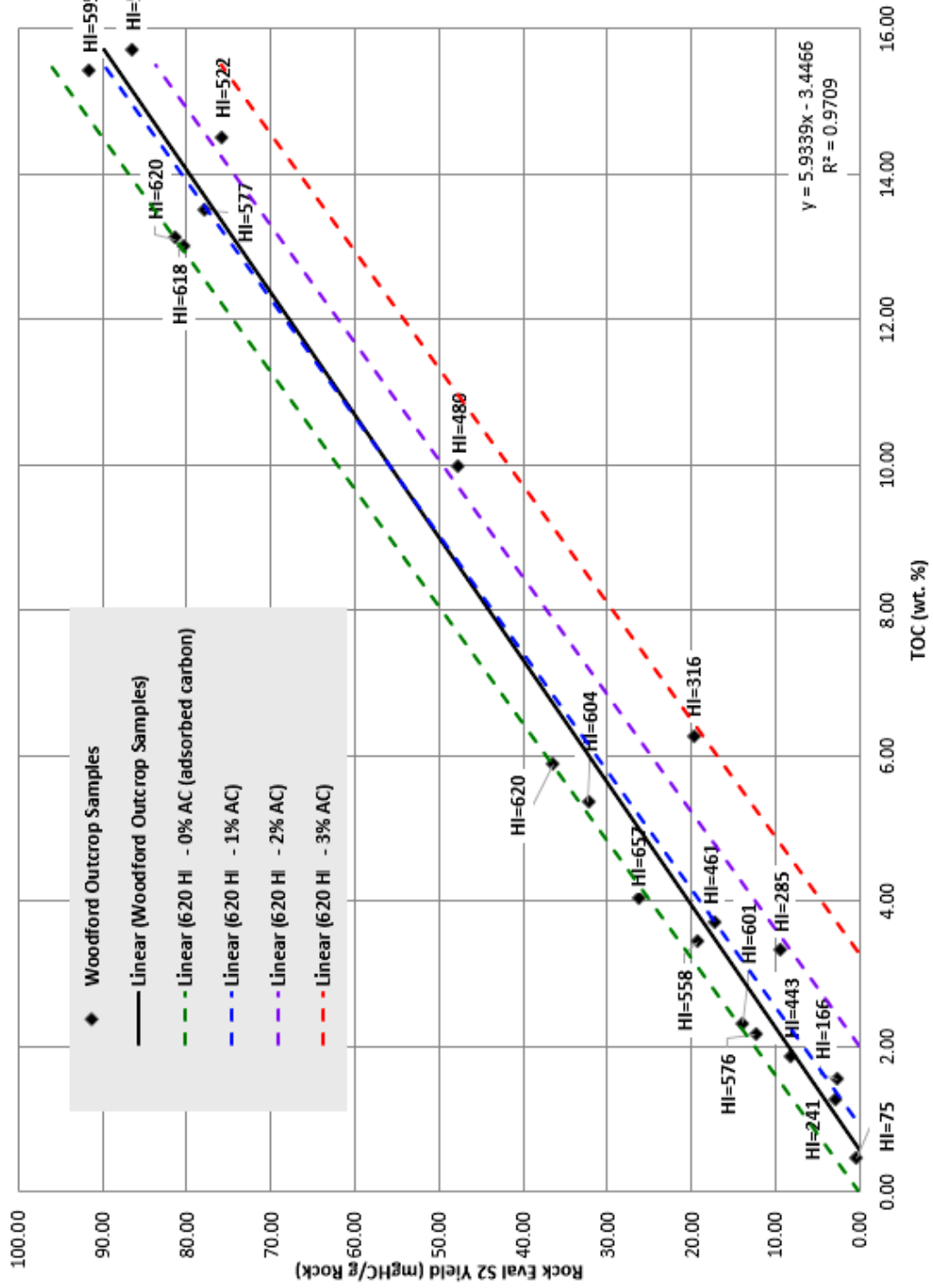


Figure 20. Modified from Langford and Blanc-Valleron's (1990) model for adsorbed carbon (%) and HI.

depict causes for variability in Rock Eval data, both from carbon adsorption in clay and variability in the amount of kerogen reworking or inert carbon between samples. Rather than attributing all variation to facies changes, this method provides another tool for explaining unusual van Krevelen signatures, and could prove useful for samples that experience a similar extent of weathering in other outcrop studies.

4.1.3. Maturity

The thermal maturity of the samples can be inferred by using Rock Eval pyrolysis T_{max} values (Table 1). T_{max} values are typically related to vitrinite reflectance maturity by the correlation proposed by Jarvie et al. (2001) using the equation:

$$R_o(\text{calculated}) = (0.0180)(T_{max}) - 7.16.$$

A plot of T_{max} versus HI shows that although the samples have a somewhat narrow range of maturity, the HI values vary greatly (Figure 21). Because these samples come from within the same 80 foot interval, the range of T_{max} values likely result from the effects of biodegradation, as opposed to thermal maturation. Oil generation from a Type II kerogen is reported to begin at $R_o=0.5\%$, although the lowest maturity with confirmed oil production in the Woodford is $R_o=0.59\%$ (Cardott, 2014). In light of this, the I-35 outcrop samples are within range to have generated oil. With that being said, the calculated R_o values present an element of error, as they do not correlate directly to measured R_o , and therefore should be validated with measured values.

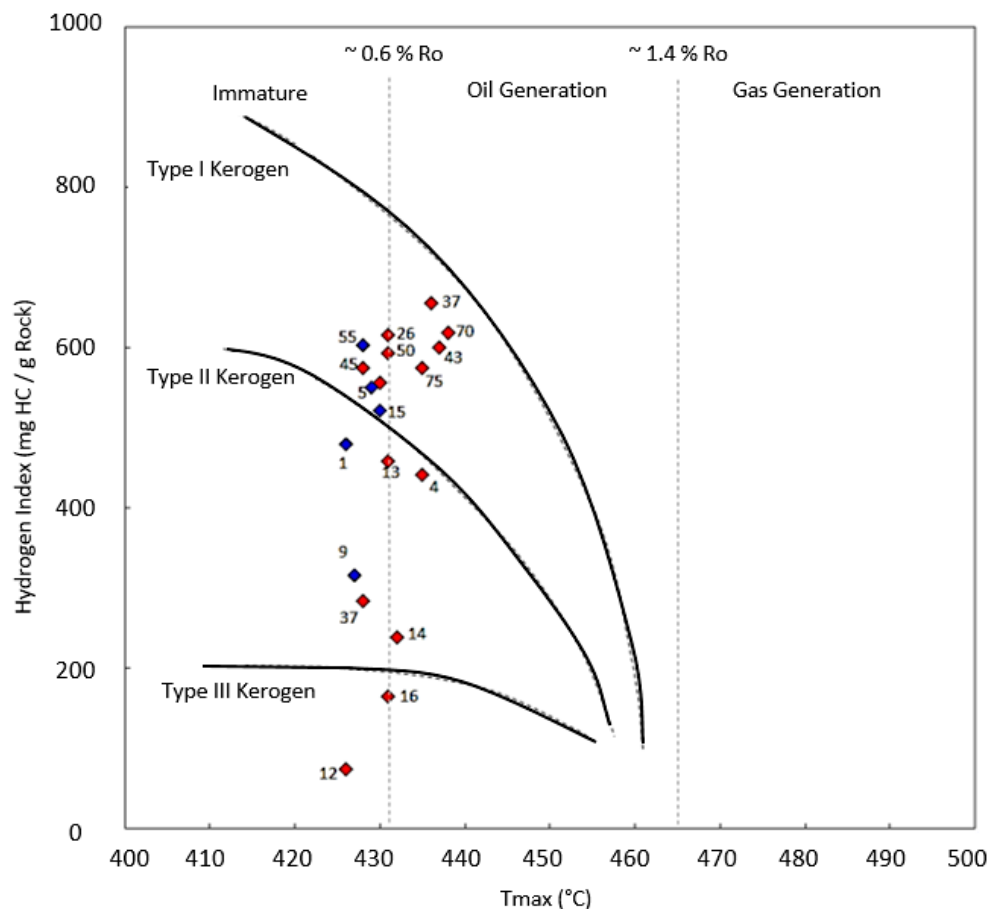


Figure 21. T_{\max} (°C) versus HI. Graph provided by GeoMark™. (red = samples used in biomarker analysis; blue = samples only analyzed by Rock Eval pyrolysis and TOC.) T_{\max} values range from 426° to 439°; HI ranges from 76 to 657.

4.1.4. Fractionation Weights

The wide range of TOCs resulted in some samples having low bitumen recovery, while other samples had >100 mg of extract. The amount of asphaltene in each sample is subject to relatively more error because for certain samples, the asphaltene adhered to the centrifuge tube and was difficult to weigh properly. The resulting weights for each fraction can be seen in Table 4. Major differences are seen in the amount of extract obtained from each sample; ranging from 14.5 mg in sample 12 to 567.0 mg in sample 50. Variability in extract amount is likely caused by 1) higher

rates of biodegradation in the case of organic-lean beds and 2) high rates of preservation in the organic-rich zones.

Table 4. Sample weights used to extract, deasphaltene, and fractionate, and the resulting yields from each step. (Soxhlet= grams of powderized rock extracted in soxhlet; Extract= weight of extract; Centifuge= recoverable extract after centrifuging; Maltene= maltene weight recovered; asphaltene= asphaltene weight recovered; Fractionated= mg of sample fractionated; Aliphatic, Aromatic, and Polar refer to final yields of each fraction).

Sample	Soxhlet (g)	Extract (mg)	Centrifuge (mg)	Maltene (mg)	Asphaltene (mg)	Fractionated (mg)	Aliphatic (mg)	Aromatic (mg)	Polar (mg)
75	49.7	127.98	125	47.04	80.28	13.36	2.77	5.25	2.89
70	48.9	78.7	78	54.23	20	13.36	5.5	4.04	1.74
65	29.9	353.3	350	244	110	19.99	10.58	5.06	2.07
50	51.9	567.13	560	161.73	342.15	18.41	4.67	12.87	3.65
45	54.7	284.2	280	185.77	85.4	13.54	4.83	3.51	1.34
43	52.1	70	69.1	44.07	23.3	11.18	2.01	3.01	4.22
37	49	44.3	42.1	19.96	14.81	9.77	1.27	1.6	3.52
32	42.1	50.2	49.34	33.5	13.7	13.5	4.75	3.55	2.38
30	48.9	34.9	33.9	22.6	10.62	14.5	5.08	4.24	3.67
26	52.1	355.4	352.5	282.1	62.21	17.7	8.38	3.9	1.99
16	51.6	50.62	48.62	28.62	11.11	10.93	3.25	2.74	1.45
14	49.2	28.5	28.2	11.93	9.8	11.93	1.86	2.25	1.54
13	52.2	55	54	17.21	35.1	10.35	3.05	2.92	1.25
12	48.1	14.5	14.31	3.72	6.49	0	0	0	0
4	49.8	20.05	18.91	8.61	6.25	8.61	2.03	2.74	1

4.2. Saturate Biomarkers

4.2.1. *n*-Alkanes and Isoprenoids

n-Alkanes dominate the saturate fractions of oils and extracts and are immediately evident by the presence of a homologous series of components in the gas chromatograms. The origin of such compounds stems primarily from lipids in living organisms such as the waxes of higher order plants (Eglinton and Hamilton, 1967), or algae in the case of lower carbon chain homologues (Smith, 1968). Thus, inferences about depositional environment can be made based on *n*-alkane distributions (i.e. predominance around C₁₇ (I; structures in Appendix A) is interpreted as algal-sourced, thus is marine or lacustrine in origin; Blumer et al. 1971).

For this study, *n*-alkane distributions were indicative of extensive biodegradation, as the *n*-alkane abundance was very low relative to the isoprenoids and weathered down to the baseline in some instances (Figure 22). Unlike oil samples, outcrop extracts tend to show greater depletion of the *n*-alkanes. Although samples from deep reservoirs tend to have more complete distributions of *n*-alkanes, samples taken at or near the surface with higher oxygen and bacterial presence have been proven to show greater rates of biodegradation (Larter et al., 2000). Samples from this study were taken 1-2 feet into the outcrop, thus making them particularly susceptible to heavy biodegradation (Figure 22).

Isoprenoids are among the most abundant compounds found in oils, and are defined as any compound that follows the biosynthetic pathway that involves the

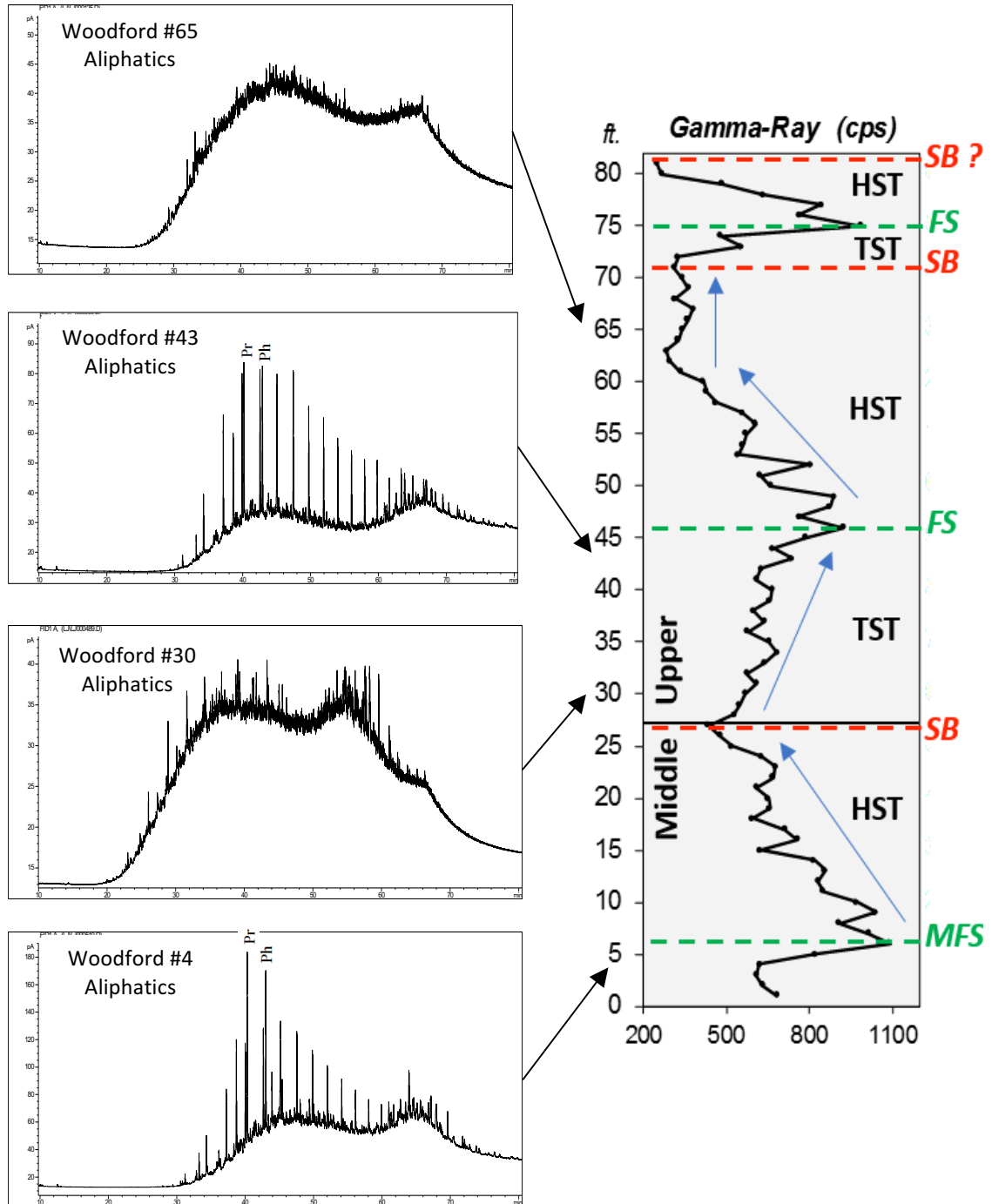


Figure 22. Chromatograms of aliphatic fractions, selected to demonstrate variable weathering up the outcrop. (Pr = pristane ; Ph = phytane). MFS = maximum flooding surface. Sequence stratigraphic interpretation based on interpretations of Galvis, 2017 and Becerra, 2017.

polymerization of C₅-isoprene units (Nes and McKean, 1977). The majority of such compounds are linked from head-to-tail between the isoprene units, while irregular isoprenoids are also synthesized in nature. Among irregular compounds are tail-to-tail linked compounds, like squalene (**II**), or head-to-head linked compounds like bisphytane (**III**), which is derived from archaea (Moldowan and Seifert, 1979; Brassell et al., 1981). Regular isoprenoids below C₂₀ in length are generally considered to come from the phytol side-chain from chlorophyll (Rontani and Volkman, 2003). This includes pristane (**IV**) and phytane (**V**), which are frequently used biomarkers for discerning redox conditions. In general, reducing conditions favor the dehydration and reduction of phytol to form phytane, while oxic conditions promote the oxidation and decarboxylation of phytol to pristane (Didyk et al., 1978). Higher pristane to phytane ratios can be indicative of higher thermal maturity (Alexander et al., 1981), but for samples of similar maturity, as is the case for samples in the same 80 foot interval of the I-35 outcrop, this is not a factor.

Due to preferential removal of alkanes following biodegradation, isoprenoids were relatively more abundant compared to alkanes in the more degraded samples. In this study, the pristane/phytane ratio in samples fluctuated from 0.9 to 1.1. Unfortunately, the values were relatively difficult to determine in some cases where the peaks in the GC traces were too low to accurately identify the compounds or make any meaningful measurements.

Alternatives to the classic pristane/phytane ratios have been proposed for those samples which have undergone removal of isoprenoid signatures in order to assess redox conditions and hypersalinity. For example, methyl-trimethyl-tridecyl-chromans

(MTTCs; **VI**) have been proposed as a potential replacement because of their susceptibility to oxygenation, but relative resistance to biodegradation (Brassell et al., 1983; Goossens et al., 1984; Sinninghe Damste et al., 1987). The MTTCs are derived from tocopherols, or vitamin E, and have been recognized in ancient sediments and oils as biological precursors to pristane (Sinninghe Damste et al., 1987). The compounds serve as antioxidants to protect lipids, and thus can indicate relative levels of oxidation. An MTTC ratio is calculated by dividing the sum of the trimethyl MTTCs (**VIII**) by the sum of the methyl MTTCs (Sinninghe Damste et al., 1987; Gross et al., 2015). Higher values of the ratio indicate more oxic conditions and correlate with lower pristane/phytane ratios (Sinninghe Damste et al., 1987). Using GC/MS/MS, MTTCs were identified in sample #14, but were present in too low concentration to be recognized by GCMS or quantify in a meaningful way (Appendix D). Therefore, other parameters associated with redox conditions, like a ratio of dibenzothiophenes to phenanthrenes, were used for this study, but the identification of MTTCs in the Woodford Shale should be mentioned as they may prove useful for future studies in other parts of the formation.

4.2.2. Steranes

Steroids from the lipid membranes of eukaryotic cells are the precursors for steranes, which are abundant in sediments, source rocks and oils (Mackenzie et al., 1982). Because of their widespread abundance, steranes make useful biomarkers for interpreting depositional environment, source derivation, and lithology. Different types of sterols predominate depending on the kind of organisms (Mackenzie et al., 1982).

For example, organisms such as vertebrates and plankton serve as sources of cholesterol (Gagosian et al., 1979), land plants produce stigmasterol and sitosterol, and ergosterols tend to be derived from fungi (Volkman et al., 1986).

Steranes were detected and identified by GCMS analysis using m/z 217.3, and then confirmed using GC/MS/MS (Figure 23 and Figure 24, respectively). For this analysis, C_{27} through C_{30} steranes and diasteranes were identified in the study samples. Comparison of relative amounts of C_{27} (**IX**), C_{28} (**X**), and C_{29} (**XI**) steranes have been used to differentiate source rocks from different environmental settings (Huang and Meinschein, 1979; Moldowan et al., 1985). The method implemented for this involves plotting the relative amounts of C_{27} , C_{28} , and C_{29} steranes on a ternary plot (i.e. $\% C_{27} = C_{27}/[C_{27}+C_{28}+C_{29}]$; Moldowan et al., 1985) resulting in established areas that correlate with a particular type of source rock. Although the application of this theory to oils results in much overlap, these diagrams are useful for correlating source rocks and oils (Peters et al, 2005). Because of some coelution between $5\alpha 14\beta 17\beta$ 20R cholestane and diastigmastane, only the $5\alpha 14\alpha 17\alpha$ 20S & 20R isomers and epimers were used for calculating sterane ratios. The plotted data for the I-35 outcrop samples, with the various depositional environments labeled are shown in Figure 25. The sterane distributions from this study's data display high relative amounts of C_{29} steranes, pushing the samples into the plot region for marine shales greater than 350 mya, with some overlap in the marine carbonate zone. Because it is an established Devonian-Early Mississippian source rock with Rock Eval signatures characteristic of a Type II source (Lewan, 1983), the ternary sterane diagram agrees with previous interpretations. The high relative amounts of C_{29} sterane compared to C_{27} and C_{28} homologs could be an

indication of a land plant source (Czochanska et al., 1988). The evolution of land plants during the Devonian could make this interpretation likely considering the influx of plant material which has been proposed as a factor contributing to the end-Devonian mass extinction (Algeo and Scheckler, 1998). With that being said, caution must be applied when interpreting a land-plant source from C₂₉ steranes alone, as there are documented instances of C₂₉ predominance in Precambrian rocks, which has been attributed to algae because land plants had not evolved yet (Grantham, 1986; Volkman et al., 1986).

Woodford #4 – Aliphatics

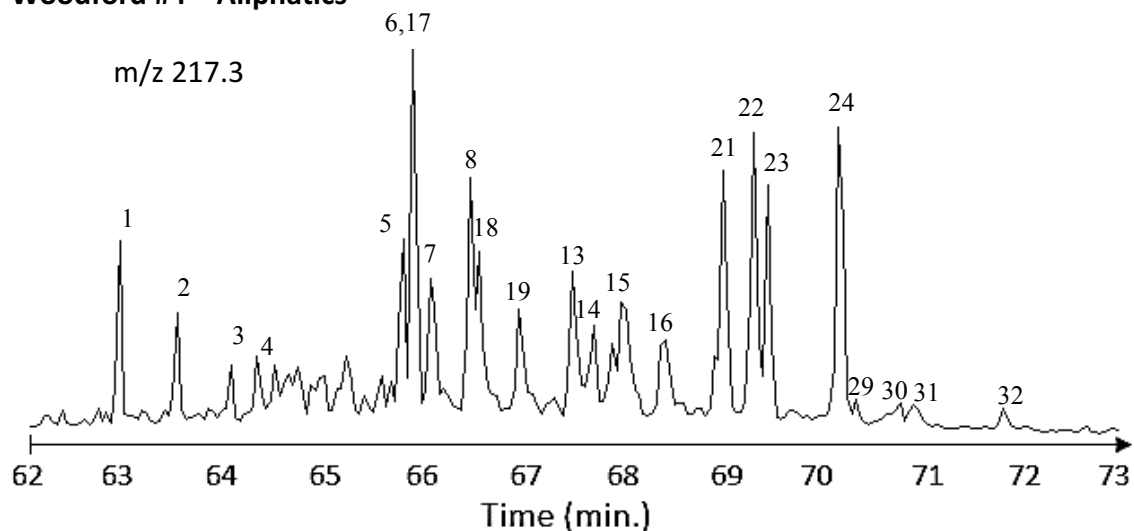


Figure 23. GCMS m/z 217.3 fragmentogram identifying C₂₇-C₃₀ steranes and diasteranes. Peak identities in Table 5.

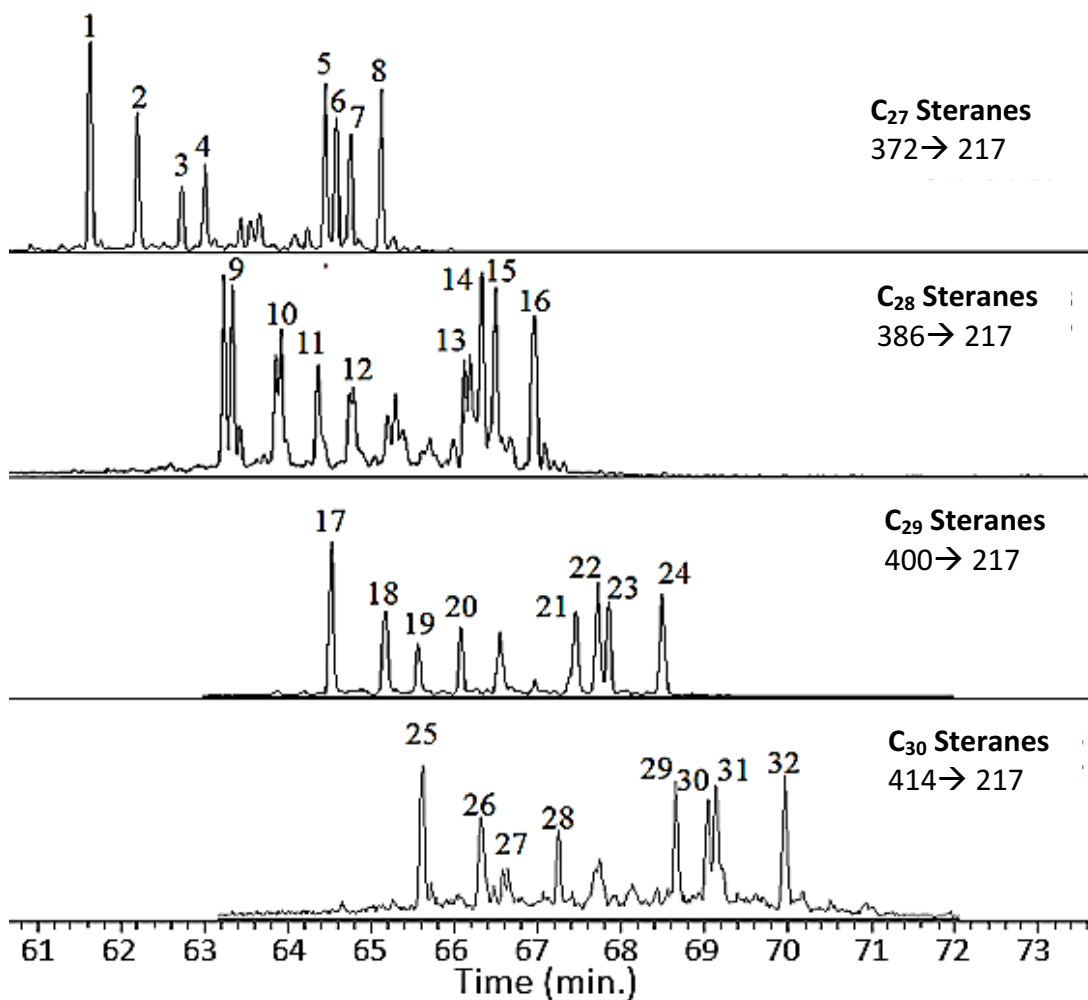


Figure 24. GC/MS/MS Identifications of C₂₇-C₃₀ sterane and diasterane isomers.

Table 5. Sterane identities of numbered GC/MS/MS peaks. Names in parentheses refer to abbreviations used in Figure 26 and Table 6.

Sterane Identification			
1	C ₂₇ 13β17α diasterane 20S (C ₂₇ βaS)	17	C ₂₉ 13β17α diasterane 20S
2	C ₂₇ 13β17α diasterane 20R (C ₂₇ βaR)	18	C ₂₉ 13β17α diasterane 20R
3	C ₂₇ 13α17β diasterane 20S	19	C ₂₉ 13α17β diasterane 20S
4	C ₂₇ 13α17β diasterane 20R	20	C ₂₉ 13α17β diasterane 20R
5	C ₂₇ 5α14α17α 20S cholestane (C ₂₇ aaaS)	21	C ₂₉ 5α14α17α 20S stigmastane (C ₂₉ aaaS)
6	C ₂₇ 5α14β17β 20R cholestane	22	C ₂₉ 5α14β17β 20R stigmastane
7	C ₂₇ 5α14β17β 20S cholestane	23	C ₂₉ 5α14β17β 20S stigmastane
8	C ₂₇ 5α14α17α 20R cholestane (C ₂₇ aaaR)	24	C ₂₉ 5α14α17α 20R stigmastane (C ₂₉ aaaR)
9	C ₂₈ 13β17α diasterane 20S	25	C ₃₀ 13β17α diasterane 20S
10	C ₂₈ 13β17α diasterane 20R	26	C ₃₀ 13β17α diasterane 20R
11	C ₂₈ 13α17β diasterane 20S	27	C ₃₀ 13α17β diasterane 20S
12	C ₂₈ 13α17β diasterane 20R	28	C ₃₀ 13α17β diasterane 20R
13	C ₂₈ 5α14α17α 20S ergostane (C ₂₈ aaaS)	29	C ₃₀ 5α14α17α 20S 24- <i>n</i> -propylcholestane (C ₃₀ aaaS)
14	C ₂₈ 5α14β17β 20R ergostane	30	C ₃₀ 5α14β17β 20R 24- <i>n</i> -propylcholestane
15	C ₂₈ 5α14β17β 20S ergostane	31	C ₃₀ 5α14β17β 20S 24- <i>n</i> -propylcholestane
16	C ₂₈ 5α14α17α 20R ergostane (C ₂₈ aaaR)	32	C ₃₀ 5α14α17α 20R 24- <i>n</i> -propylcholestane (C ₃₀ aaaR)

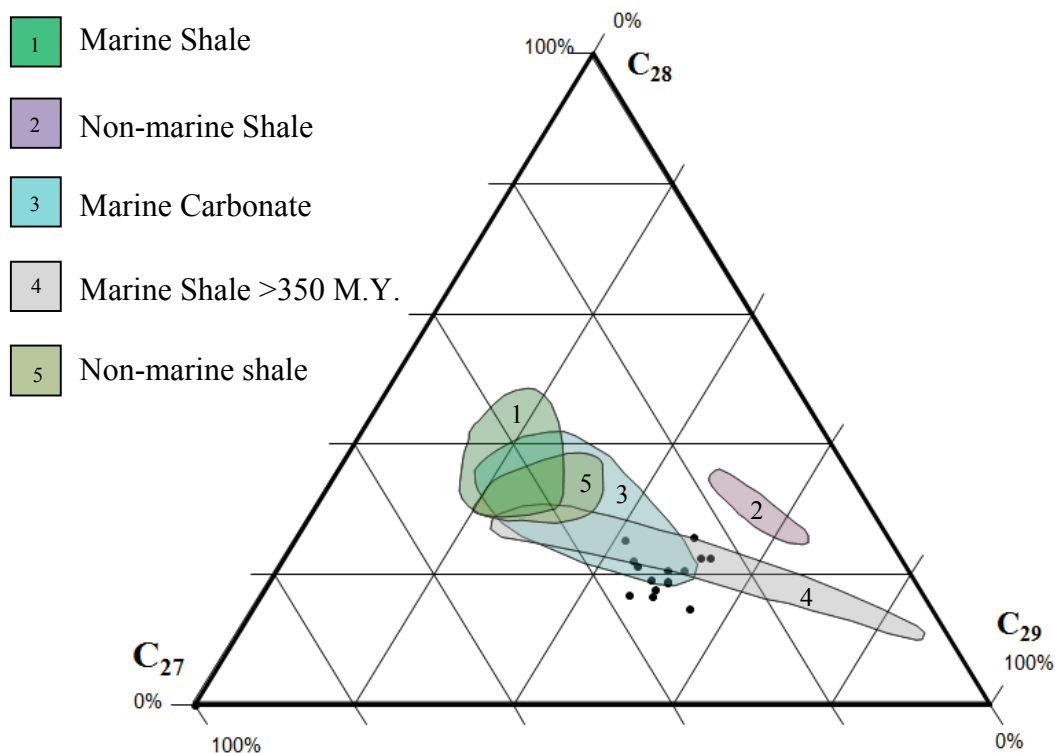


Figure 25. Ternary plot showing the relative proportions of the C_{27} : C_{28} : C_{29} steranes compared to distributions originally proposed by Moldowan (1985) for source rocks of varying ages.

The presence of C_{30} steranes (**XII**) is considered to be an indicator of a marine source input. The confirmation of this compound was done by GC/MS/MS using the 414→217 parent daughter ion transition. The C_{30} steranes, or 24-n-propylcholestanes, are derived from sterols present in chrysophyte algae, and in the marine invertebrates that ingest such algae (Raederstorff and Rohmer, 1984; Moldowan et al., 1985).

Because the presence of C_{30} steranes is the most powerful sterane indicator of marine input, the sterane index, defined as the ratio of C_{30} / C_{27} - C_{30} steranes using $5\alpha,14\alpha,17\alpha$ 20S & 20R isomers and epimers, can be used to discern zones that include

more/less marine biotic input (Figure 26; Moldowan et al., 1992). For the I-35 outcrop data set, the results show some variability, indicating changes in the deposition, likely associated with parasequences within the section (Figure 26). With the exception of the uppermost samples (70 and 75), the overall value of the C₃₀ sterane index tends to decrease with falling sea level, away from the MFS. Higher sea level would coincide with intervals deposited furthest from the shoreline, and therefore the highest relative amounts of marine-sourced organic matter. Therefore, the C₃₀ abundance toward the bottom of the section (<45 ft.) is consistent with the sequence stratigraphic interpretation, which places the MFS 6 feet from the base of the outcrop (Becerra-Rondon, 2017).

The rearrangement of steranes to diasteranes (**XIII**) occurs in the presence of clay via acid catalysis (Rubinstein et al., 1975). For this reason, lithology of a source rock can be discerned to include clay minerals, such as montmorillonite or illite, when diasteranes are found in oils and extracts. The diasterane/sterane index, defined as the ratio of C₂₇ diasterane/ (C₂₇ diasteranes + C₂₇ steranes), can be used to approximate conditions in which this conversion is favorable, as increased diasterane concentration requires greater clay content to catalyze the reaction. A lower value of this ratio is linked with more anoxic, clay-poor conditions. Rubinstein et al., (1975) suggested this trend may occur in zones where the diagenesis of carbonate minerals occurs, causing subsequent bicarbonate and ammonium production from bacteria. Such conditions would cause increased pH and low Eh, which are conducive to the rearrangement of steranes to diasteranes (Mello et al., 1988).

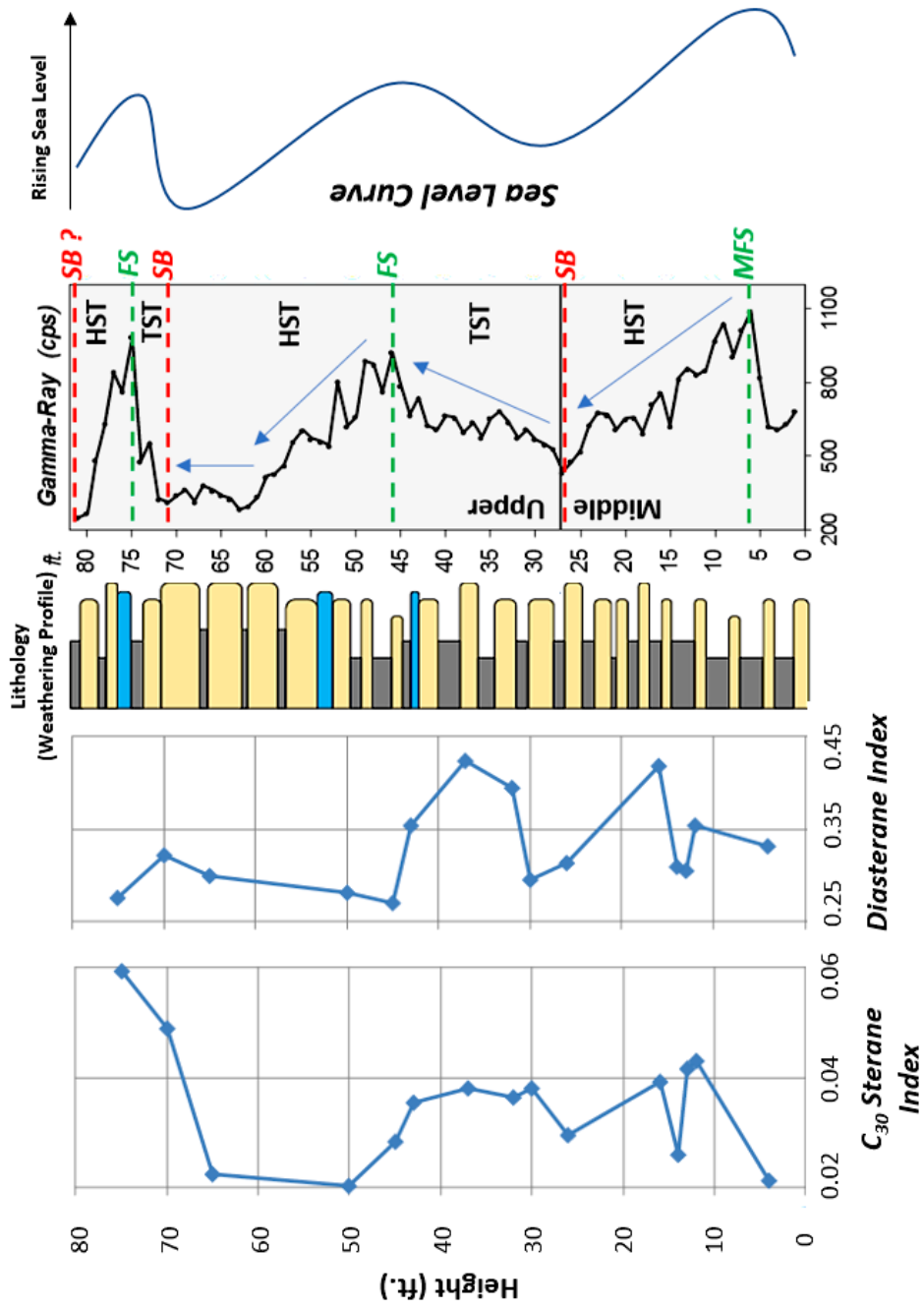


Figure 26. Sterane Index and diasterane ratio versus lithostratigraphic column, gamma ray (Becerra-Rondon, 2017) and interpreted sequence stratigraphy and sea level. (Sterane Index = $C_{30\alpha\alpha\alpha} / (C_{27\alpha\alpha\alpha} + C_{30\alpha\alpha\alpha})$ steranes; Diasterane Index = $C_{27\beta\alpha} \text{ diasteranes} / (C_{27\beta\alpha} \text{ diasteranes} + C_{27\alpha\alpha\alpha} \text{ steranes})$).

For this set of samples, cholestanes and diacholestanes were most easily identified in the GCMS traces among steranes. Diacholestanes were found throughout the entire data set, inherent as a feature of a clay-rich shale where the conversion of steranes would be expected. Because of overlap between C_{27} $13\alpha17\beta$ diasterane 20S and C_{28} $13\beta17\alpha$ diasterane 20S, the C_{27} $13\beta17\alpha$ diasterane 20S and 20R epimers were used against the C_{27} $5\alpha14\alpha17\alpha$ 20S & 20R steranes. The ratio of diacholestanes/cholestanes shows several inflections in the trend, with more concentrated diacholestanes at the bottom of the outcrop (samples 16 and 37; Figure 26). This is reflective of a general reduction in the clay material being deposited as you go from the predominantly siliceous shale at the base of the outcrop, toward the mostly chert lithology in the upper Woodford portion. The highest relative amounts of diasteranes occur in the interval of transgression (30-45 ft.), which coincides with areas of more clay content and higher gamma ray response. The lowest values of the diasterane/sterane ratio corresponds to the lowest sterane index values (45, 50, 65 ft.). This correlation is likely the result of increased carbonate, decreased clay mineralogy in those zones (noted in the XRF data from Table 10), which is common of samples with low sterane index values (Moldowan et al., 1992) and decreased diasterane abundance (Mello et al., 1988). The values and ratios for sterane analysis are reported in Table 6.

Table 6. Integrated areas and calculated values for steranes calculated for the various parameters used to interpret sterane distributions. (C_{27} SI = C_{27} sterane ratio = $C_{27}aaa/[C_{27}aaa + C_{28}aaa + C_{29}aaa]$; C_{28} SI = C_{28} sterane ratio = $C_{28}aaa/[C_{27}aaa + C_{28}aaa + C_{29}aaa]$; C_{29} SI = C_{29} sterane ratio = $C_{29}aaa/[C_{27}aaa + C_{28}aaa + C_{29}aaa]$; C_{30} SI = C_{30} Sterane Index = $C_{30}aaa/[C_{27}aaa + C_{28}aaa + C_{29}aaa + C_{30}aaa]$; C_{27} DR = Diasterane ratio = $C_{27}\beta\alpha$ diasteranes/[$C_{27}\beta\alpha$ diasteranes + $C_{27}aaa$ steranes]). Ratios calculated adding R and S isomers together .

Sample	C_{27} $\beta\alpha S$	C_{27} $\beta\alpha R$	C_{27} $aaaS$	C_{27} $aaaR$	C_{28} $aaaS$	C_{28} $aaaR$	C_{29} $aaaS$	C_{29} $aaaR$	C_{30} $aaaS$	C_{30} $aaaR$	C_{27} SI	C_{28} SI	C_{29} SI	C_{30} SI	C_{27} DR
75	32894	19071	38934	97589	33556	32842	94320	101930	11590	13579	0.34	0.17	0.49	0.06	0.28
70	59718	39667	105714	103863	59218	61353	142965	158409	14665	17780	0.33	0.19	0.48	0.05	0.32
65	44044	25858	65549	97613	41866	33013	99570	104202	8396	1691	0.37	0.17	0.46	0.02	0.3
50	49318	19343	94733	80627	63118	65490	124749	192971	6506	6384	0.28	0.21	0.51	0.02	0.28
45	73178	43655	188046	128754	94141	73042	181097	283959	9760	17902	0.33	0.18	0.49	0.03	0.27
43	373745	227188	298358	800487	486051	269348	748239	1036682	62106	71421	0.3	0.21	0.49	0.04	0.35
37	333774	206316	411292	323111	395600	290307	688808	940839	52636	67716	0.24	0.22	0.53	0.04	0.42
32	266471	163996	317245	343504	412974	278311	447217	897101	34403	67532	0.25	0.26	0.5	0.04	0.39
30	164989	118371	468568	205509	212409	190355	494054	580045	32982	52153	0.31	0.19	0.5	0.04	0.3
26	133119	67013	269090	169333	107269	103726	374182	412748	18206	25650	0.31	0.15	0.55	0.03	0.31
16	161965	95385	144870	213242	158792	163335	305550	438979	18795	39296	0.25	0.23	0.52	0.04	0.42
14	349219	204013	351510	885506	461735	322287	681245	963036	35090	62855	0.34	0.21	0.45	0.03	0.31
13	177453	54996	302796	225111	191196	129579	376059	467914	39212	34371	0.31	0.19	0.5	0.04	0.31
12	83873	46909	115221	122933	116955	63634	105788	190944	7463	24721	0.33	0.25	0.41	0.04	0.35
4	477689	317790	978714	628495	567551	490686	747234	1348112	23949	79988	0.34	0.22	0.44	0.02	0.33

4.2.3. Hopanes

Hopanes (**XIV**) are pentacyclic terpanes that occur in oils and result from the breakdown of bacteriohopanetrol in the lipid membranes of anaerobic bacteria (Ourisson et al., 1979). Hopanoids are ubiquitous in soils, sediments, and oils (Ourisson and Albrecht, 1992) and can be derived from marine and terrestrial bacteria (Rohmer et al., 1984; Cooke et al., 2008). The determination of hopanoid compounds is accomplished through the m/z 191.3 ion fragment on GCMS, which is also the mass fragment used to determine tricyclic terpanes in saturate fractions (Figure 27). While the relative amounts of the tricyclic terpanes and hopanes vary in the I-35 outcrop, the predominant compound class throughout the section is the hopanes, which is a common observation made for oils and extracts (Figure 27, Zumberge, 1984). Bacteriohopanetetrols require polar and non-polar ends in order to exist within a cell membrane wall. For this reason, the stereochemical arrangement of hopane precursors are relatively unstable and susceptible to variability in abundance depending on depositional conditions and maturation (Seifert and Moldowan, 1980; Peters et al., 2005).

Gammacerane (**XV**) is a heavily utilized biomarker in geochemical analyses, classically representative of water column stratification associated with hypersaline environments (Moldowan et al., 1985). The total concentration of gammacerane is plotted in Figure 28, demonstrating higher abundance in the lower part of the outcrop, especially at the 26 and 45 ft. beds. These intervals could therefore be interpreted as instances of water column stratification in the history of upper Woodford deposition,

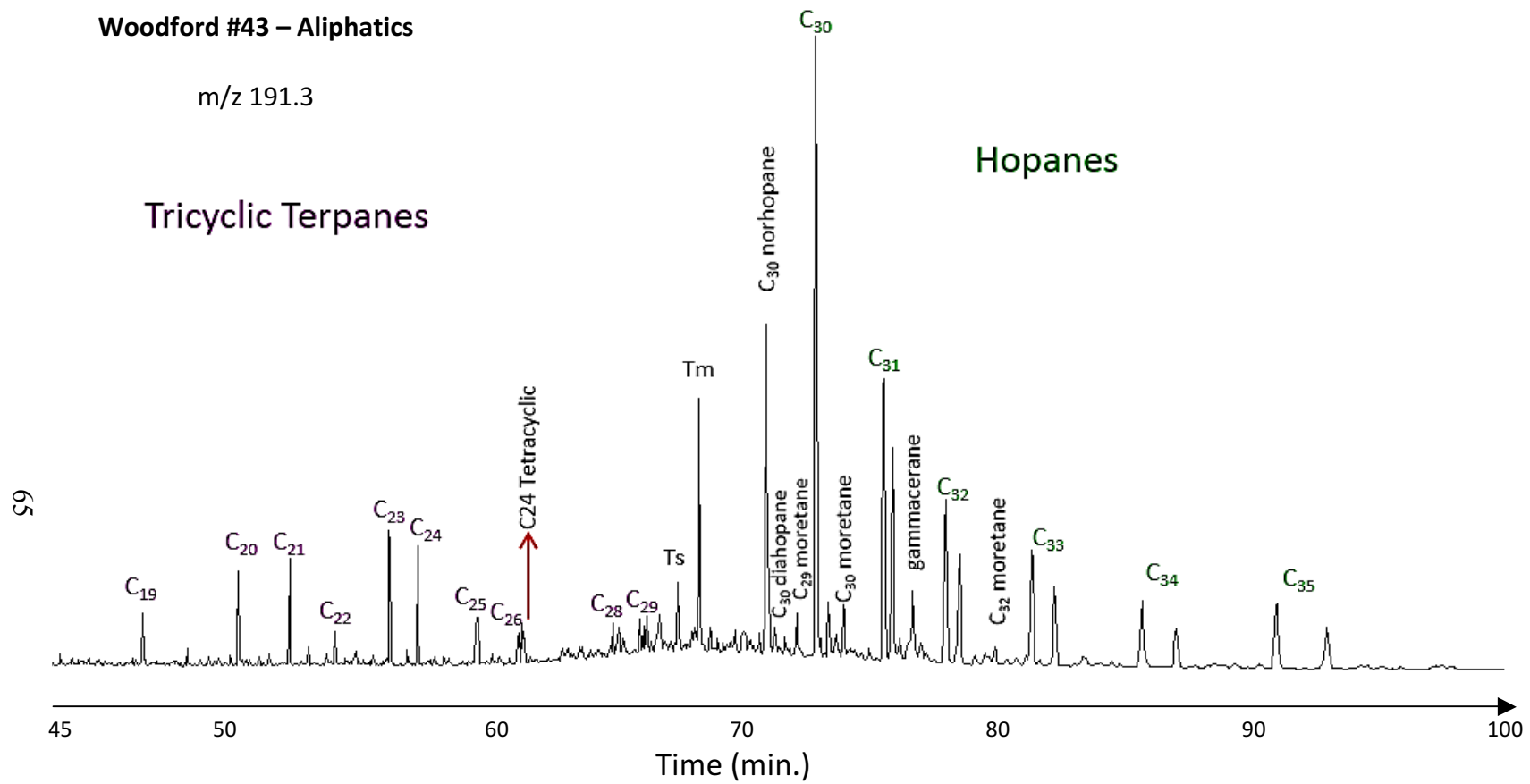


Figure 27. Tricyclic terpane and hopane identification using m/z 191.3 plot of sample 43.

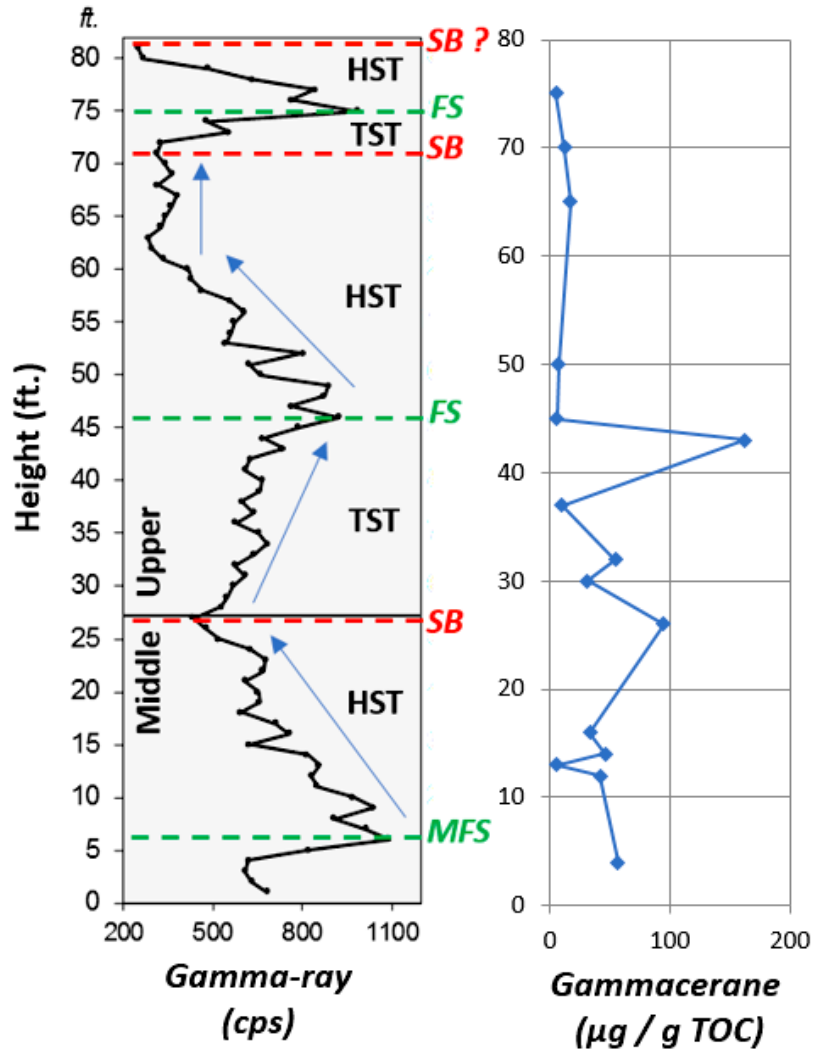


Figure 28. Gammacerane concentration up the outcrop, and gamma ray curve.

thus contributing to the likelihood of anoxic events that could lead to high rates of organic preservation. Intervals toward the base of the outcrop represent more distal position from land, which for this set of samples, seems to correlate with increased gammacerane concentration, and therefore, a greater chance of water column stratification. In terms of a sequence stratigraphic trend, gammacerane is most abundant at 26 feet (middle/upper Woodford boundary) and after a transgressive parasequence

(30-45 ft.), showing that despite elevated sea level, water column stratification occurred to some degree in the upper Woodford. As will be seen in later sections, these data are useful to compare with other proxies for stratification, including carotenoids and aryl isoprenoids.

4.2.4. Tricyclic Terpanes

Tricyclic terpanes (**XVI**), evident in a m/z 191.3 chromatogram, are found in oils, source rocks, and sediments from marine and lacustrine settings (Figure 27; Aquino Neto et al., 1983; Volkman et al., 1989). Although the definitive sourcing of such compounds is still not fully established, their presence has been attributed to cytotoxins in sponges (Manes et al., 1988), Cheilanthes ferns (Khan et al., 1971), prokaryotes (Ourisson et al., 1982) and algal blooms from *Tasmanites* and *prasinophyceae* in marine source rocks (Aquino Neto et al., 1982; Brocks and Summons, 2014), which are well established contributors of the Woodford Shale. The role of *Tasmanites* in the Woodford is important, as it contributes to the original production of the TOC and biogenic silica, which play a role in the mechanics that make ‘frackable’ intervals for unconventional plays (Slatt, 2013).

Throughout the entire outcrop, the hopanes predominate over the tricyclic terpanes, and among the tricyclic terpanes, the C₂₃ homologue represented the highest peak in all the samples as observed in many oils and extracts (Figure 27; Connan et al., 1980). The abundance of the tricyclic terpanes can be compared to that of the hopanes as a means of establishing relative amounts of input from algal blooms as opposed to marine bacteria contribution, using a ratio of C₂₈-C₂₉ tricyclic terpanes / C₂₉-C₃₃

hopanes (Stout et al., 2001). The results of this ratio indicate that the relative amounts of algae and marine prokaryotes were not constant through time, but rather, varied with depositional conditions. In particular, the ratio shows a bimodal trend, with relative highs at 26 and 65 feet up the outcrop (Figure 29). The two zones of higher tricyclic terpane abundance correspond to intervals of increased chert lithology. In fact, the highest abundance is found in the upper zone with higher concentration of chert beds and likely consistent with more open-marine, unrestricted, distal conditions. Intermittent chert deposition has been attributed to periodic upwelling (Roberts and Mitterer, 1992), which would increase available nutrients that may account for increased bioproductivity of algae in the chert beds of this outcrop. The break in the trend occurs at about the middle of the outcrop (30-45 ft.) and corresponds to the interpreted minor transgression that occurred in that zone. Decreased values of the tricyclic terpane to hopane ratio may be the result of increased prokaryotic marine organic matter preservation due to increasing sea level.

Cross plots of specific tricyclic terpanes and hopanes have been used as source rock proxies for depositional environments (Hays et al., 2012). The parameter hinges on the fact that C₂₆ tricyclic terpanes predominate over C₂₅ tricyclics for lacustrine source rocks (C₂₆/C₂₅ > 1.4), but are lower in abundance for marine shales and carbonates (Aquino Neto et al., 1983; Hays et al., 2012). There is a general inverse relationship between C₂₆/C₂₅ tricyclic terpane and C₃₁R/C₃₀ hopane ratios, such that a higher value of the hopane ratio indicates a marine shale (>0.25), or carbonate (0.45) lithology. The I-35 outcrop samples plotted using the tricyclic terpane and hopane ratios are shown in Figure 30. Despite the presence of some dolomitic mudstones in the

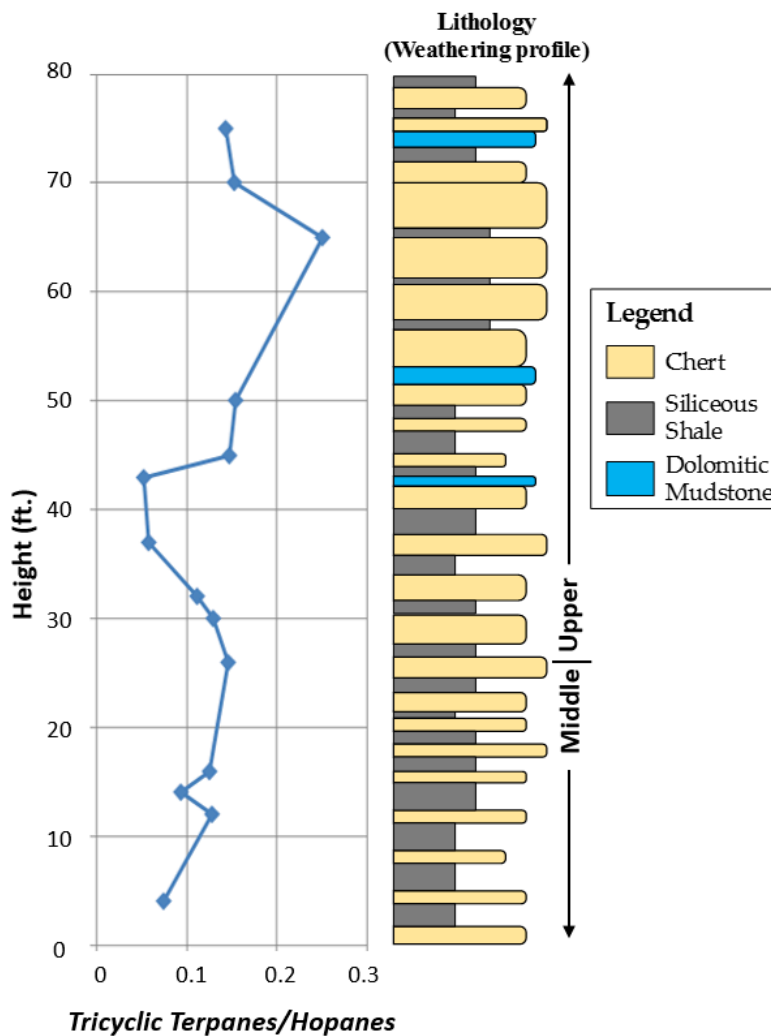


Figure 29. Comparison of tricyclic terpene/hopane abundance, as compared to lithofacies. (Tricyclic terpene / hopane ratio = $[C_{28}\text{-}C_{29}$ tricyclic terpanes / $C_{29}\text{-}C_{33}$ hopanes]).

chemofacies identification (samples 37, 43, 75; Becerra-Rondon, 2017), the data points for the I-35 outcrop fall in the region for marine shales (Figure 30). While Rock Eval data with high HI values characteristic of Type I lacustrine sources were found in the data set (Peters and Cassa, 1994; Table 1), the C_{26} tricyclic terpanes do not demonstrate

a lacustrine setting. This agrees with the lack of other indicators characteristic of lacustrine sources, such as the trace amounts of tetracyclic polyprenoids (Section 4.2.5.).

One sample (#13) had an anomalously high $C_{31}R/C_{30}$ ratio, thus indicating a ‘carbonate’ lithology (Figure 30). It was also found via gas chromatography and mass spectrometry that this particular sample displayed biomarker signatures unique from the other samples, especially in the aromatic fraction. Regularly spaced peaks within the aromatic fraction, similar to the profile seen for the n-alkanes, provide the best visual cue of the samples unusual signature (Figure 31). After re-extraction of sample #13 to ensure contamination from sample handling did not affect the results, the GCMS analysis demonstrated the same unique chromatogram trace. Using the MSDS Chemstation database, the tallest peak in the aromatic fraction was found to be a 98% match with methyl palmitate. The unusual hopane signature in the saturate fraction helped confirm the identification. Hopanes which are especially susceptible to thermal maturation, are biologically produced in the R configuration at C-22 position (Ensminger et al., 1977). With thermal maturation, hopanes will isomerize into the 22S configuration (Schoell et al., 1983). The anomalously high $C_{31} R$ homohopane/ C_{30} hopane is accompanied by a relatively high $22S/[22R+22S]$ C_{31} hopane ratios in sample 13 (Table 7), thus demonstrating higher maturity than the rest of the samples. This signature would be expected of biodiesels or hydrocarbons that have been processed and incorporated into plastics, causing isomerization of hopanes to the 22S configuration. Thus, sample 13 likely demonstrates some form of contamination.

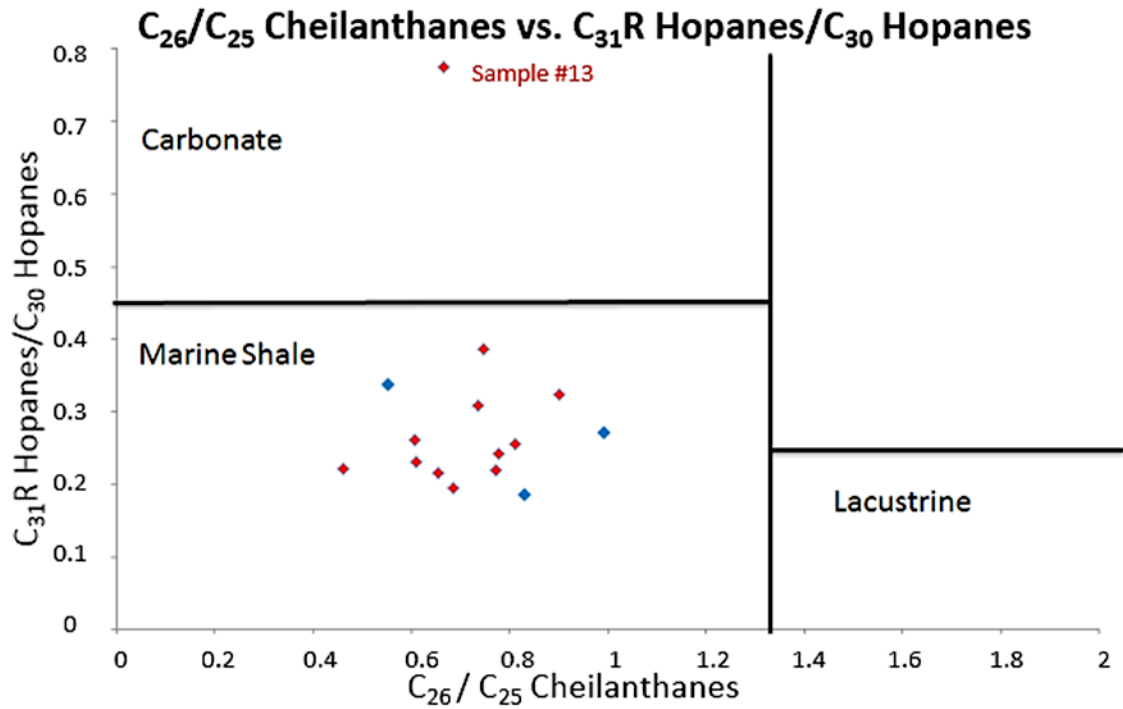


Figure 30. C₂₆/C₂₅ Cheilanthanes vs. C₃₁R Hopanes/C₃₀ Hopanes. (Blue = samples designated as dolomitic mudstone by Becerra-Rondon, 2017).

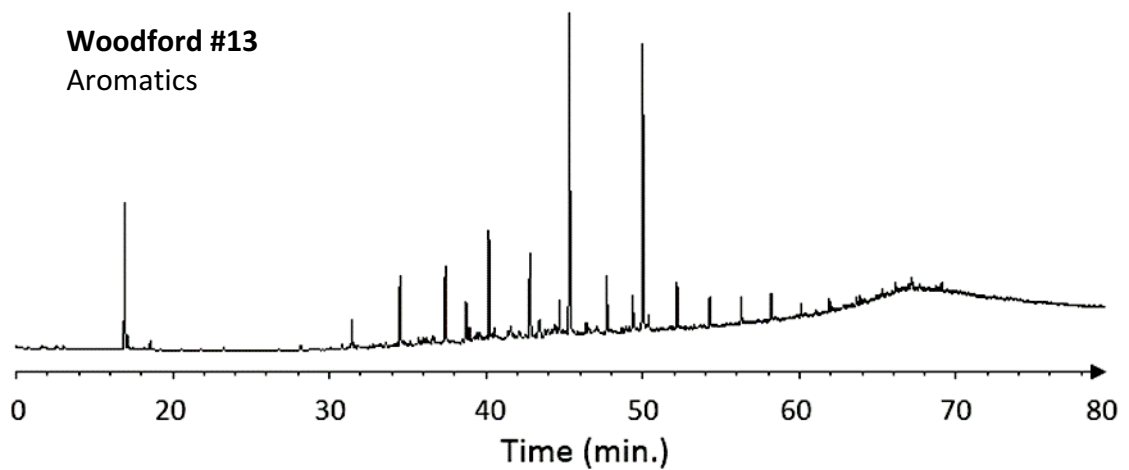


Figure 31. Sample 13 aromatics, with apparent contamination.

Because this flaw was recognized in sample #13, the sample was excluded when assessing biomarker parameters that used hopanes.

4.2.5. Tetracyclic Polyprenoids

Tetracyclic polyprenoids (TPP; **XVII**) were tentatively identified by GC/MS/MS using the m/z 414→259 transition, however, they were found in such low abundance that they could not be distinguished on GCMS. These biomarkers are highly specialized for lacustrine brackish environments, most likely from freshwater algae (Holba et al., 2000). The low concentration of such biomarkers is an indication of little input from brackish or freshwater algae. Although the upper Woodford is predominantly characterized by regressive systems tract, the distal setting and distance from the shoreline resulted in little input from brackish or freshwater algae sources. This corresponds to the relatively low C_{26} to C_{25} tricyclic terpane ratio (<1.4), which is also characteristic non-lacustrine algal input (Aquino Neto et al., 1983; Table 7).

Table 7. Hopane and tricyclic terpene ratios used. (Gammacerane Index = 10* gammacerane / [gammacerane + C₃₀ hopane]; C₂₆/C₂₅ TT = C₂₆/C₂₅ tricyclic terpanes; C₃₁R/ C₃₀ = C₃₁R/ C₃₀ hopanes; TT/Hop = [C₂₈ + C₂₉ tricyclic terpanes] / [C₂₉ -C₃₃ hopanes] ; 22S/[22S+22R] ratio calculated for C₃₁ hopane).

Sample	Gammacerane (µg / g TOC)	Gammacerane index	C ₂₆ /C ₂₅ TT	C ₃₁ R/ C ₃₀	22S/(22S+22R)	TT/Hop
75	5.06	9.81	0.78	0.24	0.56	0.14
70	11.83	9.76	0.83	0.19	0.6	0.15
65	17.06	9.92	0.69	0.19	0.59	0.25
50	7.29	9.64	0.46	0.22	0.56	0.15
45	6.07	9.85	0.66	0.22	0.59	0.15
43	162.48	6.07	0.75	0.39	0.6	0.05
37	9.82	8.85	0.55	0.34	0.57	0.06
32	54.54	8.49	0.99	0.27	0.56	0.11
30	31.34	8.68	0.81	0.25	0.58	0.13
26	94.45	9.14	0.61	0.23	0.57	0.15
16	33.52	9.06	0.61	0.26	0.6	0.13
14	46.07	8.1	0.74	0.31	0.57	0.09
13	5.95	9.72	0.67	0.77	0.66	N/A
12	41.85	9.09	0.77	0.22	0.62	0.13
4	56.61	7.79	0.9	0.32	0.56	0.07

4.3. Aromatic Biomarkers

4.3.1. Identifying Photic Zone Euxinia: Carotenoids and Aryl Isoprenoids

Carotenoids are a class of aromatic C₄₀ compounds that are derived from photosynthetic pigments (Summons and Powell, 1987). Specifically, carotenoids in shallow marine settings are most often attributed to green sulfur-reducing bacteria (GSB) from the *Chlorobiaceae* family, which require photic zone euxinia (PZE) in order to survive (Summons and Powell, 1986; Imhoff, 1995; Brocks and Summons, 2014). Photic zone euxinia refers to the environmental conditions involving sunlight exposure in a setting with anoxia, resulting in sulfur-reducing conditions and water column stratification. The basal Woodford Sea, which was relatively shallow in Oklahoma, went through periods of restricted circulation, giving way to conditions that would cause PZE (Comer, 2008; Connock, 2015). Because GSB synthesize C₄₀ carotenoids in the marine setting, the presence of such compounds has strong implications for a euxinic depositional environment (Philp, 2013; Connock, 2015). Within the family of sulfur-reducing bacteria, a purple and green strain exist, and offer slightly different paleoenvironmental interpretations, as green sulfur bacteria appears to be more resilient to changes in chemocline depth, light availability and pH (Repeta et al., 1989; Vila and Abella, 1994; Brocks and Schaeffer, 2008; Connock, 2015). A simplified model of overlapping photic zone and stratified water column is shown in Figure 32, demonstrating the position of sulfur reducing bacteria. Aryl isoprenoids are the products of green sulfur bacteria breakdown, and therefore, also provide indication

of PZE during deposition of a source rock (Summons and Powell, 1986, Grice et al. 1996).

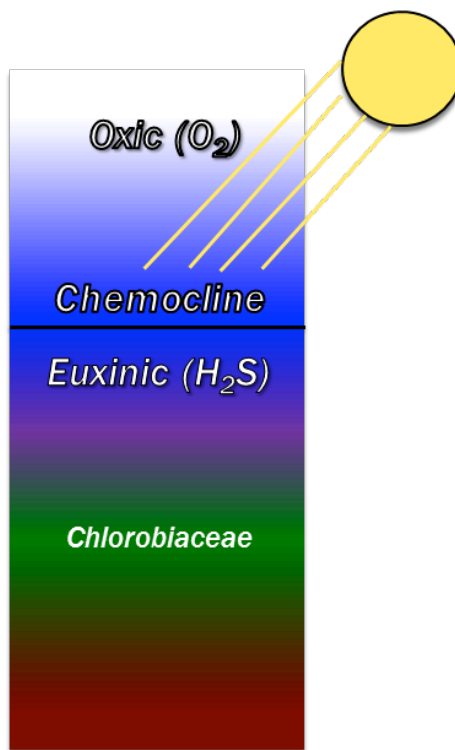


Figure 32. Generalized model for photic zone euxinia, after Connock, 2015. Colors indicate relative positions of sulfur bacteria species, with brown GSB existing deeper than PSB, which inhabits deeper position than PSB.

The distribution and identification for aryl isoprenoids and carotenoids on the I-35 outcrop using m/z 133 and 134 are shown in Figure 33 and Figure 34. It is important to note that for this method, the C₁₃- C₃₁ aryl isoprenoids appeared in the saturate fraction despite having aromatized structures, which is a common occurrence for typical oil fractionations (Brown and Kenig, 2004). The C₃₂+ aryl isoprenoids and C₄₀ carotenoids appeared in the aromatic fraction. There are two prominent stratigraphic instances of aryl isoprenoids (26 and 43 feet), with the most significant being at 26 feet

(Figure 35; Table 8). The 2,3,6-trimethylsubstituted aryl isoprenoids (m/z 133; **XVII**) are derived from both β -isorenieratane and β -carotane (**XX**), which come from green sulfur bacteria and cyanobacteria, respectively. The 3,4,5-trimethyl-substituted aryl isoprenoids (**XIX**), are derived solely from isorenieratane from *Chlorobiaceae*, and therefore make for a more direct indicator of euxinia (Koopmans et. al, 1996; Brown and Kenig, 2004; Miceli-Romero and Philp, 2012). A depth plot of 3,4,5-trimethyl-substituted aryl isoprenoids, 2,3,6-trimethyl aryl isoprenoids, and total sum of aryl isoprenoids demonstrate similar covariations from the base of the outcrop (Figure 35). This may imply that the source of the 2,3,6-trimethyl aryl isoprenoids in the zone that covaries may also be mainly from isorenieratane (**XXI**) and therefore a sign of PZE. The C_{18} aryl isoprenoid ratio (2,3,6- / 3,4,5-trimethyl-substituted) can be utilized to assess relative amounts of aryl isoprenoids from *Chlorobiaceae*, where lower values correspond with more green sulfur bacteria input, as opposed to cyanobacteria input. Usually, a lower value corresponds to more anoxic conditions and lower Pr/Ph ratios (Miceli-Romero, 2010), however, the total concentrations show that the 2,3,6- and 3,4,5- trimethyl-substituted aryl isoprenoid isomers have matching trends and inflections in abundance (Figure 35). Previous C_{18} AIR calculations have also modeled high values in the upper Woodford (6.09-12.80), which were attributed to relatively oxic conditions (Miceli-Romero and Philp, 2012), but the high preservation of aryl isoprenoids and carotenoids between 30-45 feet in the I-35 outcrop would suggest otherwise. In the case of the upper Woodford, differences in the C_{18} AIR between this and previous studies may arise from regional differences in organic deposition.

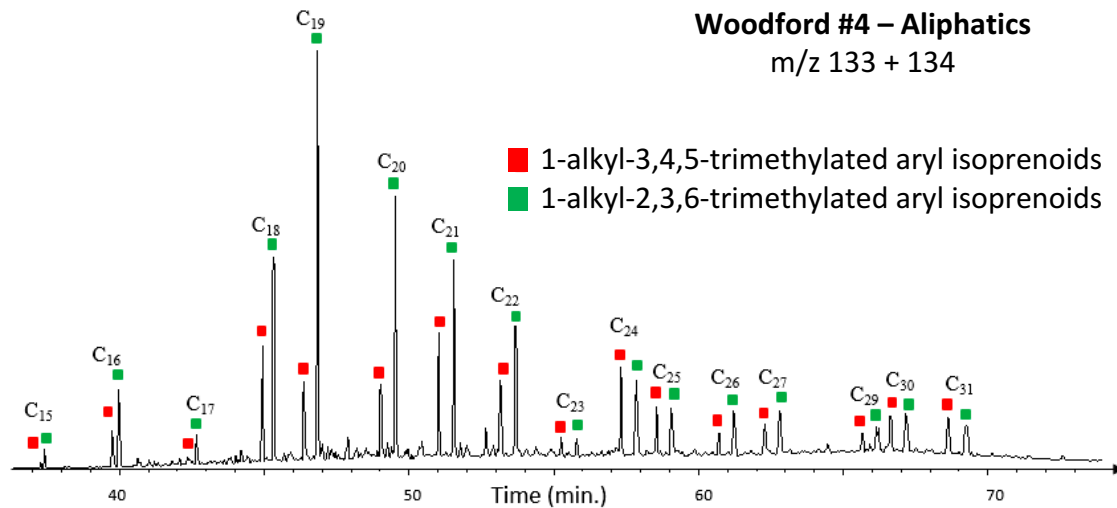


Figure 33. Identification of aryl isoprenoids using added mass fragments (m/z 133 +134).

Woodford #4 – Aromatics
m/z 133 + 134

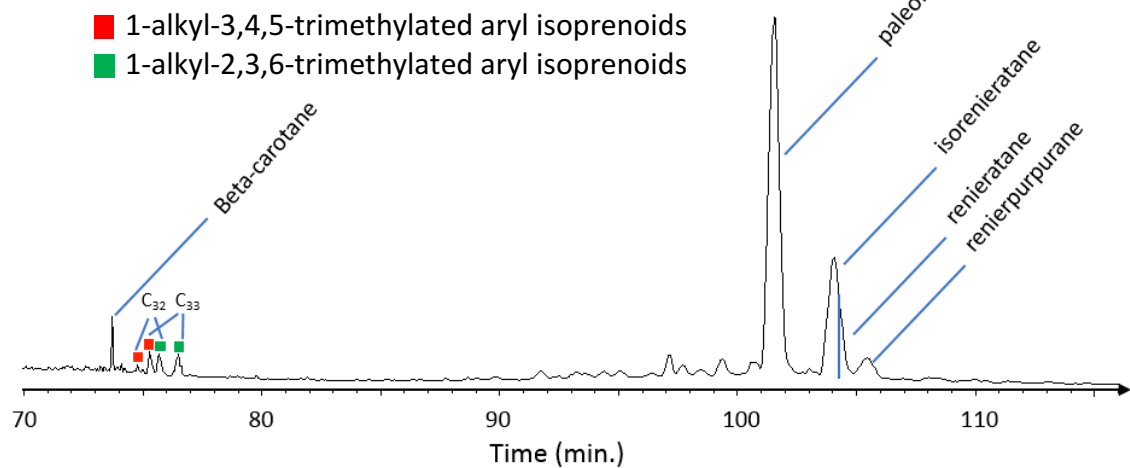


Figure 34. Identification of beta-carotane, C₃₂ and C₃₃ aryl isoprenoids, and C₄₀ Carotenoids using m/z 133 + 134.

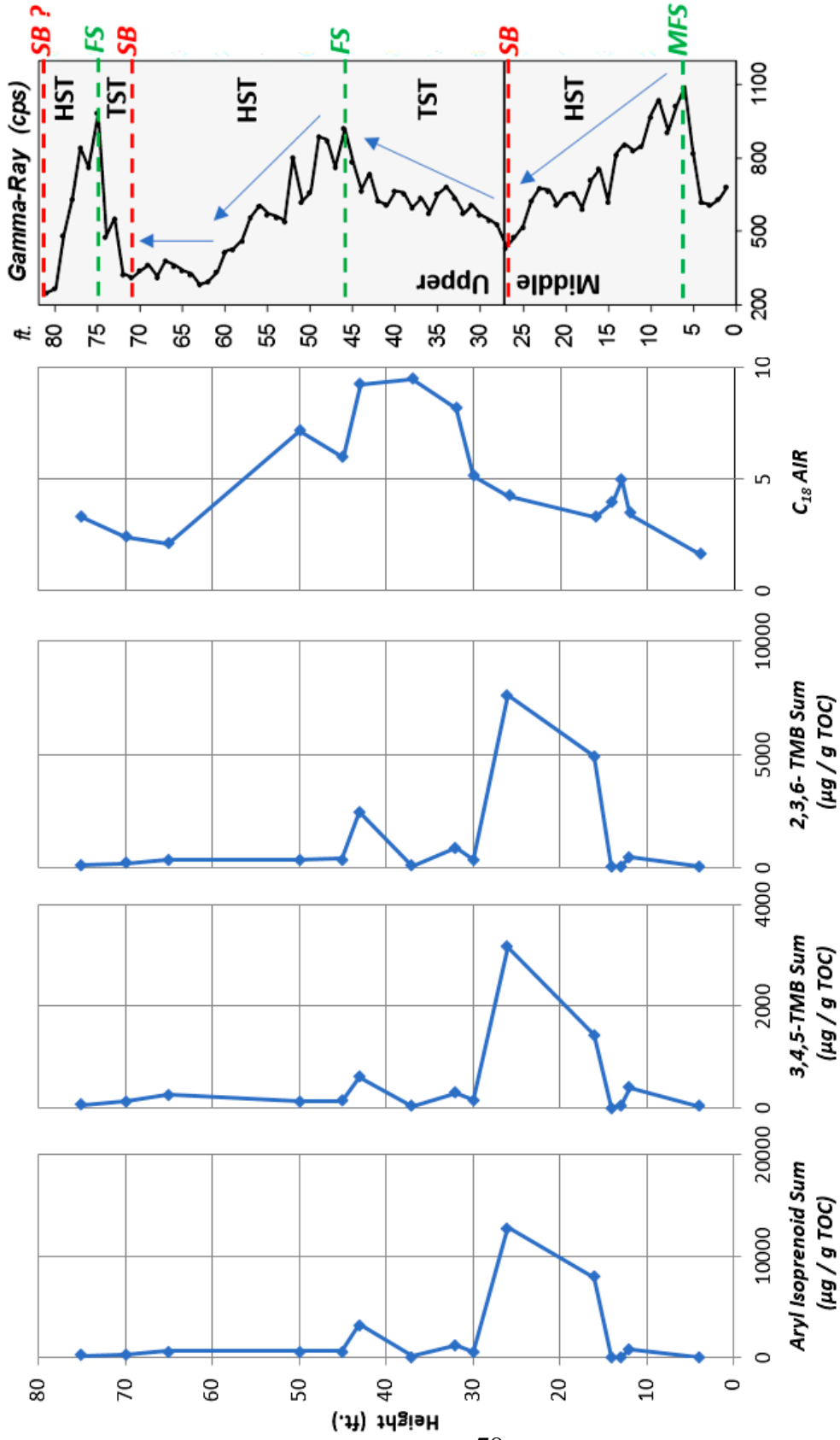


Figure 35. Aryl isoprenoid sum (3,4,5- + 2,3,6- trimethyl-substituted aryl isoprenoids); total 3,4,5-trimethyl substituted aryl isoprenoids; total 2,3,6-trimethyl substituted aryl isoprenoids; and C_{18} AIR = 3,4,5- / 2,3,6- trimethyl-substituted

The length of aryl isoprenoid chains are commonly associated with the degree of oxicity in a marine setting (Miceli-Romero and Philp, 2012). Oxic-suboxic conditions and thermal maturation tend to break isoprene units from long chains to shorter chains, so another aryl isoprenoid ratio is frequently employed to analyze the stability of the stratified water column (Schwark and Frimmel, 2004). For this, the sum of C₁₃₋₁₇ aryl isoprenoids are compared to the sum of C₁₈₋₂₂, where values less than 1 indicate persistent euxinia, whereas values greater than 1 suggests more episodic incidence of PZE. A plot showing the ratio of C₁₃₋₁₇ / C₁₈₋₂₂ is seen in Figure 36, with the areas highlighted to show the persistence of euxinic conditions compared to the concentration of gammacerane, another indicator of stratification (Sinninghe Damste et al., 1995). Most of the samples for this set fall below 1, which would suggest a more persistent stratified water column capable of preserving the longer aryl isoprenoid chains (Table 8). The C₁₃₋₁₇ / C₁₈₋₂₂ AIR values below 0.5 for the interval between 30 and 45 feet correlates with high gammacerane concentration. Alternatively, the same zone has the highest C₁₈ AIR values, resulting in disagreement between the two parameters, and further suggesting the lack of utility of the C₁₈ AIR for this particular outcrop. The C₁₃₋₁₇ / C₁₈₋₂₂ AIR ratio below 0.5 is characteristic of persistent euxinic conditions, which is unique for the upper Woodford, as previous studies have shown a tendency toward oxic conditions that either displayed only intermittent instances of euxinia, or did not foster anaerobic, autotrophic bacteria at all due to a total lack of aryl isoprenoids and C₄₀ carotenoids (Miceli-Romero and Philp, 2012; Connock, 2015; Degarmo, 2015). Only Villalba (2016) showed low C₁₃₋₁₇ / C₁₈₋₂₂ AIR values in the upper Woodford section of cores from the Cherokee Platform, and attributed it to a persistent deep chemocline that

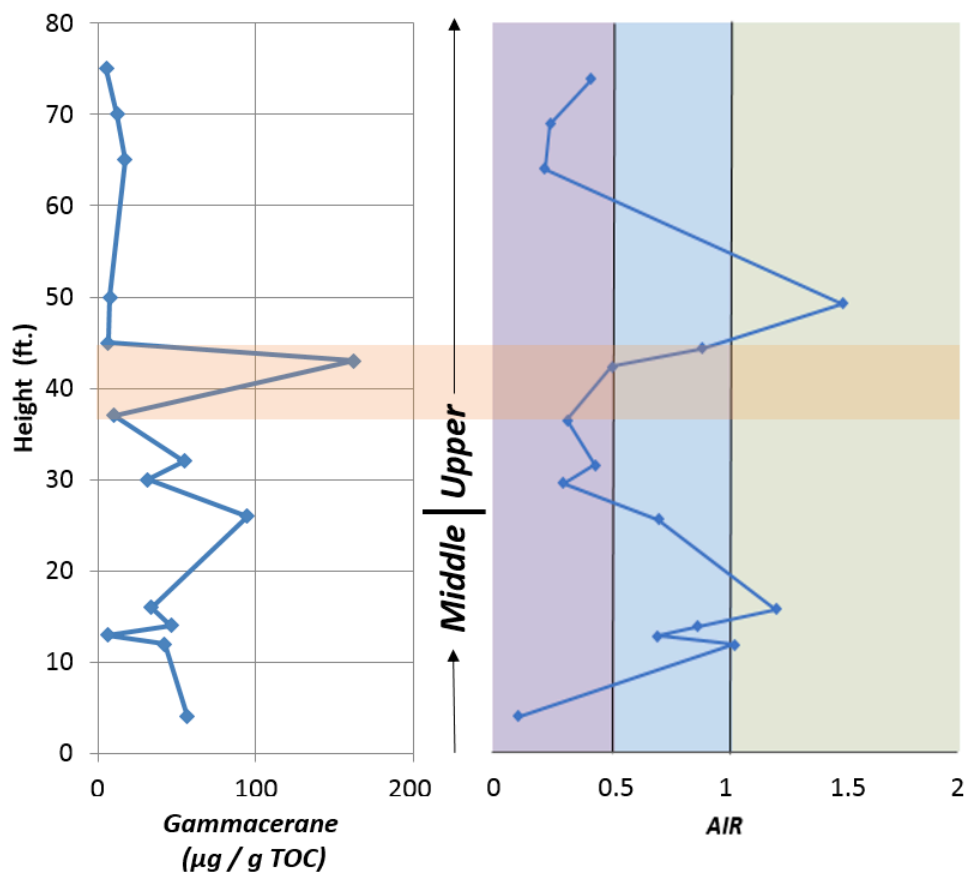


Figure 36. Gammacerane concentration versus AIR. (AIR= C_{13-17} aryl isoprenoids / C_{18-22} aryl isoprenoids. Green= intermittent PZE, blue=transitional conditions, purple= persistent PZE; Orange zone demonstrating gammacerane and AIR correlation.)

existed during that period. The anomalously low C_{13-17} / C_{18-22} AIR values in the I-35 upper Woodford and Cherokee Platform compared with other Woodford studies are likely the result of variability in PZE conditions throughout the Woodford Sea. This occurrence may suggest the need for better regional modeling of PZE conditions throughout the history of Woodford deposition. The AIR values characteristic of persistent euxinia may also demonstrate variable weathering and preservation of upper

Woodford sections, as previous studies only included about 30 ft. of upper Woodford section (Connock, 2015; Degarmo, 2015).

In addition to aryl isoprenoids, C₄₀ carotenoids were also identified in the m/z 133+134 mass chromatograms (Figure 33). The overall concentrations of isorenieratane (XXI), paleorenieratane (XXII), renieratane (XXIII), and renierpurpurane (XXIV) were highest in samples at 4, 16, and 43 ft. (Figure 37; Table 8). These episodes of high *Chlorobiaceae* input would ultimately suggest some change in depositional environment that is either related to: 1) increased sunlight to assist with GSB bioproductivity; or 2) increased restriction that allowed for pervasive euxinia. Examples of high carotenoid abundances are seen globally for upper Devonian shallow marine source rocks, e.g. the Holy Cross Mountains, Poland (Marynowski et al., 2000), and the Canning Basin, Australia (Edwards et al., 1997; Long and Trinajstić, 2010). Elevated amounts of isorenieratane and renieratane at 43 feet correlate with zones of low AIR values (Figure 37), and thus provide further identification of a deep chemocline and PZE at that stratigraphic location. Below the 43 foot bed, peak amounts of carotenoids are slightly offset from the highest concentrations of aryl isoprenoids; aryl isoprenoids are present at 12 and 26 feet, whereas carotenoids are present at 4, 14 and 16 feet (Figure 35, 37). This stratigraphic differentiation in aryl isoprenoid and carotenoid abundances may indicate more persistent euxinia for beds with higher carotenoid preservation, and diminishing euxinia for the overlying beds, causing diagenesis of carotenoids into aryl isoprenoids. The fluctuation in abundance would suggest 3 cases of PZE onset beginning at 4, 14, and 43 feet, each followed by water column destabilization and diminishing euxinia.

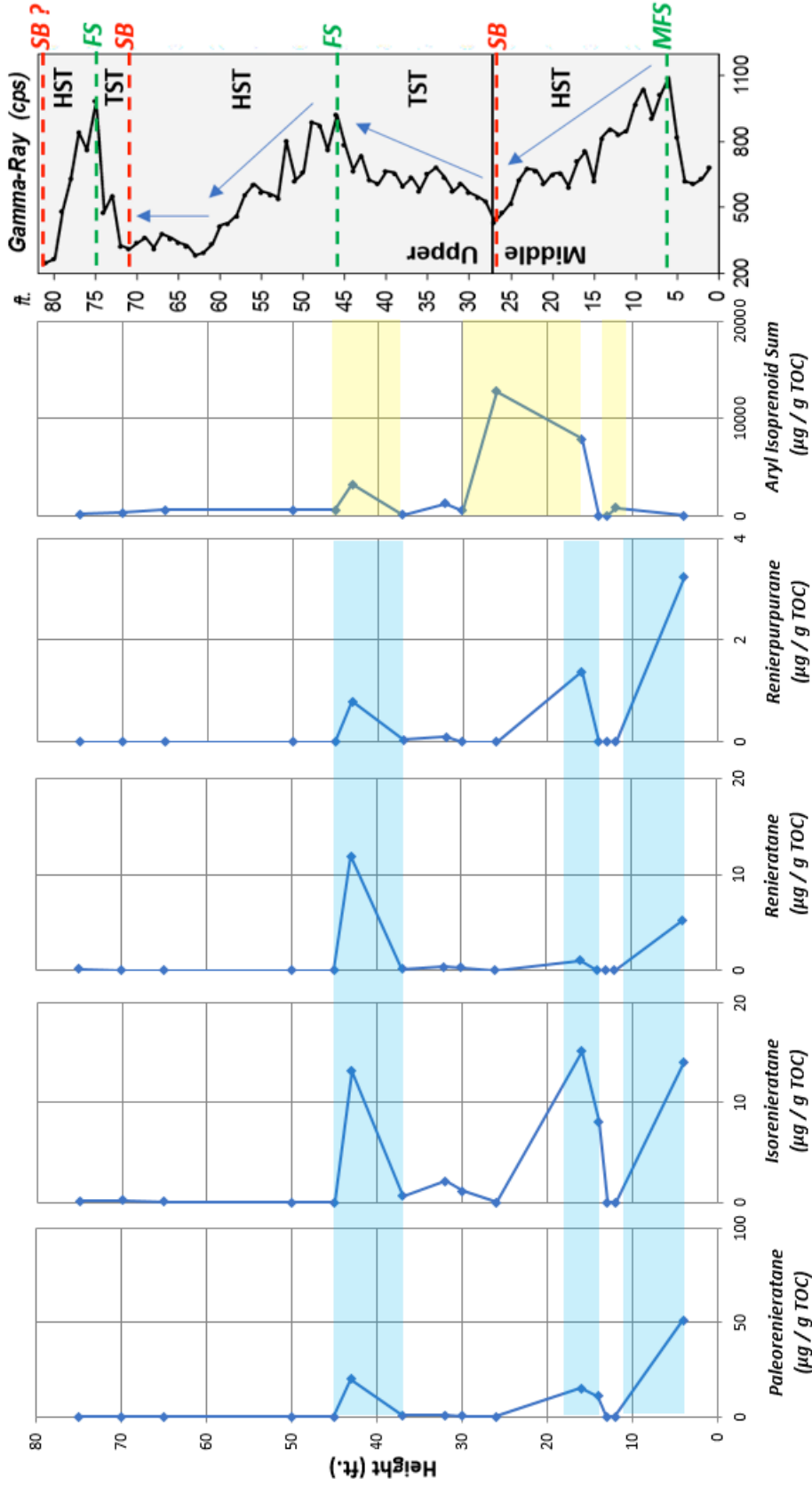


Figure 37. C40 carotenoid concentrations and aryl isoprenoid sum ($\mu\text{g} / \text{g TOC}$). Blue = elevated carotenoids, persistent euxinia, yellow = elevated aryl isoprenoids.

As mentioned previously, the various strains of GSB offer slightly different interpretations of chemocline depth and stability (Repeta et al., 1989; Vila and Abella, 1994; Brocks and Schaeffer, 2008; Connock, 2015). Fluctuations in the relative amounts of C₄₀ carotenoids arise from the fact that strains of carotenoid producing sulfur bacteria are known to thrive in different settings, demonstrated by the generalized water column structure in Figure 32. Isorenieratane comes from the brown strain of *Chlorobiaceae*, which can tolerate deeper chemocline (<80-100 meters; Repeta et al., 1989). Paleorenieratane is interpreted to have been biosynthesized at shallower depths than the brown strains, by an extinct strain of GSB (Connock, 2015). Renierapurpurane is derived from the purple strain, which is considered to be less tolerant to chemocline instability than the green and brown strains of sulfur-reducing bacteria, thus inhabiting shallower depths than green or brown sulfur bacteria (Brocks and Schaeffer, 2008). For this reason, a comparison of PSB/GSB can possibly lend insight to times of relatively more stable depositional conditions (French et al., 2015). Renierapurpurane barely occurs in this section (max~ 4 µg/ g TOC) relative to paleorenieratane (~50 µg/g TOC; Figure 37), indicating a deeper chemocline and unstable pH and temperature in the uppermost Woodford. Table 8 includes all the values and ratios calculated for C₄₀ carotenoids and aryl isoprenoids.

Table 8. Ratios and concentrations expressed in $\mu\text{g} / \text{g TOC}$, calculated for aryl isoprenoids and carotenoids. (Paleo=paleorenieratane; Iso=isorenieratane; Ren=renieratane; RPur=renierapurpurane; AIR=(C_{13-17}/C_{18-C22}); 3,4,5-TMB= Σ [3,4,5 trimethylated aryl isoprenoids]; 2,3,6-TMB= Σ [2,3,6 trimethylated aryl isoprenoids]).

Sample	Σ (Aryl isoprenoid)	Paleo	Iso	Ren	RPur	AIR	3,4,5-TMB	2,3,6-TMB
75	181.94	0.09	0.13	0.14	0	0.43	61.09	119.44
70	334.13	0.24	0.22	0	0	0.25	124.66	209.04
65	644.93	0.03	0.02	0	0	0.23	265.72	379.21
50	642.44	0	0	0	0	1.5	122.88	365.41
45	666.08	0	0	0.02	0	0.9	130.91	405.85
43	3282.38	19.86	13.19	11.86	0.78	0.52	609.13	2459.04
37	110.78	0.76	0.62	0.14	0.04	0.32	21.67	86.29
32	1257.68	0.9	2.09	0.34	0.1	0.44	287.94	886.97
30	551.88	0.64	1.13	0.31	0	0.31	146.92	389.25
26	12791.3	0.13	0	0	0	0.72	3162.9	7648.2
16	7920.18	15.21	15.19	1	1.38	1.22	1430.59	4924.67
14	14.9	10.9	8.11	0	0	0.88	4.4	8.8
13	80.05	0	0	0	0	0.71	20.3	53.42
12	873.03	0.15	0	0	0	1.04	389.4	451.77
4	87.96	51.31	14.11	5.14	3.23	0.12	28.34	58.45

4.4. Polycyclic Aromatic Hydrocarbons

Polycyclic aromatic hydrocarbons (PAH) are the result of diagenetic and catagenic processes, causing the aromatization of organic compounds prevalent in sediments and oils, and therefore do not specifically meet the definition of biomarkers (Alexander et al., 1992; Stout et al., 2015). Because of the derivation of these compounds from catagenesis and diagenesis, information related to levels of maturation, oxidation, and transport can be inferred from their quantification and analysis. Identification of PAHs can be difficult and were made by comparison to a coal tar sample, ‘Standard Reference Material 1597’ from the National Bureau of Standards. The PAHs identified in the I-35 outcrop include phenanthrenes, dibenzothiophenes, dibenzofurans, fluoranthene, benzofluoranthenes, perylenes, benzoperylene, pyrenes, benzopyrenes, biphenyl, cadalene, chrysene, benzoanthracene, and triphenylene. The significance and abundance of these compounds are discussed in the following sections. Compounds including naphthalenes (XXXIX) and retene (XXXX) were scanned for, however, naphthalenes were found to be virtually absent throughout the outcrop, while retene was not found at all.

4.4.1. Terrestrial Plant Biomarkers

A number of PAHs were identified which can be indirectly associated with organic input from terrestrial plants. When found in marine-sourced organic matter, the presence of terrestrial material would require 1) transport of material from the continent to the marine setting and 2) preservation of organic material (Tissot and Welte, 1984). Because most plant material is destroyed during transportation, the aromatized and

unsaturated compounds can act as proxy for terrestrial organic matter if they can be traced back to their biological origin (van Aarssen et al., 1999). The occurrence of terrestrial plant biomarkers in a marine setting would require transportation of continental material from river runoff, progradation, or transgression onto a previous exposed soil horizon where PAHs may have accumulated. Thus, terrestrial indicators, which have been detected in this set of middle and upper Woodford samples, have implications for the sequence stratigraphic framework of the basin, as a higher concentration would be expected closer to the shoreline when sea level is lower.

To give an example, dibenzofuran (**XXVII**), a prototypical biomarker used to identify plant input from continental sourcing, was tentatively identified from the m/z 168 mass fragment (Figure 38). Dibenzofuran (DBF) is a product of weathered terrestrial organic matter, and thus is commonly used as an indicator of soil erosion (Septhon et al., 2005; Mizukami et al., 2014). The formation of dibenzofurans occurs due to oxidative coupling of phenols (Born et al., 1989), dehydration of polysaccharides (Pastorova et al., 1994) and oxidation of lignin in woody plants (Radke et al., 2000; Fenton et al., 2007; Nabbefeld et al., 2010). Other PAHs detected in these samples also known to be derived from similar terrestrial plant origins include cadalene (a bicyclic compound derived from sesquiterpenoids; **XXXV**) and biphenyl (from woody plants; **XXXIV**; van Aarssen et al., 2000; Fenton et al., 2007). Perylene (**XXX**) is not thought of as a direct product of higher plants, but is instead considered a product wood-degrading fungus, thus making it an indicator of terrestrial plant input (Marynowski et al., 2015). Sources of other terrestrial-derived PAHs are more ambiguous in that the extent to which they are derived from diagenesis, or alternatively by combustion of

plant material, remains somewhat unclear. Compounds which are more definitively produced by combustion, include fluoranthene (**XXVIII**), benzofluoranthene (**XXIX**), benzoanthracene (**XXXVIII**), and pyrene (**XXXII**), which were identified in the samples (Killops and Massoud, 1992; Nabbefeld et al., 2010; Fang et al., 2015).

The PAHs discussed above were detected in extracts from the I-35 Woodford outcrop. The identifications are verified by comparing to the coal tar standard in Figure 38, Figure 39, and Figure 40. Cadalene was not in the coal tar standard, so a separate compound verification was done by coinjection with a cadalene standard. In Figure 41, the m/z 183 fragment from the aromatic fraction of sample #4 is shown before and after coinjection with cadalene standard. Increased peak height in the bottom fragmentogram demonstrates coelution with cadalene in the standard and cadalene in the sample. The concentrations of specific PAHs are plotted against height from the base of the outcrop in Figures 42 and 43, except for those that are analyzed in more depth in subsequent sections. Trends in the abundances of polycyclic aromatics tend to track each other and show inflections at similar heights, likely reflecting their derivation from similar terrestrial sources. Calculated concentrations are recorded in Table 9.

More specifically, PAHs tied to decomposed terrestrial plants, including biphenyl, DBF, and cadalene, showed increased concentrations in the middle Woodford portion (16 feet from the base), followed by diminishing values thereafter (Figure 42). The sample at 16 feet displays the most distinct instance of increased influx of plant matter. Concentrations of biphenyl and dibenzofuran compounds begin to recover again in the upper Woodford portion of the outcrop, but in lower concentrations than seen toward the base of the outcrop (at 50 feet for biphenyl; at 43 feet for dibenzofuran).

Cadalene concentrations are actually higher in the upper Woodford section (at 43 ft.). In general, these data aligned with the gamma ray seem to suggest that a greater amount of terrestrial organic matter is deposited during regression, which could be explained by closer proximity to the shoreline and progradation of sediment rich in terrestrial organic matter. The fact that the maximum concentration of cadalene falls in the transgressive portion of the upper Woodford provides an outlier to this trend, although this could be explained by increased productivity of species cadalene is derived from during that period. The covariation of biphenyl and dibenzofuran, evident by the matching stratigraphic locations of increased concentration (16 and 45 feet), indicate that both compounds may in fact be derived from woody, conifer-type species, as suggested by Mizukami et al. (2013).

Evidence of combusted plant material based on the presence of pyrene, fluoranthene, and benzofluoranthene generally correlate with the stratigraphic instances of plant indicators, although peak abundances are slightly offset. Based on those four compounds, the greatest prevalence of pyrogenic material occurred at 16 feet from the base (middle Woodford; Figure 42 and 43). Reappearance of combustion proxies at 50 feet indicates a second apparent instance of recurring forest fires within the upper Woodford portion.

All the PAHs thus far seem to demonstrate intervals of increased prevalence from 14-16 feet (middle Woodford), as well as 45-50 feet (upper Woodford). The concentration of terrestrial sourced biomarkers in these specific intervals reflects increased continental organic matter input, especially during times of regression when

the location of deposition was closer in proximity to the shoreline. Subsequent sections investigate more PAH data to analyze these trends further.

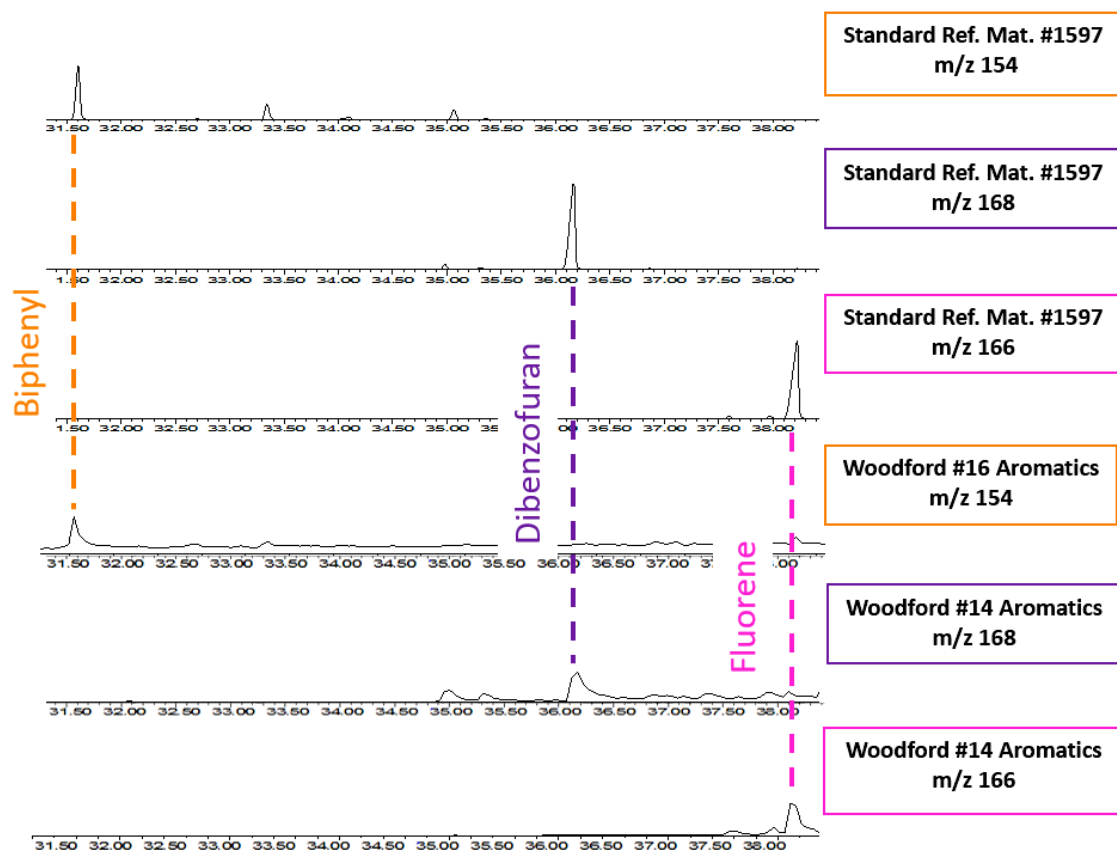


Figure 38. GC/MS identification of biphenyl, dibenzofuran, and fluorene by comparing previously identified peaks for the coal tar standard with peaks in the aromatic fraction of sample 14 and 16. Peak numbers defined in table on the right.

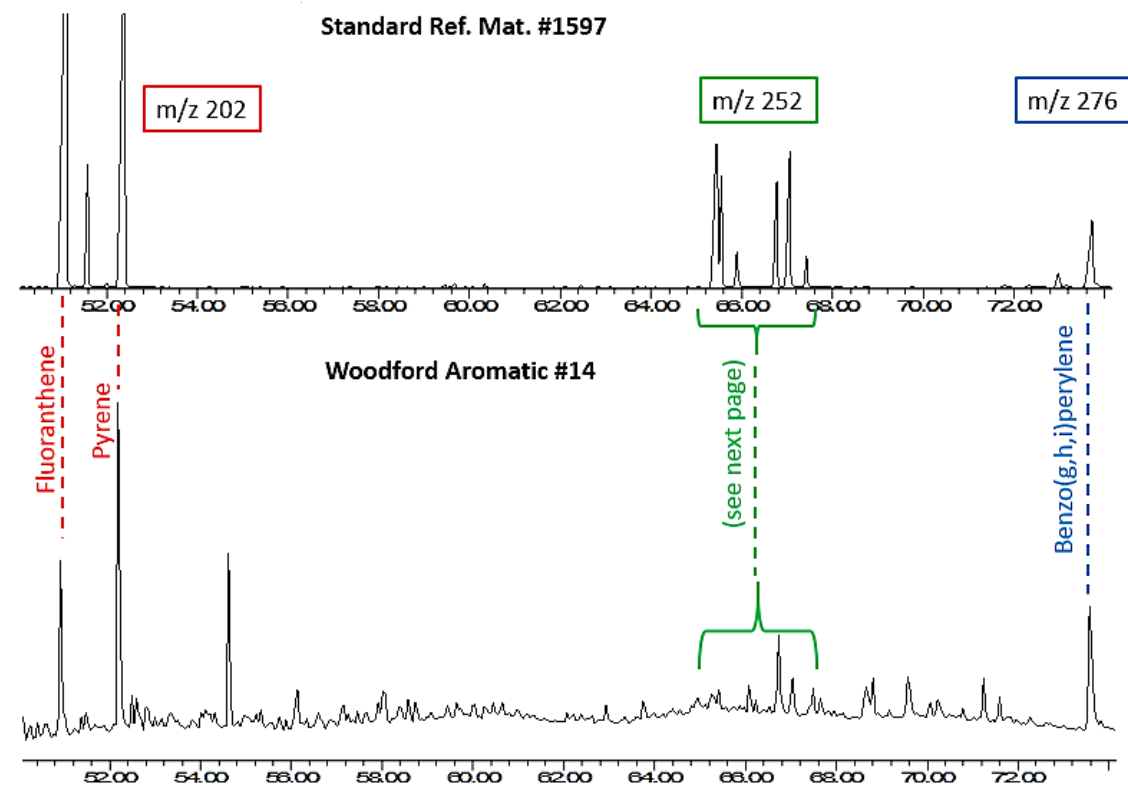


Figure 39. GC/MS identification of fluoranthene, pyrene, benzofluoranthenes, benzopyrenes, and perylene, by comparing previously identified peaks for the coal tar standard with peaks in the aromatic fraction of sample 14.

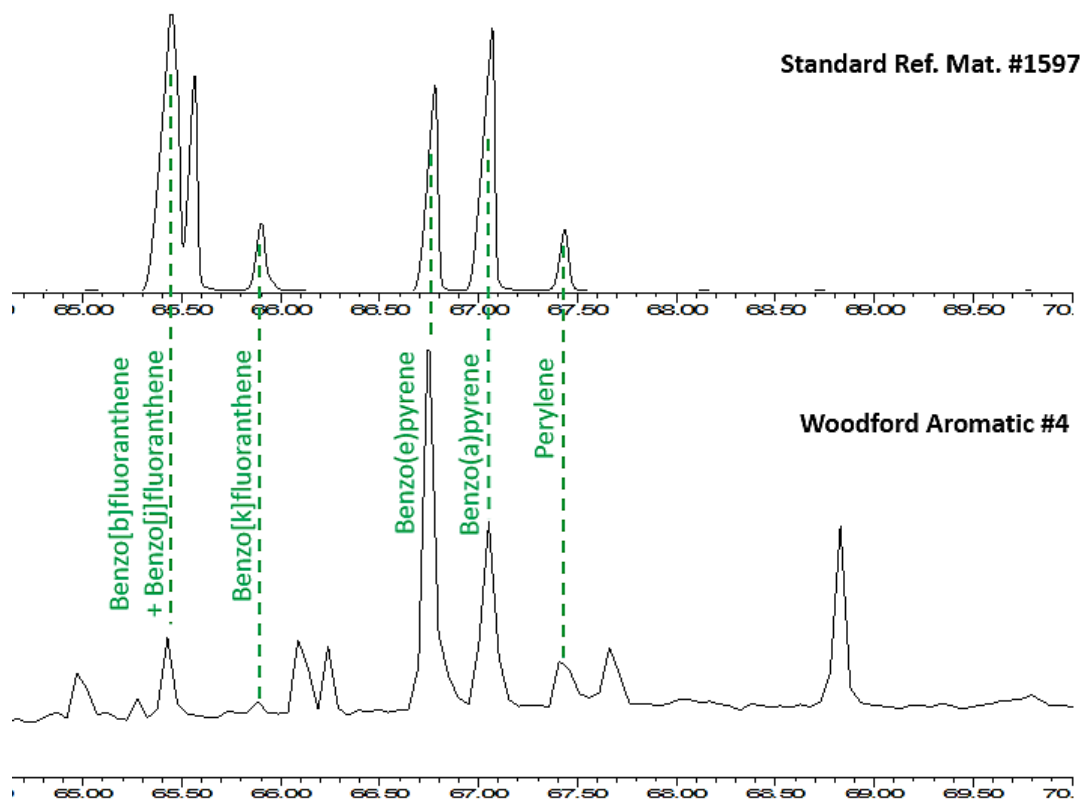


Figure 40. Zoomed in m/z 252 of Standard Ref. Mat #1597 and Woodford Aromatic #4.

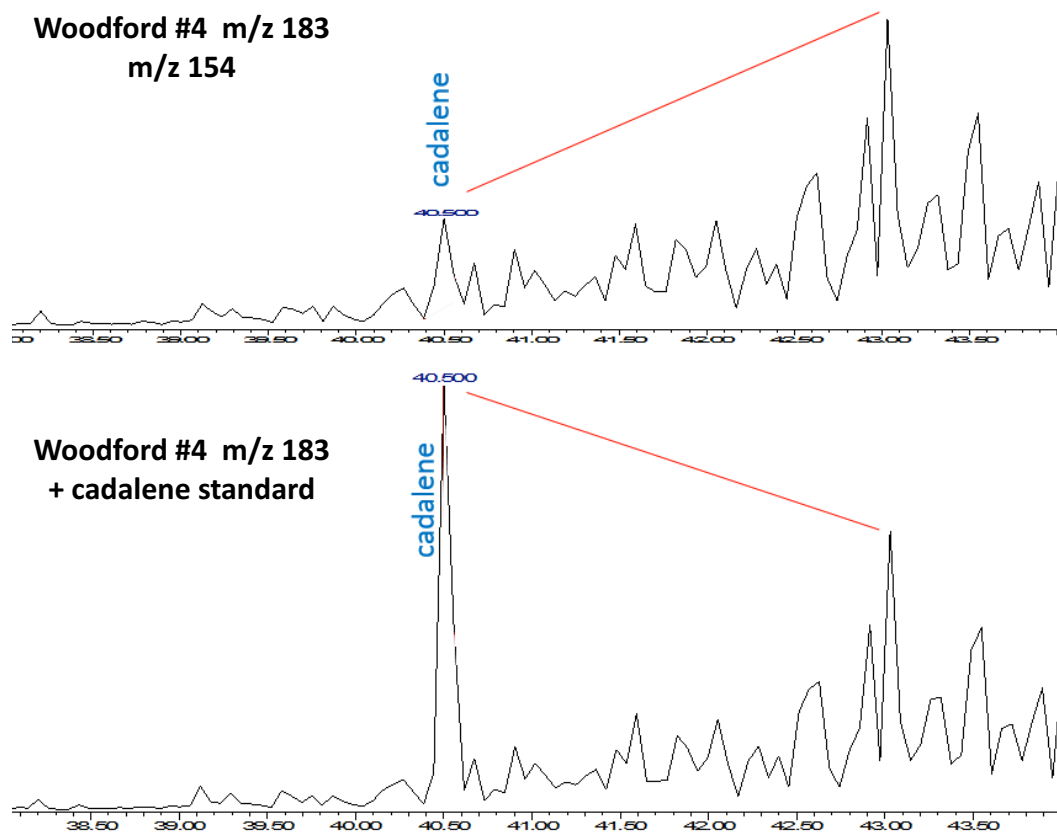


Figure 41. m/z 183 from aromatic fraction of Woodford sample #4 before and after coinjection with cadalene standard. Increased peak height in bottom fragmentogram demonstrates coelution with cadalene in the standard and cadalene in the sample.

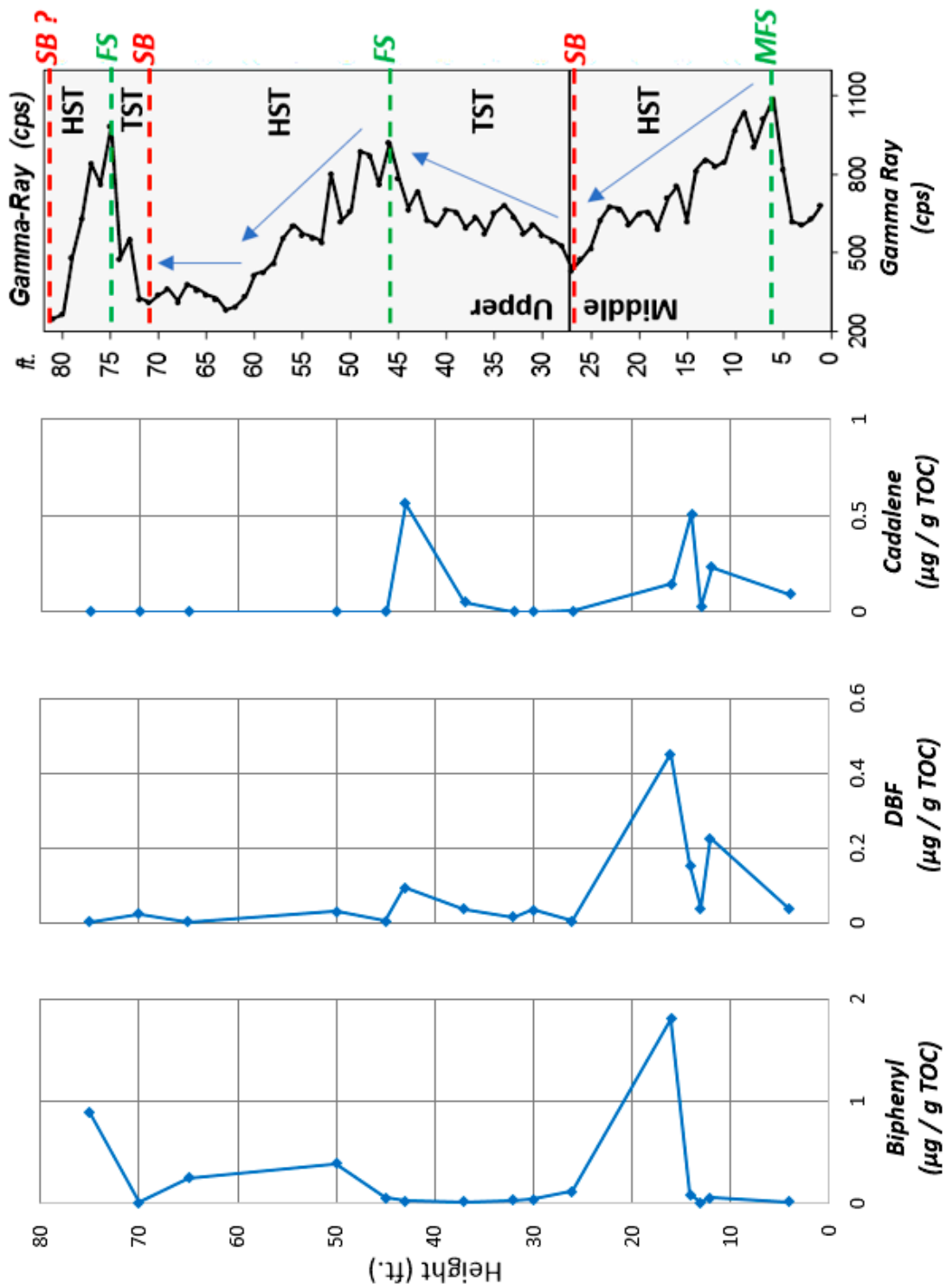


Figure 42. Concentrations of dibenzofuran, biphenyl, and cadalene by height from outcrop base.

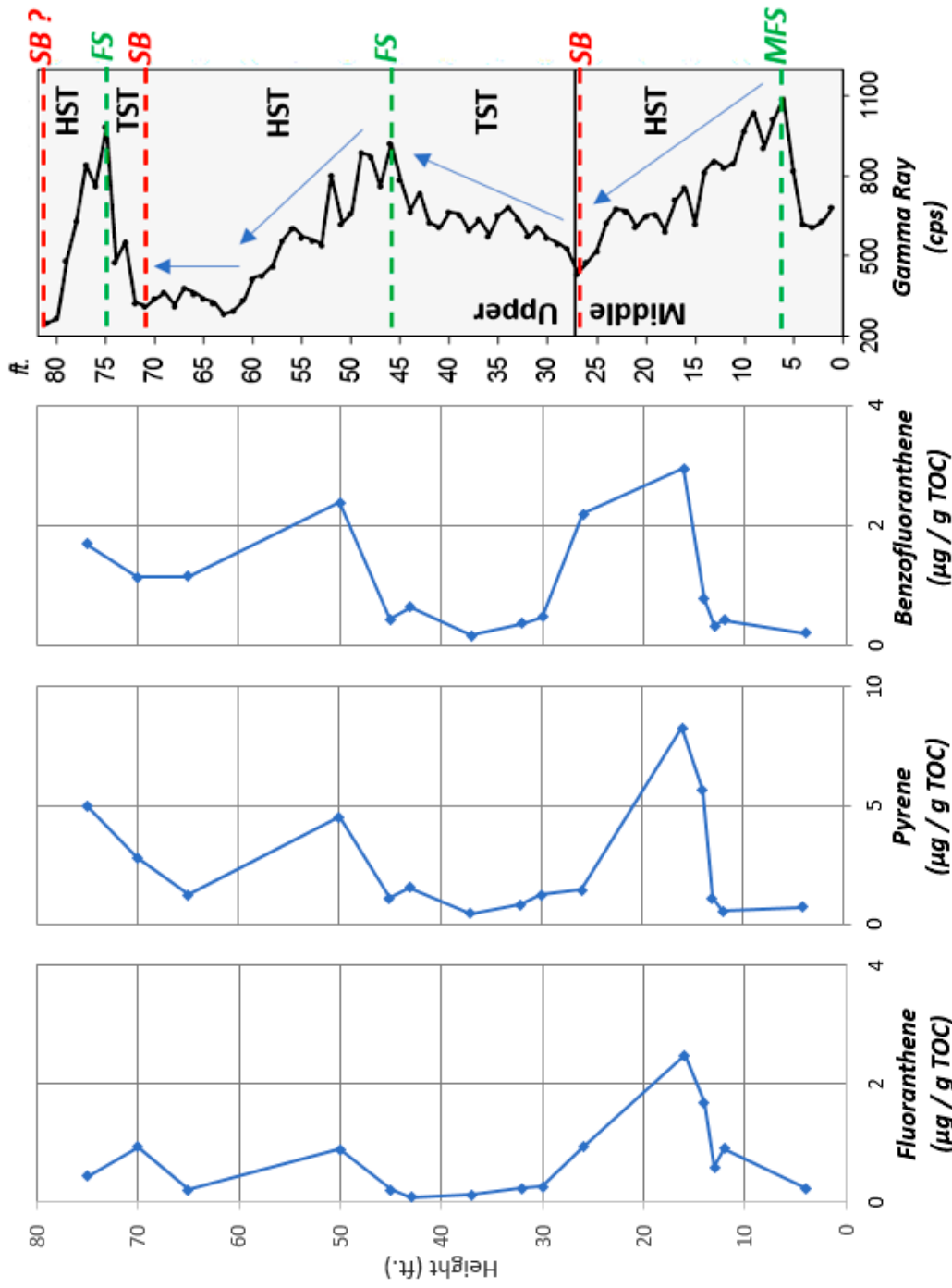


Figure 43. Concentrations of fluoranthene, pyrene, and benzofluoranthenes by height from base of outcrop.

Table 9. Concentrations of various PAHs in extracts, expressed in $\mu\text{g} / \text{g}$ TOC. (biP= biphenyl; Cad= cadalene; DBF= dibenzofuran; Py= pyrene; Fl= fluoranthene; BFl= benzofluoranthene).

Sample	biP	Cad	DBF	Py	Fl	BFl
75	0.89	0	0	5	0.44	1.68
70	0	0	0.02	2.81	0.93	1.14
65	0.24	0	0	1.24	0.21	1.14
50	0.39	0	0.03	4.51	0.88	2.38
45	0.05	0	0	1.1	0.21	0.44
43	0.02	0.56	0.09	1.53	0.09	0.63
37	0.01	0.05	0.04	0.44	0.13	0.16
32	0.03	0	0.02	0.83	0.23	0.36
30	0.03	0	0.03	1.22	0.27	0.47
26	0.11	0	0	1.45	0.93	2.19
16	1.8	0.15	0.45	8.27	2.48	2.94
14	0.09	0.51	0.15	5.64	1.68	0.76
13	0.01	0.03	0.04	1.1	0.58	0.32
12	0.05	0.23	0.23	0.55	0.91	0.41
4	0.02	0.09	0.04	0.72	0.23	0.2

4.4.2. Diagenesis vs. Combustion Derived PAHs

As Marynowski et al. (2015) pointed out, there are many precautions necessary in applying any novel PAH interpretations. One issue with PAH analyses arises from the fact that for many of the compounds, the formation has been attributed to both combustion and diagenesis, thus leaving some uncertainty in the interpretation (Li et al., 2013). Thus, interpretations of paleo-wildfires can be hindered by potentially non-specific PAH signatures. One method of overcoming this ambiguity in compound origin is identifying those compounds that are only derived from one or the other process. A comparison of chrysene and triphenylene to benzo(a)anthracene (BaA) has been suggested as a means to resolve the source of PAHs (Yunker et al., 2002).

Chrysene (**XXXVI**) and triphenylene (**XXXVII**) are known diagenetic products from terrestrial plant precursors, although there is also an element of combustion associated with their formation (Killops and Massoud, 1992). Benzo(a)anthracene (**XXXVIII**), however, is solely combustion-derived (Laflamme and Hites, 1978; Jiang et al., 1998). The original parameter used by Yunker et al. (2002) involved the ratio of $BaA / (BaA + \text{chrysene})$, where values <0.2 indicate chrysene derived from combustion of terrestrial plants, and values >0.35 indicate aromatization from diagenetic processes for PAH sourcing in recent sediments. Li et al. (2012) noted that a similar relationship can be made with ancient sediments, but the $BaA / (BaA + \text{chrysene})$ ratio is generally in a lower range (0-0.15). For this reason, the cutoffs used by Yunker et al. (2002) to define combustion vs. thermally matured PAHs may be specific to the basin in that study (Fraser River Basin, Canada), and need to be modified for the Woodford. It is important to note that chrysene and triphenylene are usually found to co-elute in

samples, but that the ratio of BaA / (BaA + chrysene + triphenylene) can still be used because triphenylene is also considered a diagenetic product of plant material (Grice et al., 2007; Li et al., 2012).

Both BaA and chrysene/triphenylene were identified in the I-35 outcrop using m/z 228, and by comparing with the coal standard (Figure 44). The concentrations of these compounds were higher at 16 feet (middle Woodford), and at 50 feet (upper Woodford), but the highest values of chrysene/triphenylene are seen at 16 feet while the highest amount of BaA is seen at 50 feet (Figure 45). This may demonstrate relatively more pyrogenic input in the middle Woodford. When employing the ratio, samples near the middle/upper Woodford boundary (from 16-45 feet) are enriched in BaA relative to the samples at either end of the outcrop. Specifically, sample 32 demonstrates the highest combustion-derived input relative to diagenetic products. In the case of the Woodford, a better parameter may be >0.05 for primarily diagenetic PAHs, whereas <0.15 could provide the limit characteristic of high amounts of combustion material.

In terms of the sequence stratigraphic model for the upper Woodford, the zone of highest BaA concentration (16 feet) correlates with high PAH abundances seen previously (DBF, biphenyl, fluoranthene, benzofluoranthene, pyrene; Figure 42 and 43), but the peak BaA ratio values occur during a transgressive period. This observation indicates lesser deposition of diagenetically-aromatized plant material between 16 and 45 feet, which is consistent with the relatively distal location during a transgressive period. The concentrations and BaA ratio calculations are listed in Table 10.

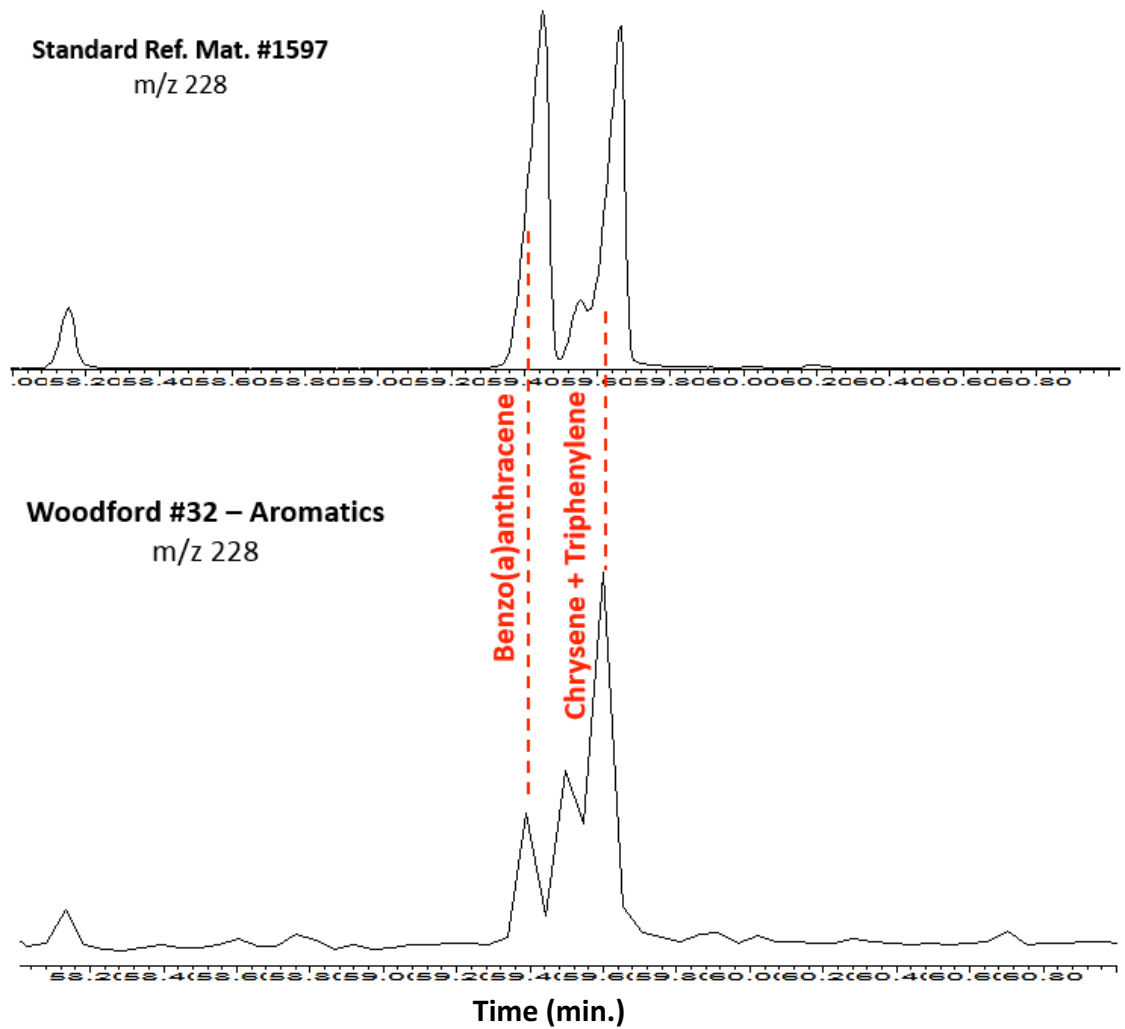


Figure 44. Comparison of benzoanthracene and chrysene/triphenylene between the Woodford #32 sample and the coal standard.

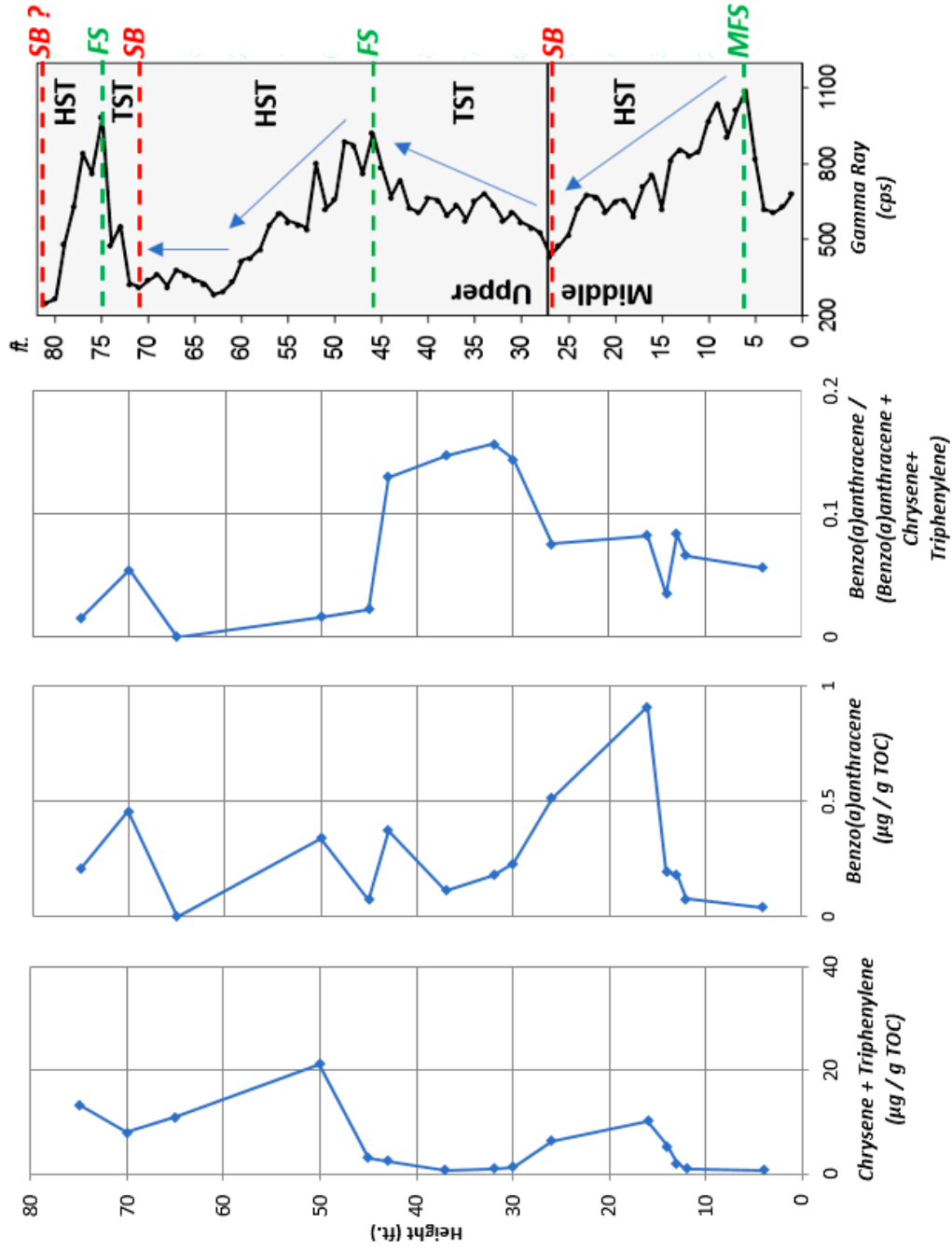


Figure 45. Concentrations of benzo(a)anthracene, chrysene, and BaA ratio from the base of the outcrop compared with interpreted gamma ray, PZE conditions and interpreted sequence stratigraphy. BaA ratio = benzo(a)anthracene / (benzo(a)anthracene + chrysene + triphenylene). Blue = PZE onset, yellow = diminishing PZE conditions.

Table 10. Chrysene and Benzo(a)anthracene concentrations expressed in $\mu\text{g} / \text{g}$ TOC. (BaA Ratio = $\text{BaA} / (\text{BaA} + \text{Triphenylene} + \text{Chrysene})$).

Sample	BaA	Chrysene/Triphenylene	BaA Ratio
75	0.2	13.27	0.02
70	0.46	7.99	0.05
65	0	10.9	0
50	0.34	21.19	0.02
45	0.07	3.11	0.02
43	0.37	2.5	0.13
37	0.11	0.65	0.15
32	0.18	0.97	0.16
30	0.23	1.35	0.14
26	0.51	6.31	0.08
16	0.91	10.14	0.08
14	0.19	5.29	0.04
13	0.18	2.02	0.08
12	0.07	1.06	0.07
4	0.04	0.64	0.06

4.4.3. Perylene and Alteration Products

Perylene (**XXX**) is a polycyclic aromatic hydrocarbon (PAH) found in petroleum, sediments, coals, peats, oils and extracts from marine, lake and river sediments, associated with a variety of marine and terrestrial organisms, such as fossil crinoids and tropical termite mounds (Laflamme and Hites, 1978; Silliman et al., 2000). Additionally, it has been reported that the concentration of perylene decreases basinward, providing further evidence of terrestrial-sourcing for this compound (Dahle et al., 2003). Consequently, the origin of the compound is still debated, but its elevated abundance in beds with high amounts of fungal spores associated with woody vegetation ultimately resulted in its correlation with wood-degrading fungi (Blumer, 1960; Grice et al., 2009; Nabbefeld et al., 2010; Marynowski et al., 2015). The inverse relationship between lignin marker guaiacol and perylene concentrations, as well as progressive decrease in $\delta^{13}\text{C}$ isotope values of perylene with simultaneous lignin degradation, have been cited as evidence for the compound's diagenetic origin (Grice et al., 2009).

Perylene is frequently found with a suite of PAHs related to the partial combustion of organic matter from both forest fires and petroleum, including benzo(e)pyrene (BeP), benzo(a)pyrene (BaP; **XXXIII**), and benzo(g,h,i)perylene (BghiP; **XXXI**) all of which have been identified in the I-35 Woodford samples (Figure 46; Laflamme and Hites, 1978; Lichtfouse et al., 1997; Nabbefeld et al., 2010). Marynowski et al. (2015), who used artificial maturation to track transformation and degradation of perylene into its thermal products (Figure 47). When heated to 300°C,

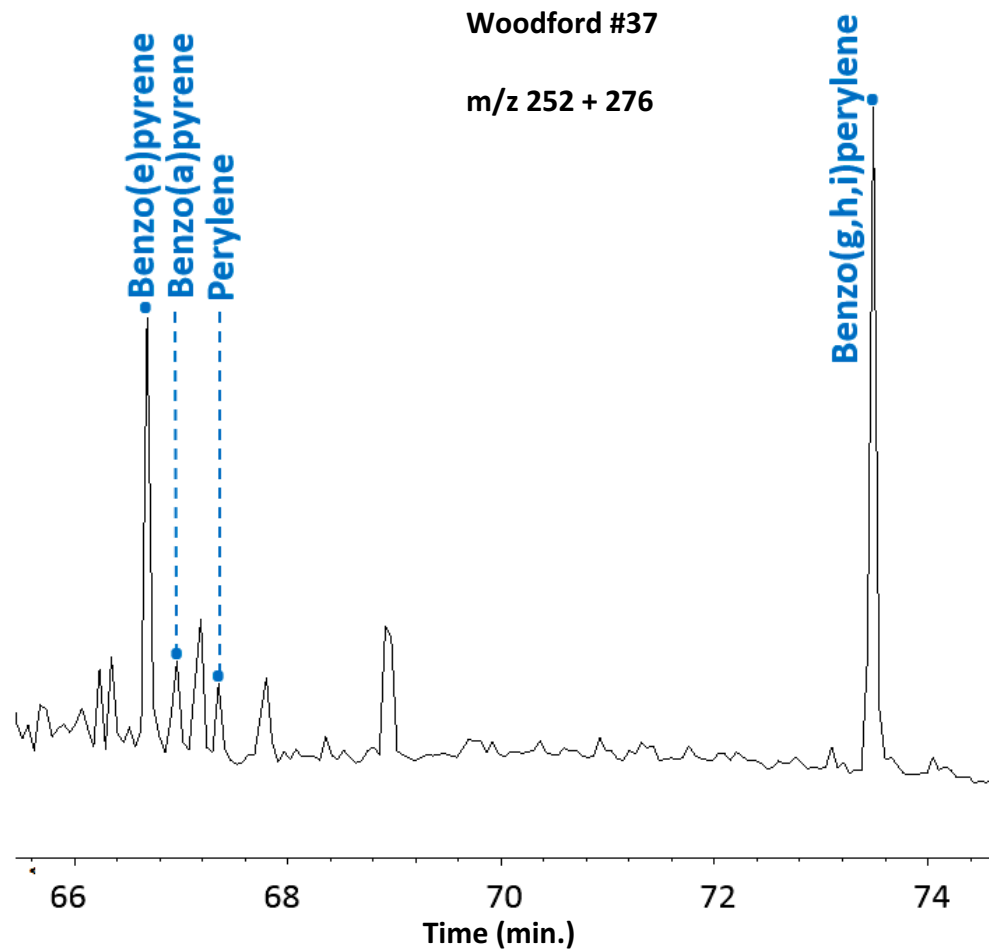


Figure 46. Identification of perylene, benzo(e)pyrene, benzo(a)pyrene, and benzo(g,h,i)perylene using m/z 252 and 276.

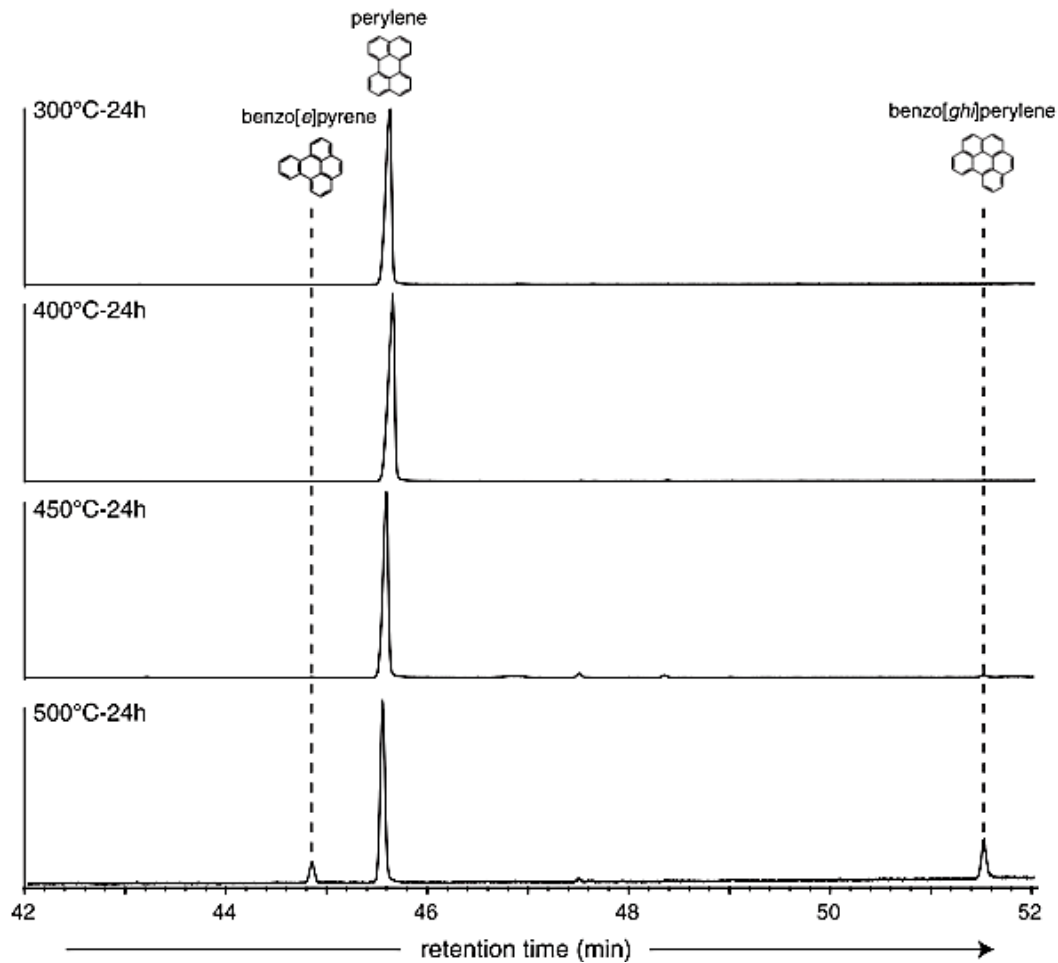


Figure 47. Artificial maturation of perylene (from Marynowski et al., 2015).

400°C, 450°C, and 500°C for 24 hours, BeP and BghiP only begins to appear at 450°C, and are quantifiable at 500°C. BaP is not formed with increasing maturation, but rather, demonstrates degradation at high temperatures. The implications for this study suggest thermal instability for BaP, and therefore limited use as a proxy for burning biomass for samples that are mature enough to display perylene thermal degradation. Because the I-35 outcrop samples fall between immature and early oil window and come from within

80 feet of each other, the usefulness of this parameter for Devonian wood combustion should still be valid.

Perylene, benzo(g,h,i)perylene, benzo(e)pyrene, and benzo(a)pyrene were identified and quantified using mass ion fragments 252 and 276 (Figure 46). The compounds showed relatively higher concentrations at 16 feet, and 50 feet (for BeP) (Figure 48; Table 11). These likely represent instances of higher amounts of terrigenous input, although based on BghiP concentrations, the degree of combustion associated with each sample varies. Concentrations of BghiP compared to the other compounds demonstrates more concentrated markers for wildfires in the zone between 14 and 26 feet, which coincides with the stratigraphic interval that had the highest BaA (Figure 48). Interestingly, the peak concentrations of BaP, BghiP, and perylene at 16 correlates with middle Woodford zone characterized by increased carotenoids, aryl isoprenoids, gammacerane, and other terrestrial biomarkers such as cadalene and DBF. This correlation provides further evidence to terrestrial organic matter as a contributing factor for euxinic conditions. Calculations of ratios and concentrations are listed in Table 11.

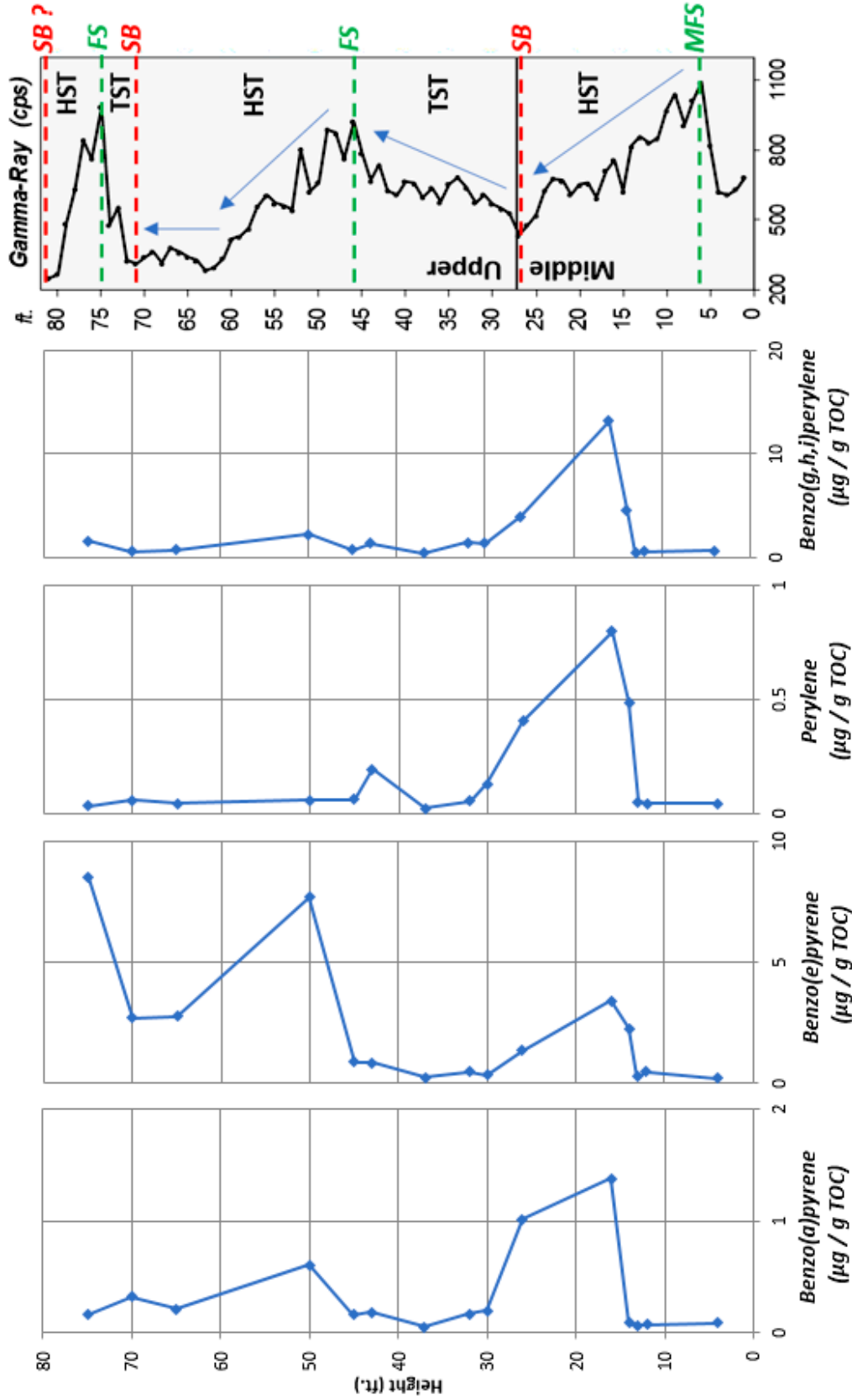


Figure 48. Quantity of perylene, benzo(a)pyrene, benzo(e)pyrene, and benzo(g,h,i)perylene in $\mu\text{g/g TOC}$.

Table 11. Concentrations ($\mu\text{g} / \text{g}$ TOC) and relative amounts of perylene and derivatives.
(BeP= benzo(e)pyrene; BaP=benzo(a)pyrene; P= perylene; BghiP= benzo(g,h,i)perylene).

Sample	BeP	BaP	P	BghiP
75	8.49	0.16	0.03	1.57
70	2.71	0.32	0.06	0.52
65	2.77	0.21	0.04	0.68
50	7.67	0.6	0.06	2.2
45	0.89	0.16	0.06	0.71
43	0.85	0.18	0.19	1.36
37	0.23	0.05	0.02	0.41
32	0.49	0.17	0.05	1.42
30	0.34	0.2	0.13	1.33
26	1.36	1.01	0.41	3.94
16	3.39	1.38	0.8	13.18
14	2.27	0.09	0.49	4.6
13	0.29	0.07	0.05	0.43
12	0.50	0.07	0.04	0.52
4	0.21	0.09	0.04	0.65

4.4.4. Maturity and Biodegradation: Phenanthrenes

Phenanthrenes (**XXV**) and alkyl-phenanthrenes derivatives were identified by GCMS for this set of samples using fragment ions m/z 178, 192, 206, 220, and 234 (Figure 49). The origin of these compounds is non-specific, as they have been attributed to the aromatization of steroids, and diterpenoids (Tissot and Welte, 1984; Simoneit, 1986). This would tie phenanthrene occurrence to the diagenesis of plant material, which has been reported in previous studies (Jiang, 1998; Grimalt et al., 2004), however, phenanthrenes are most commonly attributed to sterane diagenesis (Hall et al, 1984).

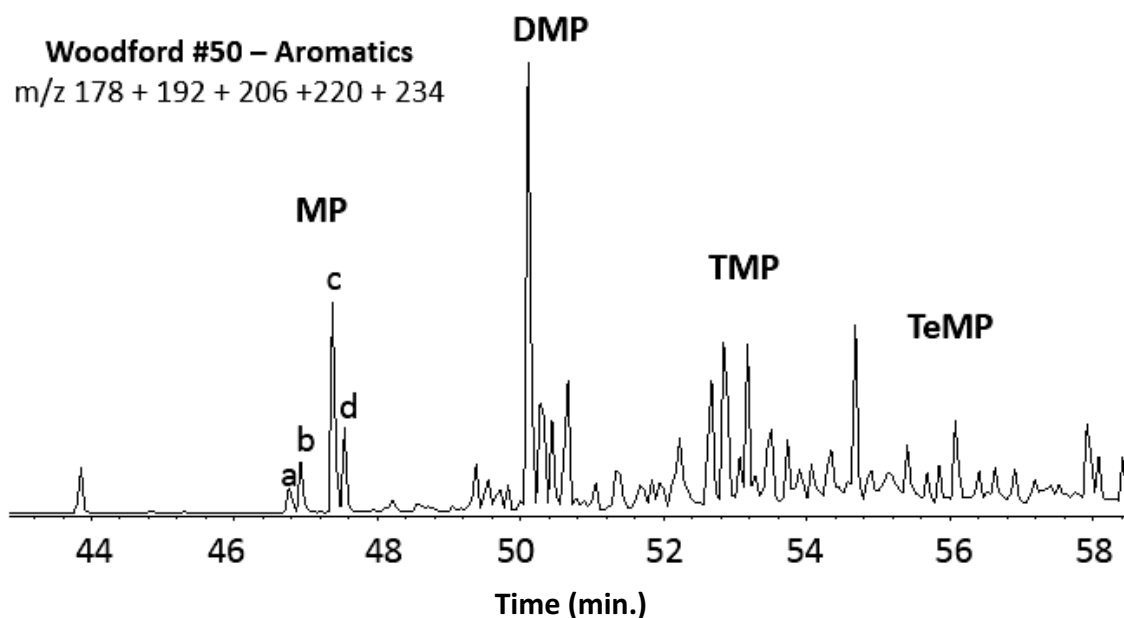


Figure 49. Identification of phenanthrene, methyl-phenanthrenes, dimethylphenanthrenes, trimethylphenanthrenes, and tetramethylphenanthrenes using and mass fragments (m/z 178 + 192 + 206 + 220 + 234). (a= 3-methylphenanthrene; b= 2-methylphenanthrene; c= 9-methylphenanthrene; d=1-methylphenanthrene).

A methyl-phenanthrene index (MPI) is frequently used in order to assess maturity in a source rock and provide a vitrinite reflectance proxy (Radke and Welte, 1981). The value for this parameter is calculated using the formula $MPI = 1.5 * (2-MP + 3-MP) / (P + 1-MP + 9-MP)$. For oils and extracts falling within the oil window, a calculated vitrinite reflectance (R_c) can be modeled using the equation $R_c = 0.6(MPI) + 0.4$. Considering the samples of this study all fall within an 80-foot interval, the MPI should be consistent throughout the section. Upon calculating the values, R_c range from 0.55 to 1.02 (Table 12).

, which characterize samples ranging from immature to late in the oil window, thus demonstrating an issue with applying this parameter for this study. Williams et al. (1986) found progressive removal of methyl-phenanthrenes in biodegraded oils, which may explain the variation in MPI for the I-35 outcrop, despite having the same maturity. A ratio of phenanthrene / (phenanthrene + 2-, 3-, 1-, and 9- methylphenanthrenes) yield results that help explain the failure of MPI application to this outcrop. Based on Williams et al. (1986) observation, values should be highest in the most biodegraded beds. In this case, sample 12 demonstrates the highest degree of biodegradation, which correlates with the sample with the least extractable bitumen (Table 4).

4.4.5. Sulfate Reduction: Dibenzothiophenes

Dibenzothiophene (**XXVI**) is a sulfur-bearing compound that has been used as a proxy for H_2S buildup in an anoxic environment (Hughes et al., 1995). Its formation requires reaction of inorganic sulfur with organic matter, which likely occurs syndepositionally or in early diagenesis (Hughes, 1984; Sinninghe Damste and de

Leeuw, 1990). Dibenzothiophene and its methylated homologues have been noted to be abundant in siliceous rocks (Chakhmakhchev and Suzuki, 1995), such as the Woodford.

Mizukami et al. (2014) noted increased DBT in beds with evidence of high rates of terrestrial input. Zhou et al., (2016) suggested that because terrestrial organic input provides a flux of nutrients to the marine setting, triggering planktonic blooms and bioproductivity, oxygen would be consumed and causing favorable conditions for euxinia. Therefore, DBT concentrations would increase due to the sulfur-reducing conditions brought on by the terrigenous input. This model could explain why DBT has been found to correlate with DBF and biphenyl (terrestrial plant biomarkers) during euxinic conditions at the PTB (Sephton et al., 2005; Fenton et al., 2007; Xie et al., 2007).

Dibenzothiophene is generally found with its methylated dibenzothiophenes and dimethylated dibenzothiophenes. Fan et al. (1990) suggested that hypersalinity increased the rate of methylation, though the reason for this is not completely understood. Both DBT and its methylated derivatives were detected in samples for this study (Figure 50), showing elevated abundance between 14 to 26 feet (Figure 51, Table 12). Hughes et al., (1995) introduced a parameter using a pristane/phytane vs. DBT/phenanthrene plot in order to approximate environmental/lithological sourcing of oil. Higher pristane/phytane values can be used to infer fluvial/deltaic from marine and lacustrine environments, whereas the ratio of DBT to phenanthrene is used as an indicator of H₂S rich depositional environment (Hughes et al., 1995). The DBT/Phen ratios can be used alone to approximate sulfur reducing conditions, where values less than 1 are associated lacustrine hypersaline environments and marine shales. In this study, DBT/Phen values

were calculated to be less than 1 for all samples except those at 4 and 43 feet (Figure 51). High values of DBT are an indicator of relatively high abundance of H₂S at those times, which line up with beds previously identified as having persistent euxinic conditions using aryl isoprenoids and carotenoids (Figure 37).

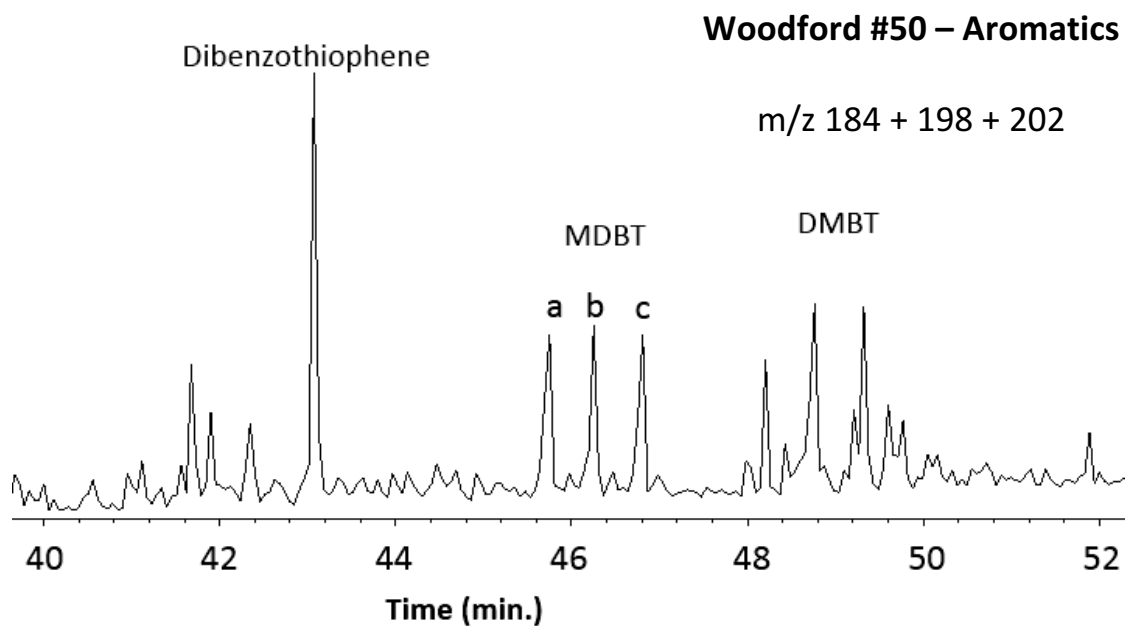


Figure 50. Identification of DBT, MDBT, and DMBT (m/z 184+198+202). (a= 4-MDBT; b= 2- + 3-MDBT; c= 1-MDBT)

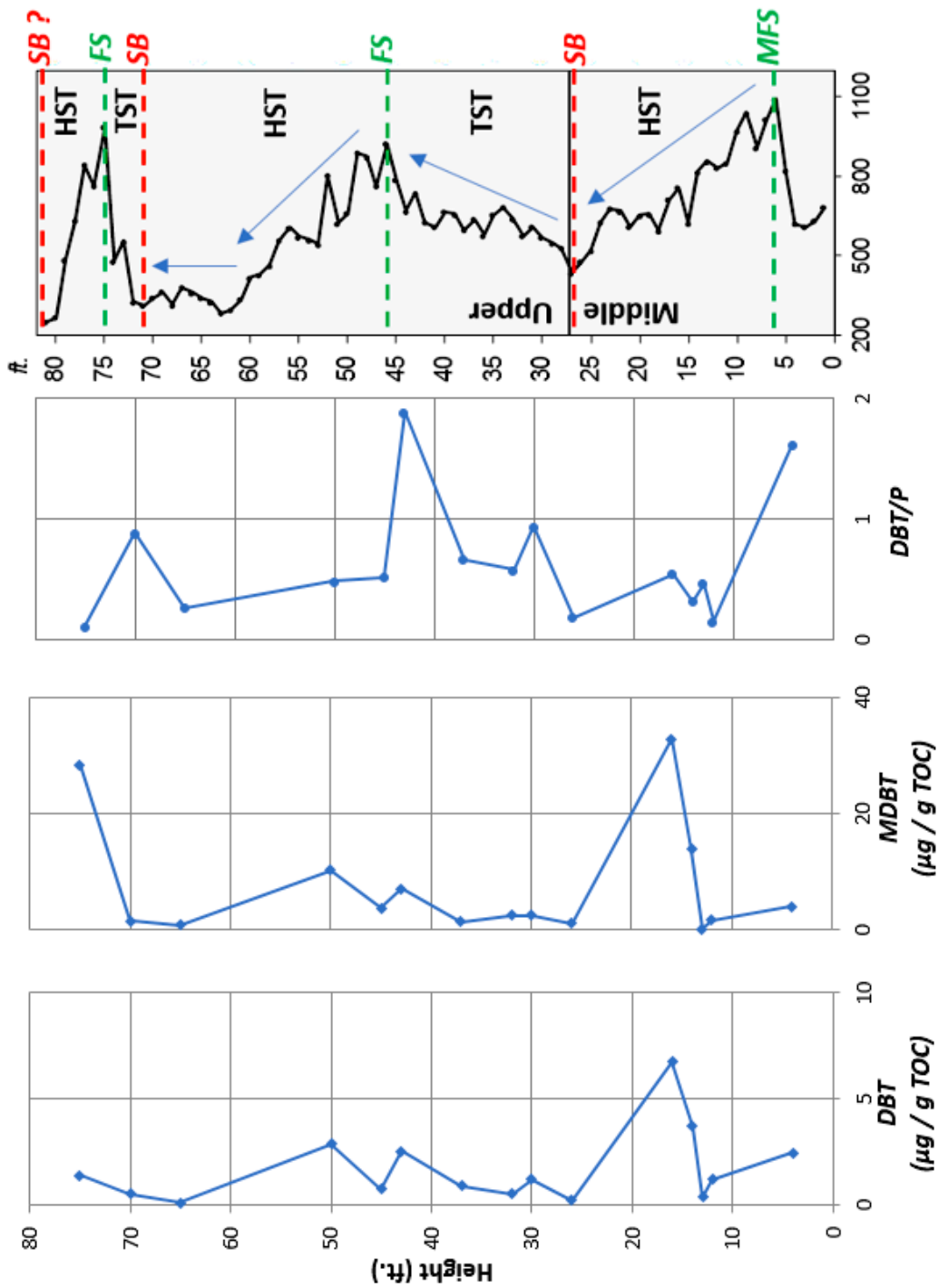


Figure 51. Concentration of DBT, MDBT by height from the base of the outcrop, as well as DBT/ P ratio. (DBT/P = dibenzothiophenes/phenanthrenes).

Table 12. Concentrations ($\mu\text{g} / \text{g TOC}$) and ratios of dibenzothiophenes (DBT), methyl-dibenzothiophenes (MDBT), phenanthrenes (P), and calculated vitrinite reflectance. (DBT ratio = $\text{DBT}/(\text{DBT}+\text{MDBT})$); MPI=methylphenanthrene index= $1.5*[2\text{-MP} + 3\text{-MP}]/[\text{P} + 1\text{-MP} + 9\text{-MP}]$; R_c= calculated vitrinite reflectance= $0.6[\text{MPI}] + 0.4$).

Sample	DBT	MDBT	DBT ratio	DBT/P	MPI	R _c
75	1.38	28.42	0.05	0.11	0.3	0.58
70	0.51	1.54	0.25	0.88	0.82	0.89
65	0.11	0.8	0.12	0.26	0.84	0.9
50	2.86	10.23	0.22	0.48	0.36	0.61
45	0.74	3.78	0.16	0.52	0.44	0.66
43	2.51	7.13	0.26	1.89	0.56	0.74
37	0.9	1.43	0.39	0.66	0.67	0.8
32	0.53	2.48	0.18	0.58	0.71	0.83
30	1.19	2.52	0.32	0.94	0.79	0.87
26	0.2	1.18	0.15	0.18	0.92	0.95
16	6.75	32.79	0.17	0.54	0.7	0.82
14	3.71	13.9	0.21	0.32	0.62	0.77
13	0.35	0.22	0.61	0.46	1.03	1.02
12	1.18	1.67	0.42	0.15	0.25	0.55
4	2.45	4.1	0.37	1.62	0.75	0.85

4.5. Evidence of Kellwasser and Hangenberg Events from PZE and Organic Input

As mentioned in the introduction, the Kellwasser Event (before the Frasnian-Famennian boundary) and Hangenberg Event (before Devonian-Carboniferous boundary), jointly contribute to one of the five largest mass extinctions in history (Kaiser et al., 2015). The marker beds, located in Germany, are black shales which have since been correlated with other shales globally (Sepkoski, 1996), including the Woodford Shale. The massive loss of life at the end of the Devonian period did not occur all at once, but rather, was characterized by bouts of extreme climatic and environmental changes between the Frasnian-Famennian boundary and D-C boundary (spanning ~13 mya), which resulted in pulses of marine and terrestrial ecosystem collapse (Becker et al., 2012). In the Woodford Shale of Oklahoma, boundaries have been identified using lithology, chemostratigraphy, and conodont biostratigraphy, such that the F-F boundary exists just below the middle/upper Woodford contact, and the D-C boundary occurs in the upper Woodford (Over, 1992; Turner, 2016). Some efforts have been made to utilize biomarker evidence of the ecosystem collapse preceding each of these boundaries (Kellwasser event before the F-F; Hangenberg event before the D-C), yet inconsistencies or limited data in previous studies makes these identifications problematic (Nowaczewski, 2011; Connock, 2015; Degarmo, 2015).

Nowaczewski (2011) attempted to locate geochemical evidence of the Hangenberg Crisis in the I-35 outcrop by assuming that it would exactly correlate with the D-C marker bed as outlined by Over (1992). In his study, Nowaczewski notes some biomarker anomalies at the boundary, such as decreased C₂₉ hopanes accompanied by elevated C₃₀ hopanes, gammacerane, and isorenieratane to demonstrate increased

marine eukaryotic preservation in stratified, anoxic waters that would be expected of the Hangenberg Crisis. With that being said, it is generally understood that the Hangenberg Crisis precedes the boundary (Sepkoski, 1996), so Nowaczewski's analysis characterizes changes at the D-C marker bed, but does not necessarily capture evidence of a biotic crisis.

Connock (2015) and Degarmo (2015) each placed the F-F boundary within their study locations, noting apparent elevated H₂S and pervasive PZE evidence prior to the collapse. Degarmo also noted a correlation between PZE conditions and abundance of terrestrial organic matter based on euxinic indicators, cadalene, and dibenzofuran, which he explains using the hypothesis that increased nutrients from terrestrial sources caused eutrophication and algal blooms (Algeo and Scheckler, 1998; Zhou et al., 2016). Interestingly, Connock (2015) places the F-F extinction in the middle Woodford, while Degarmo used a Devonian sequence stratigraphic model from Sandberg et al. (1988) in order to define a high TOC, carbonate bed in the upper Woodford for the transition bed. Although conodont stratigraphy requires the F-F boundary to be in the middle Woodford as defined by Connock, the apparent occurrence of euxinic conditions in different stratigraphic intervals in the two studies demonstrates the cyclic behavior of marine eutrophication and euxinia within the 13 mya period between the F-F and D-C boundaries (McGhee, 1996; Becker et al., 2012).

Biomarkers investigated in this thesis aimed specifically at locating anomalous signatures characteristic of an ecological crisis. These included signs of shallow marine euxinia (from carotenoids and aryl isoprenoids), accompanied by distinct fluxes in terrigenous input and algal blooms, followed by an overall depletion organic matter

deposition (Grice et al., 2005; Nabbefeld et al., 2010; Kaiho et al., 2013). Tying the sequence stratigraphy and geochemical properties of the I-35 outcrop together can inform us of paleoenvironmental changes within the Woodford Shale, and can serve as an example of the specific conditions associated with ecological collapses throughout Earth's history.

For example, the end-Permian biotic crisis saw widespread euxinia (Grice et al., 2005; Hays et al., 2007) which is usually attributed to changing circulation patterns caused by elevated sea level (Wignall and Twitchett, 1996; Nabbefeld et al., 2010). Additionally, blooming of phytoplankton communities have been recognized at times of ecosystem collapse, as seen at the Permian Triassic Boundary (PTB) in Greenland and Australia (Grice et al., 2005). In the case of the extinction that occurred at the PTB, the mechanism for ecological collapse is generally linked to the eruption of Siberian Traps, resulting in massive amounts of CO₂ emissions, thus triggering global warming (Benton and Twitchett, 2003).

The combination of parameters associated with PZE conditions allows for a more in depth interpretation of the water column stratification and euxinia throughout this portion of the Woodford. C₄₀ Carotenoids provide perhaps the best indication of photic zone euxinia due to the specificity of their biologic precursors, green and purple sulfur bacteria, which can inhabit H₂S-rich, and oxygen-poor waters (Summons and Powell, 1987; Sinninghe Damste and Schouten, 2006). Various species of sulfur bacteria provide even further environmental specificity, given that brown GSB inhabit deeper water depths than GSB or PSB (Brocks and Schaeffer, 2008). Relative

concentrations of C₄₀ carotenoids specific to each strain can therefore add to the interpretation for PZE conditions.

In the I-35 outcrop, the biomarkers specific to GSB (isorenieratane), brown GSB (paleorenieratane), and PSB (renierpurpurane) provide a base model for restriction and euxinia in the middle and upper Woodford. In Figure 52, relatively high amounts of paleorenieratane (up to 50 µg/g TOC) demonstrate a deep and persistent chemocline at 4, 16 and 43 feet. Renieratane and isorenieratane also have significant signatures at those depths, while renierpurpurane demonstrates minimal concentrations (only 4 µg/g TOC) at the bottom of the section Figure 37.

As seen in Figure 52, aryl isoprenoids do not follow a similar trend to the C₄₀ carotenoids, as peak abundance occurs at 26 feet. The fact that the intervals of higher aryl isoprenoids are slightly above the carotenoids indicates potentially declining euxinic conditions, as aryl isoprenoids are the diagenetic products of carotenoids. Using these fluctuations, a model for four instances of PZE onset and decline can be interpreted, as shown in Figure 52. Comparing evidence from other mass extinctions, such as the largest in history occurring at the Permian-Triassic transition (Erwin, 1994) can lend insight to the circumstances surrounding the Devonian biotic crisis. Similar to the late Devonian extinction, significant evidence for photic zone euxinia has also been presented for the Permian-Triassic Boundary (PTB), including elevated levels of aryl isoprenoids and C₄₀ carotenoids in the Paleotethys and Panthalassa Oceans, thus supporting global evidence of PZE (Grice et al., 2005; Hays et al., 2007).

Furthermore, the presence of DBT in the same beds with relatively high aryl isoprenoids and carotenoids is further proof of euxinia (Figure 52), as DBT is a proxy

for H₂S buildup (Hughes et al., 1995). The requirement of sulfur interaction during early diagenesis to form DBT indicates hydrogen sulfide abundance, which is a feature of PZE (Sinnighe Damste and de Leeuw, 1990).

In Figure 52, the model for PZE onset and diminishment is illustrated in context of the sequence stratigraphic model. The I-35 outcrop represents one of the few Woodford sections that have been geochemically modeled to include instances of PZE in the upper Woodford (Miceli-Romero, 2010; Connock, 2015; Degarmo, 2015; Villalba, 2016). This finding may be due to variable sampling for geochemical studies of the Woodford, or may indicate lateral variability in depositional conditions. Either way, the geochemical signatures in the I-35 outcrop definitively show the presence of deep and persistent water column stratification at several stratigraphic locations.

In light of recent models of terrigenous organic input for the PZE onset (Nabbefeld et al., 2010; Kaiho et al., 2013; Zhou et al., 2016), the I-35 outcrop provides a potential example for nutrient influx as a mechanism for oxygen consumption and depletion. As a case study, this model can be applied to the PTB as well. Fenton et al. (2007) demonstrated the elevated levels of terrestrial biomarkers (DBT, DBF, and biphenyl) just prior to the marine collapse at the PTB in Greenland, followed by an abrupt disappearance in signs of terrestrial plant input thereafter. Similar trends are displayed at other shallow marine PTB sections in Northern Italy (Sephton et al., 2005), and China (Wang and Visscher, 2007).

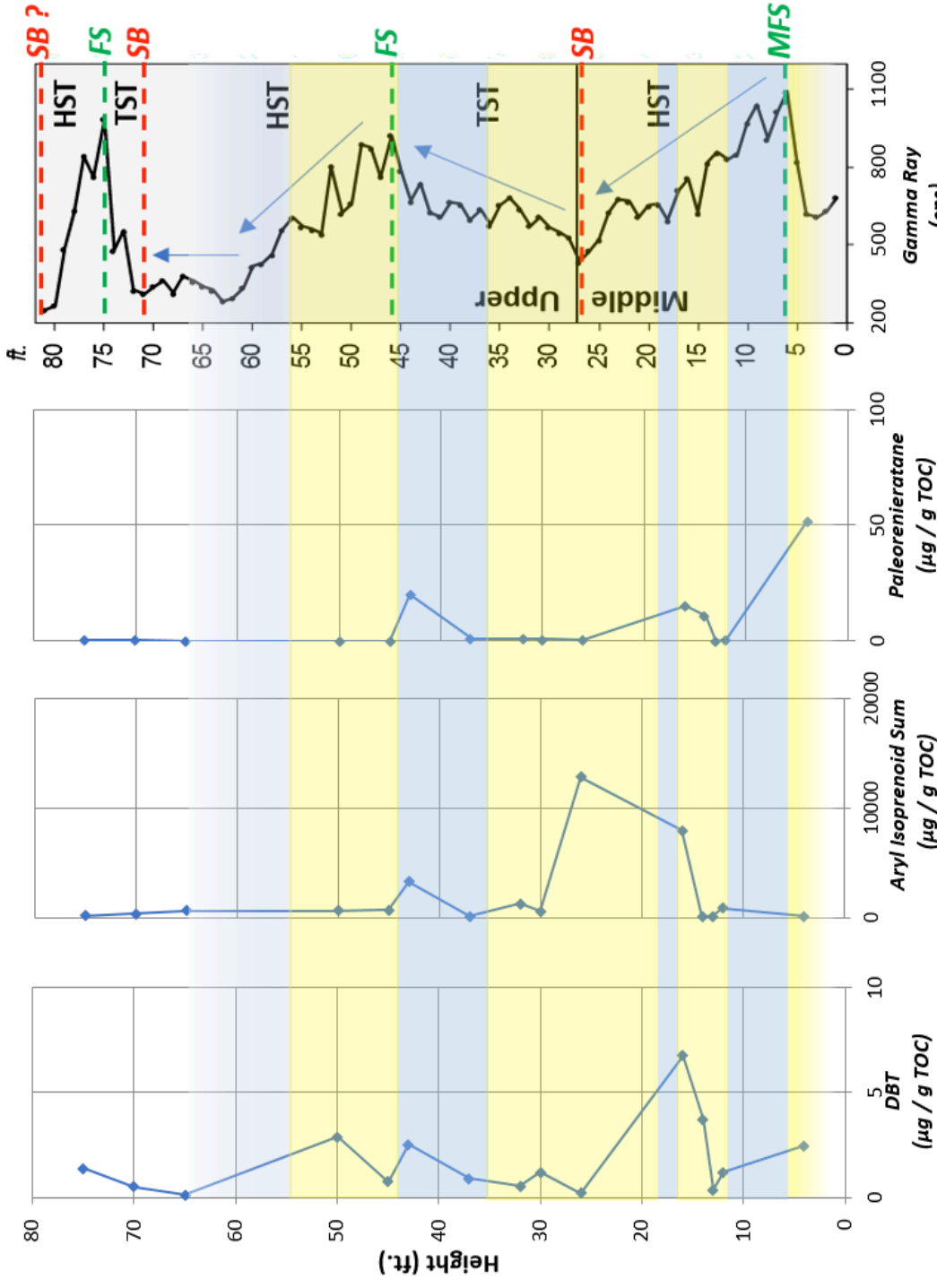


Figure 52. Inferred onset of euxinic conditions using DBT, sum of aryl isoprenoids, and paleorenieratane. Yellow= onset PZE, blue = diminishing PZE.

Using PAH biomarkers for terrestrial plant material from cadalene and DBF, and compounds known to associate specifically with conifer-type plants, like biphenyl, the signature of land plants was highest coinciding with peak PZE and gammacerane at 16 and 45-50 feet, then becomes depleted just after that depth (Marynowski et al., 2015; Figure 53). The slight difference in the prevalence of woody, conifer-type signatures (biphenyl) vs. general terrestrial plant signatures (cadalene and dibenzofuran) indicates that species of land plants were affected differently by the changing environmental conditions. The significance of terrigenous indicators coinciding with PZE and gammacerane (Figure 53) is that land plants, especially higher order, woody plants, evolved and were highly productive in the late Devonian. Kaiho et al. (2013) specifically correlated the onset of PZE with the excessive nutrient input coming from continental runoff. Based on these findings in the I-35 middle and upper Woodford, it is highly probable that the increased nutrient supply would cause marine bioproductivity, consuming the oxygen, and causing pervasive anoxic conditions. Using proxies for forest fires, such as benzo(g,h,i)perylene, increased combusted landplant signature at 16 feet seen in Figure 53 could be explained by increased forest fires during that period, which may be related to increasing global temperatures (Benton and Twitchett, 2003) and would contribute to shedding of continental organic material (Nabbefeld et al., 2010; Kaiho et al., 2013) to the Woodford basin. These instances of increased terrigenous input, potential forest fires, and PZE, followed by depletion of the signatures likely demonstrates collapses in both land and marine bioproductivity related to the F-F and D-C mass extinctions. Therefore, intervals highlighted in Figure 53, at ~16 and 50 feet have been identified as the most likely representation of the Kellwasser

and Hangenberg Crises, respectively. In light of this identification, it is plausible that that F-F boundary identified in Degarmo (2015) likely represents the Hangenberg event, rather than the F-F boundary. This would suggest that throughout much of the upper Woodford, evidence of the final ecological crisis that ended the Devonian period is present and can be identified using the biomarker and geochemical parameters used to define it in this thesis.

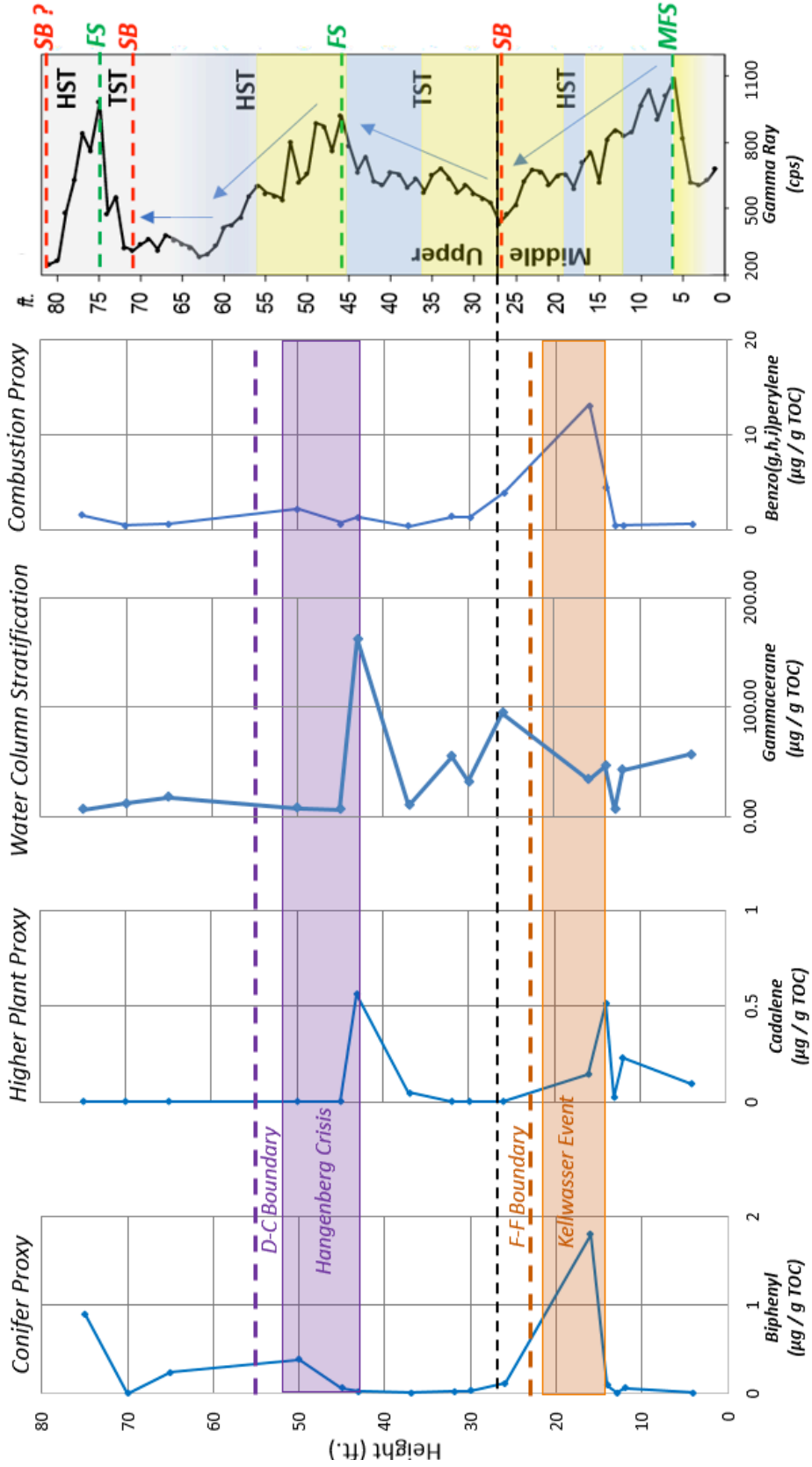


Figure 53. Comparison of interpreted Woodford PZE, higher-plant proxies, conifer proxy, water column stratification and combustion proxy.

V. CONCLUSIONS

An outcrop on I-35 in Carter County, Oklahoma, has revealed conditions associated with the Kellwasser and Hangenberg events. Previous studies of the organic geochemistry surrounding major marine biotic crises- which led to mass extinctions- have shown similar trends, including evidence of photic zone euxinia, terrestrial organic input, culminating in the collapse in both the terrestrial and marine ecosystem. In this study, the middle and upper Woodford have provided evidence for a potential mechanism for mass extinctions involving eutrophication of shallow marine settings, followed by increased bioproductivity, oxygen consumption and subsequent global euxinic seas. These harsh conditions are the likely cause of the end-Devonian mass extinction, one of the five largest in history.

The I-35 exposure of the Woodford has been identified as belonging to the middle and upper Woodford using both conodont biostratigraphy and gamma ray correlation (Over, 1990; Becerra-Rondon, 2017). Based on classic sequence stratigraphic models, its position starting near the maximum flooding surface would define this Woodford section as an HST interval with Type II marine organic sourcing (Slatt et al., 2012). Rock Eval data, sterane ratios, as well as the presence of 24-n-propylcholestanes, demonstrate the anticipated marine organic signature. Relatively higher amounts of C₂₉ sterane demonstrate the inclusion of some terrestrial input as well.

Certain biomarkers gave insight into lithologic features of the Woodford Shale. A higher presence of diasteranes, which require clay surfaces for catalysis, were most

abundant in units with the highest shale content, particularly between 30 and 45 feet. Conversely, chert-rich units were characterized by high relative amounts of tricyclic terpanes, which are indicative of *Tasmanites* and algal input. Upwellings causing chert deposition also provide nutrient-rich waters, causing algal and planktonic blooms, as seen by the tricyclic terpane signature.

By all conventional models, we would anticipate high levels of oxygenation and open marine circulation with higher sea level, yet biomarkers from this analysis point to some instances of anoxia and marine restriction. Increased abundance of gammacerane and DBT toward the bottom of the outcrop suggests water column stratification, hypersalinity, and H₂S abundance typically associated with restricted, reducing conditions. Furthermore, aryl isoprenoids and carotenoids from *Chlorobiaceae*, which require PZE for habitation, demonstrate the instances of euxinia in the basin during the end of Woodford deposition, associated with 4 periods of established water column stratification within this section of the Woodford. Two instances- once in the middle Woodford and once in the upper Woodford- demonstrate prominent stratification (~16 feet and 45-50 feet), where peak abundances of aryl isoprenoids, carotenoids, DBT, and gammacerane coincide, pointing to a distinct period of persistent PZE. It is here that this study finds evidence of ecologic stress that characterized the primary extinctions of the Devonian period; i.e. the Kellwasser and Hangenberg Events.

Biomarker evidence from terrestrial organic matter and pyrogenic origin paint a new picture for the cause of PZE. Marked by increased abundances of PAHs such as cadalene, perylene, dibenzofuran, etc., there is indication of increased terrestrial input

from land plants during the late Devonian likely upset marine life by contributing to harsh, anoxic conditions that killed off many species between the F-F and D-C boundaries. In the I-35 outcrop, the highest correlative surface of terrestrial organic matter coincides with the 16 and 45 foot beds, where the Kellwasser and Hangenberg Crises were identified. The coincidence of PZE conditions with excessive continental organic shedding demonstrates the relationship between the two features of Devonian biology. As described in recent literature, the excessive terrestrial organic matter deposited due to the diversification of land plants, likely overwhelmed the marine ecosystem, and eventually led to major destruction of Devonian life. The increased nutrients available caused blooming of marine fauna, followed by over-consumption of oxygen, and therefore O₂-poor waters. At these intervals, high amounts of organic matter are preserved under euxinic conditions, and when found, may point to a specific, regionally-correlative unit within the Woodford that could be rich in hydrocarbons. That is to say, in the case of the Woodford: characteristics necessary to develop a quality source rock occur due to the same conditions that led to one of the five largest mass extinctions in history (Nabbefeld et al., 2010; Zhou et al., 2016). The recognition of this mechanism for causing PZE in source rocks may contribute to the understanding of organic distributions in source rocks, and therefore play a potential role in oil and gas exploration.

References

- Alexander, R., Kagi, R., Woodhouse, G.W. (1981) Geochemical correlation of Windalia oil and extracts of Winning Group (Cretaceous) potential source rocks, Barrow Subbasin, Western Australia. *American Association of Petroleum Geologists Bulletin* **65**, 235-50.
- Alexander, R., Larcher, A.V., Kagi, R.I., Price, P.L. (1992) An oil-source correlation study using age-specific plant-derived aromatic biomarkers. In: Moldowan, J.M., Albrecht, P., Philp, R.P. (Eds.), *Biological Markers in Sediments and Petroleum 1992*. Prentice-Hall, Englewood Cliffs, New Jersey, 201-221.
- Algeo, T.J., Rowe, H. (2012) Paleoceanographic applications of trace-metal concentration data. *Chemical Geology* **324-325**, 6-18.
- Algeo, T.J., Scheckler, S.E. (1998) Terrestrial-marine teleconnections in the Devonian: links between evolution of land plants, weathering processes, and marine anoxic events. *Philosophical Transactions of the Royal Society of London 1998*, **353**, 113-30.
- Amsden, T.W. (1975) Hunton Group (Late Ordovician, Silurian, and Early Devonian) in the Anadarko Basin, Oklahoma. *Oklahoma Geological Survey Bulletin* **121**, 1-214.
- Aquino Neto, F.R., Restle, A., Connan, J., Albrecht P. and Ourisson, G. (1982) Novel tricyclic terpanes (C₁₉, C₂₀) in sediments and petroleums. *Tetrahedron Letters*, **23**, 2027-30.
- Aquino Neto, F.R., Trendel, J.M., Restle, A., Connan, J., Albrecht, P.A. (1983) Occurrence and formation of tricyclic terpanes in sediments and petroleums. M. Bjorøy (Ed.). In: *Advances in Organic Geochemistry 1981: International Conference Proceedings* John & Sons, New York. pp. 659-76.
- Arinobu, T., Ishiwatari, R., Kaiho, K., Lamolda, M.A., (1999) Spike in pyrosynthetic polycyclic aromatic hydrocarbons associated with an abrupt decrease in $\delta^{13}\text{C}$ of a terrestrial biomarker at the Cretaceous-Tertiary boundary at Caravaca, Spain. *Geology* **27**, 723-726.
- Becerra-Rondon, D. (2017) *University of Oklahoma M.S. Thesis*. Integrated Geological Characterization at the Bed Scale of the Woodford Shale at the I-35 Outcrop, Southern Oklahoma. 202 p.

- Becker, R.T., Gradstein, F.M., Hammer, O. (2012) The Devonian period. In: Gradstein, F.M. Ogg, J.G., Schmitz, M.D., Ogg, G.M. (Eds.), *The Geologic Time Scale 2012*. Elsevier, Amsterdam, **2**, 559-601.
- Benton, M.J., Twitchett, R.J. (2003) How to kill (almost) all life: the end-Permian extinction event. *Trends in Ecological Evolution* **18**, 358-367.
- Berner, R.A., Scott, M.R., and Thomlinson, C. (1970) Carbonate alkalinity in the pore waters of anoxic sediments. *Limnology and Oceanography*, **14**, 544-9.
- Blakey, R.C. (2011) Regional Paleogeography of North America: Late Devonian (360 Ma). Web page: <http://jan.ucc.nau.edu/rcb7/namD360.jpg>. Date accessed: March 15, 2017.
- Blumer, M. (1960) Pigments of fossil echinoderm. *Nature* **188**, 1100-1101.
- Blumer, M., Guillard, R. R. L. and Chase, T. (1971) Hydrocarbons of marine plankton. *Marine Biology*, **8**, 183-9.
- Brassell, S.C., Eglinton G., Maxwell, J.R. (1983) The geochemistry of terpenoids and steroids. *Biochemical Society Transcripts 1983*, **11**, 575-586.
- Brassell, S.C., Wardroper, A.M.K., Thompson, I.D., Maxwell, J.R. and Eglinton, G. (1981) Specific acyclic isoprenoids as biological markers of methanogenic bacteria in marine sediments. *Nature*, **290**, 693-6.
- Brocks, J.J., Schaeffer, P. (2008) Okenane, a biomarker for purple sulfur bacteria (Chromatiaceae), and other new carotenoid derivatives from the 1640 Ma Barney Creek Formation. *Geochimica et Cosmochimic Acta* **72**, 1396-1414.
- Brocks, J.J., Summons, R.E., (2014) Sedimentary Hydrocarbons, Biomarkers for Early Life. In: Turekian, K., Holland, H. (Eds.), *Treatise on Geochemistry 2nd Edition (8) 2014*. Elsevier, 61-103.
- Brown, T.C., Kenig, F. (2004) Water column structure during deposition of Middle Devonian-Lower Mississippian black and green/gray shales of the Illinois and Michigan basins: A biomarker approach. *Palaeogeography, Palaeoclimatology, Palaeoecology* **215**, 59-85.
- Cardott, B.J. (2012) Thermal maturity of Woodford Shale gas and oil plays, Oklahoma, USA. *International Journal of Coal Geology*, **103**, 109-119.

- Cardott, B.J. (2014) Woodford Shale Play Update: Expanded in the Oil Window: *American Association of Petroleum Geologists Search and Discovery Article* #80409.
- Chakhmakhchev, A., Suzuki, N. (1995) Aromatic sulfur compounds as maturity indicators for petroleum from the Buzuluk depression, Russia. *Organic Geochemistry* **23**, 617–625.
- Comer, J.B. (2008) Woodford Shale in southern Midcontinent, USA-Transgressive system tract marine source rocks on an arid passive continental margin with persistent oceanic upwelling: *American Association of Petroleum Geologists Annual Convention, San Antonio, Texas, April 20-23, 2008. Search and Discovery Article* #404026.
- Comer J. B., Hinch, H. H. (1987) Recognizing and quantifying expulsion of oil from the Woodford Shale and age-equivalent rocks in Oklahoma and Arkansas. *American Association of Petroleum Geologists Bulletin* **71**, 844-858.
- Connan J., Restle, A. and Albrecht, P. (1980) Biodegradation of crude oil in the Aquitaine Basin. A. G. Douglas and J. R. Maxwell (Eds.), *In: Advances in Organic Geochemistry 1979*. Pergamon Press, Oxford **12**, 1-17.
- Connock, G.T. (2015) Paleoenvironmental Interpretation of the Woodford Shale, Wyche Farm Shale Pit, Pontotoc County, Oklahoma with a Primary Focus on Water Column Chemistry and Structure. *M.S. Thesis, The University of Oklahoma*. 253 p.
- Cooke, M. P., Talbot, H. M. Farrimond, P. (2008) Bacterial populations recorded in bacteriohopanetriol distributions in soils from Northern England. *Organic Geochemistry* **39**, 1347-1358.
- Craig, L.C., Connor, C.W., Armstrong, A.K., Varnes, K.L., Mast, C.A., Kiteley, L.W., (1979) Paleotectonic investigations of the Mississippian System in the United States. *United States Geological Survey Professional Paper* **1010**, 1-559.
- Curiale J.A., Cole R.D., Witmer R.J. (1992) Application of organic geochemistry to sequence stratigraphic analysis. Four Corners Platform area, New Mexico, U.S.A., *Organic Geochemistry*, **19 (1-3)**, 53-75.
- Czochanska, Z., Gilbert, T.D., Philp, R.P. (1988) Geochemical application of sterane and triterpene biomarkers to a description of oils from the Taranaki Basin in New Zealand. *Organic Geochemistry* **12**, 123-35.

- Dahle, S., Savinov, V.M., Matishov, G.G., Evenset, A., Naes, K. (2003) Polycyclic aromatic hydrocarbons (PAHs) in bottom sediments of the Kara sea shelf, Gulf of Ob and Yenisei bay. *The Science of the Total Environment* **306**, 57-71.
- Didyk, B.M, Simoneit, B.R.T., Brassell, S.C., and Eglinton, G. (1978) Organic geochemical indicators of palaeoenvironmental conditions of sedimentation. *Nature* **272**, 216-22.
- DeGarmo, D. C. (2015) Geochemical Characterization of the Woodford Shale (Devonian-Mississippian), McAlister Cemetery Quarry, Criner Hills Uplift, Ardmore Basin, Oklahoma. *University of Oklahoma M.S. Thesis*. 198 p.
- Durand, B. (1980) Kerogen. *Insoluble Organic Matter From Sedimentary Rocks*. Editions Technip, Paris. 13-14.
- Edwards, D.S., Summons, R.E., Kennard, J.M., Nicoll, R.S., Bradshaw, J., Bradshaw, M., Foster, C.B., O'Brien, G.W., Zumberge, J.E. (1997) Geochemical characterization of Paleozoic petroleum systems in northwestern Australia. *The APPEA Journal* **37**, 351-379.
- Eglinton G. and Calvin M. (1967) Chemical fossils. *Scientific American* **261**, 32-43.
- Eglinton G. and Hamilton R.J. (1967) Leaf epicuticular waxes. *Science*, **156**, 1322-35.
- Ellison, S.P. Jr. (1950) Subsurface Woodford black shale, west Texas and southeast New Mexico: University of Texas, Bureau of Economic Geology, Report of Investigations **7**, 20.
- Ensminger, A., Albrecht, P., Ourisson, G., and Tissot, B. (1977) Pentacyclic triterpanes of the hopane type as ubiquitous geochemical markers: origin and significance. B. Tissot and F. Bienner, (Eds.) In: *Advances in Organic Geochemistry 1973 Editions Technip, Paris*, 245-66.
- Erwin, D.H. (1994) The Permo-Triassic extinction. *Nature* **367**, 231-236.
- Fang, R., Li, M., Wang, T.-G., Zhang, L., Shi, S. (2015). Identification and distribution of pyrene, methylpyrenes and their isomers in rock extracts and crude oils. *Organic Geochemistry* **83-84**, 65-76
- Fenton, S., Grice, K., Twitchett, R.J., Böttcher, M.E., Looy, C.V., Nabbefeld, B. (2007) Changes in biomarker abundances and sulfur isotopes of pyrite across the Permian-Triassic (P/Tr) Schuchert Dal section (East Greenland). *Earth Planetary Science Letters* **262**, 230-239.

- Gagosian, R.B., Smith, S.O., Lee, C., Farrington, J.W. (1979) Douglas, A.G., Maxwell, J.R. (Eds.). Steroid transformation in recent marine sediments. *Advances in Organic Geochemistry 1979*, 407-419.
- Galvis, H.A., 2017. Detailed Lithostratigraphic Characterization and Sequence Stratigraphy of a complete Woodford Shale Outcrop Section in Southern Oklahoma. M.S. thesis, University of Oklahoma, 169 p.
- Galvis-Portilla, H., Becerra-Rondon, D., Duarte, D., and Slatt, R.M. (2016) Rock and Fracture Characterization of the Woodford Shale along the I-35 Outcrop. *American Association of Petroleum Geologists Search and Discovery Article #51240*.
- Galvis-Portilla, H., Becerra-Rondon, D., Slatt, R.M. (2017) Let's Make Outcrops Recover Their Value, Understanding the Rocj on the Surface for Predicting into the Subsurface: Woodford Shale Case Study, Ardmore Basin, Oklahoma. *American Association of Petroleum Geologists Search and Discovery Article #10907*.
- Goossens, H., De Leeuw, J.W., Schenk, P.A. and Brassell S.C. (1984) Tocopherols as likely precursors of pristane in ancient sediments and crude oils. *Nature* **184**, 440-442.
- Grantham, P.J (1986) The occurrence of unusual C27 and C29 sterane predominances in two types of Oman crude oil. *Organic Geochemistry* **9**, 1-10.
- Grice K., Schaeffer P., Schwark L., Maxwell, J.R. (1996) Molecular indicators of palaeoenvironmental conditions in an immature Permian shale (Kupferschiefer, Lower Rhine Basin, north-west Germany) from free and S-bound lipids. *Organic Geochemistry* **25**, 131-147.
- Grice, K., Backhouse, J., Alexander, R., Marshall, N., Logan, G.A. (2005) Correlatin terrestrial signatures from biomarker distributions , $\delta^{13}C$, and palynology in fluvio-deltaic deposits from NW Australia (Triassic-Jurassic). *Organic Geochemistry* **36**, 1347-1358.
- Grice, K., Nabbefeld, B., Maslen, E. (2007). Source and significance of selected polycyclic aromatic hydrocarbons in sediments (Hovea-3 well, Perth Basin, Western Australia) spanning the Permian-Triassic boundary. *Organic Geochemistry* **38**, 1795-1803.

- Grice, K., Lu, H., Atahan, P., Asif, M., Hallman, C., Greenwood, P., Maslen, E., Tulipani, S., Williford, K., Dodson, J. (2009) New insights into the origin of perylene in geological samples. *Geochimica et Cosmochimica Acta* **73**, 6531
- Grimalt, J.O., van Drooge, B.L., Ribes, A., Fernandez, P., Ableby, P. (2004) Polycyclic aromatic hydrocarbon composition in soils and sediments of high altitude lakes. *Environmental Pollution* **131**, 13-24.
- Gross, D., Sachsenhofer, R.F., Bechtel, A., Pytlak, L., Rupprecht, B., Wegerer, E. (2015) Organic geochemistry of Mississippian shales (Bowland Shale Formation) in central Britain: Implications for depositional environment, source rock and gas shale potential. *Marine and Petroleum Geology* **59**, 1-21.
- Hackley, P.C., Cardott, B.J. (2016) Application of organic petrography in North American shale petroleum systems: A review. *International Journal of Coal Geology*, **163**, 8-51.
- Hall, P.B., Schou, L., Bjoroy, M., (1984) Aromatic hydrocarbon variations in North Sea Wells. In: Thomas, B.M., et al. (Eds.), *Petroleum Geochemistry in Exploration of Norwegian Shelf*, Norwegian Petroleum Society . Graham and Trotman Ltd., London, U.K., 293-301.
- Ham, W.E., Denison, R.E., Merritt C.A. (1964) Basement rocks and structural evolution of Southern Oklahoma. *Oklahoma Geological Survey Bulletin* **95**, 1-302.
- Ham, W.E., Wilson, J.L. (1967) Paleozoic epeirogeny and orogeny in the central United States. *American Journal of Science* **265**, 332-407.
- Hays, L.E., Beatty, T., Henderson, C.M., Love, G.D., Summons, R.E. (2007) Evidence for photic zone euxinia through the end-Permian mass extinction in the Panthalassic Ocean (Peace River Basin, Western Canada). *Paleoworld* **16** (1-3), 39-50.
- Hays, L.E., Grice, K., Foster, C.B., Summons, R.E. (2012) Biomarker and isotopic trends in a Permian-Triassic sedimentary section at Kat Stosch, Greenland. *Organic Geochemistry* **43**, 67-82.
- Hester, T.C., Sahl, H.L., Schmoker, J.W. (1988) Cross sections based on gamma-ray, density and resistivity logs showing stratigraphic units of the Woodford Shale, Anadarko basin, Oklahoma. *United States Geological Survey Bulletin* **1866-D**, 1-38.

- Hester, T.C., Schmoker, J.W., Sahl, H.L. (1990) Log-derived regional source rock characteristics of the Woodford Shale, Anadarko basin, Oklahoma: U.S. *Geological Survey Bulletin* **1866-D**, 38 p.
- Holba, A.G., Tegelaar, E., Ellis, L., Singletary, M.S., Albrecht, P. (2000) Tetracyclic polyprenoids: indicators of freshwater (lacustrine) algal input. *Geology* **28**, 251-254.
- Huang W. Y., Meinschein, W. G. (1979) Sterols as ecological indicators. *Geochimica et Cosmochimica Acta* **43**, 739-45.
- Hughes W. B. (1984) Use of thiophenic organosulfur compounds in characterizing crude oils derived from carbonate versus siliclastic sources. In Petroleum Geo-chemistry and Source Rock Potential of Carbonate Rocks. Palacas J. B. (Eds.), *American Association of Petroleum Geologists Student Geology 1984* **18**, 181-196.
- Hughes, W. B., Holba, A. G., Dzou, L. I. P. (1995) The ratios of dibenzothiophene to phenanthrene and pristane to phytane as indicators of depositional environment and lithology of petroleum source rocks. *Geochimica et Cosmochimica Acta*, **59** 3581-3598.
- Imhoff, J.F. (1995) Taxonomy and physiology of phototrophic purple bacteria and green sulfur bacteria. *Anoxygenic Photosynthetic Bacteria* 1-15.
- Infante-Paez, L., Cardona, L-F., McCullough, B., and Slatt, R. (2016) Seismic analysis of paleotopography and stratigraphic controls on total organic carbon: Rich sweet spot distribution in the Woodford Shale, Oklahoma, USA. *Interpretation*, **5**, T33-T47.
- Isaksen G. H. and Bohacs K.M. (1995) Geologic Controls of Source Rock Geochemistry Through Relative Sea Level: Triassic, Barents Sea. B. J. Katz (Eds.), In: *Petroleum Source Rocks*. Springer-Verlag, Berlin Heidelberg. 25-50.
- Jarvie, D.M. (2001) Williston Basin petroleum systems: inferences from oil geochemistry and geology. *Mountain Geologist* **38**, 19-42.
- Jiang, C., Alexander, R., Kagi, R.I., and Murray, A.P. (1998) Polycyclic aromatic hydrocarbons in ancient sediments and their relationships to paleoclimate. *Organic Geochemistry*, **29 (5-7)**, 1721-1735.

- Jiang, C. (1998). Polycyclic Aromatic Hydrocarbons and their Geochemical Significance. Application to Sediments from the Northern Carnarvon Basin. *Ph.D. Thesis, Curtin University of Technology, Australia.*
- Johnson, J.G., Klapper, G., Sandberg, C.A. (1985) Devonian eustatic fluctuations in Euramerica. *Geological Society of America Bulletin*, **96**, 567-587.
- Johnson, K.S. (2008) Geologic History of Oklahoma. *Oklahoma Geological Survey: Educational Publication 9*, 2-9.
- Johnson K. S., Amsden T. W., Denison R. E., Dutton S. P., Goldstein A. G., Rascoe Jr. B., Sutherland P. K. and Thompson D. M. (1989) Geology of the southern Midcontinent. *Oklahoma Geological Survey Special Publication 89-2*, 1-53.
- Johnson K. S. and Cardott B. J. (1992) Geologic framework and hydrocarbon source rocks of Oklahoma. *Oklahoma Geological Survey Circular 93*, 21-37.
- Jones, R. W., (1987). Organic facies. J. Brooks and D. Welte, (Eds.), In: *Advances in Petroleum Geochemistry 1987*. Academic Press, New York, 1-90.
- Kaiho, K., Yatsu, S., Oba, M., Gorjan, P., Casier, J.G. Ikeda, M. (2013) A forest fire and soil erosion event during the Late Devonian mass extinction. *Palaeogeography, Palaeoclimatology, Palaeoecology* **392**, 272-280.
- Kaiser, S.I., Aretz, M., Becker, R.T. (2015) The global Hangenberg Crisis (Devonian-Carboniferous transition): review of a first-order mass extinction. *Geological Society of London, Special Publications 2015*, **423**, 387-437.
- Katz, B. J. (1995) Petroleum Source Rocks- an Introductory Overview. In: *Petroleum Source Rocks*. Springer-Verlag, Berlin Heidelberg, 1-8.
- Khan, H., Zaman, A., Chetty, G.L., Gupta, A.S. Dev, S. (1971) Cheilanthatriol a new fundamental type in sesterpenes. *Tetrahedron Letters* **12**, 4443-4446.
- Killops, S.D., Massoud, M.S., (1992) Polycyclic aromatic hydrocarbons of pyrolytic origin in ancient sediments: evidence for Jurassic vegetation fires. *Organic Geochemistry* **18**, 1-17.
- Köster, J., Van Kaa-Peters, H.M.E., Koopmans, M.P. (1997) Sulphurisation of homohopanoids: effects on carbon number distribution, speciation, and 22S/22R epimer ratios. *Geochimica et Cosmochimica Acta* **61**, 2431-52.

- Laflamme, R.E., Hites, R.A. (1978) The global distribution of polycyclic aromatic hydrocarbons in recent sediments. *Geochimica et Cosmochimica Acta* **42**, 289-303.
- Langford, F.F., Blanc-Valleron (1990) Interpreting Rock-Eval Pyrolysis Data Using Graphs of Pyrolizable Hydrocarbons vs. Total Organic Carbon. *American Association of Petroleum Geologists Bulletin*, **74**, 799-804.
- Larter S. R., Bowler, F. Li, M., et al. (1996) Benzocarbozoles as molecular indicators of secondary oil migration distance. *Nature* **383**, 593-7.
- Lewan, M.D. (1983) Effects of thermal maturation on stable organic carbon isotopes as determined by hydrous pyrolysis of Woodford Shale. *Geochimica et Cosmochimica Acta* **47**, 1471-1479.
- Lewan, M.D. (1992) Primary oil migration and expulsion as determined by hydrous pyrolysis. *13th World Petroleum Congress* **2**, 215-223.
- Li, M., Shi, S., Wang T.-G. (2012) Identification and distribution of chrysene, methylchrysenes and their isomers in crude oils and rock extracts. *Organic Geochemistry* **52**, 55-66.
- Li, M., Zhong, N., Shi, S., Zhu, L., Tang, Y. (2013) The origin of trimethyldibenzothiophenes and their application as maturity indicators in sediments from the Liaohe Basin, East China. *Fuel* **103**, 299-307.
- Lichtfouse, E., Budzinski, H., Garrigues, P., Eglinton, T.I. (1997) Ancient polycyclic aromatic hydrocarbons in modern soils: ¹³C, ¹⁴C and biomarker evidence. *Organic Geochemistry* **26**, 353-359.
- Lo, H.B., Cardott, B.J. (1995) Detection of natural weathering of Upper McAlester coal and Woodford Shale, Oklahoma, U.S.A. *Organic Geochemistry* **22**, 73-83.
- Long, J.A., Trinajstic, K. (2010) The Late Devonian Gogo Formation lagerstatten of Western Australia: exceptional early vertebrate preservation and diversity. *Annual Review of Earth and Planetary Science* **38**, 255-279.
- Mackenzie, A.S., Lamb, N.A., Maxwell, J.R. (1982) Steroid hydrocarbons and the thermal history of sediments. *Nature* **295**, 223-6.
- Manes, L.V., Crews, P., Kernan, M.R., Faulkner, D.J., Fronczek, F.R., Gandour, R.D., 1988. Chemistry and revised structure of suvanine. *Journal of Organic Chemistry* **53**, 570-575.

- Marynowski, L., Filipiak, P. (2007) Water column euxinia and wildfire evidence during the deposition of the Upper Famennian Hangenberg event horizon from the Holy Cross Mountains (Central Poland). *Geology Magazine* **144**, 569-595.
- Marynowski, L., Kubik, R., Uhl, D., Simoneit, B.R.T. (2014) Molecular composition of fossil charcoal and relationship with incomplete combustion of wood. *Organic Geochemistry* **77**, 22-31.
- Marynowski L., Narkiewicz M., Grelowski C. (2000) Biomarkers as environmental indicators in a carbonate complex, examples from the Middle Devonian, the Holy Cross Mountains, Poland. *Sedimentary Geology* **137**, 187-212.
- Marynowski L., Rakociński M., Borcuch E., Kremer B., Schubert B. A. and Jahren A. H. (2011) Molecular and petrographic indicators of redox conditions and bacterial communities after the F/F mass extinction (Kowala, Holy Cross Mountains, Poland). *Palaeogeography, Palaeoclimatology, Palaeoecology* **306**, 1-14.
- Marynowski, L., Smolarek, J., Hautevelle, Y. (2015) Perylene degradation during gradual onset of organic matter maturation. *International Journal of Coal Geology* **139**, 17-25.
- McCullough, B.J., 2014, Sequence-stratigraphic Framework and Characterization of the Woodford Shale on the Southern Cherokee Platform of Central Oklahoma. *M.S. Thesis, University of Oklahoma, Norman, Oklahoma*, 212 p.
- McGhee, G.R. (1981) Evolutionary replacement of ecological equivalents in Late Devonian benthic marine communities. *Palaeogeography, Palaeoclimatology, Palaeoecology* **34**, 267-283.
- McGhee, George R. (1996) The Late Devonian Mass Extinction: The Frasnian/Famennian Crisis. *Columbia University Press*, 303.
- Mello, M.R., Gaglianone, P.C., Brassel, S.C., Maxwell, J.R. (1988) Geochemical and biological marker assessment of depositional environments using Brazilian offshore oils. *Marine and Petroleum Geology* **5**, 205-23.
- Meissner, F. F. (1978) Petroleum Geology of the Bakken Formation, Williston Basin, North Dakota, and Montana. In: *Williston Basin Symposium 1978*, Billings, Montana, 207-227.

- Miceli-Romero, A.A. (2010) Geochemical Characterization of the Woodford Shale, Central and Southeastern Oklahoma. *M.S. Thesis, The University of Oklahoma*. 289 p.
- Miceli-Romero, A., Philp, R.P. (2012) Organic geochemistry of the Woodford Shale, southeastern Oklahoma: How variable can shales be? *American Association of Petroleum Geologists Bulletin*, **96**, 493-517.
- Mizukami, T., Kaiho, K., Oba, M. (2013) Significant changes in land vegetation and oceanic redox across the Cretaceous/Paleogene boundary. *Palaeogeography, Palaeoclimatology, Palaeoecology* **369**, 41-47.
- Mizukami, T., Kaiho, K., Oba, M. (2014). A spike of woody plant biomarkers in the deep-sea iridium layer at the Cretaceous/Paleogene boundary. *Palaeogeography, Palaeoclimatology, Palaeoecology* **412**, 241-248.
- Moldowan, J.M., Lee, C.Y., Sundararaman, P. (1992) Source correlation and maturity of select oils and rocks from the Central Adriatic Basin (Italy and Yugoslavia). J.M. Moldowan, P. Albrecht and R.P. Philp, (Eds.), In: *Biological Markers in Sediments and Petroleum*. Prentice-Hall, Englewood Cliffs, NJ, 370-401.
- Moldowan, J. M., Seifert, W. K. (1979) Head-to-head linked isoprenoid hydrocarbons in petroleum. *Science* **204**, 169-71.
- Moldowan, J. M., Seifert, W. K. and Gallegos, E. J. (1985) Relationship between petroleum composition and depositional environment of petroleum source rocks. *American Association of Petroleum Geologists Bulletin* **69**, 1255-68.
- Nabbefeld, B., Grice, K., Summons, R.E., Lindsay, E.H., Cao, C. (2010) Significance of polycyclic aromatic hydrocarbons (PAHs) in Permian/Triassic boundary sections. *Applied Geochemistry* **25**, 1374-1382.
- Nes, W.R., McKean, M.L. (1977) *Biochemistry of Steroids and Other Isopentenoids*. University Park Press, Baltimore. 690 p.
- Nowaczewski, V. (2011) Biomarker and paleontological investigations of the late Devonian extinctions, Woodford Shale, Southern Oklahoma. *University of Kansas M.S. Thesis*. 96 p.
- Ourisson, G., Albrecht, P., Rohmer, M. (1979) The hopanoids. Palaeochemistry and biochemistry of a group of natural products. *Pure and Applied Chemistry* **51**, 706-729.

- Over, D.J. (1990) Conodont Biostratigraphy of the Woodford Shale (Late Devonian-Early Carboniferous) In the Arbuckle Mountains, South-Central Oklahoma. *Texas Tech University Ph.D. Dissertation*. 174 p.
- Over, D.J. (1992) Conodonts and the Devonian-Carboniferous Boundary in the Upper Woodford Shale, Arbuckle Mountains, South-Central Oklahoma. *Journal of Paleontology* **66**, 293-311.
- Ourisson, G., Albrecht, P., Rohmer, M. (1982) Predictive microbial biochemistry – from molecular fossils to prokaryotic membranes. *Trends in Biochemical Sciences* **7**, 236-239.
- Ourisson, G., Albrecht P. (1992) hopanoids: 1. Geohopanoids: The most abundant natural products on Earth? *Accounts of Chemical Research* **25**, 398-402.
- Pastorova, I., Botto, R.E., Arisz, P.W., Boon, J.J. (1994) Cellulose char structure: a combined analytical Py-GC-MS, FTIR, and NMR study. *Carbohydrate Research* **262**, 27-47.
- Paxton, S.T., Olsen, T., Price, C., Gross, E., and Allison, S. 2015. Spectral Gamma-Ray Profile of Woodford Shale - OHMEGCO Locality, Oklahoma. PowerPoint presentation prepared for Ardmore Geological Society, January. 108 slides.
- Peters, K. E. (1986) Guidelines for evaluating petroleum source rock using programmed pyrolysis. *American Association of Petroleum Geologists Bulletin*, **70**, 318-29.
- Peters, K.E. and Cassa, M.R. (1994) Applied source rock geochemistry. L.B. Magoon and W.G. Dow (Eds.), In: *The Petroleum System – From Source to Trap*, American Association of Petroleum Geologists, Tulsa, OK, 93-117.
- Peters, K.E., Walters, C.C., Moldowan, J.W. (2005) *The Biomarker Guide; Volume 1- Biomarkers and Isotopes in the Environment and Human History, 2nd Edition*. p. 1155. Cambridge University Press, New York.
- Peters, K.E., Walters, C.C., Moldowan, J.W. (2005) *The Biomarker Guide; Volume 2- Biomarkers and Isotopes in Petroleum Exploration and Earth History, 2nd Edition*. p. 471. Cambridge University Press, New York.
- Radke M., Welte, D.H. (1981) The Methylphenanthrene Index (MPI): A maturity parameter based on aromatic hydrocarbons. *Advances in Organic Geochemistry*, 504-512.

- Radke, M., Vriend, S.P., Ramanampisoa, L.R. (2000) Alkyldibenzofurans in terrestrial rocks: influence of organic facies and maturation. *Geochimica et Cosmochimica Acta* **64**, 275-286.
- Raederstorff, D. and Rohmer, M. (1984) Sterols of the unicellular algae *Nematochryopsis roscoffensis* and *chrysochlorella lamellosa*: isolation of (24E)-24-n-propylidenecholesterol and 24-n-propylcholesterol. *Phytochemistry*, **23**, 2835-8.
- Repeta, D.J., Simpson, D.J., Jorgenson, B.B., Jannasch HW (1989) Evidence for anoxygenic photosynthesis from the distribution of bacteriochlorophylls in the Black Sea. *Nature*, **342**, 69-72.
- Requejo A. G., Allan J., Creaney S., Gray N. R. and Cole K. S. (1992) Aryl isoprenoids and diaromatic carotenoids in Paleozoic source rocks and oils from the Western Canada and Williston Basins. In *Advances in Organic Geochemistry 1991* (Edited by Eckardt C. B. et al.), *Organic Geochemistry* **19**, 245-264. Pergamon Press, Oxford.
- Roberts, C.T. and Mitterer R.M. (1992) Laminated black shale-bedded chert cyclicity in the Woodford Formation, southern Oklahoma, In: *K.S. Johnson and B.J. Cardott, eds., Source rocks in the southern Midcontinent, 1990 symposium: OGS Circular* **93**, 330-336.
- Rodriguez, N. D., and Katz, B. J. (2017). The Effect of Oil Based Drilling Mud (OBM) on the Assessment of Hydrocarbon Charge Potential: Are We Underestimating Source Rock Potential? *Presented at the Annual Meeting of the American Association of Petroleum Geologists*. April 2-5, 2017, Houston, Texas.
- Rohmer, M., Bouvier-Nave, P., Ourisson, G., (1984) Distribution of hopanoid triterpanes in prokaryotes. *Journal of General Microbiology* **130**, 1137-1150.
- Rontani, J. F. and Volkman J. K. (2003) Phytol degradation products as biogeochemical tracers in aquatic environments. *Organic Geochemistry*, **34**, 1-35.
- Rubinstein, I., Sieskind, O., and Albrecht, P. (1975) Rearranged sterenes in a shale: occurrence and simulated formation. *Journal of Chemical Society, Perkin Transaction I*, 1833-6.
- Sandberg, C.A., Ziegler, W., Dreesen, R., Butler, J.L. (1988) Part 3: Late Frasnian mass extinction: conodont event stratigraphy, global changes, and possible causes. *Courier Forschung-Intitut Senckenberg* **102**, 263-307.

- Schoell, M., Teschner, M., Wehner, H., Durand, B., and Oudin, J.L. (1983) Maturity related biomarker and stable isotope variations and their application to oil/source rock correlation in the Mahakam Delta, Kalimantan. In: *Advances in Organic Geochemistry 1981*, 156-63.
- Seifert W. K. and Moldowan J. M. (1980) The effect of thermal stress on source-rock quality as measured by hopane stereochemistry. *Physics and Chemistry of the Earth* **12**, 229-237.
- Sepkoski, J. J., Jr. (1996) Patterns of Phanerozoic Extinction: a Perspective from Global Data Bases; in Walliser, Otto H. (ed.), *Global Events & Event Stratigraphy in the Phanerozoic*, 35-51.
- Serna-Bernal, A. (2013) Geological Characterization of the Woodford Shale, McAlister Cemetary Quarry, Criner Hills, Ardmore Basin, Oklahoma. *M.S. Thesis, The University of Oklahoma*. 141 p.
- Sephton, M.A., Looy C.V., Brinkhuis, H., Wignall, P.B., de Leeuw, J.W., Visscher, H. (2005) Catastrophic soil erosion during the end-Permian biotic crisis. *Geology* **33**, 41-944.
- Silliman, J.E., Meyers P.A., Ostrom, N.E., Eadie, B.J. (2000) insights into the origin of perylene based on its low abundance in sediments of Green Bay, Wisconsin. *Chemical Geology*, **177**, 309-322.
- Simoneit, B.R.T. (1986) Cyclic terpenoids of the geosphere. In: Johns, R.B. (Ed.), *Biological Markers in the Sedimentary Record*. Elsevier, New York, 43-99.
- Sinninghe Damste, J.S., Kenig, F., Koopmans, M.P. (1995) Evidence of gammacerane as an indicator of water column stratification. *Geochimica et Cosmochimica Acta* **59**, 1895-1900.
- Sinninghe Damste, J.S., Kock-Van Dalen, A.C., de Leeuw, Schneck, P.A., Sheng, G., Brassell, S.C. (1987) The identification of mono-, di-, and trimethyl 2-methyl-2-(4,8,12-trimethyltricyclic)chromans and their occurrence in the geosphere. *Geochimica et Cosmochimica Acta*, **51**, 2393-2400.
- Sinninghe Damsté, J.S., de Leeuw, J.W. (1990) Analysis, structure and geochemical significance of organically-bound sulfur in the geosphere: state of the art and future research. *Organic Geochemistry* **16**, 1077-1101.
- Sinninghe Damste, J.S., Schouten, S. (2006) Biological markers for anoxia in the photic zone of the water column. In: Volkman, J. (Ed.), *Marine Organic*

Matter: Biomarkers, Isotopes and DNA. *The Handbook of Environmental Chemistry*, 127-163. Springer, Berlin/Heidelberg.

- Slatt, R. M. (2013) *Stratigraphic Reservoir Characterization For Petroleum Geologists, Geophysicists, and Engineers: Origin, Recognition, Initiation, and Reservoir Quality*. In: *Developments in Petroleum Science*. Second Edition. p. 1-671. Elsevier, Netherlands.
- Slatt, R.M., Molinares-Blanco, C. , Amorocho, J.D., Cabarcas, C.L., Torres-Parada, E. (2014) Sequence Stratigraphy, Geomechanics, Microseismicity, and Geochemistry Relationships in Unconventional Resource Shales. *Proceedings from the 2nd Unconventional Resources Technology Conference: URTeC #1934195*.
- Slatt, R.M., and Abousleiman Y. (2011) Merging sequence stratigraphy and geomechanics. *Lead Edge*, March 2001, 274-282.
- Slatt, R.M., Philp, R.P., Abousleiman, Y., Singh, P., Perez, R., Portas, R., Marfurt, K.J., Madrid-Arroyo, S., O'Brian, N., Eslinger, E., Baruch, E.T. (2012) Pore-to-regional-scale integrated workflow for the unconventional gas shales, in J. A. Breyer, ed., *Shale reservoirs- Giant resources for the 21st century: American Association of Petroleum Geologists Memoir 97*, 127-150
- Slatt R. M., and Rodriguez N. D. (2012) Comparative sequence stratigraphy and organic geochemistry of gas shales: Commonality or coincidence? *Journal of Natural Gas Science and Engineering* **8**, 68-84.
- Slatt R.M. (2013) Paleotopographic and Depositional Environment Control on 'Sweet Spot' Locations in Some Unconventional Resource Shales. *Presented at Houston Geological Society, 2013*.
- Smith, H. M. (1968) Qualitative and quantitative aspects of crude oil composition. *US Bureau of Mines Bulletin*, **642**, 1-136.
- Stout, S.A., Emsbo-Mattingly, S.D., Douglas, G.S., Uhler, A.D., McCarthy, K.J., (2015) Beyond 16 Priority Pollutant PAHs: A Review of PACs used in Environmental Forensic Chemistry. *Polycyclic Aromatic Compounds*, **35**, 285-315.
- Stout, S.A., Uhler, A.D., McCarthy, K.J. (2001) A Strategy and Methodology for Defensibly Correlating Spilled Oil to Source Candidates. *Environmental Forensics* **2**, 87-98.

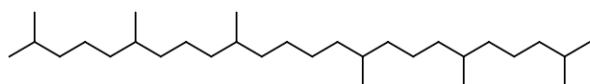
- Summons R.E., Powell, T.G. (1986) chlorobiaceae in Paleozoic seas revealed by biological markers, isotopes and geology. *Nature* **319**, 763-765.
- Summons R.E., Powell, T.G. (1987) Identification of arylisoprenoids in source rocks and crude oils: Biological markers for the green sulfur bacteria. *Geochimica et Cosmochimica Acta* **51**(3), 557-566.
- Tissot, B.P., Welte, D.H (1984) Petroleum formation and occurrence. Berlin Springer-Verlag, 699.
- Turner, B.W. (2016) Utilization of Chemostratigraphic Proxies for Generating and Refining Sequence Stratigraphic Frameworks in Mudrocks and Shales. *Ph.D. dissertation, The University of Oklahoma*. 135 p.
- Turner B.W., Slatt, R.M. (2016) Assessing bottom water anoxia within the Late Devonian Woodford Shale in the Arkoma Basin, southern Oklahoma. *Marine and Petroleum Geology* **78**, 536-546.
- Turner B. W., Molinares-blanco C. E. and Slatt R. M. (2015) Special section: Shale paleoenvironments stratigraphic analysis of the Woodford Shale , Wyche Farm Quarry, Pontotoc County, Oklahoma. *Interpretation* **3**, SH1–SH9.
- U.S. Energy Information Administration, 2015. 2014 Annual Energy Outlook.
- van Aarssen, B.G.K., Bastow, T.P., Alexander, R., Kagi, R.I. (1999). Distribution of methylated naphthalenes in crude oils: indicators of maturity, biodegradation, and mixing. *Organic Geochemistry* **30**, 1213-1227.
- van Aarssen, B.G.K., Alexander, R., and Kagi, R.I. (2000) Higher plant biomarkers reflect paleovegetation changes during the Jurassic times. *Geochimica et Cosmochimica Acta* **64**, 1417-1424.
- van Krevelen, D.W. (1961) *Coal*. Elsevier, New York. 113-120.
- Van Wagoner J. C., Posamentier H.W., Mitchum R. M., Vail P. R., Sarg J. F., Louit T. S. and Hardenbol J. (1988) An Overview of the fundamentals of sequence stratigraphy and key definitions. In: *Sea-Level Changes—An Integrated Approach*. Society of Economic Paleontology and Mineralogy Special Publication **42**, 39-45.
- Vila, X., Abella, C.A. (1994) Effects of light quality on the physiology and the ecology of planktonic green sulfur bacteria and lakes. *Photosynthesis Research* **41**, 53-65.

- Villalba, D.M. (2016) Organic geochemistry of the Woodford Shale, Cherokee Platform, OK and its role in a complex petroleum system. *M.S. thesis, The University of Oklahoma*. 126 p.
- Volkman, J.K., Allen, D.I., Stevenson, P.L., Burton, H.R. (1986) Bacterial and algal hydrocarbons in sediments from a saline Antarctic lake, Ace Lake. *Organic Geochemistry* **10**, 671-81.
- Volkman, J.K., Banks, M.R., Denwer, K., Aquino Neto, F.R. (1989) Biomarker composition and depositional setting of Tasmanite oil shale from northern Tasmania, Australia. *Presented at the 14th International Meeting on Organic Geochemistry*, September 18-22, 1989, Paris.
- Wang, C., Visscher, H. (2007) Abundance anomalies of aromatic biomarkers in the Permian-Triassic boundary section at Meishan, China – Evidence of end-Permian terrestrial ecosystem collapse. *Palaeogeography, Palaeoclimatology, Palaeoecology* **252** (1-2), 291-303.
- Wignall, P.B., Twitchett, R.J. (1996) Oceanic anoxia and the end Permian mass extinction. *Science* **272** (5265), 1155-1158.
- Williams, J.A., Bjoroy, M., Dolcater, D.L., Winters, J.C. (1986) Biodegradation of South Texas Eocene oils – effects on aromatics and biomarkers. *Organic Geochemistry* **10**, 425-9.
- Xie, S., Pancoast, R.D., Huang, X., Jiao, D., Lu, L., Huang, J., Yang, F., Evershed, R.P. (2007) Molecular and isotopic evidence for episodic environmental change across the Permo/Triassic Events boundary at Meishan in South China. *Global Planetary Change* **55**, 56-65.
- Yunker, M.B., Macdonald, R.W., Vingarzan, R., Mitchell, R.H., Goyette, D., Sylvestre, S. (2002) PAHs in the Fraser River basin: A critical appraisal of PAH ratios as indicators of PAH source and composition. *Organic Geochemistry* **33**, 489–515.
- Zhou, W., Algeo, T.J., Ruan, X., Genming, L., Chen, Z., Xie, S. (2016) Expansion of photic-zone euxinia during the Permian-Triassic biotic crisis, and its causes: Microbial biomarker records. *Palaeogeography, Palaeoclimatology, Palaeoecology*, **47**, 140-151.
- Zumberge, J.E. (1984) Source rock of the La Luna Formation (U. Cretaceous) in the Middle Magdalena Valley, Columbia. *Stud. Geol.* **18**, 127-134.

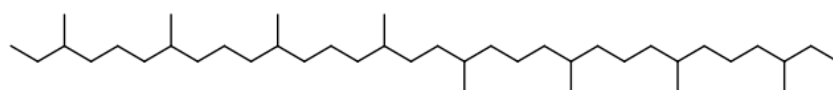
Appendix A: Compound Structures



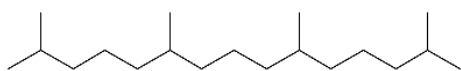
I: C₁₇ n-Alkane



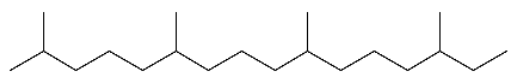
II: Squalene (tail-to-tail example)



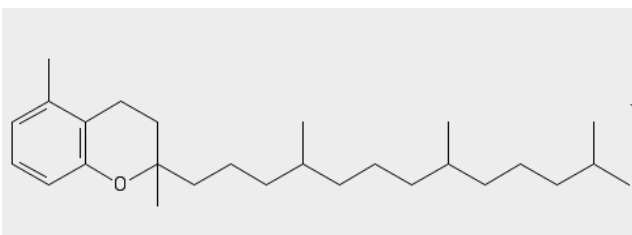
III: Bisphytane (head-to-head)



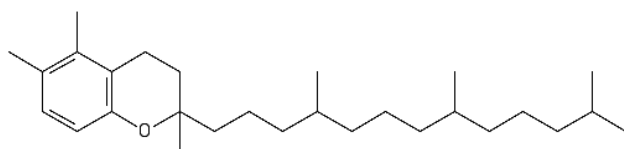
IV: Pristane



V: Phytane

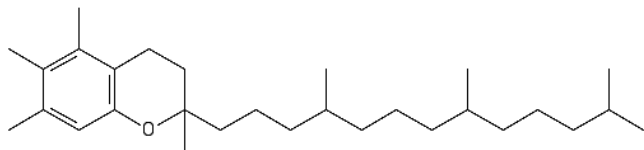


VI: MTTC

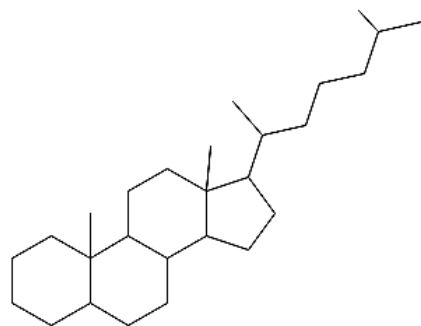


VII: diMe-MTTC

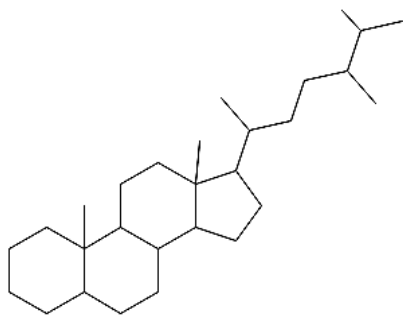
VIII: triMe-MTTC



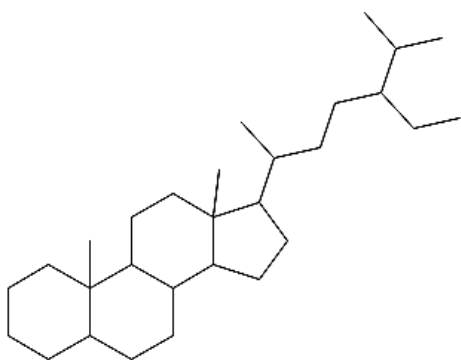
IX: C₂₇ Sterane

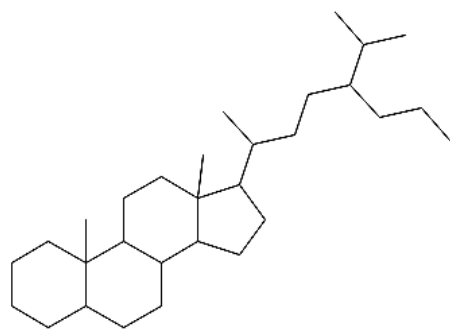


X: C₂₈ Sterane

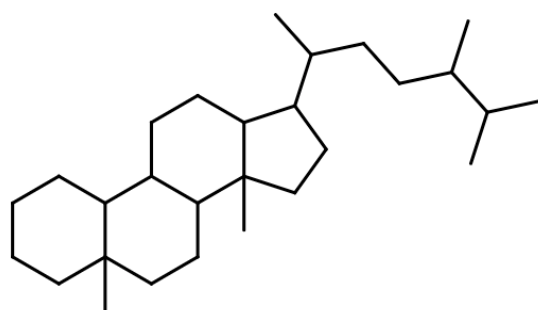


XI: C₂₉ Sterane

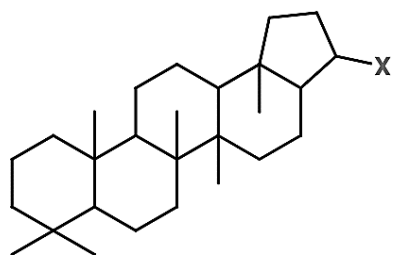




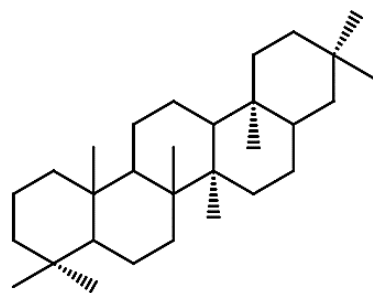
XII: C₃₀ Sterane



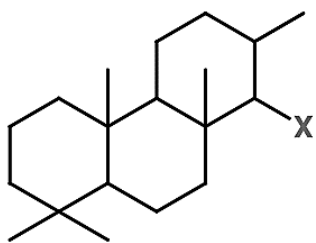
XIII: C₂₇ Diasterane



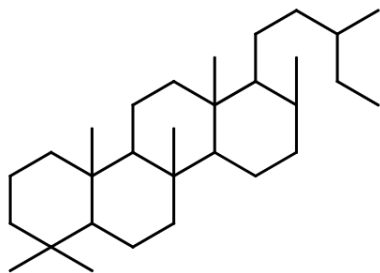
XIV: Hopane



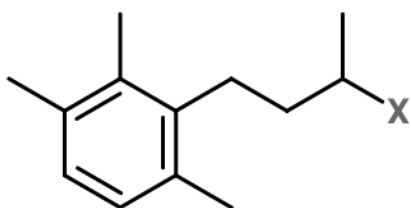
XV: Gammacerane



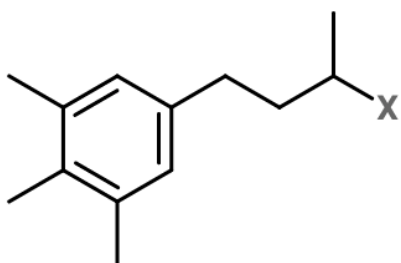
XVI: Tricyclic Terpane



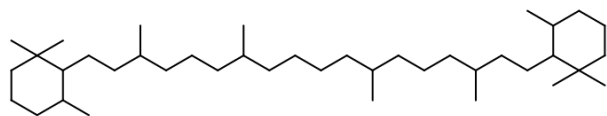
XVII: Tetracyclic Polyprenoid (C₃₀)



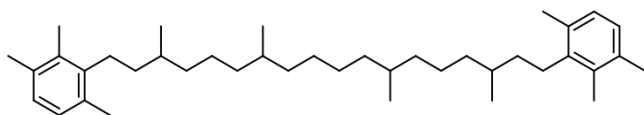
XVIII: 2,3,6- trimethylbenzene



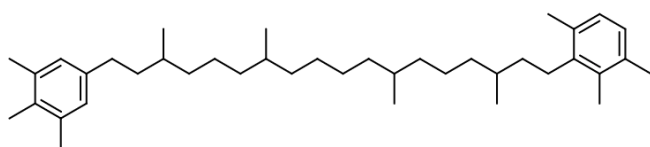
XIX: 3,4,5- trimethylbenzene



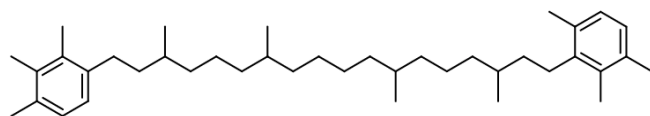
XX: B-Carotane



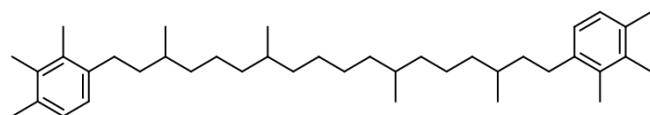
XXI: Isorenieratane



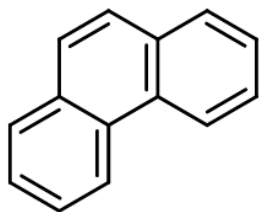
XXII: Paleorenieratane



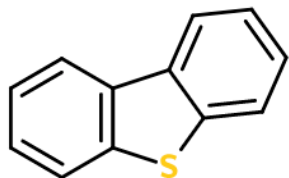
XXIII: Renieratane



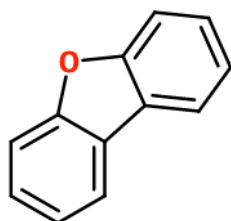
XXIV: Renierpurpurane



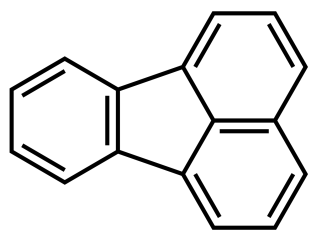
XXV: Phenanthrene



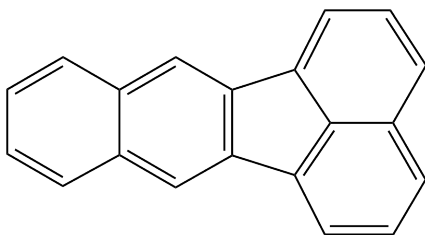
XXVI: Dibenzothiophene



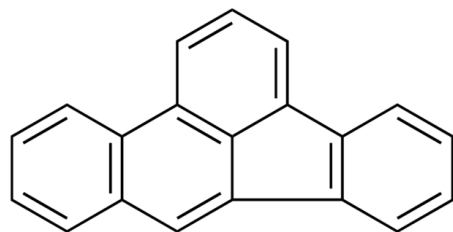
XXVII: Dibenzofuran



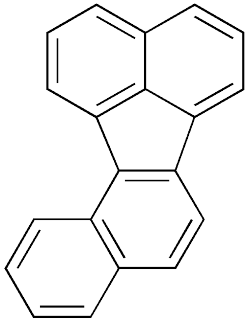
XXVIII: Fluoranthene



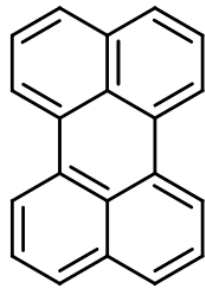
XXIX: Benzo(k)fluoranthene



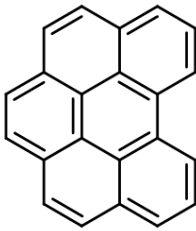
Benzo(b)fluoranthene



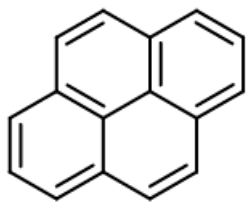
Benzo(j)fluoranthene



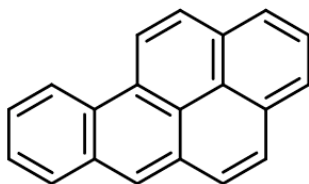
XXX: Perylene



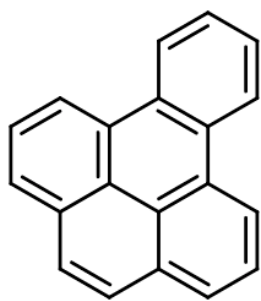
XXXI: Benzo(ghi)perylene



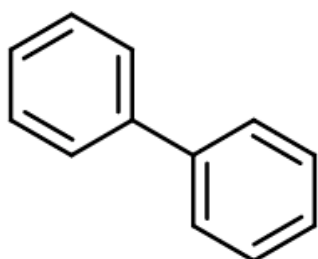
XXXII: Pyrene



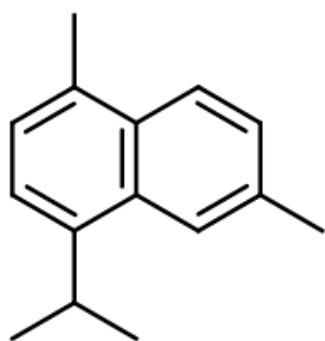
XXXIII: Benzo(a)pyrene



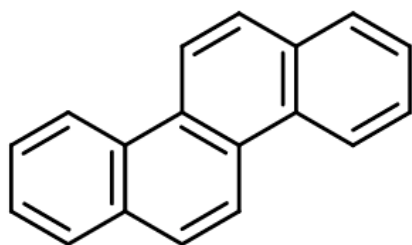
Benzo(e)pyrene



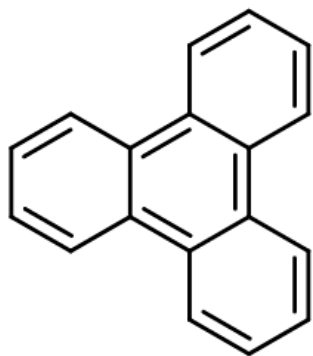
XXXIV: Biphenyl



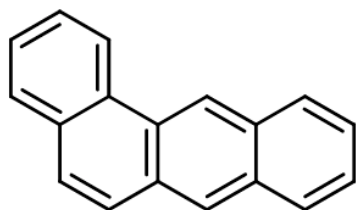
XXXV: Cadalene



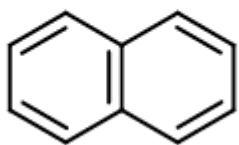
XXXVI: Chrysene



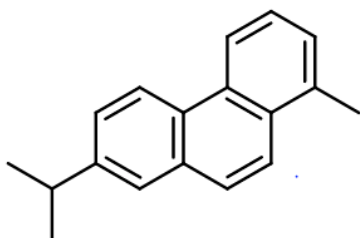
XXXVII: Triphenylene



XXXVIII: Benzoanthracene

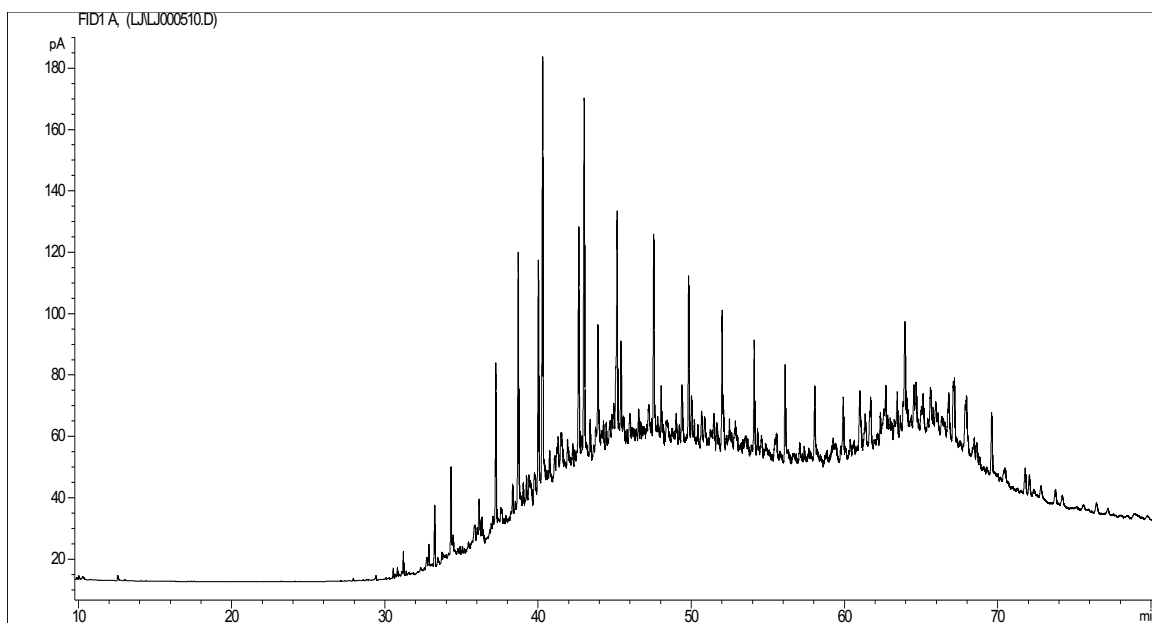


XXXIX: Naphthalene

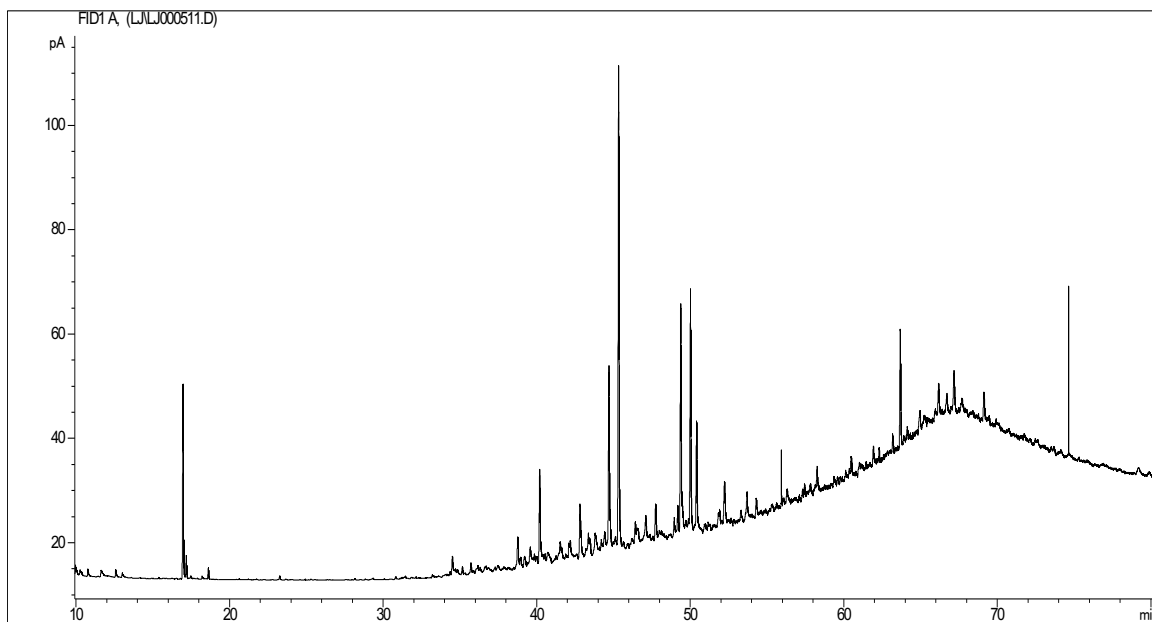


XXXX: Retene

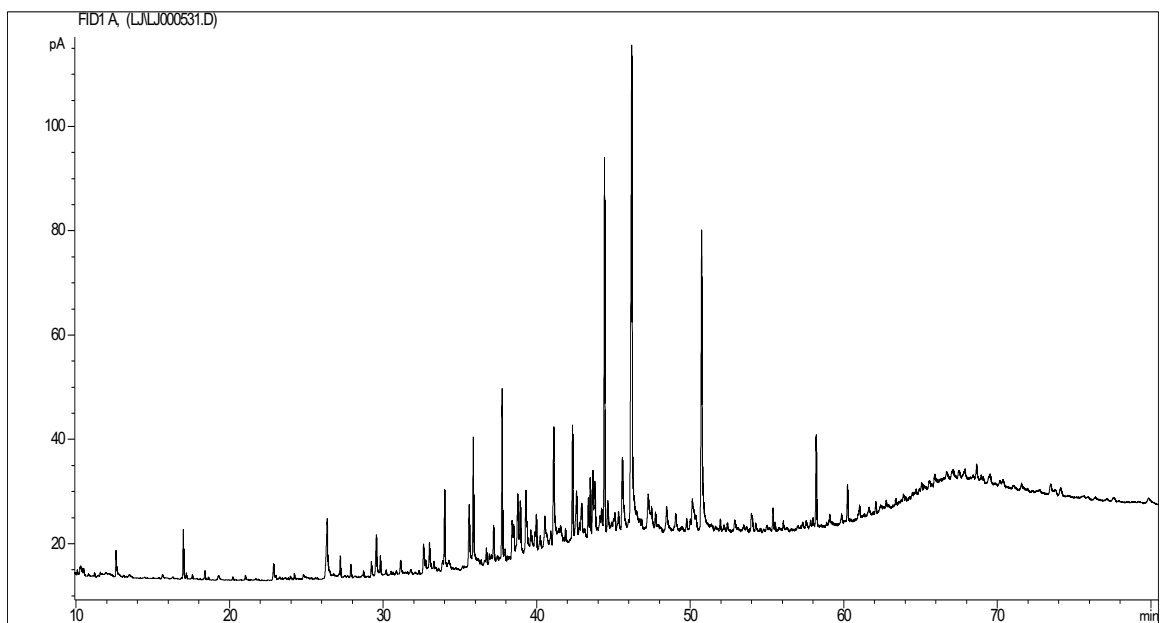
Appendix B: Gas Chromatography Results



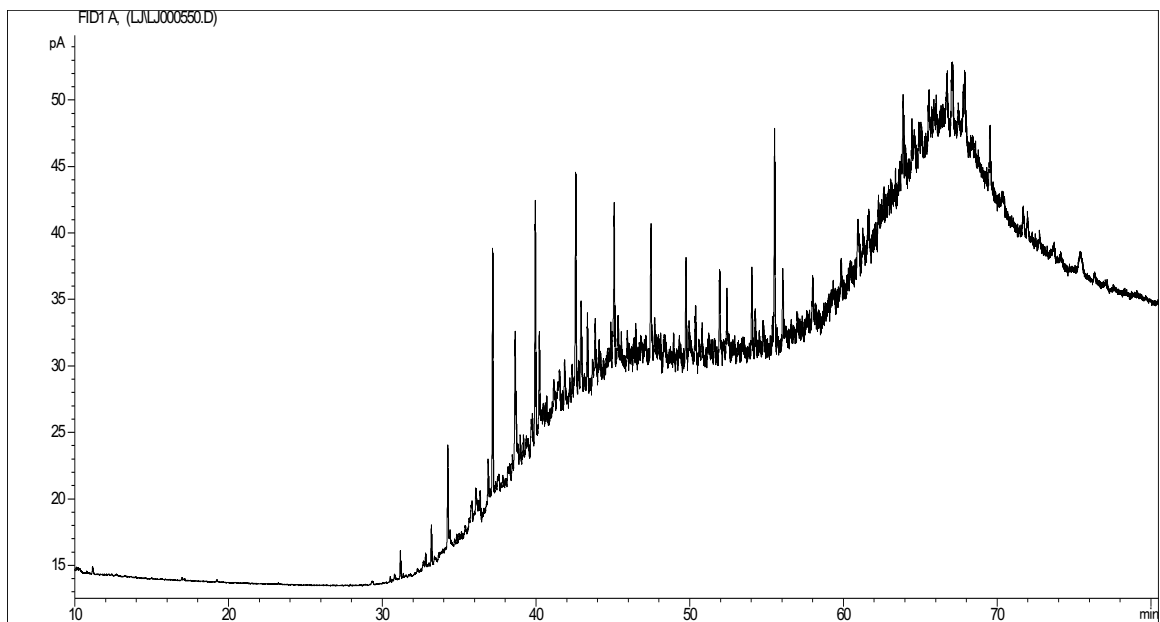
Woodford #4 - Aliphatics



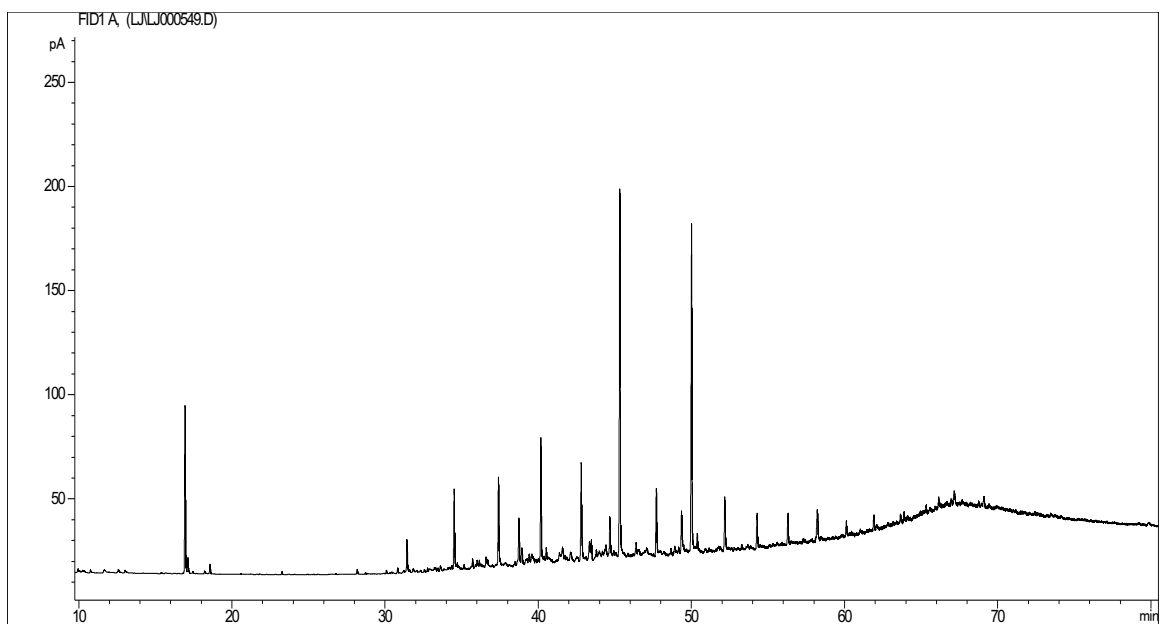
Woodford #4 - Aromatics



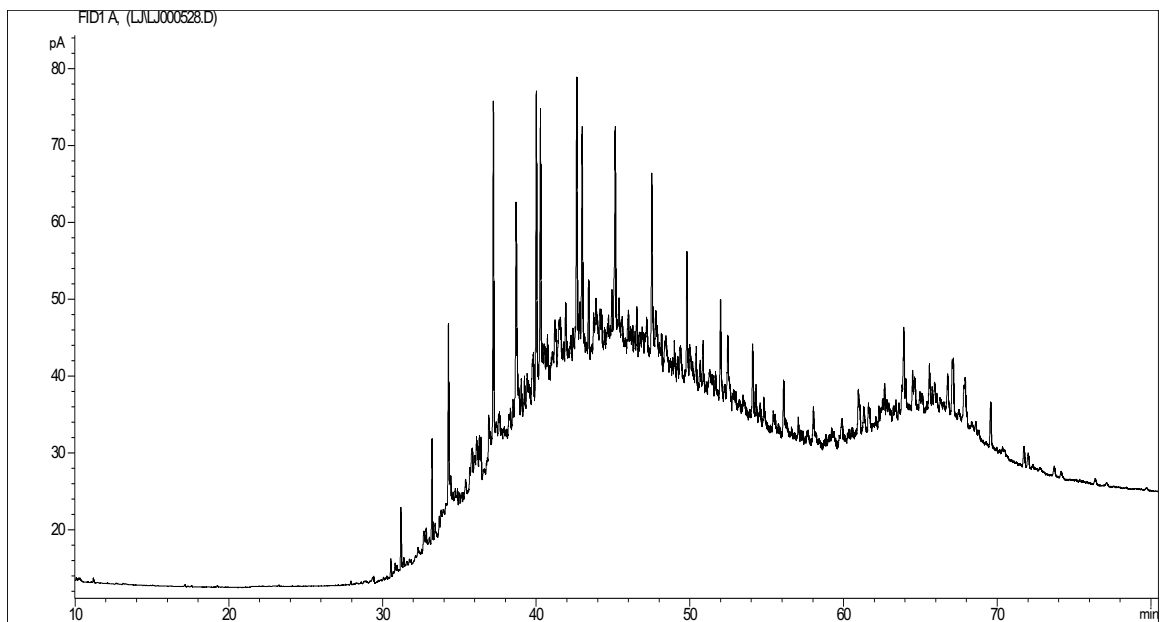
Woodford #12 - Maltenes



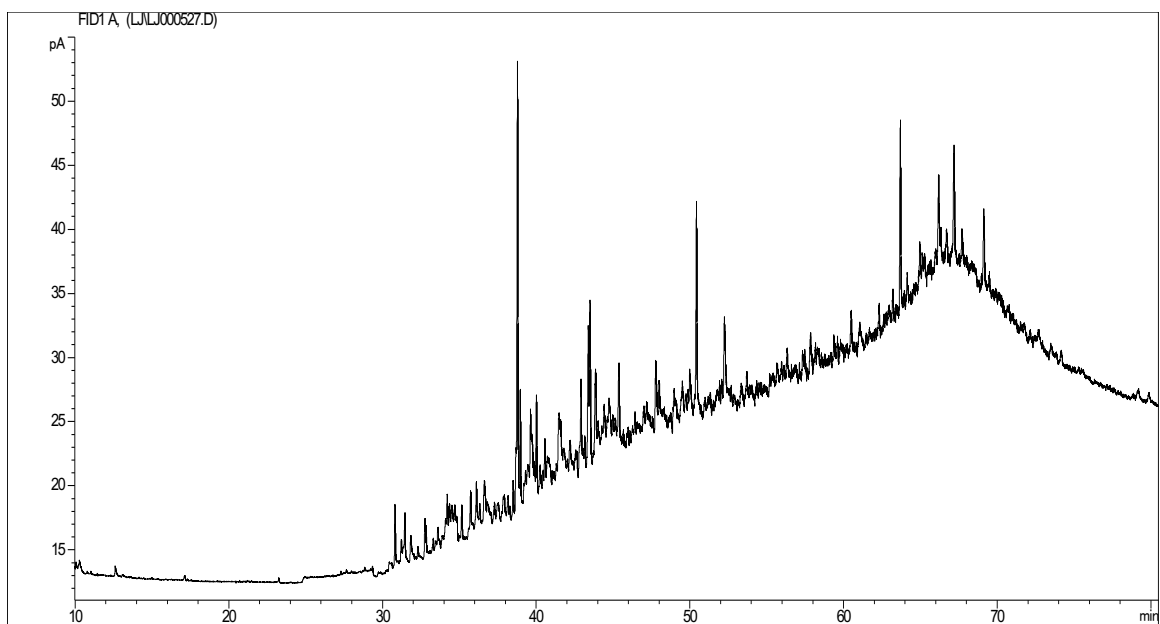
Woodford #13 - Aliphatics



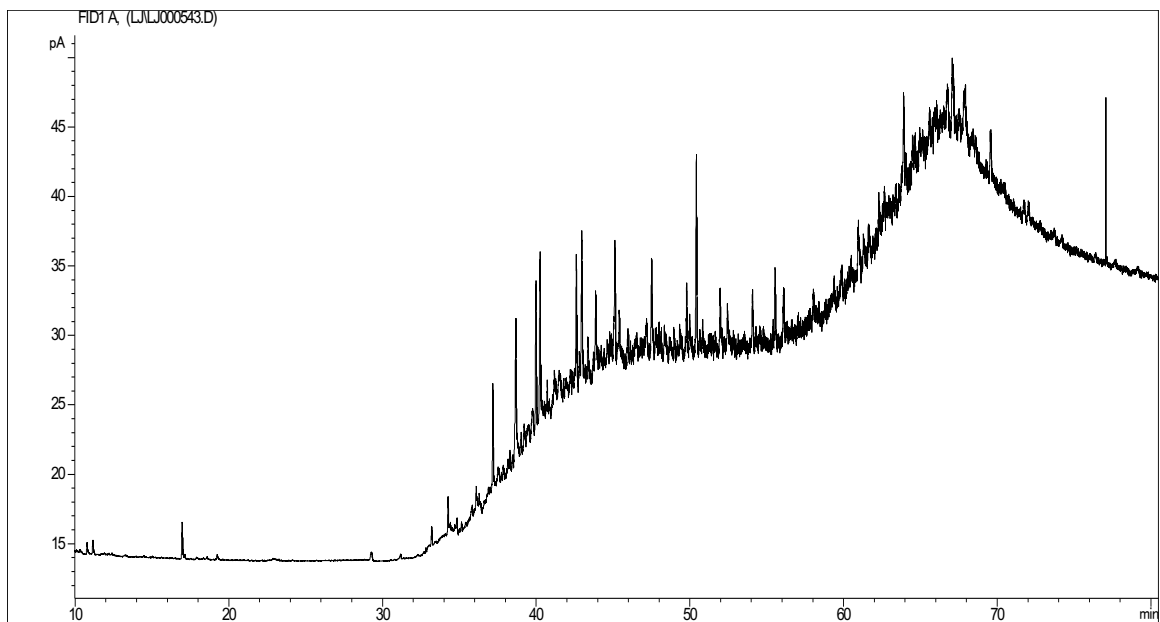
Woodford #13 - Aromatics



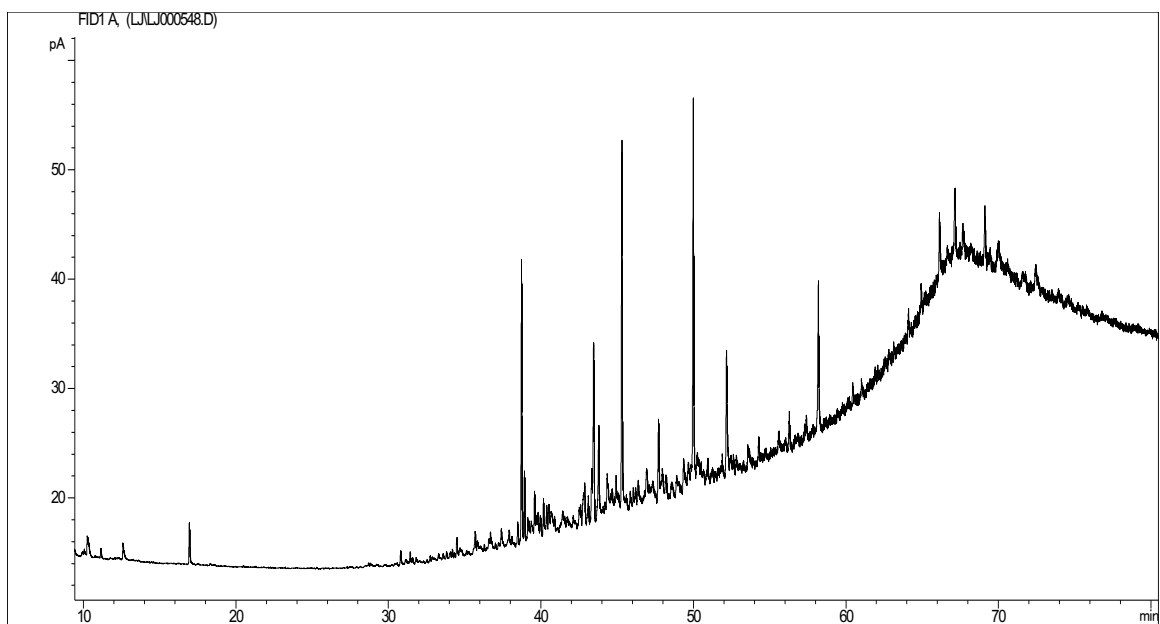
Woodford #14 – Aliphatics



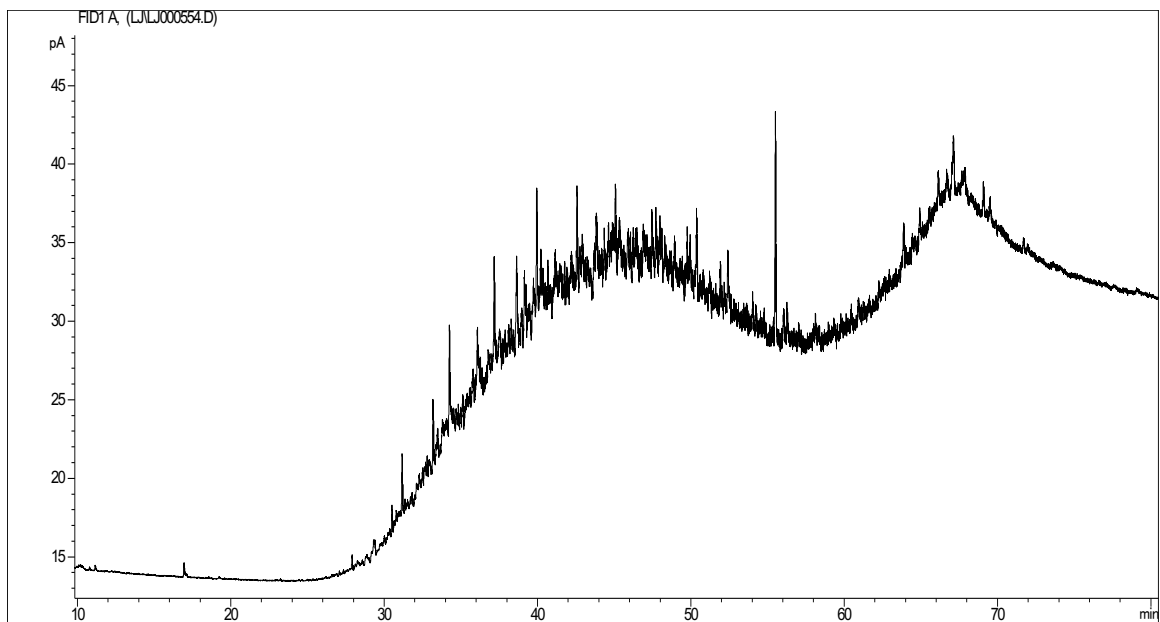
Woodford #14 – Aromatics



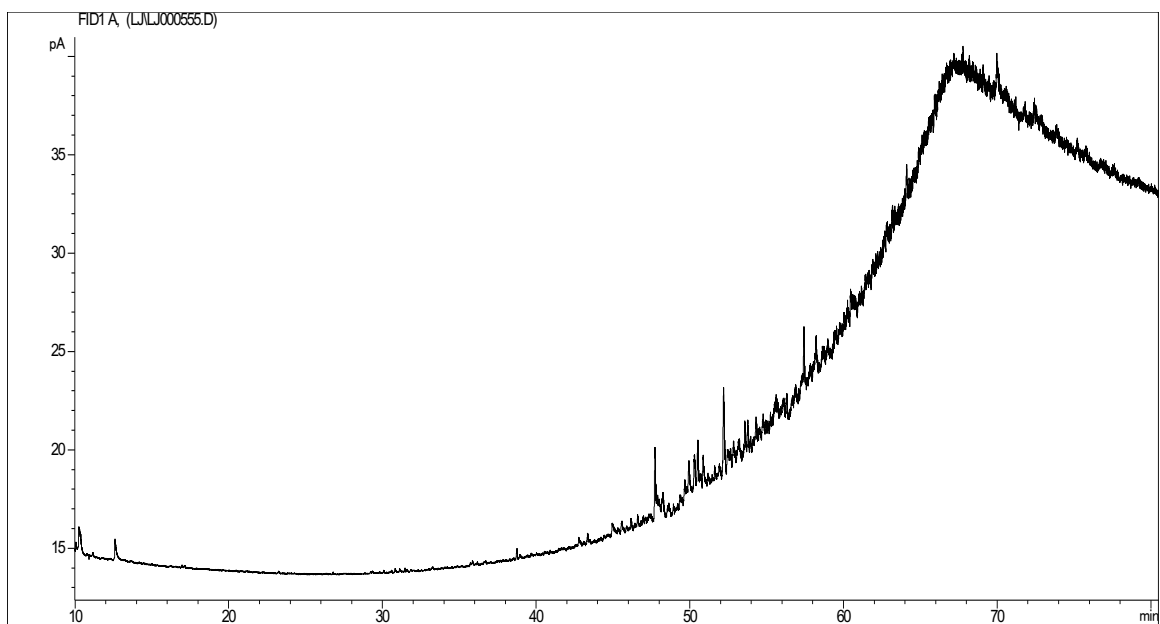
Woodford #16 - Aliphatics



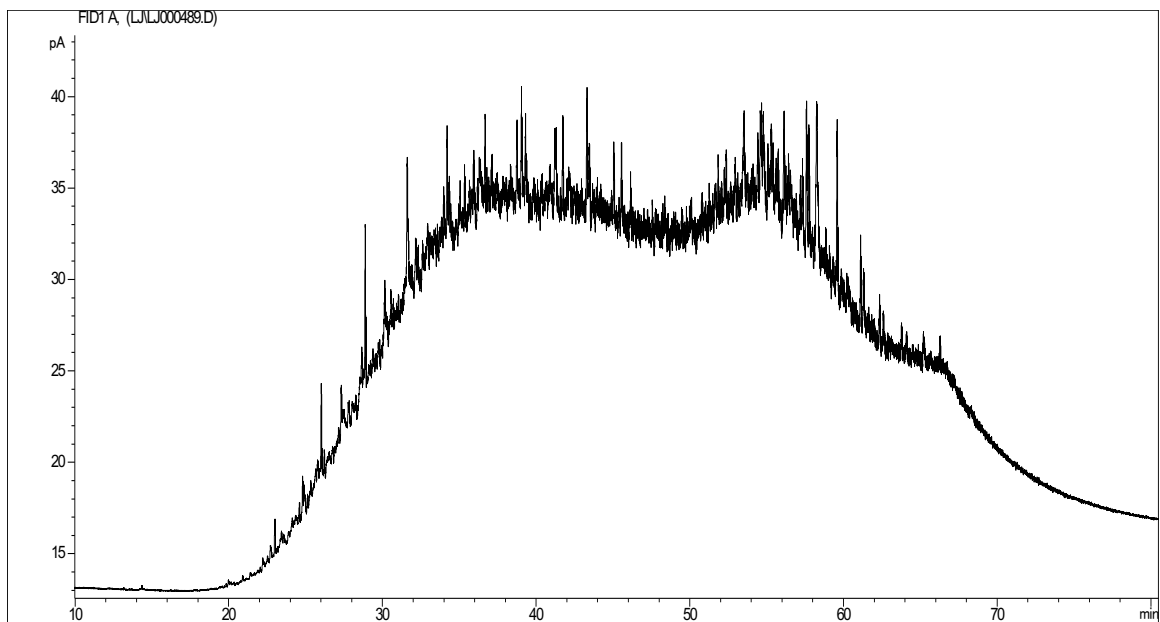
Woodford #16 - Aromatics



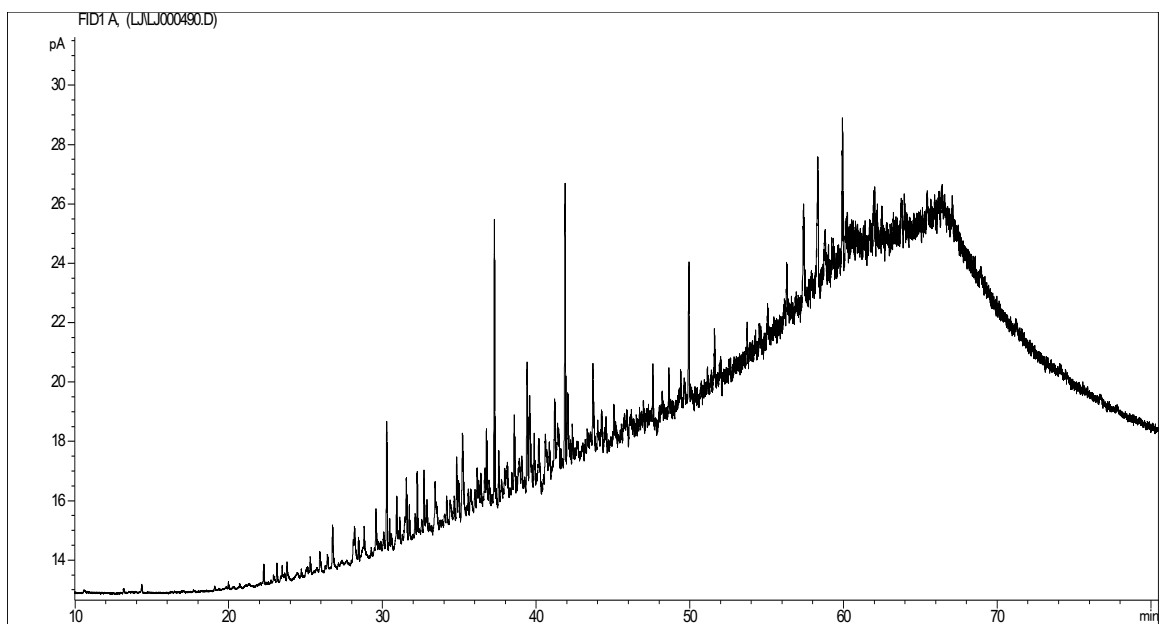
Woodford #26 - Aliphatics



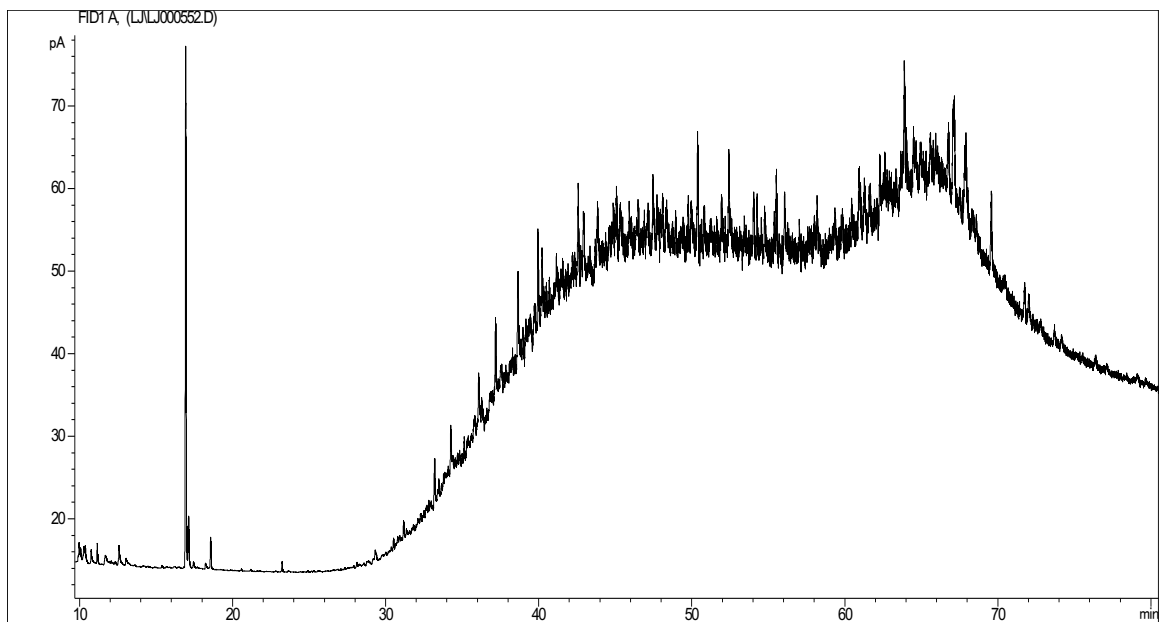
Woodford #26 - Aromatics



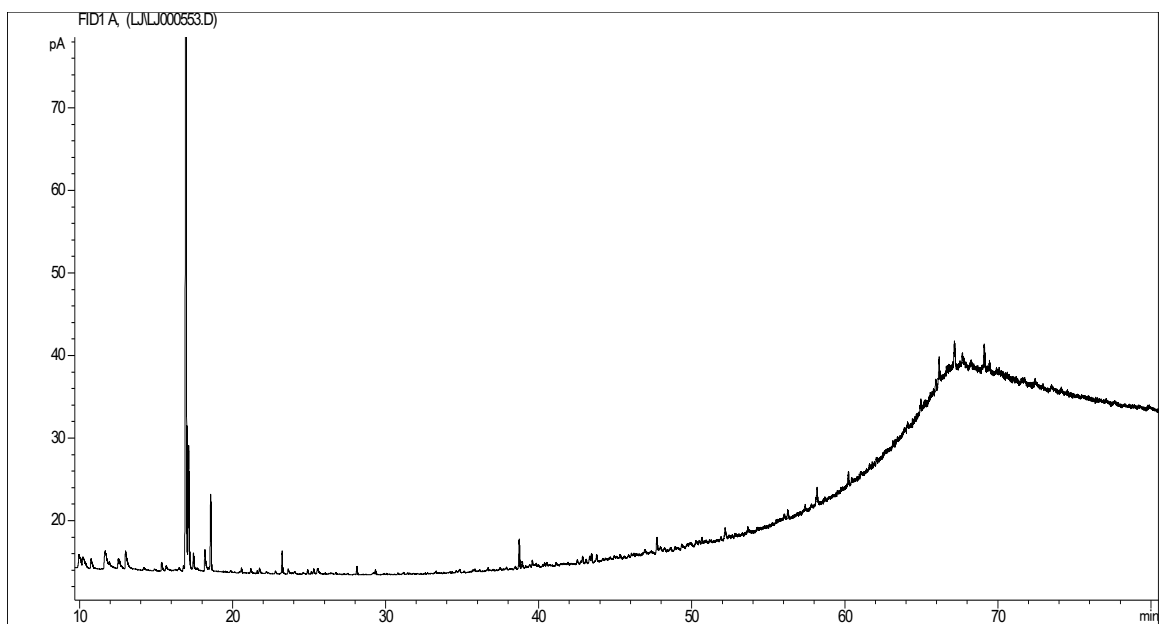
Woodford #30 - Aliphatics



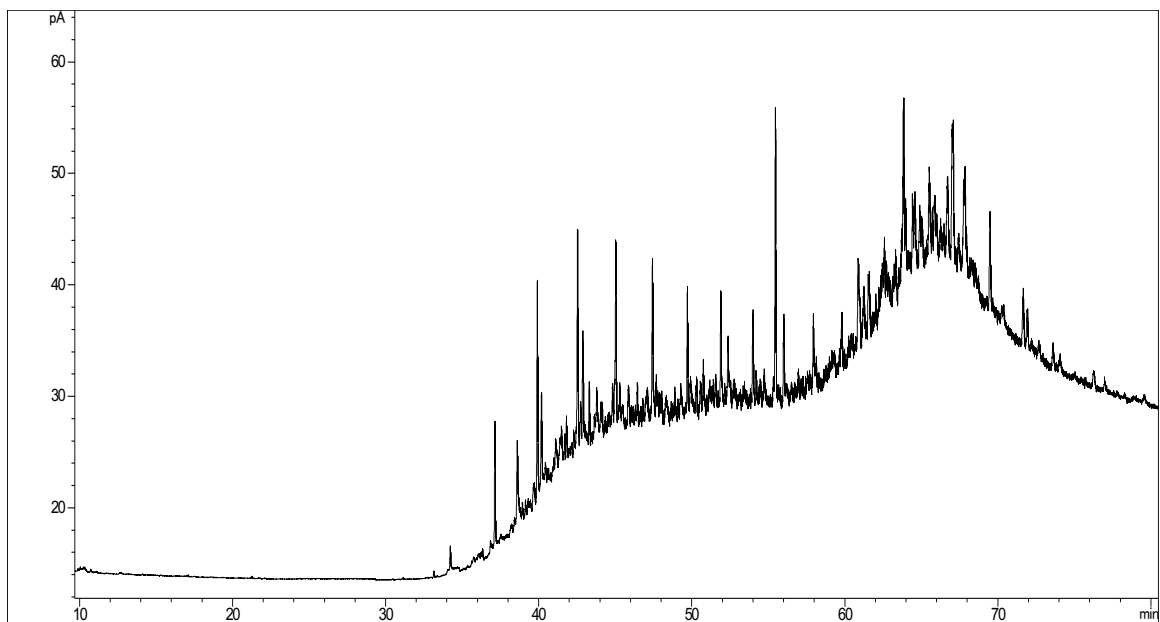
Woodford #30 - Aromatics



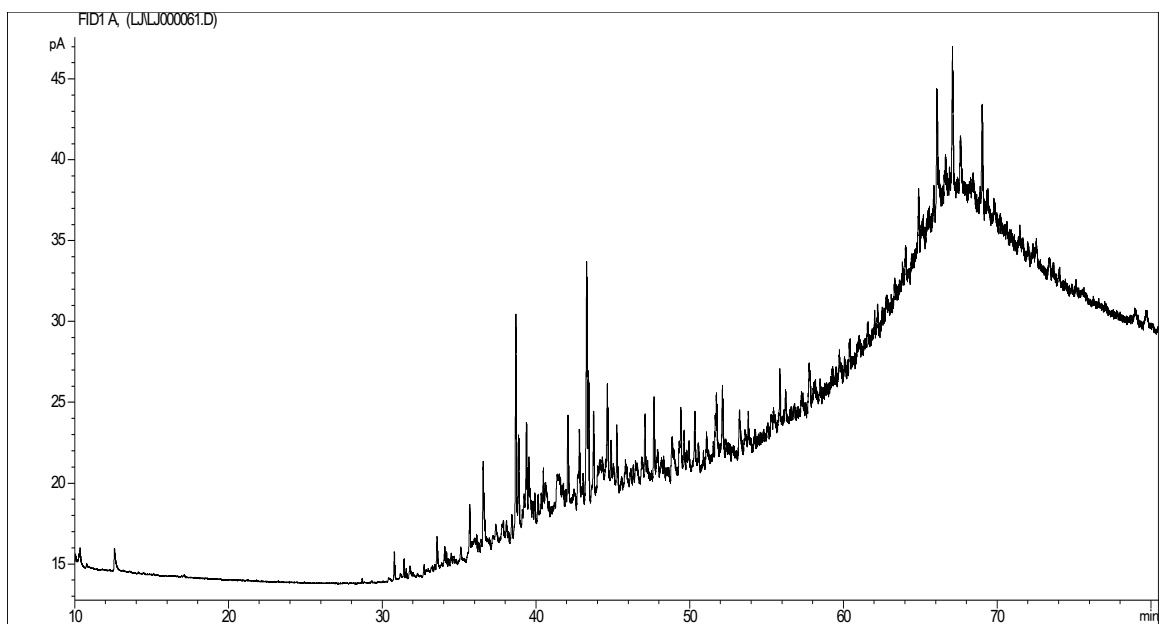
Woodford #32 – Aliphatics



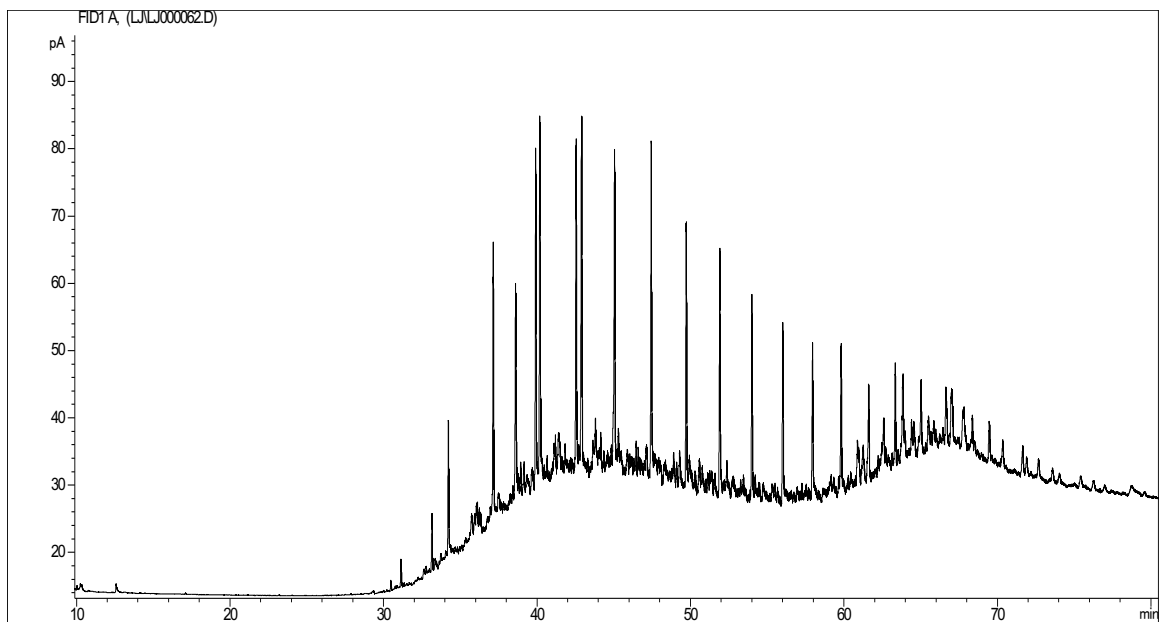
Woodford #32 - Aromatics



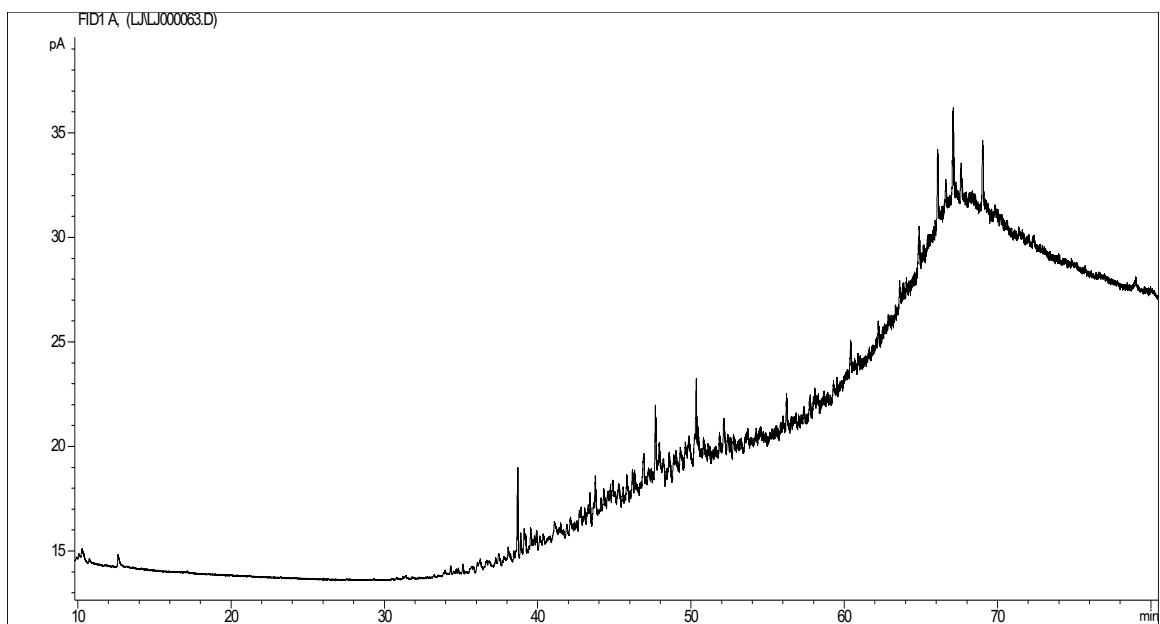
Woodford #37 - Aliphatics



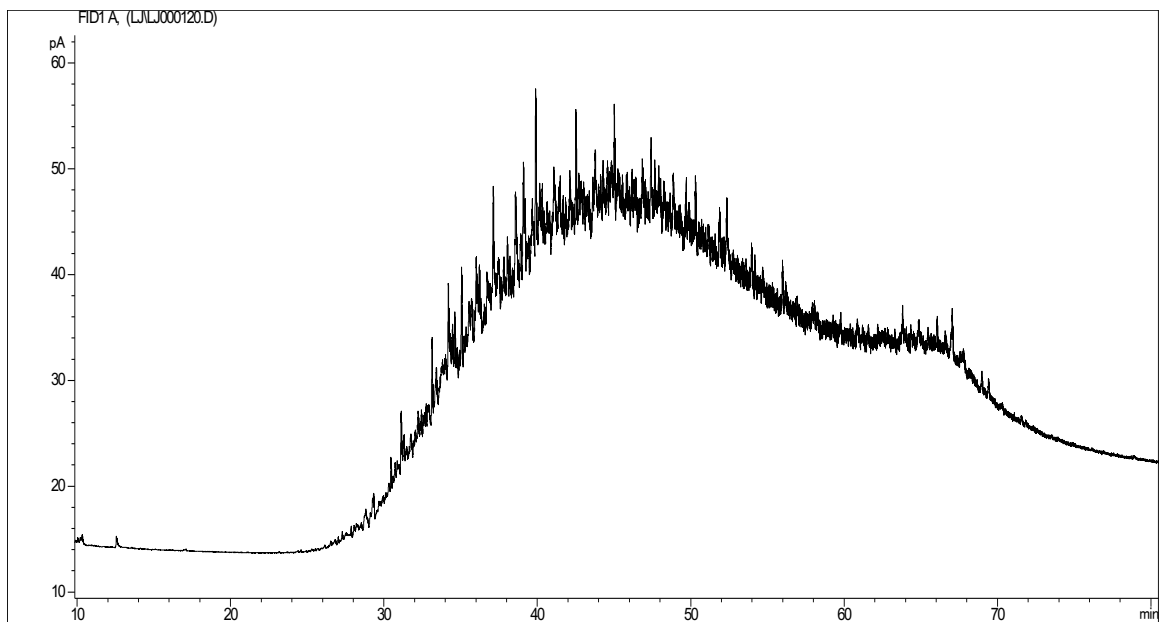
Woodford #37 - Aromatics



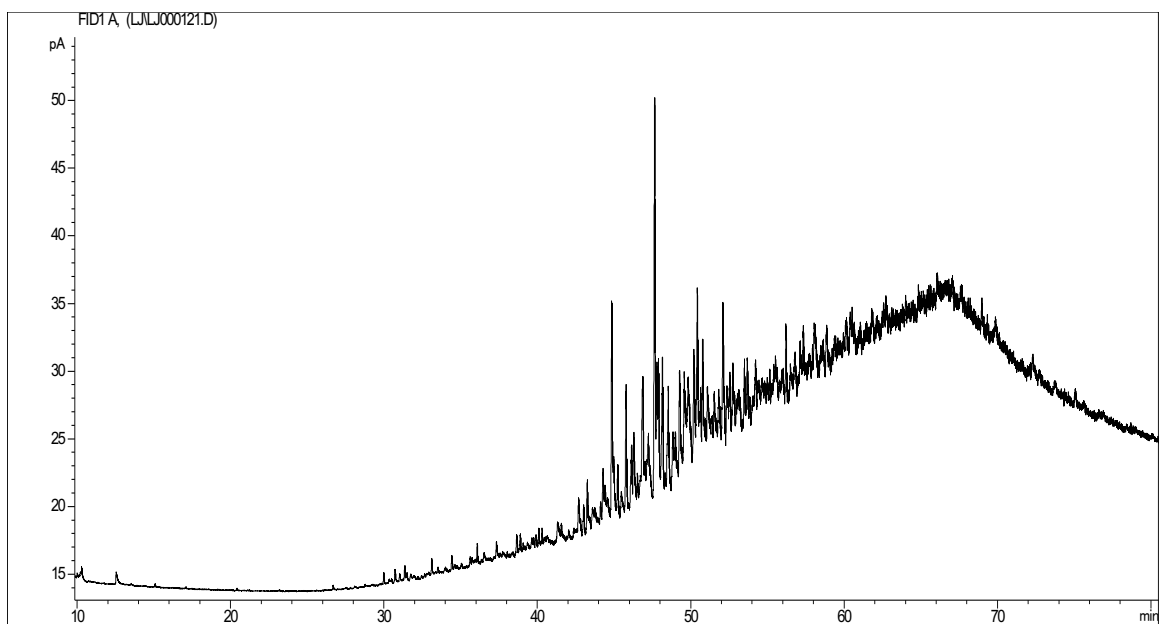
Woodford #43 - Aliphatics



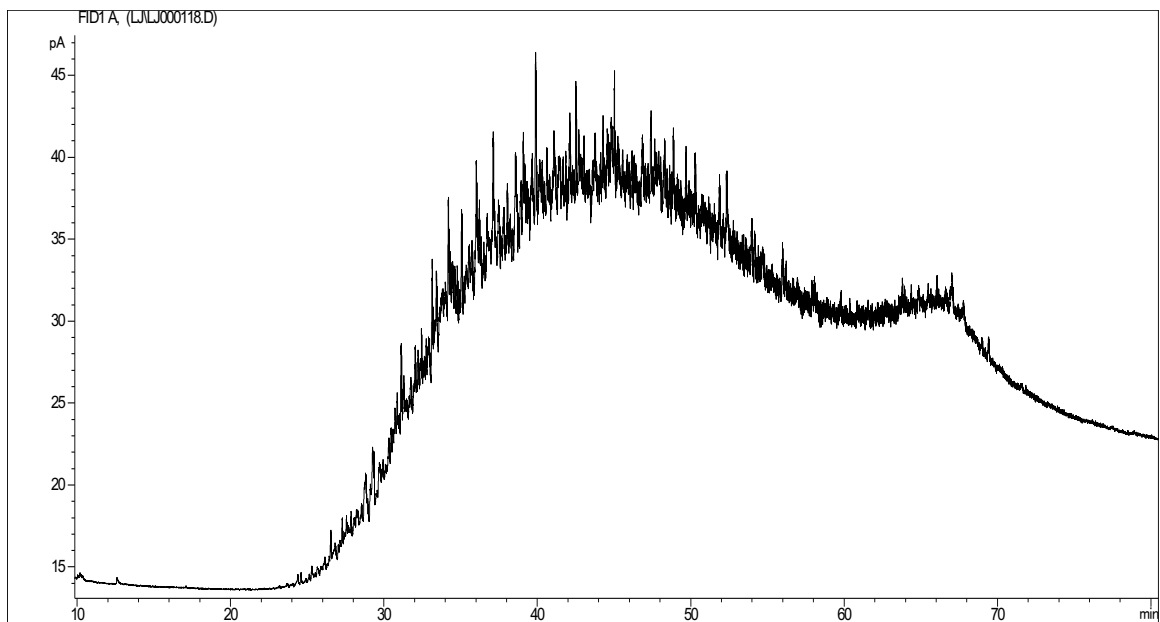
Woodford #43 - Aromatics



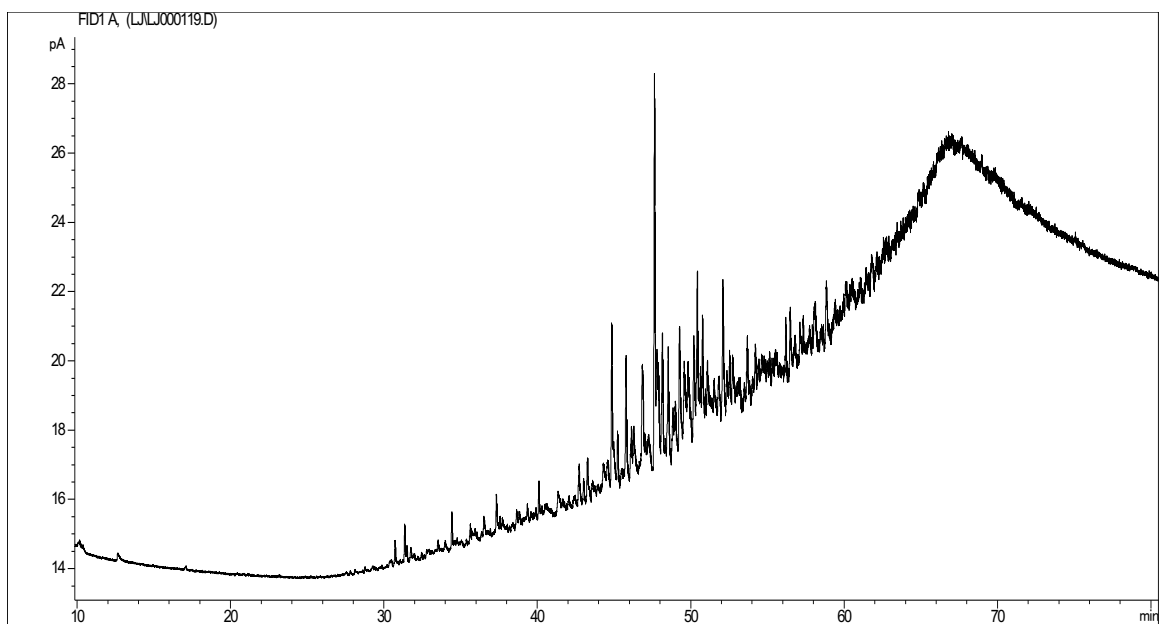
Woodford #45 - Aliphatics



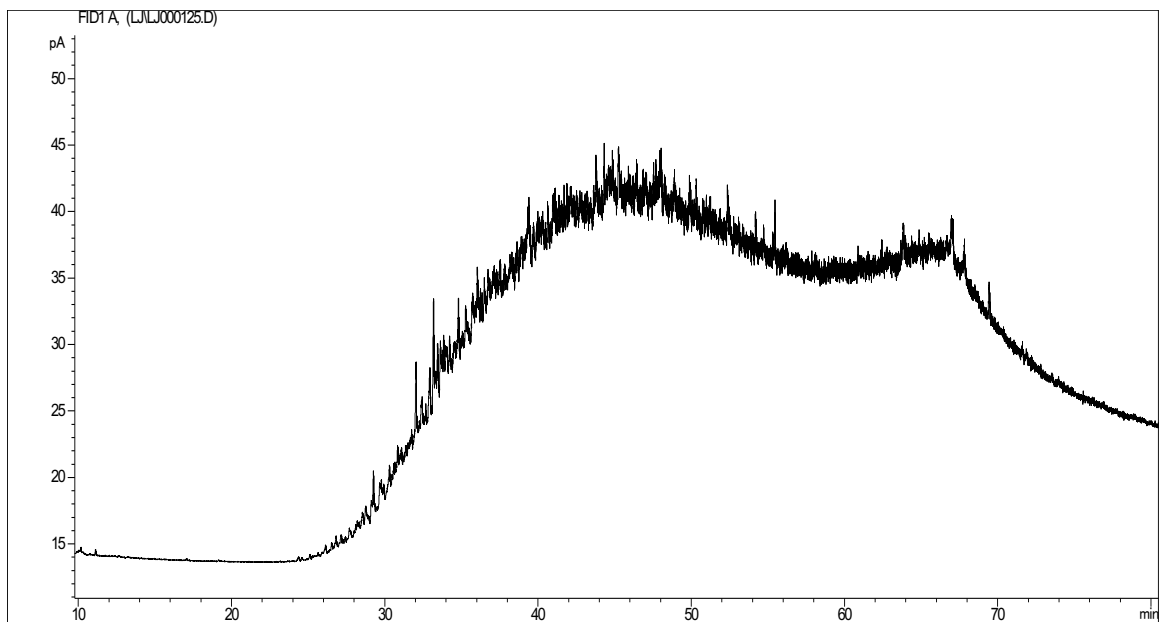
Woodford #45 - Aromatics



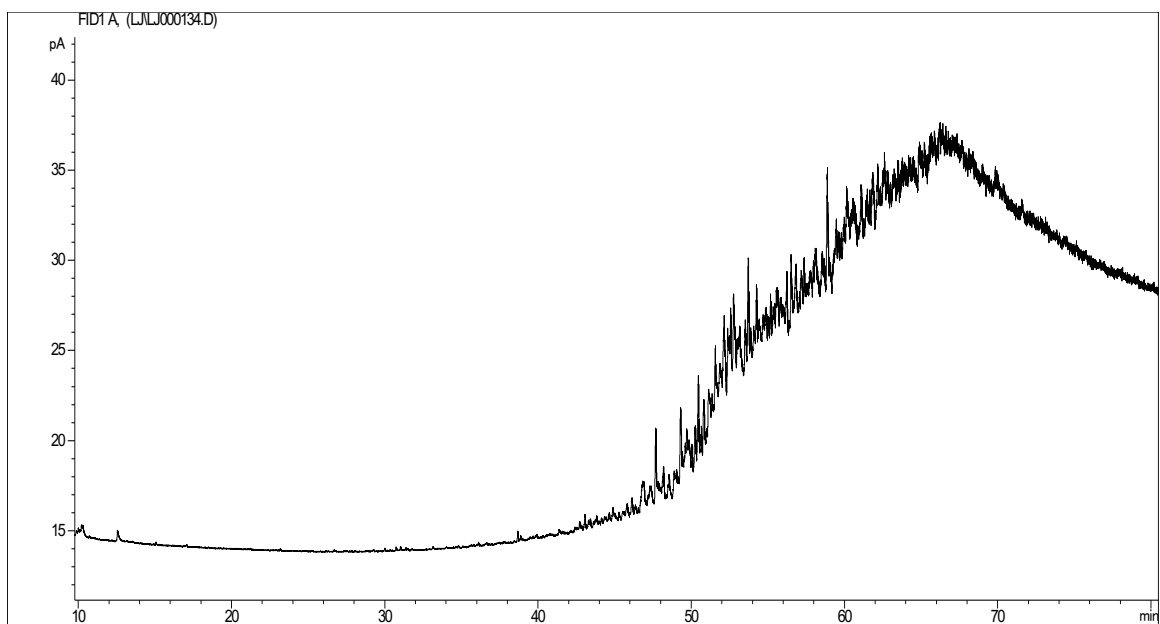
Woodford #50 - Aliphatics



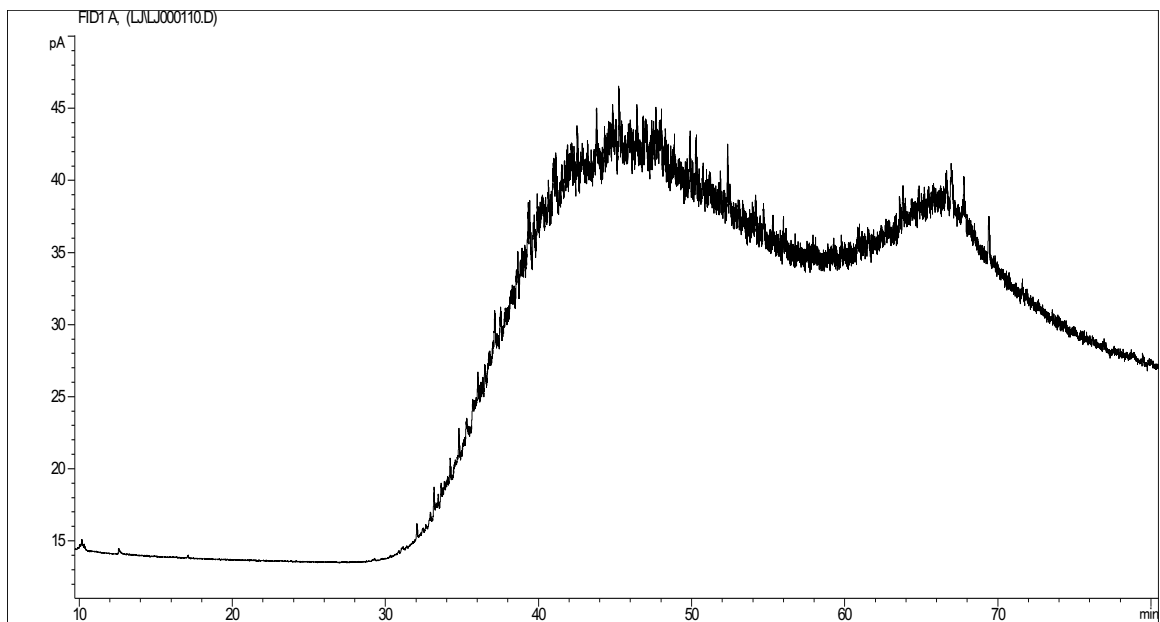
Woodford #50 - Aromatics



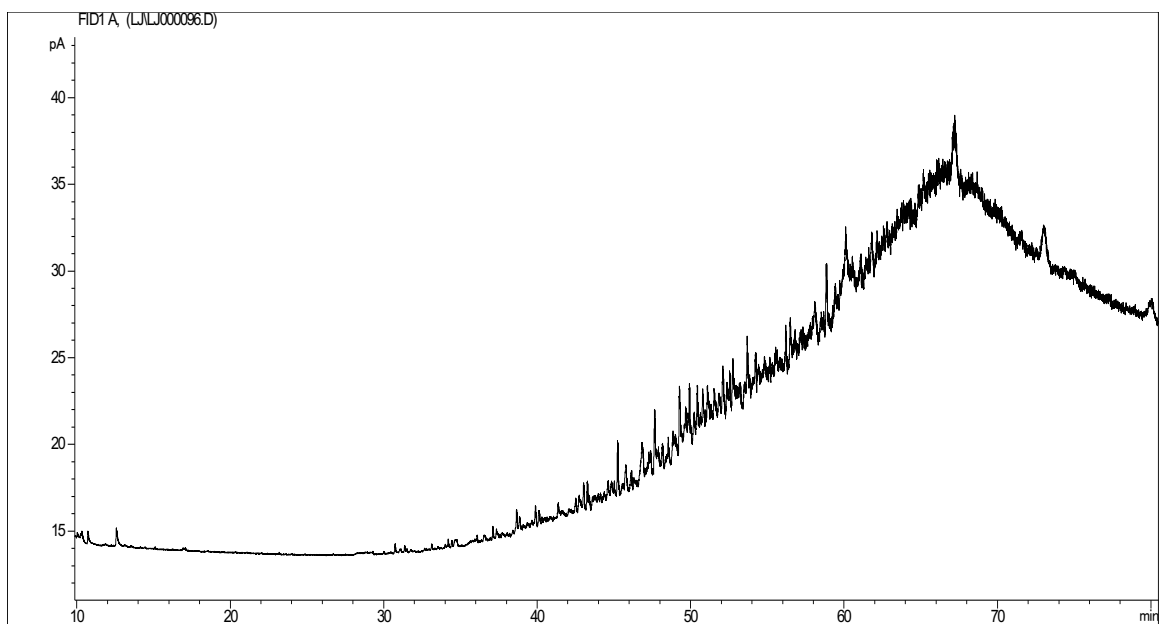
Woodford #65 - Aliphatics



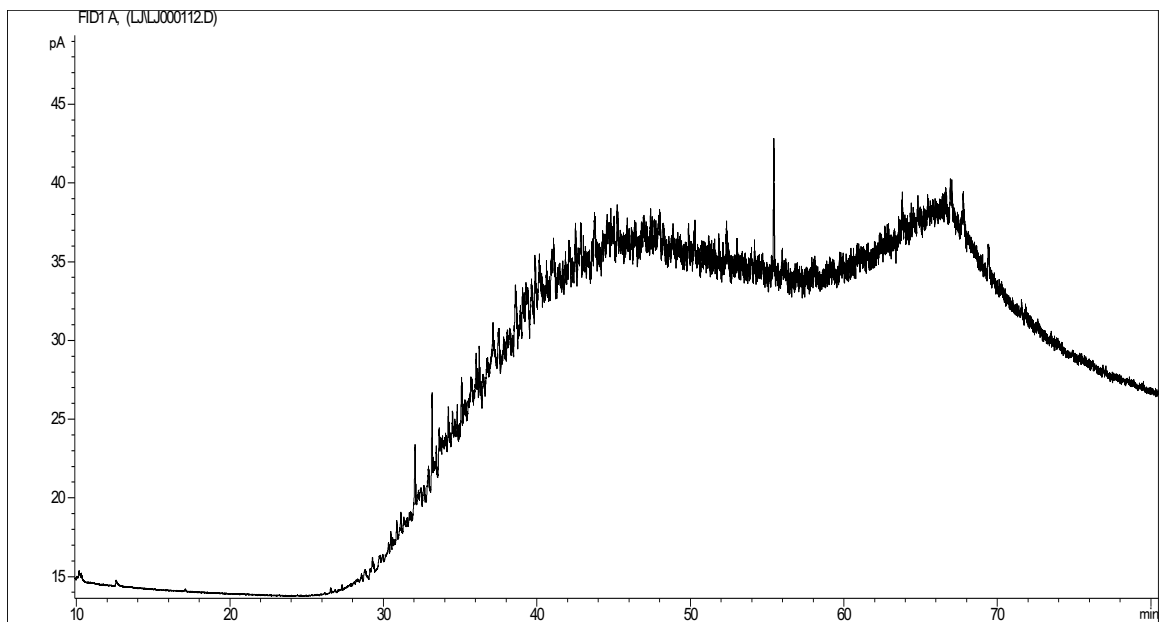
Woodford #65 - Aromatics



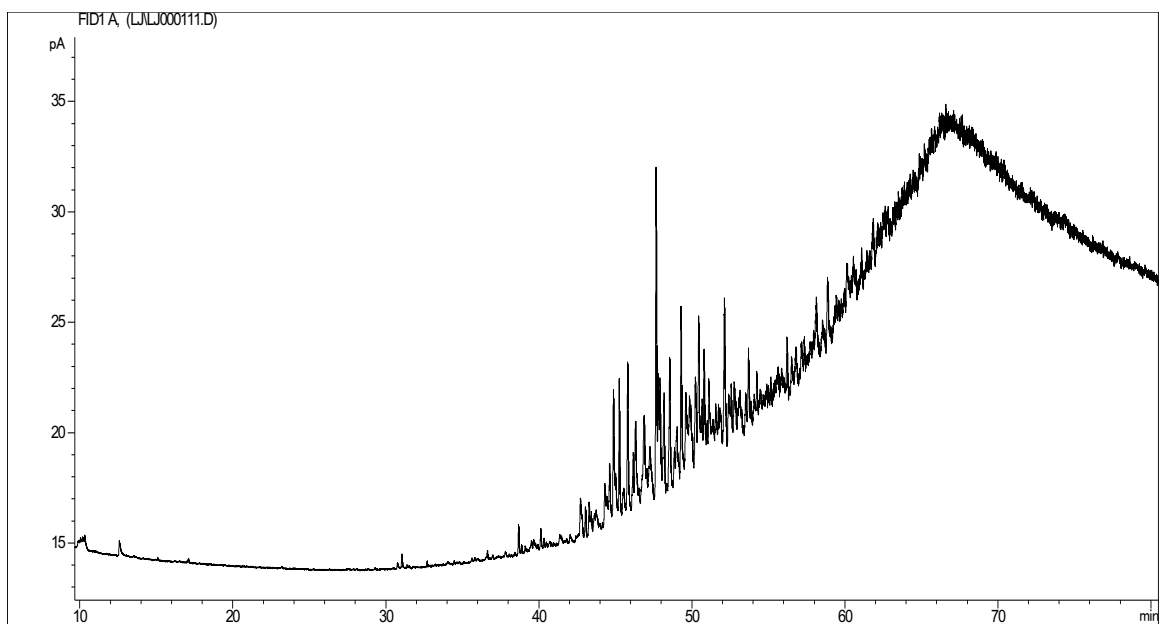
Woodford #70 - Aliphatics



Woodford #70 - Aromatics



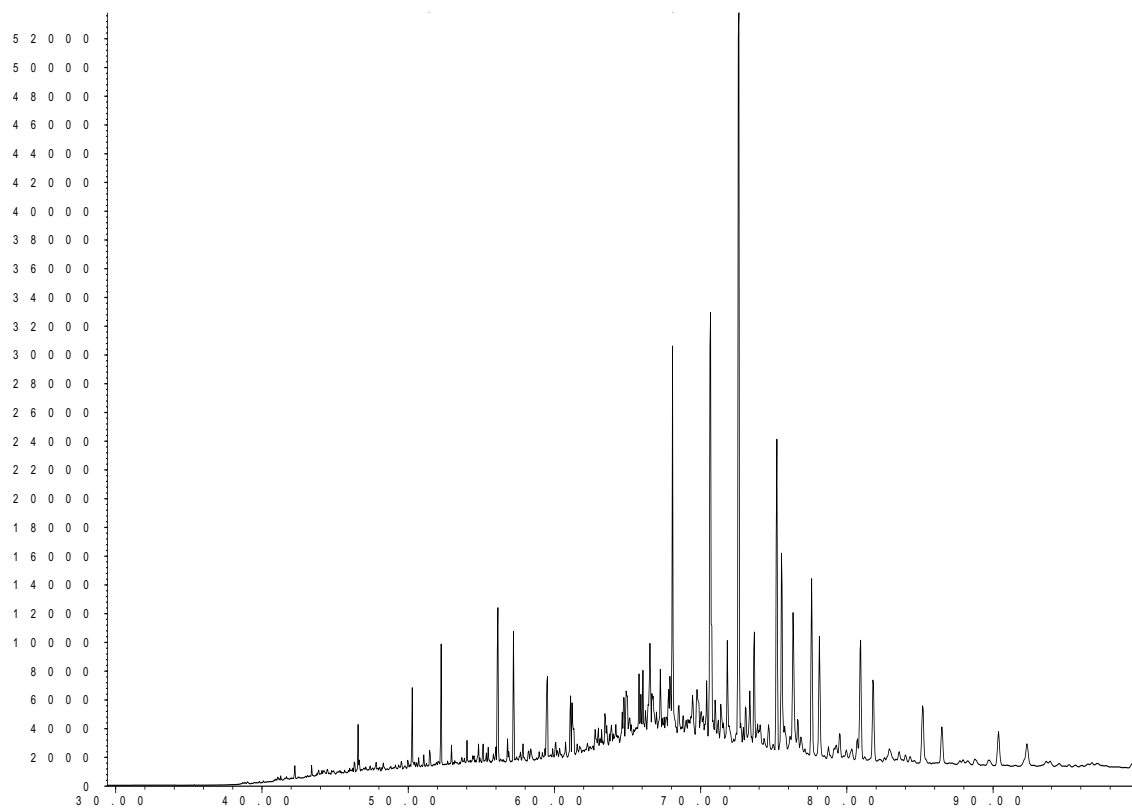
Woodford #75 – Aliphatics



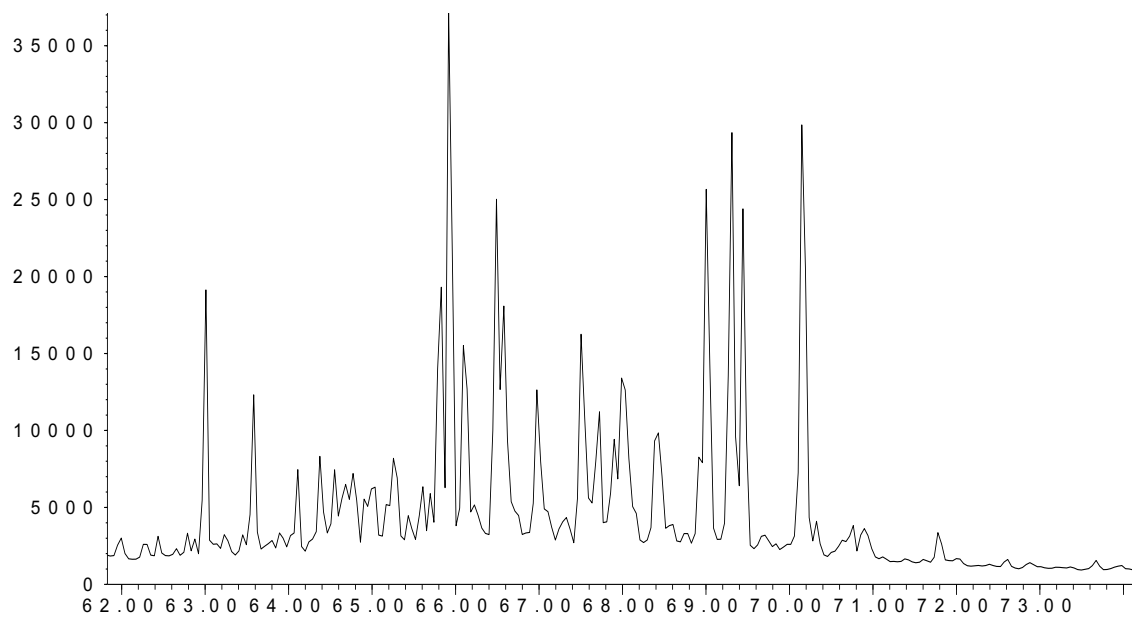
Woodford #75 - Aromatics

Appendix C: GCMS Results

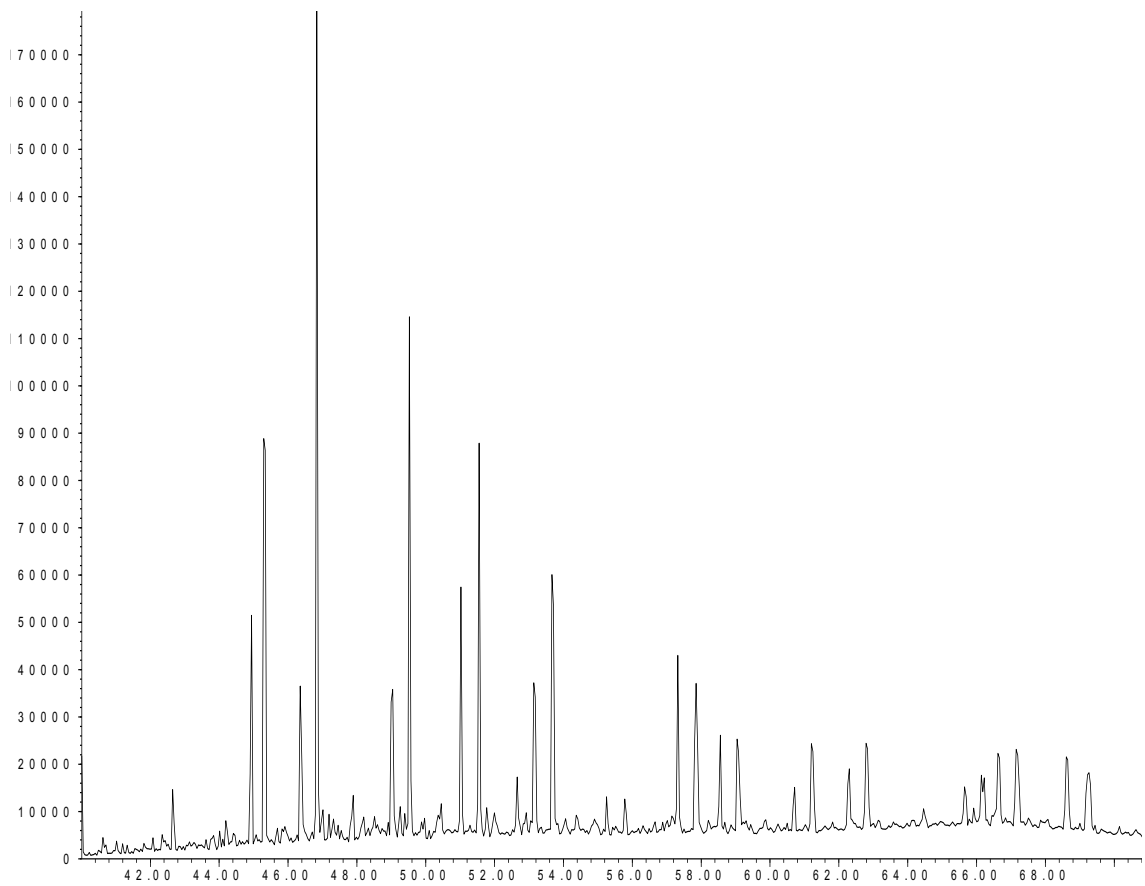
Woodford #4 Aliphatics – m/z 191.3



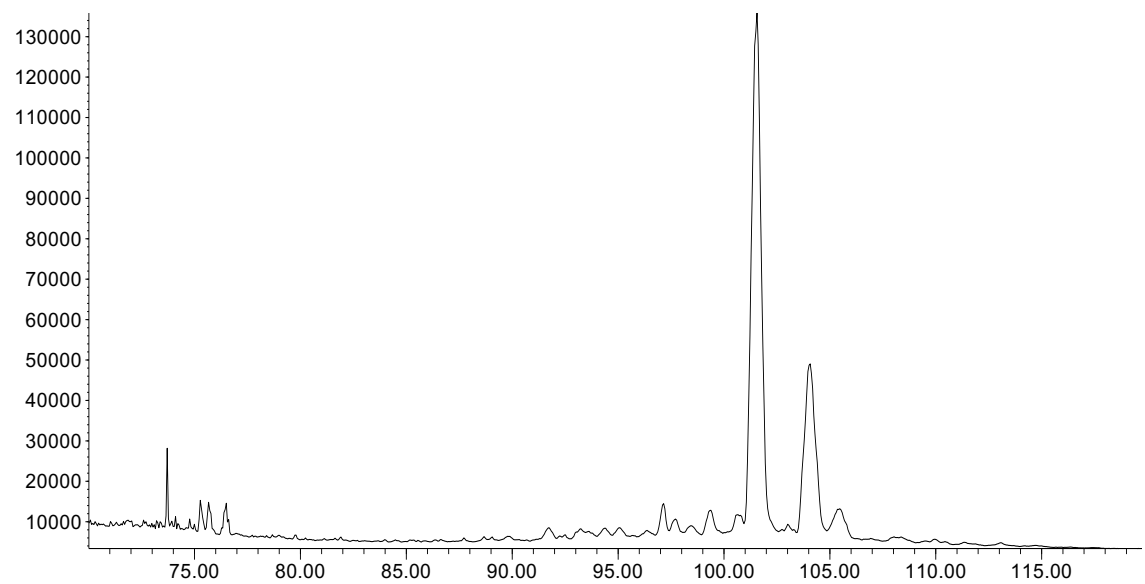
Woodford #4 Aliphatics – m/z 217.3



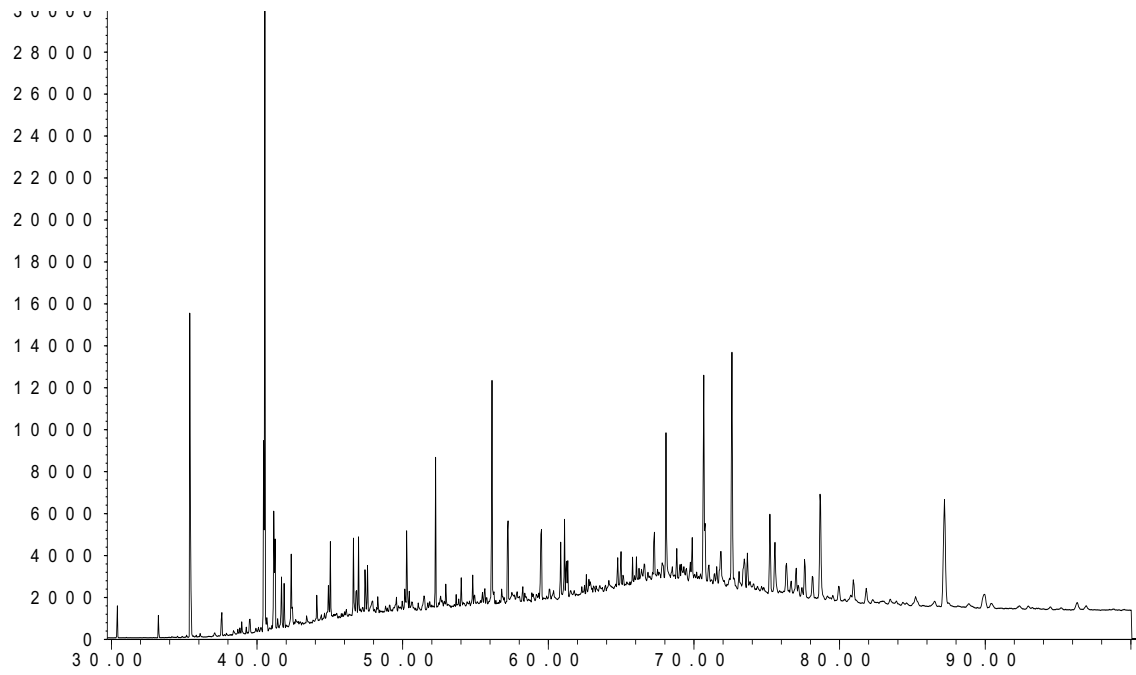
Woodford #4 Aliphatics – m/z 133.3 +134.3 (40-70 min.)



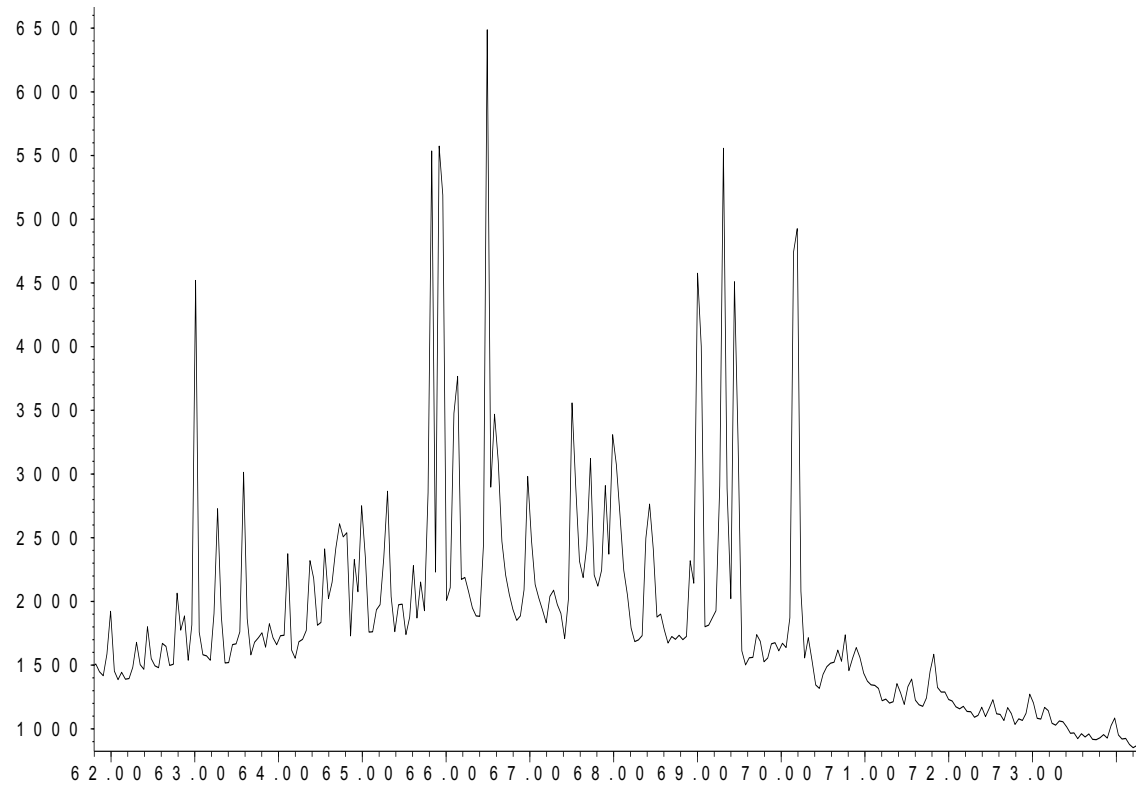
Woodford #4 Aromatics – m/z 133.3 + 134.3 (70-120 min.)



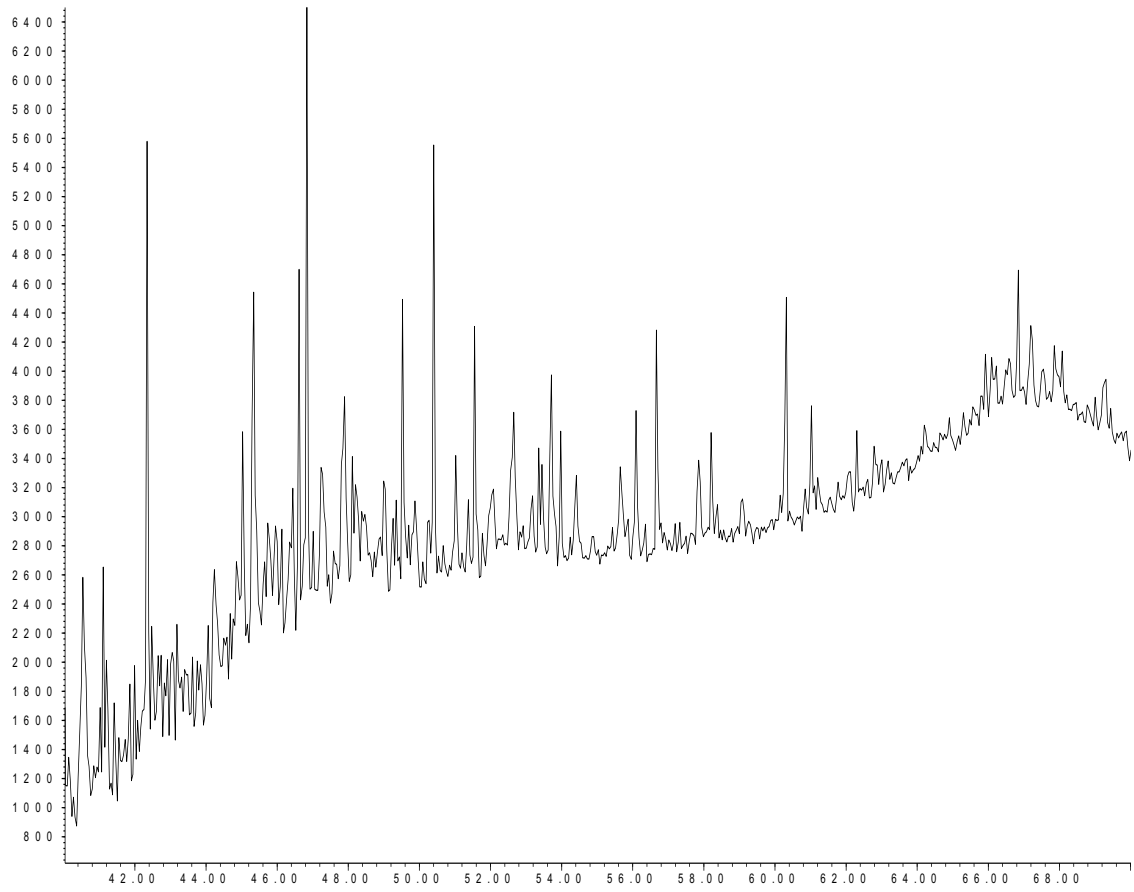
Woodford #12 Aliphatics – m/z 191.3



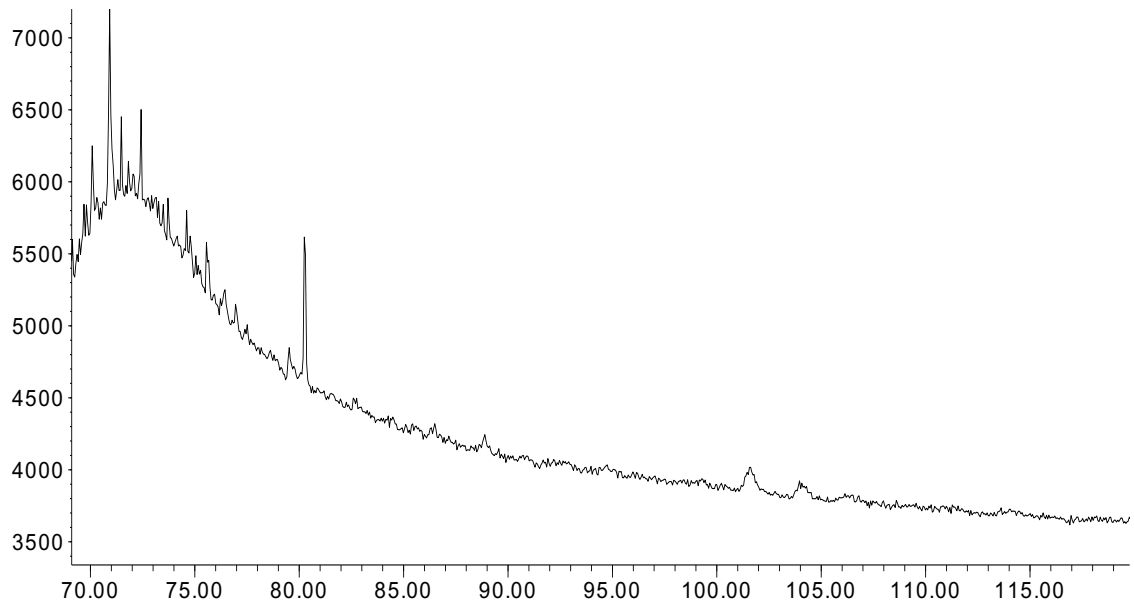
Woodford #12 Aliphatics – m/z 217.3



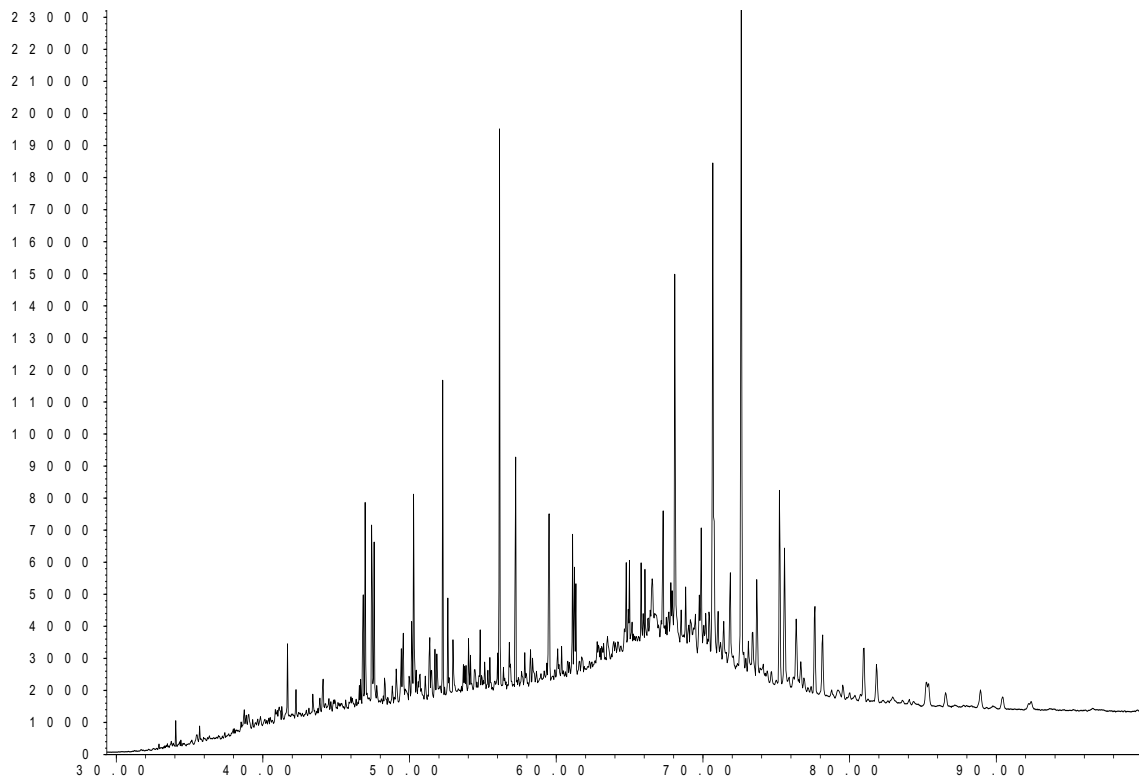
Woodford #12 Aliphatics – m/z 133.3 +134.3 (40-70 min.)



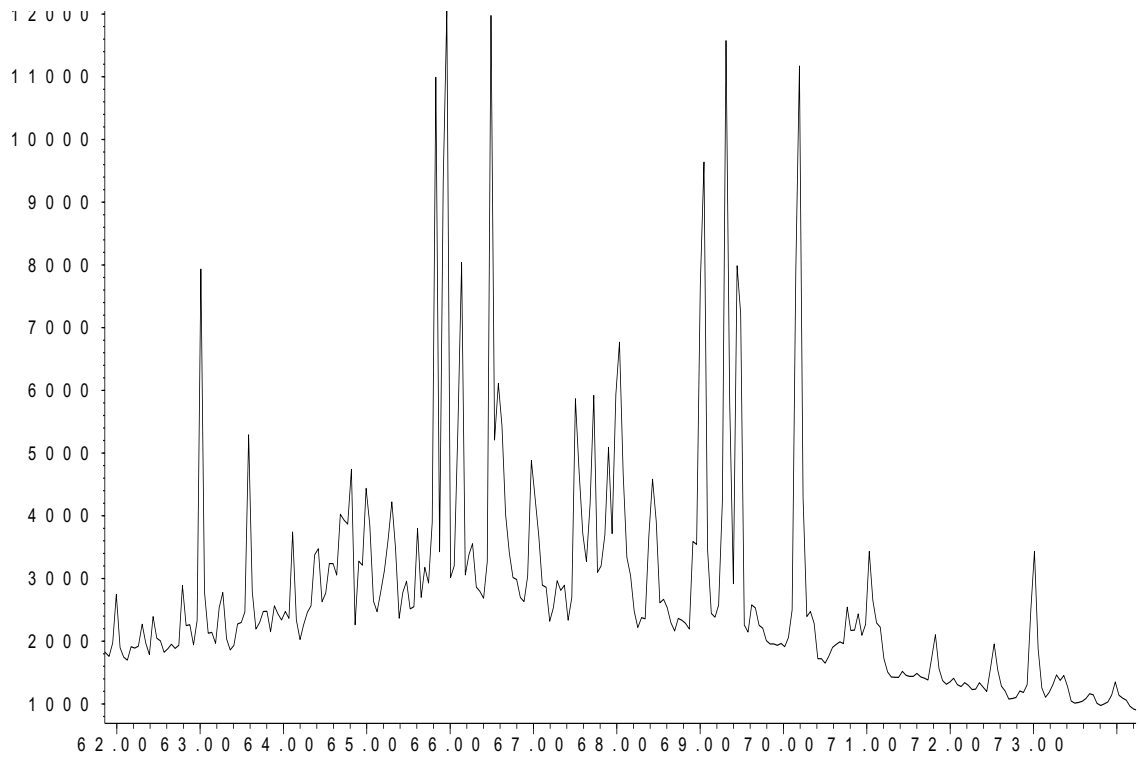
Woodford #12 Aromatics– m/z 133.3 +134.3 (70-120 min.)



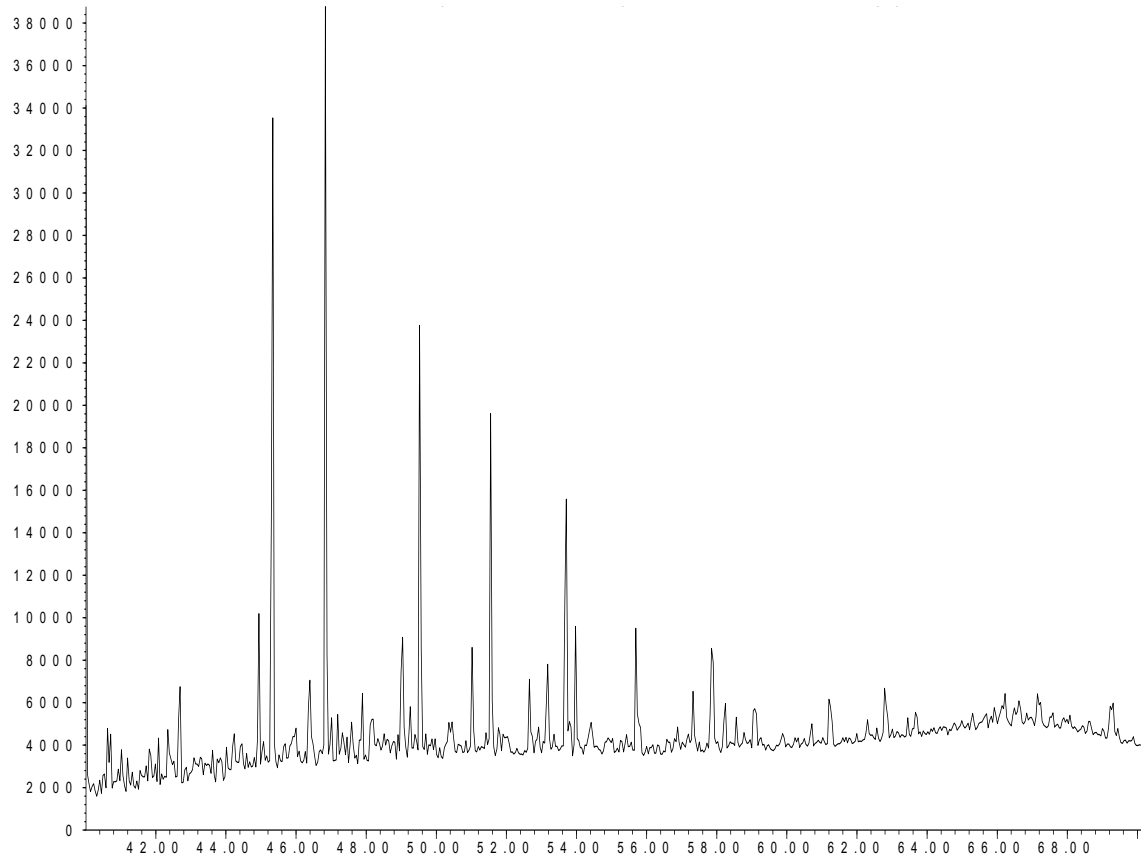
Woodford #13 Aliphatics– m/z 191.3



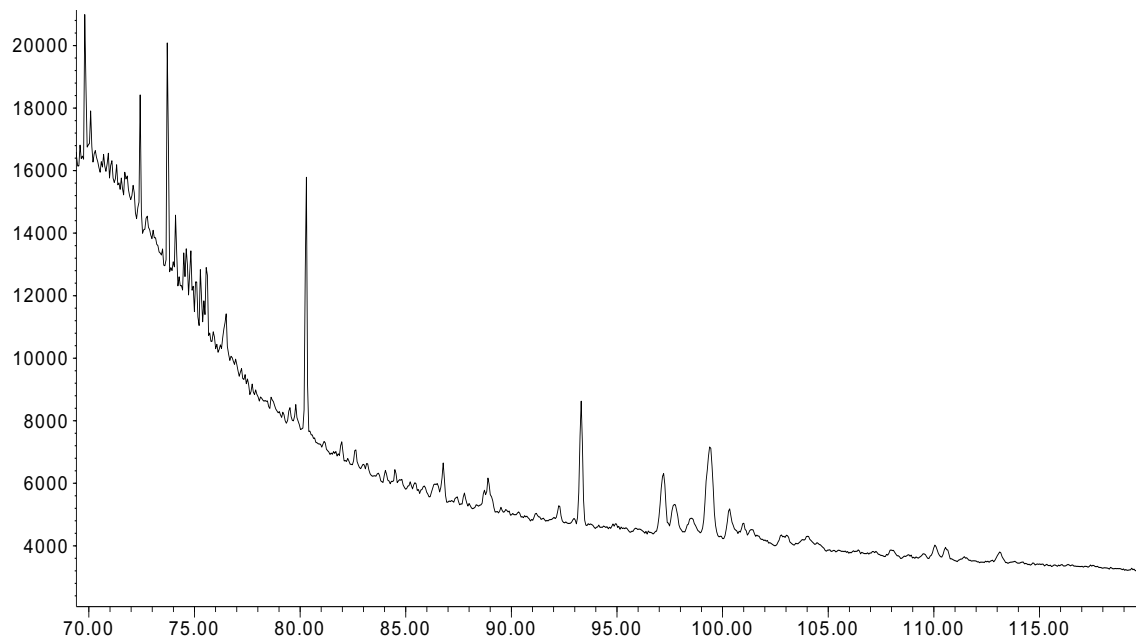
Woodford #13 Aliphatics– m/z 217.3



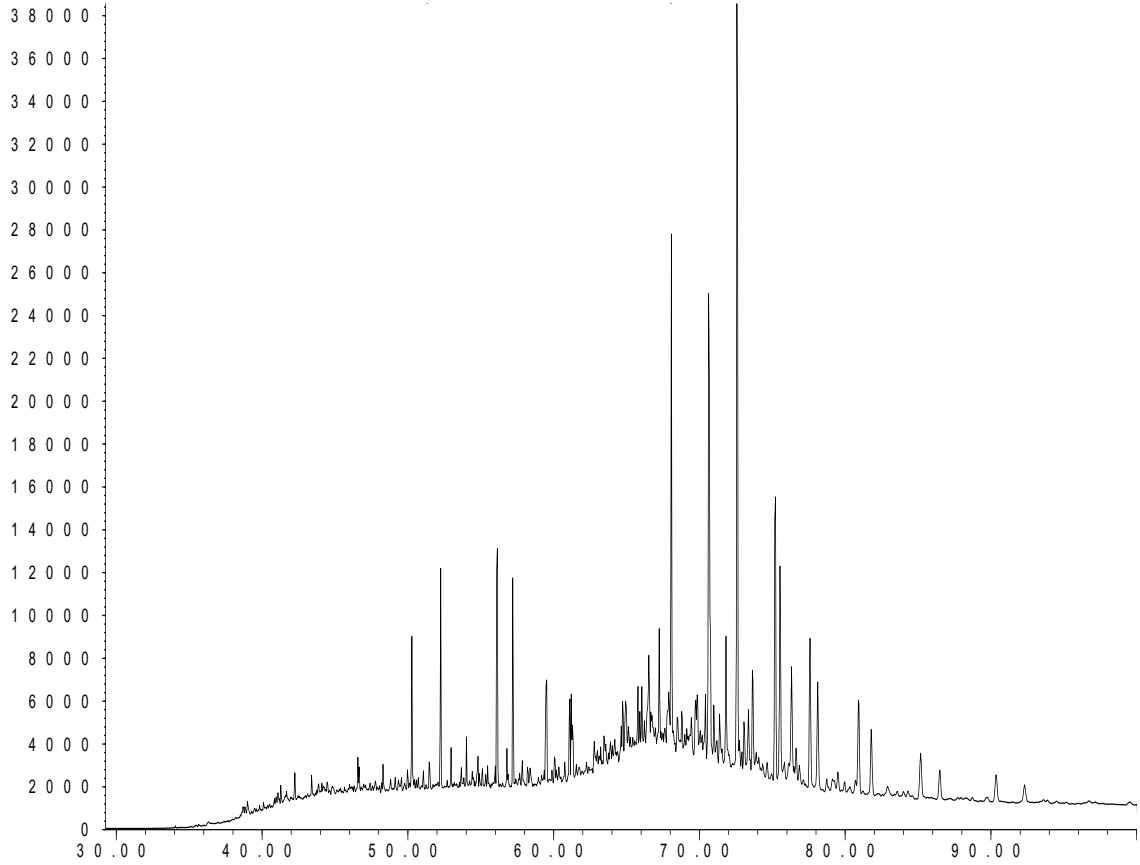
Woodford #13 Aliphatics– m/z 133.3 + 134.3 (40-70 min.)



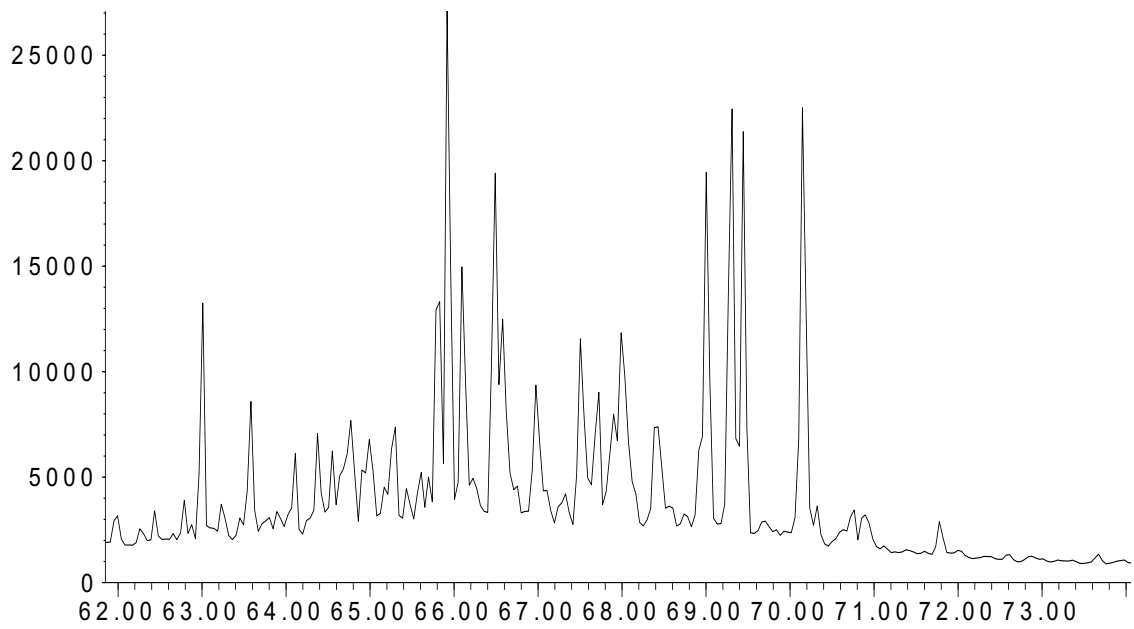
Woodford #13 Aromatics– m/z 133.3 + 134.3 (70-120 min.)



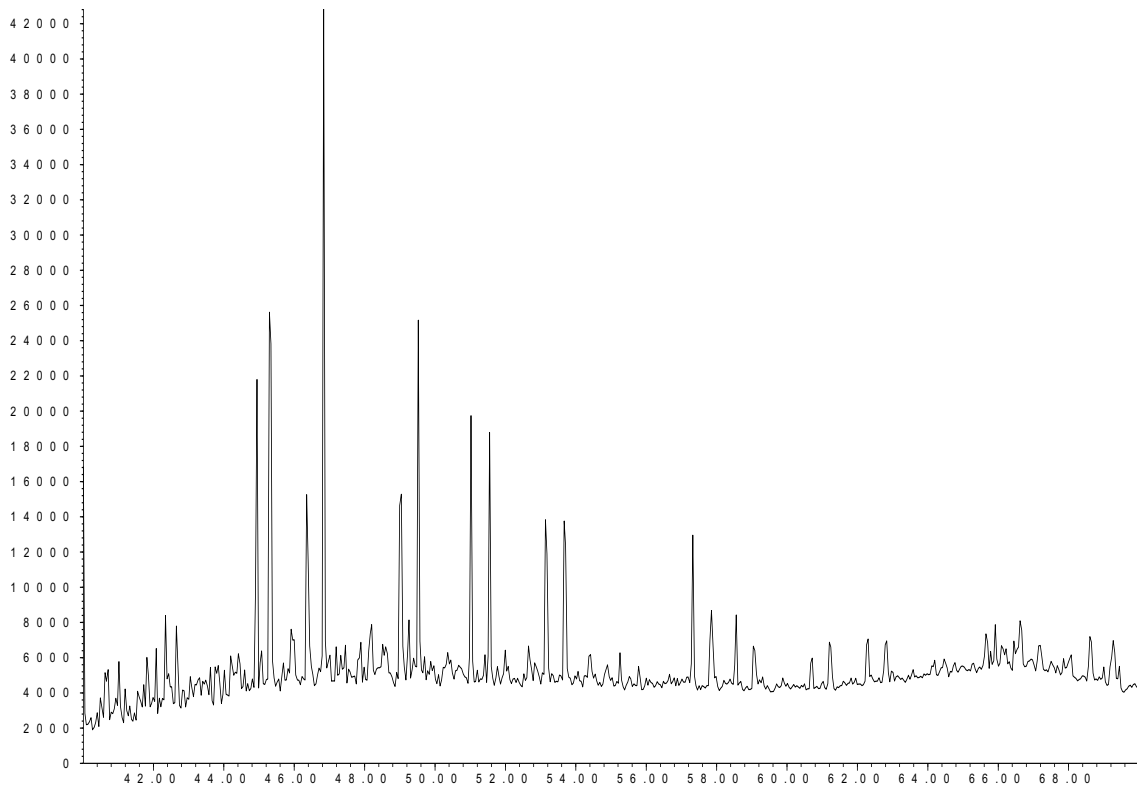
Woodford 14 Aliphatics – m/z 191.3



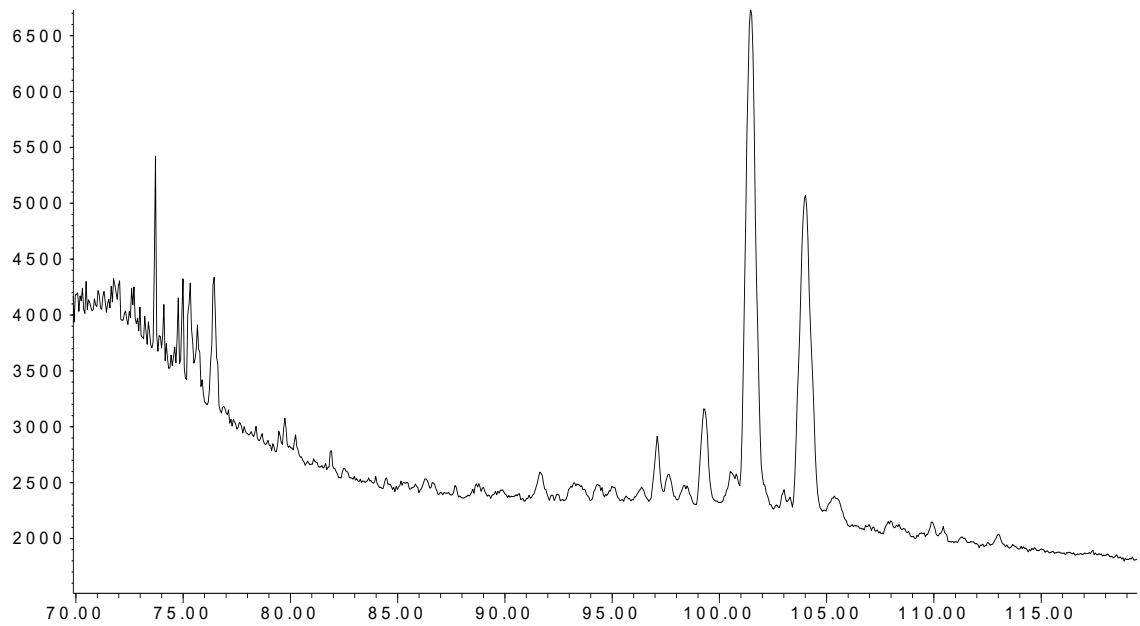
Woodford 14 Aliphatics – m/z 217.3



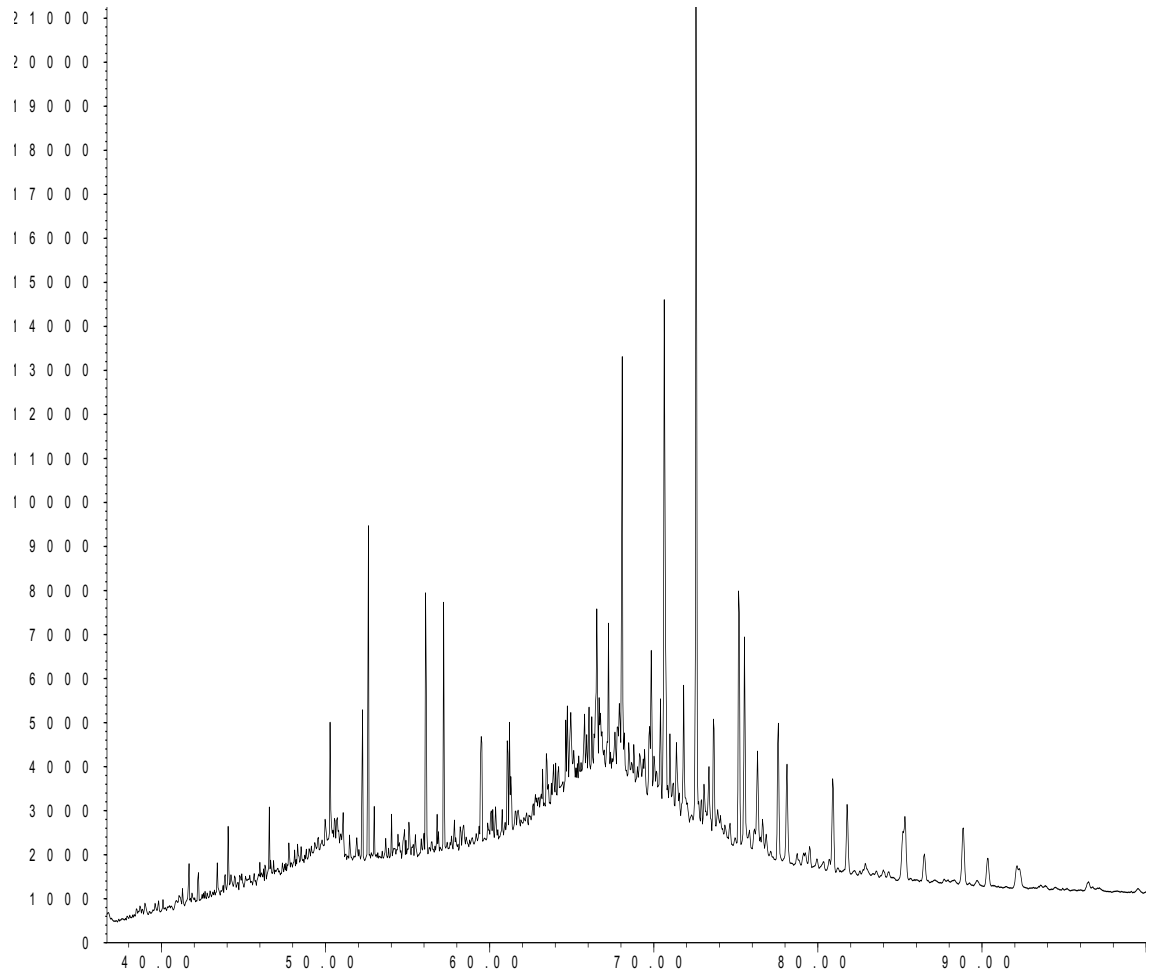
Woodford 14 Aliphatics – m/z 133.3 + 134.3 (40-70 min.)



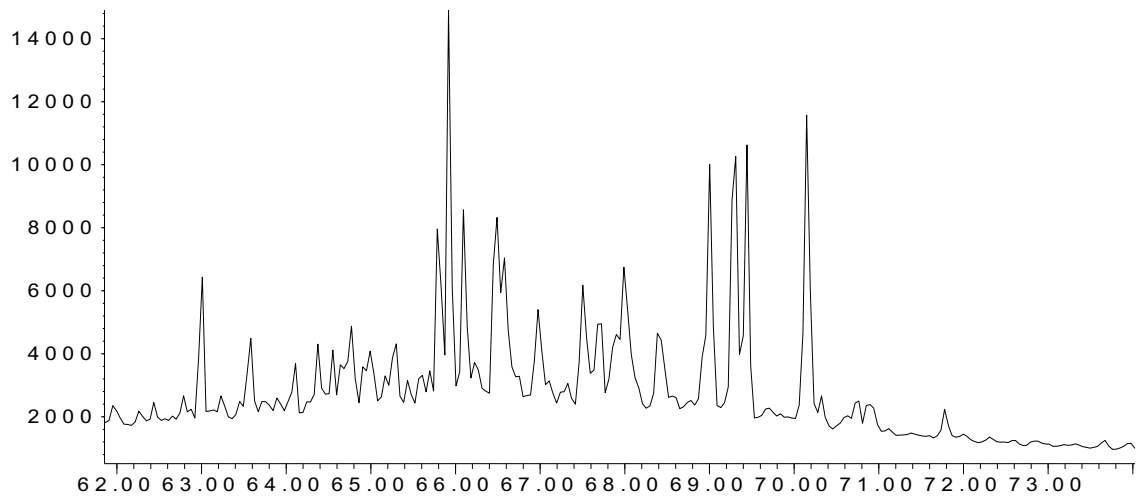
Woodford 14 Aromatics – m/z 133.3 + 134.3 (70-120 min.)



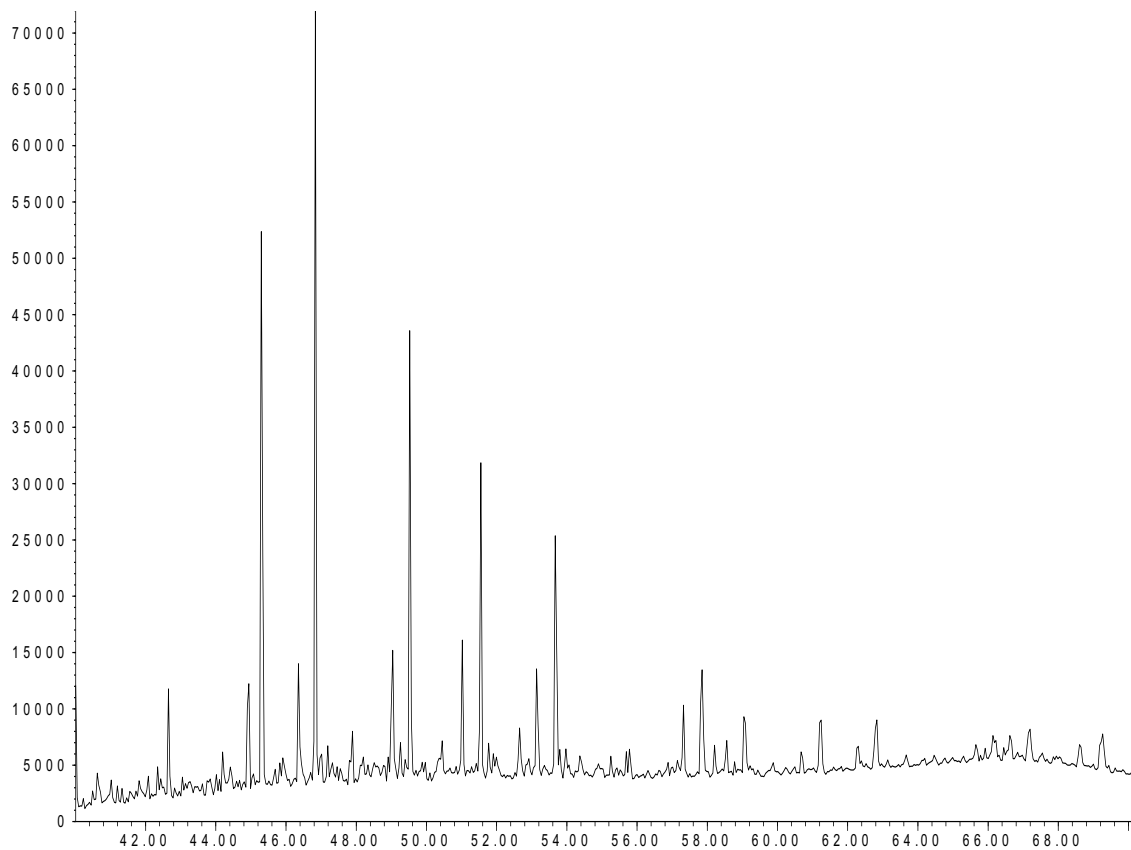
Woodford 16 Aliphatics – m/z 191.3



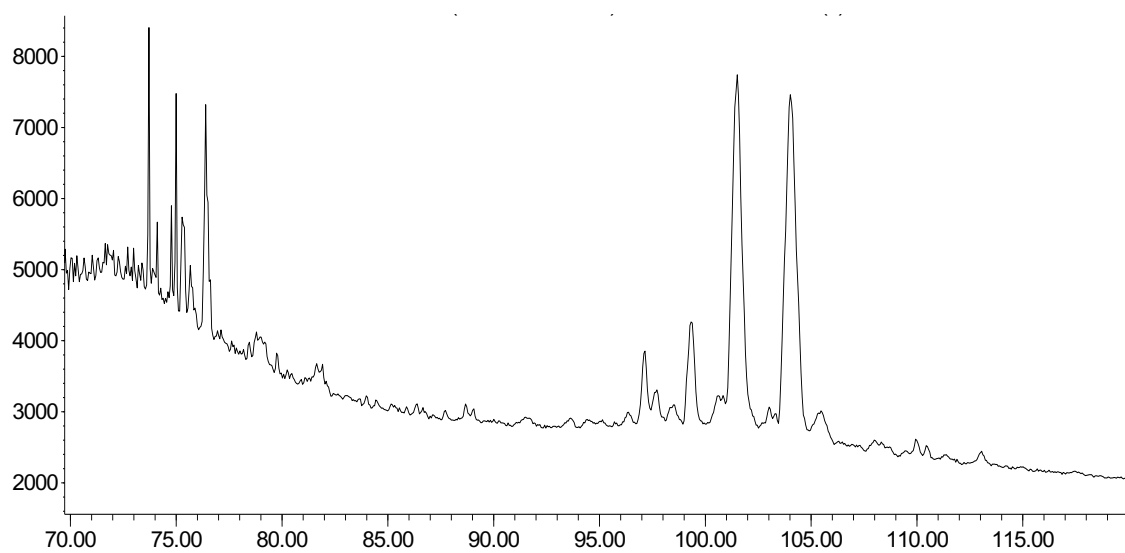
Woodford 16 Aliphatics – m/z 217.3



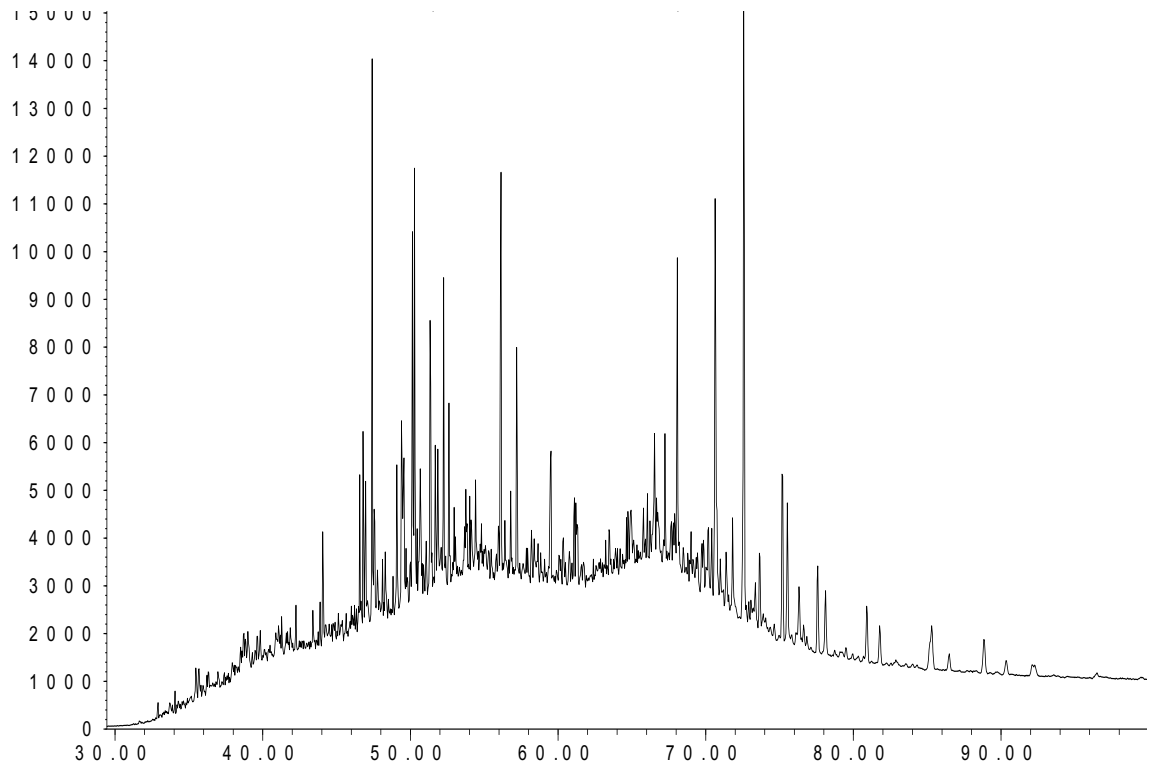
Woodford 16 Aliphatics – m/z 133.3 + 134.3 (40-70 min.)



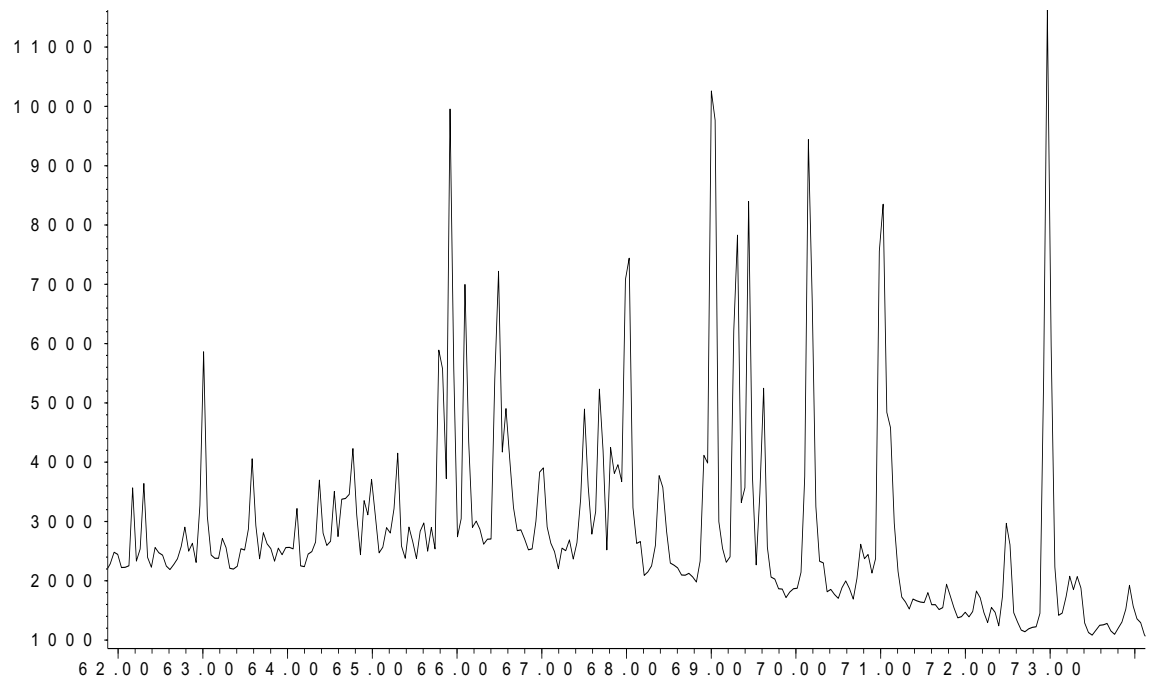
Woodford 16 Aromatics – m/z 133.3 + 134.3 (70-120 min.)



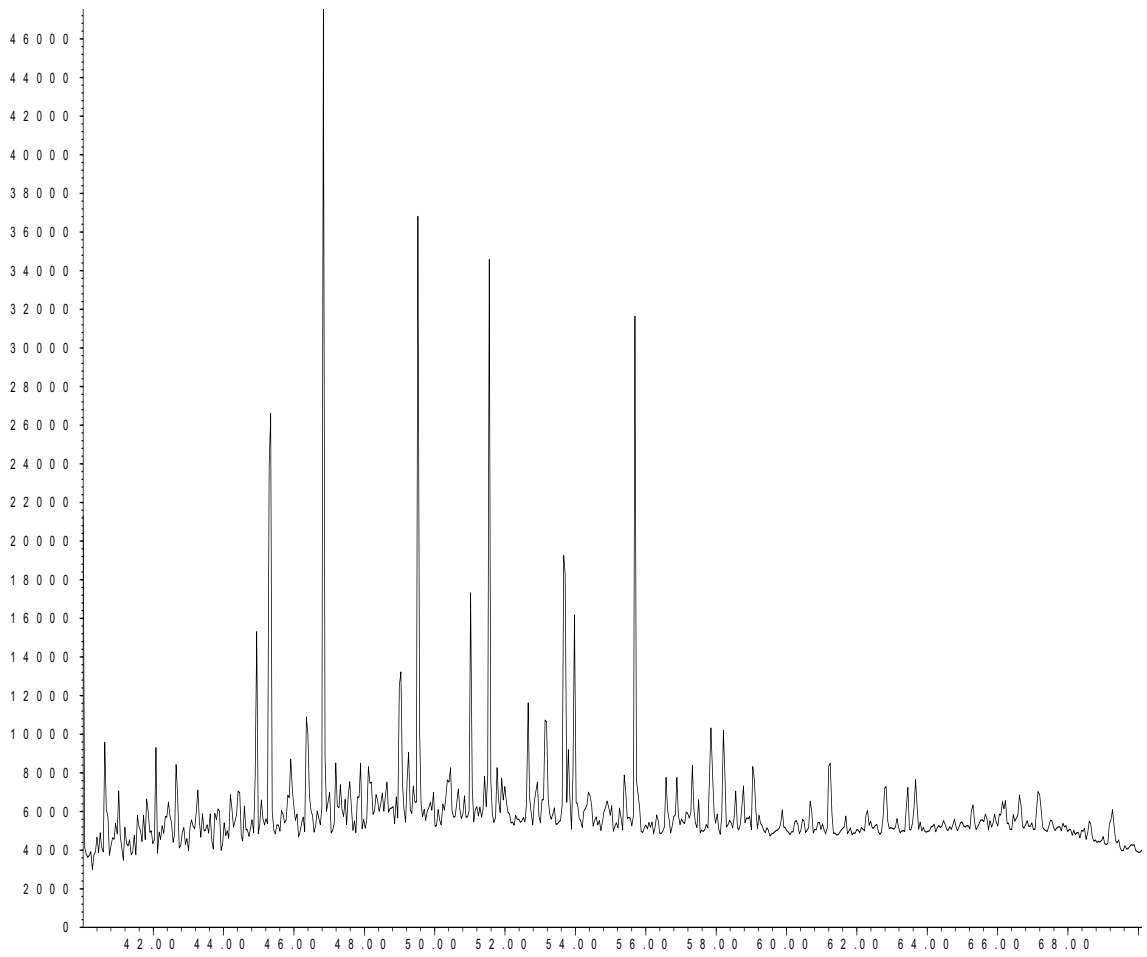
Woodford 26 Aliphatics – m/z 191.3



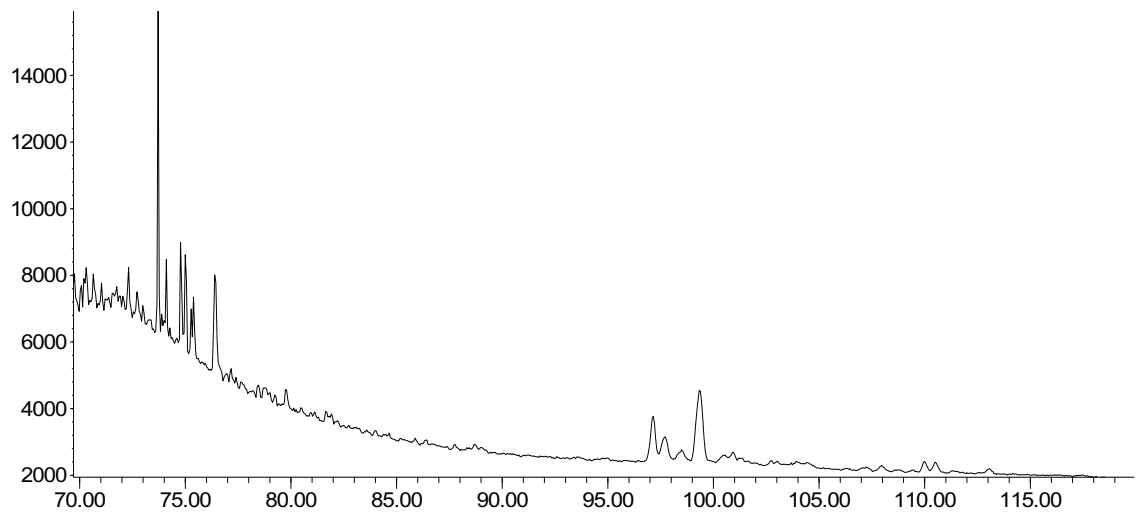
Woodford 26 Aliphatics – m/z 217.3



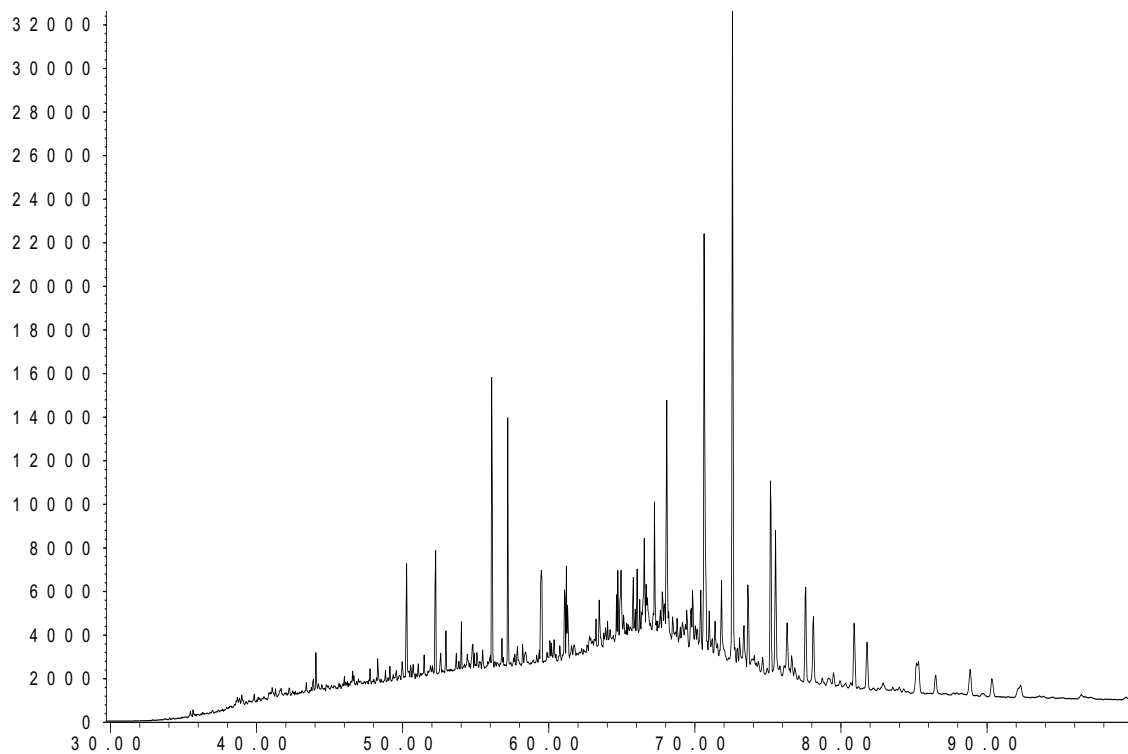
Woodford 26 Aliphatics – m/z 133.3 +134.3 (40-70 min.)



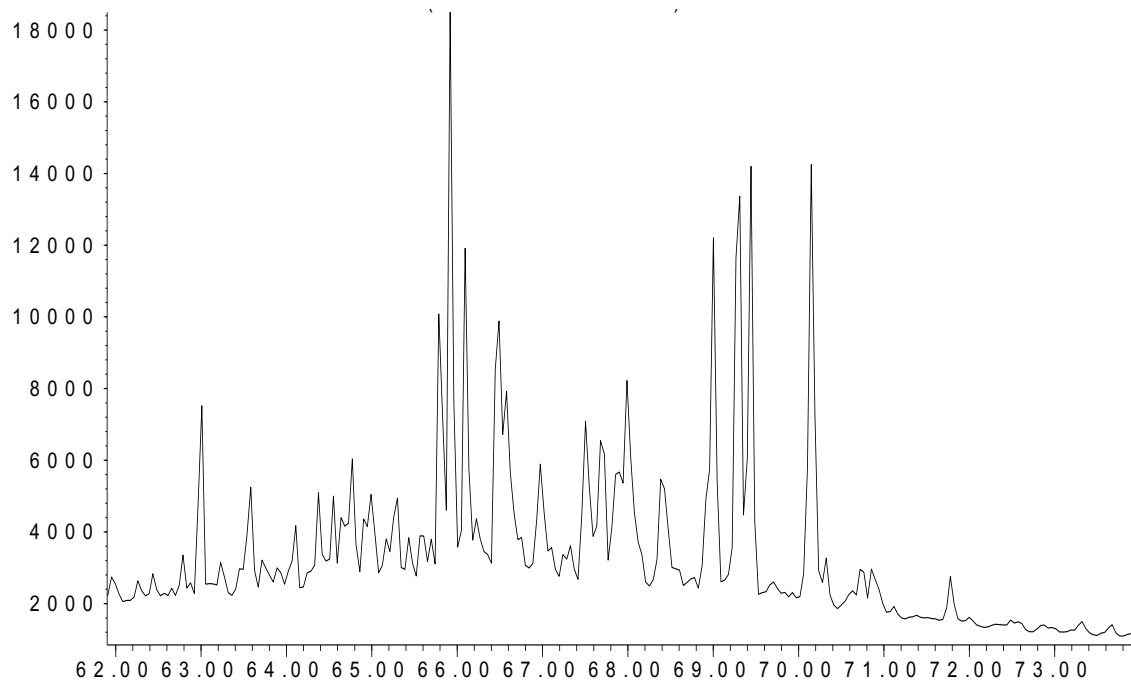
Woodford 26 Aromatics – m/z 133.3 +134.3 (70-120 min.)



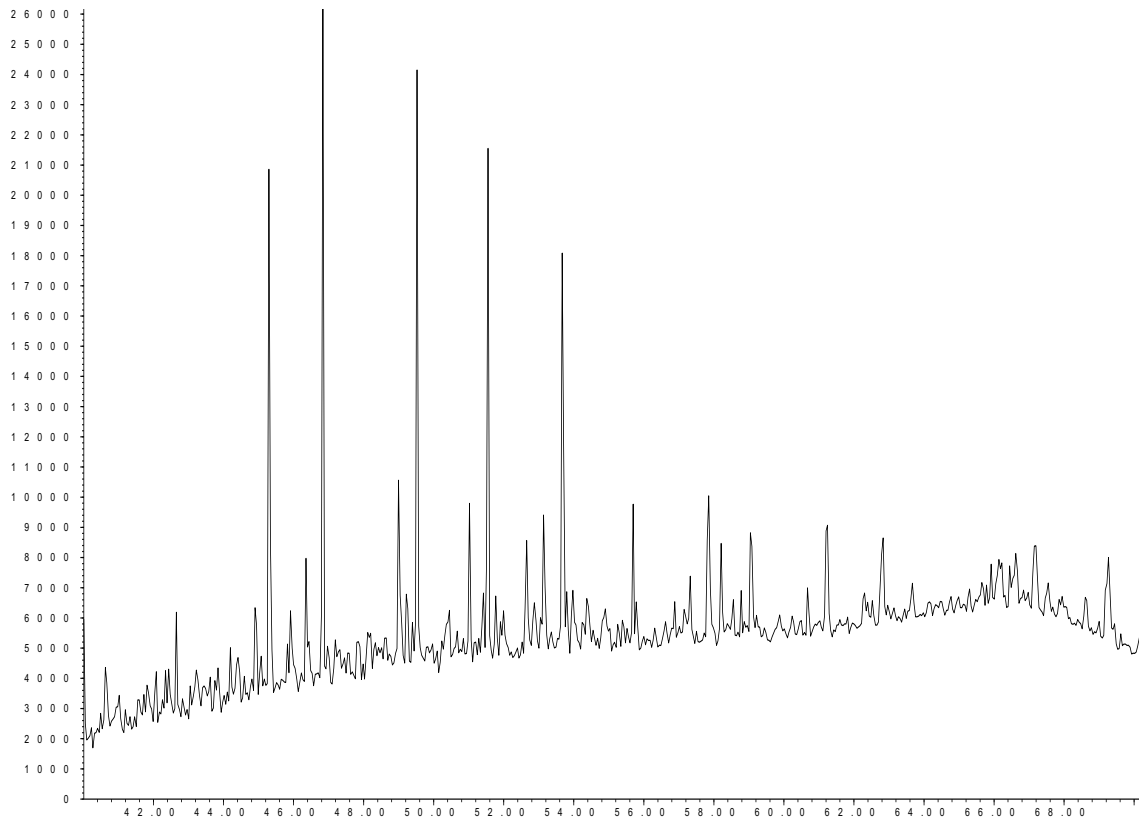
Woodford 30 Aliphatics – m/z 191.3



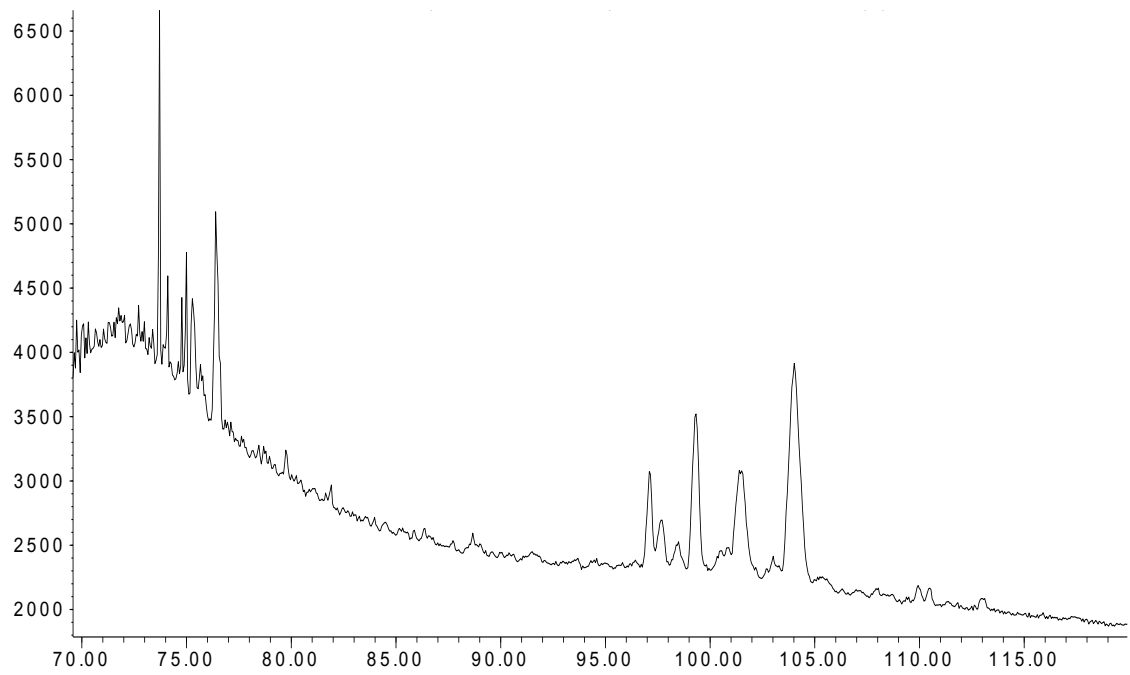
Woodford 30 Aliphatics – m/z 217.3



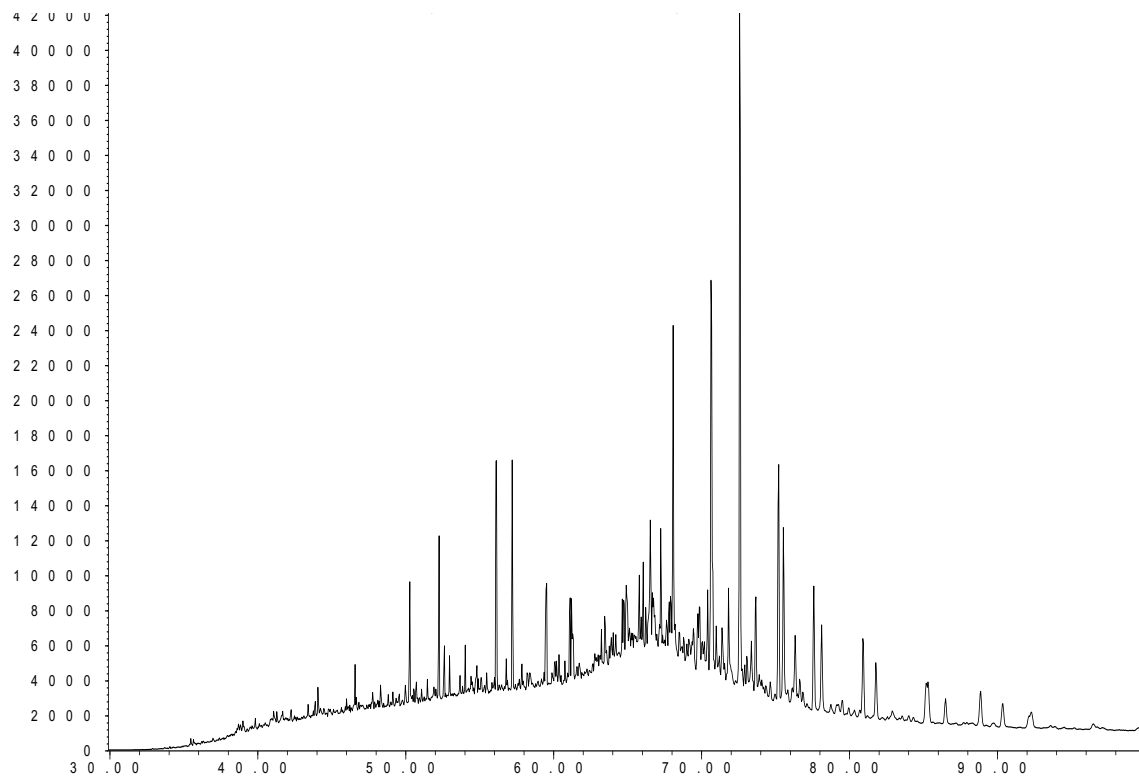
Woodford 30 Aliphatics – m/z 133.3 + 134.3 (40-70 min.)



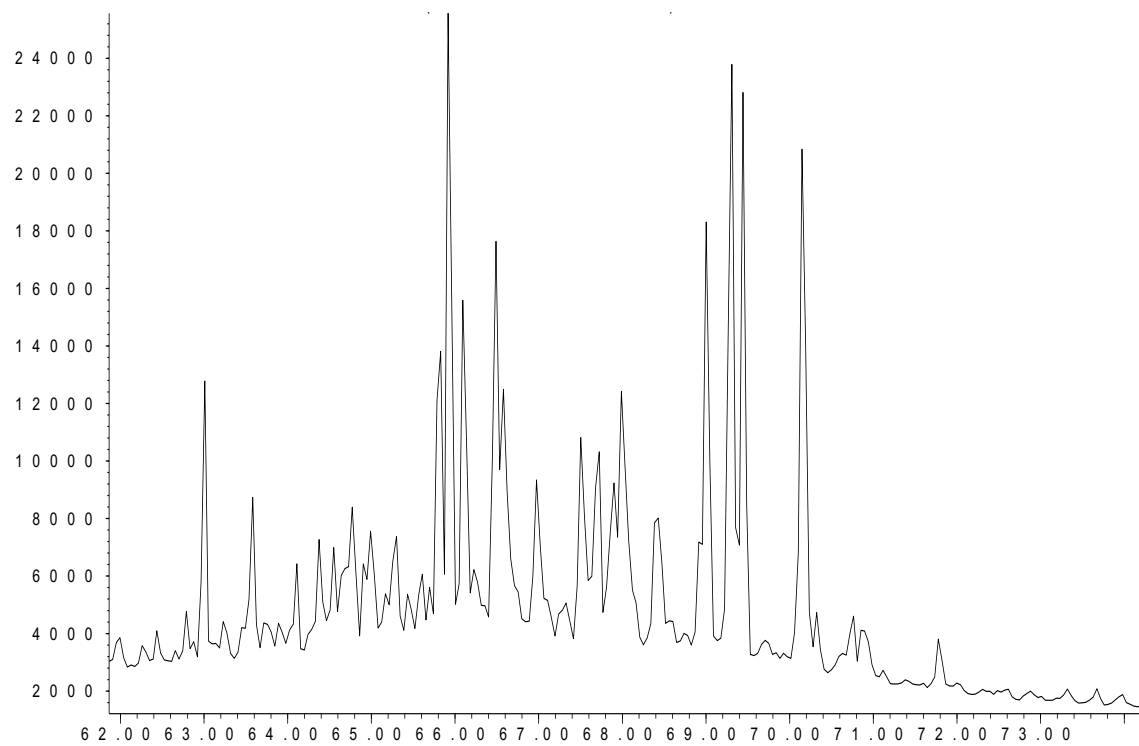
Woodford 30 Aromatics – m/z 133.3 + 134.3 (70-120 min.)



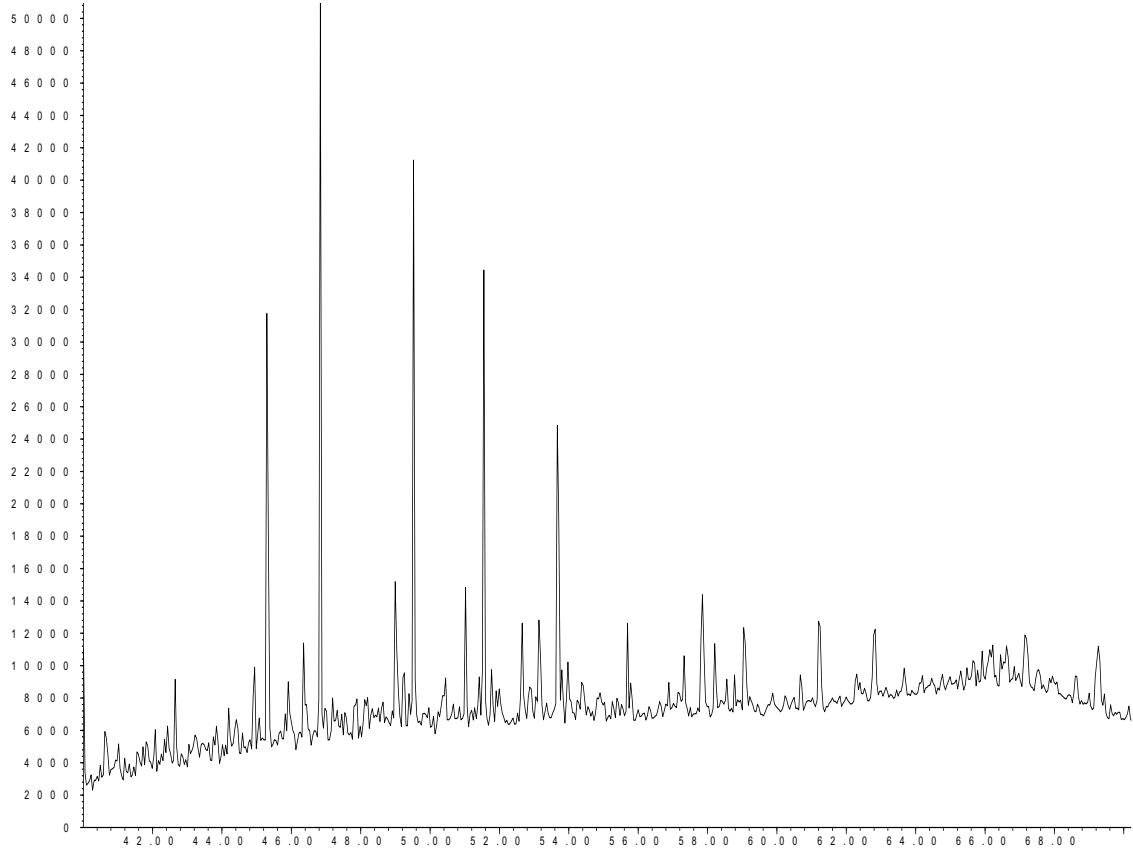
Woodford 32 Aliphatics – m/z 191.3



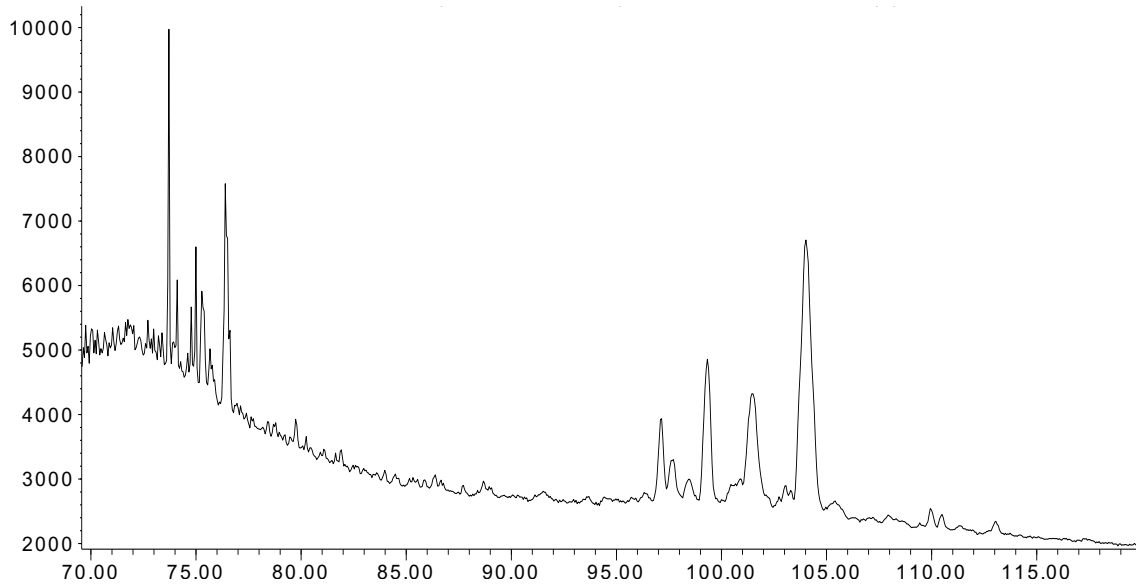
Woodford 32 Aliphatics – m/z 217.3



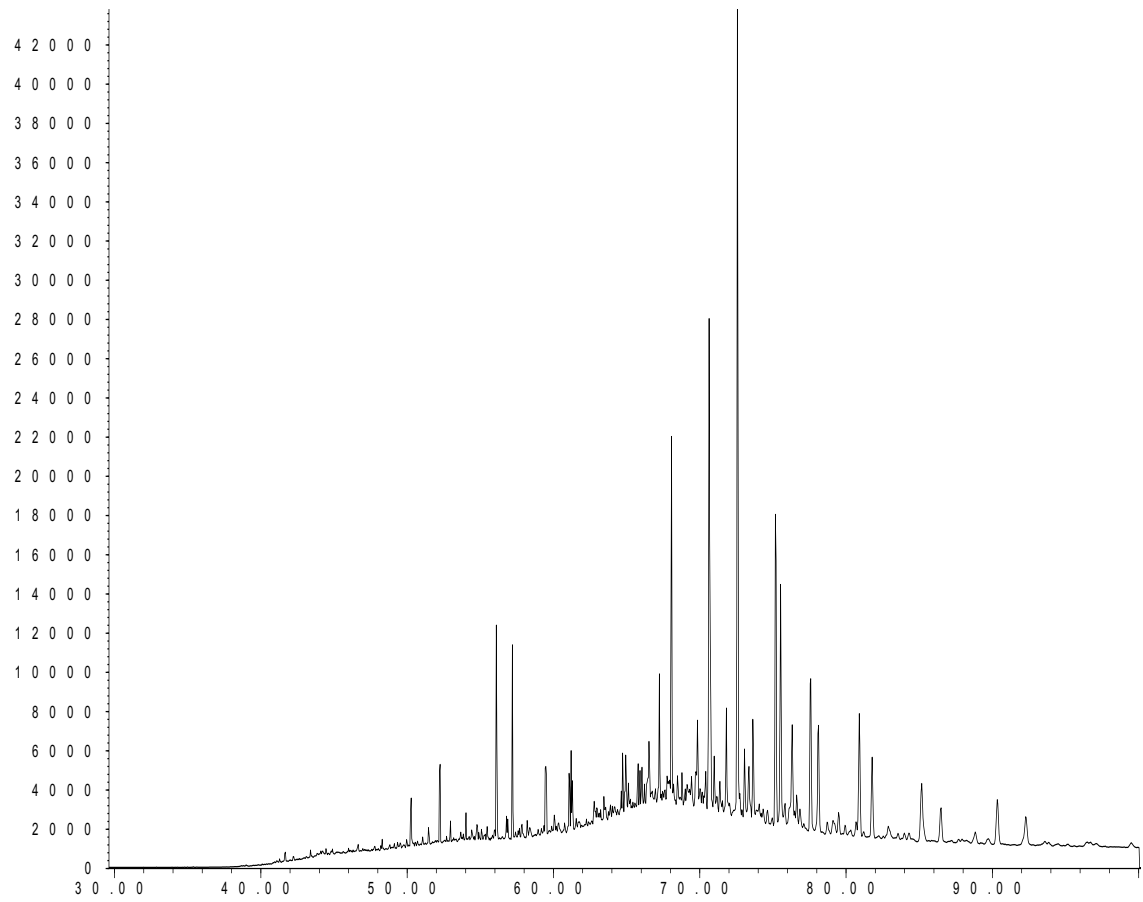
Woodford 32 Aliphatics – m/z 133.3 + 134.3 (40-70 min.)



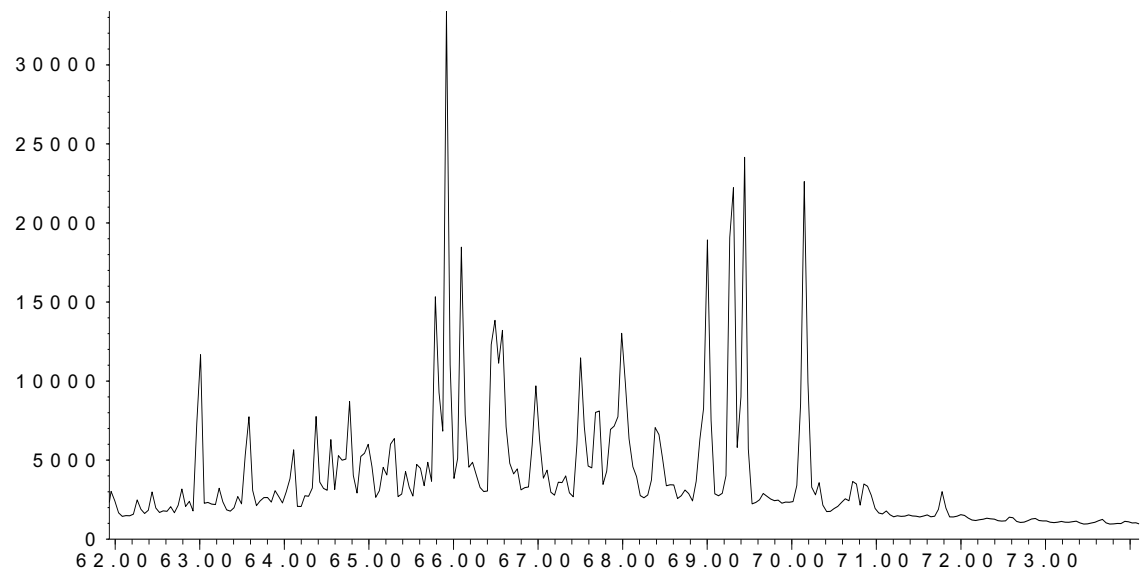
Woodford 32 Aromatics – m/z 133.3 + 134.3 (70-120 min.)



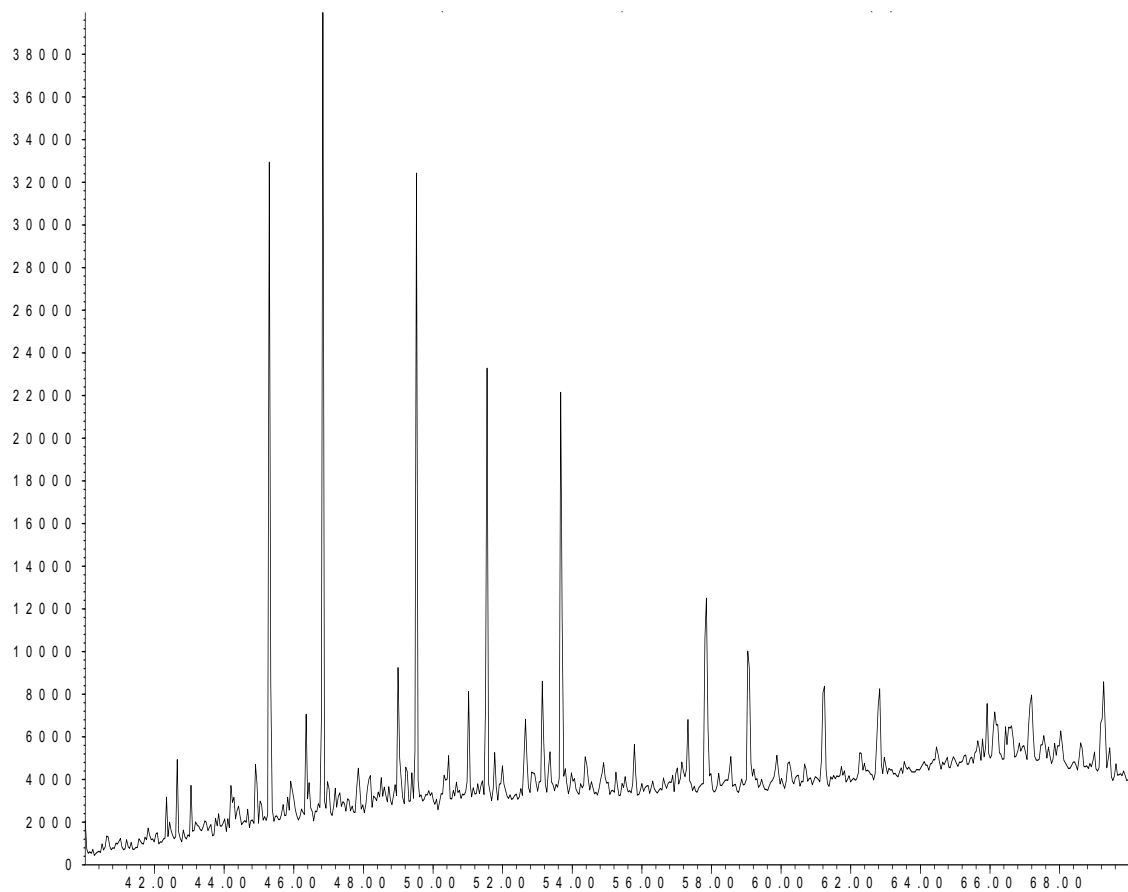
Woodford 37 Aliphatics – m/z 191.3



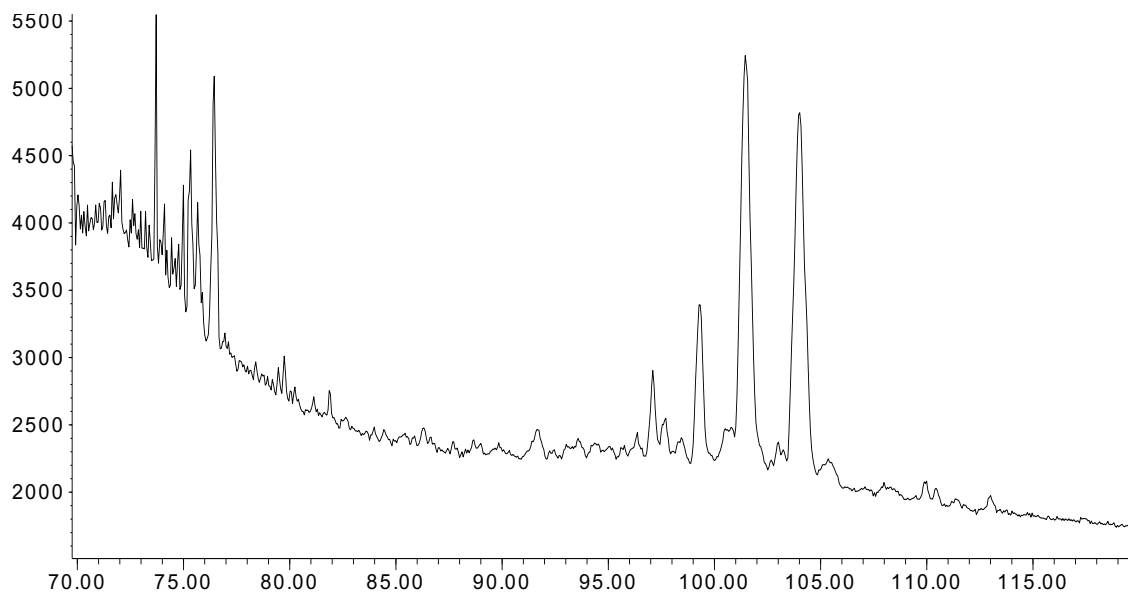
Woodford 37 Aliphatics – m/z 217.3



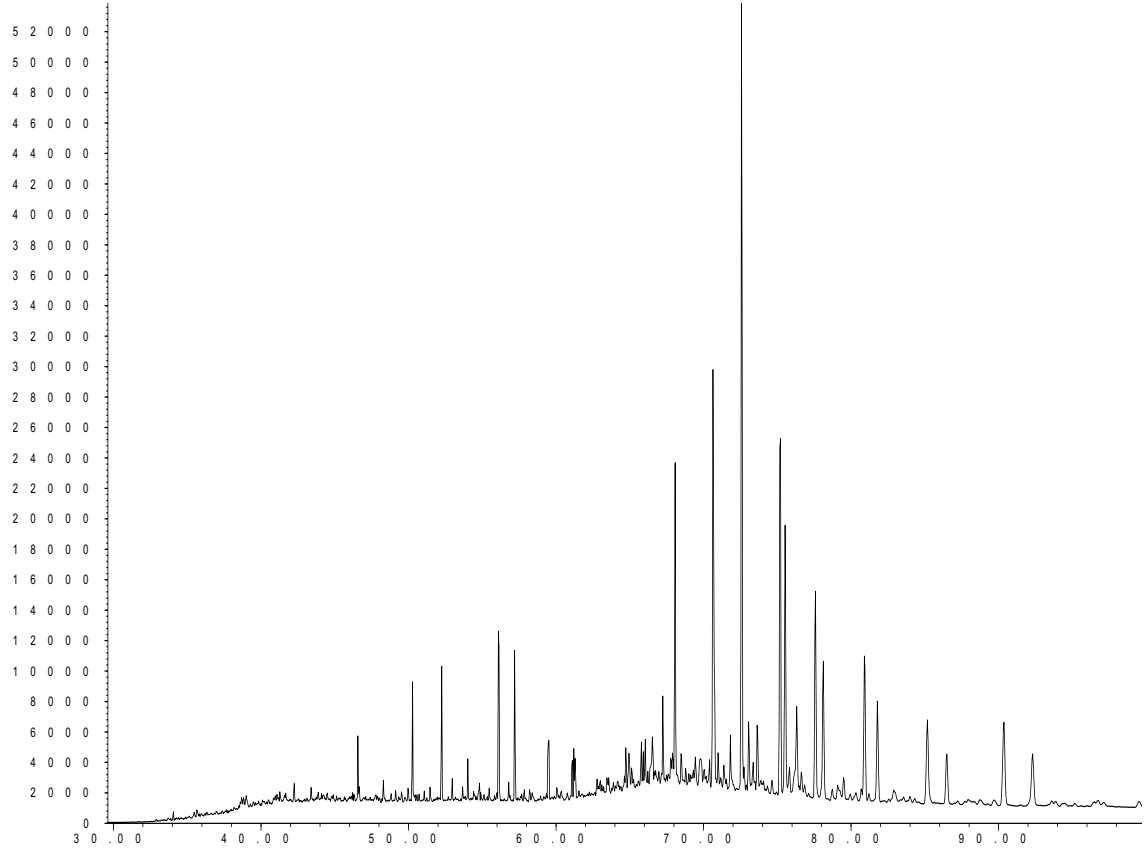
Woodford 37 Aliphatics – m/z 133.3 + 134.2 (40-70 min.)



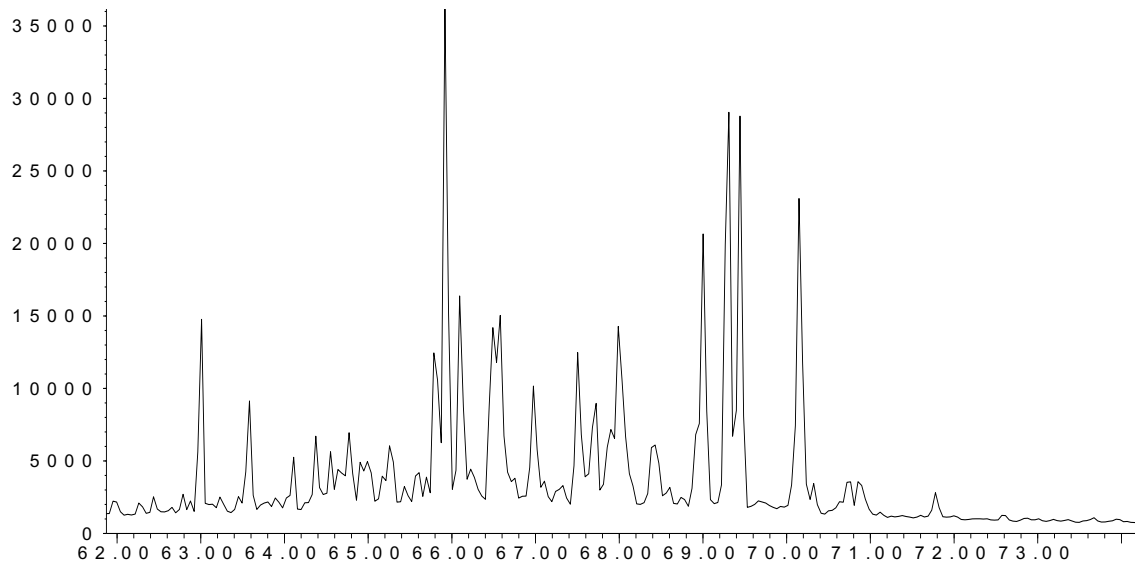
Woodford 37 Aromatics – m/z 133.3 + 134.3 (70-120 min.)



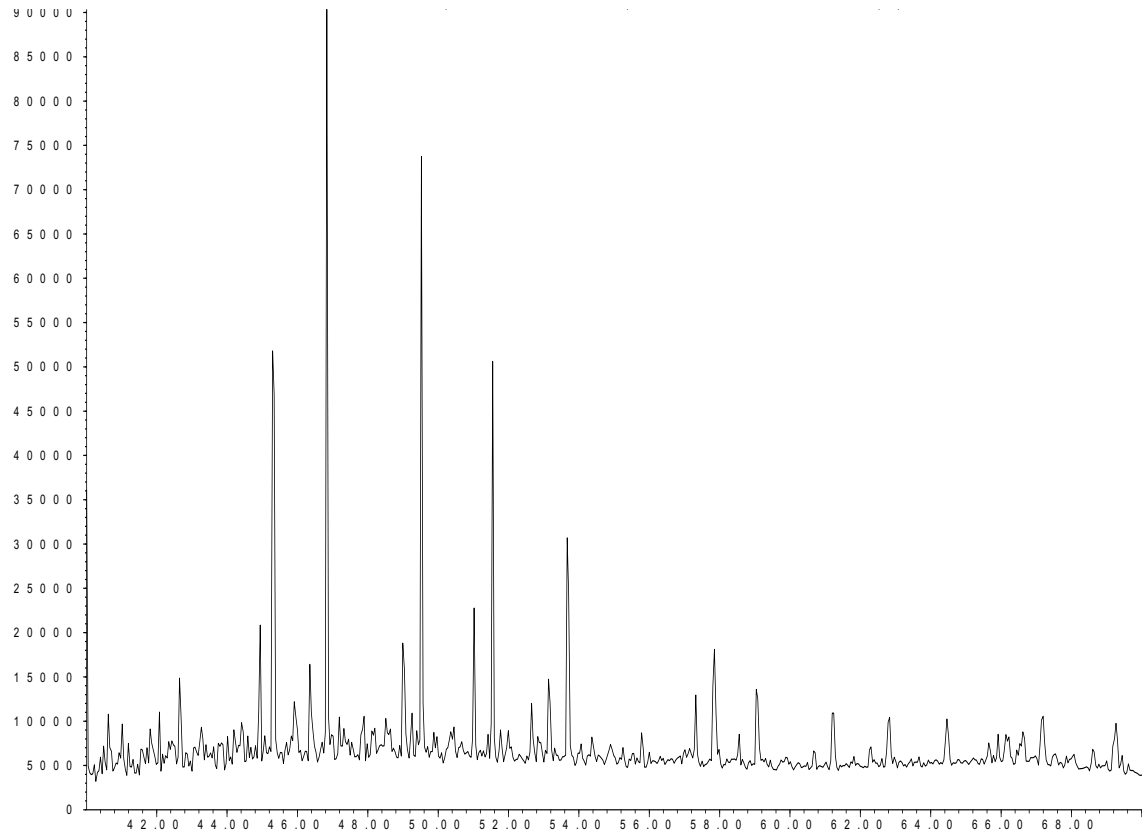
Woodford 43 Aliphatics – m/z 191.3



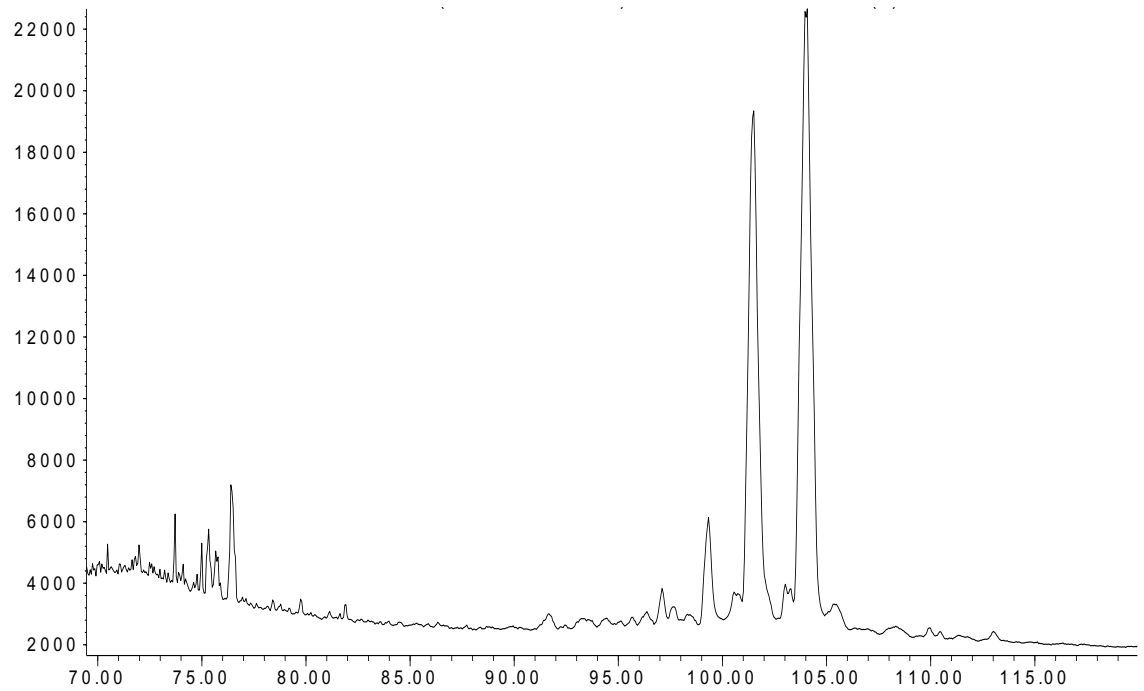
Woodford 43 Aliphatics – m/z 217.3



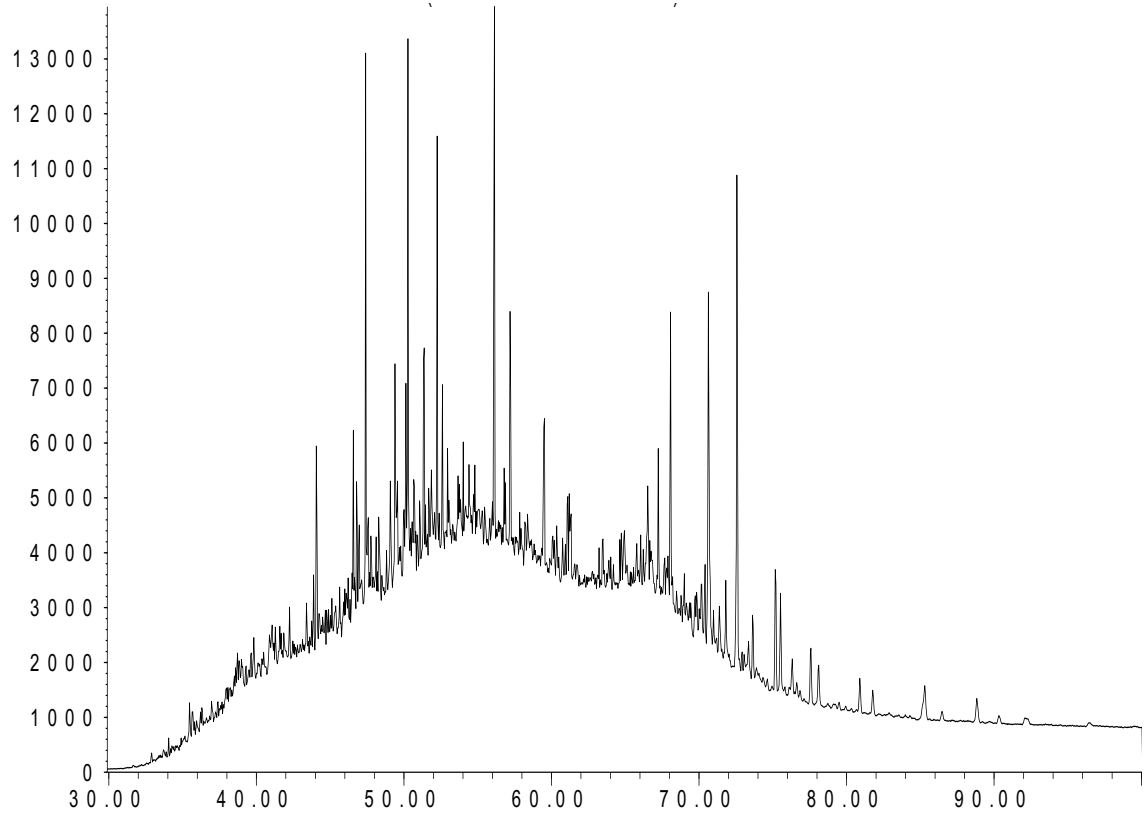
Woodford 43 Aliphatics – m/z 133.3 + 134.3 (40-70 min.)



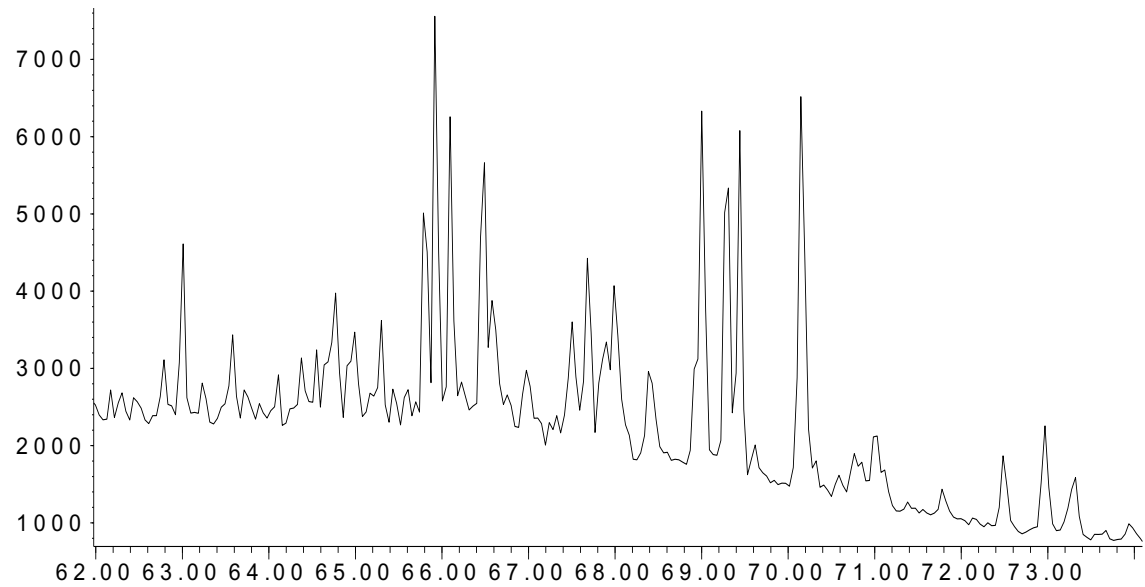
Woodford 43 Aromatics – m/z 133.3 + 134.3 (70-120 min.)



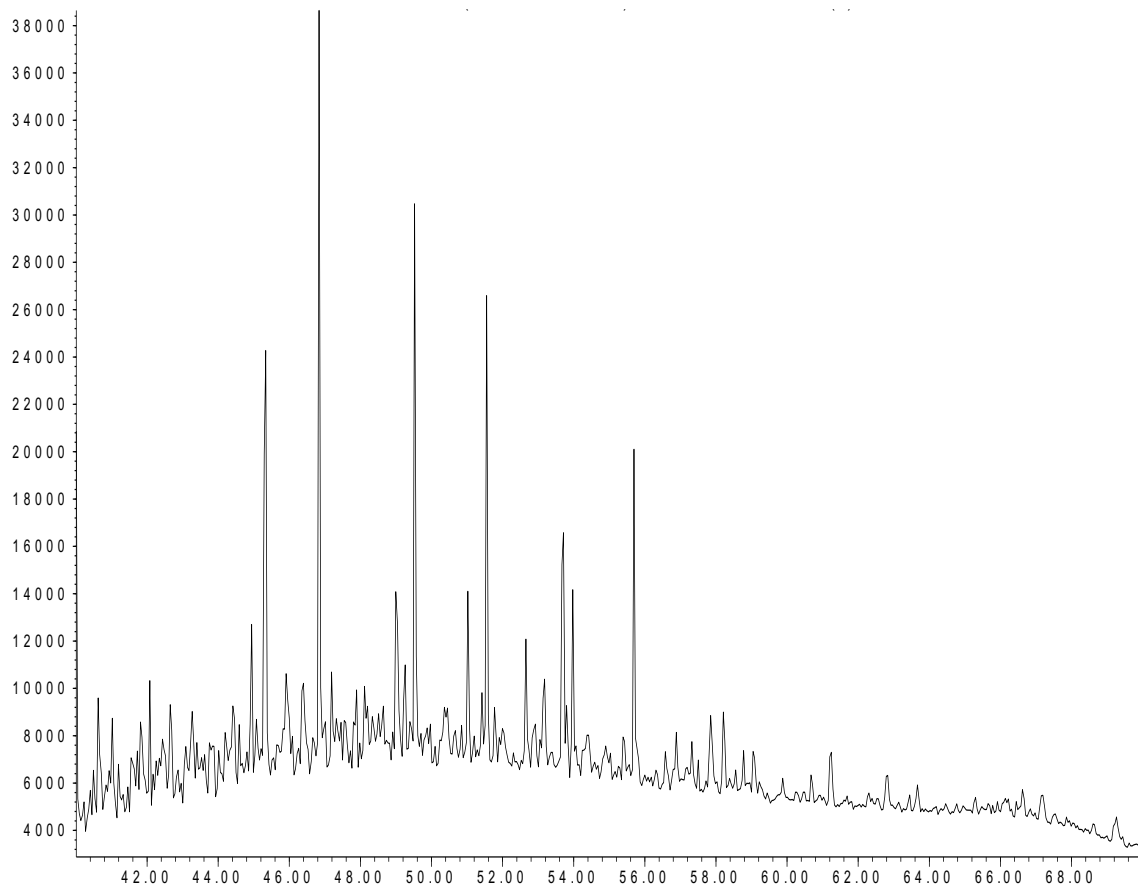
Woodford 45 Aliphatics – m/z 191.3



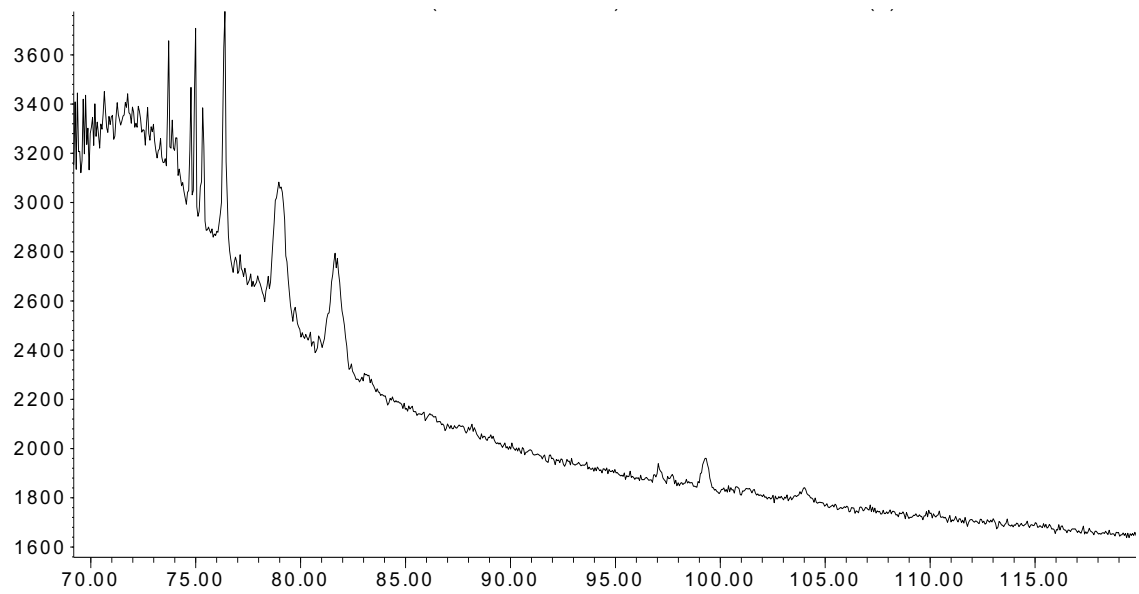
Woodford 45 Aliphatics – m/z 217.3



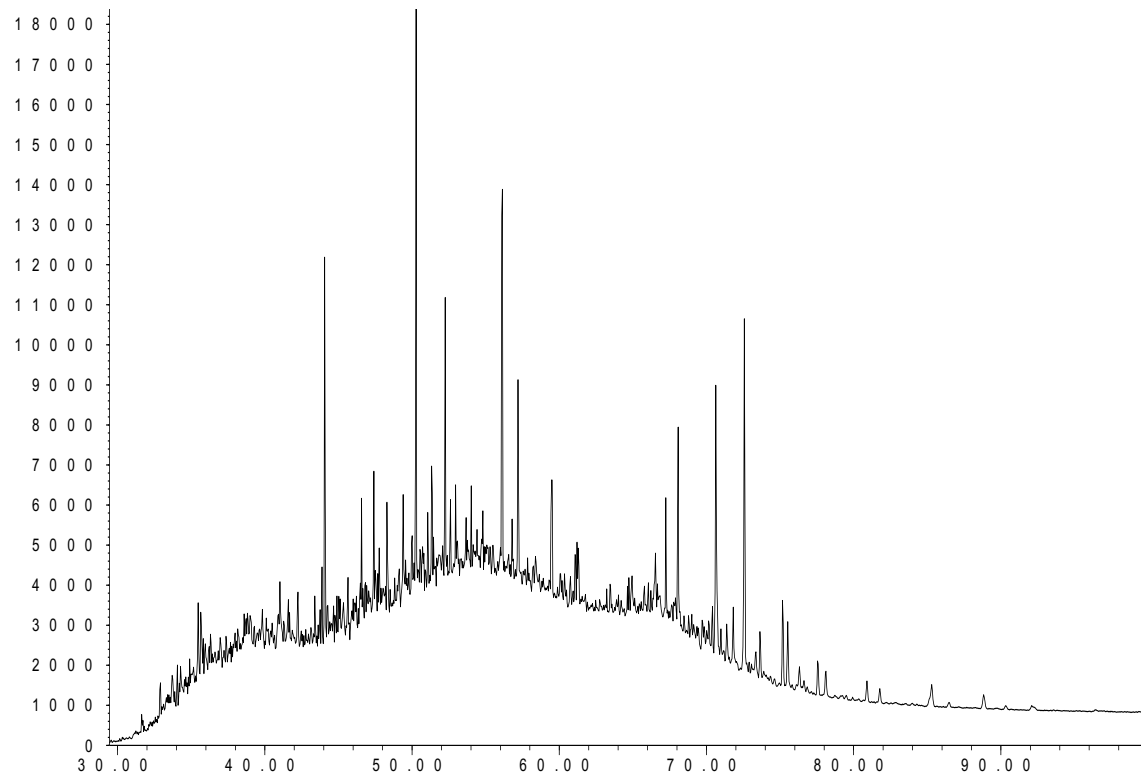
Woodford 45 Aliphatics – m/z 133.3 + 134.3 (40-70 min.)



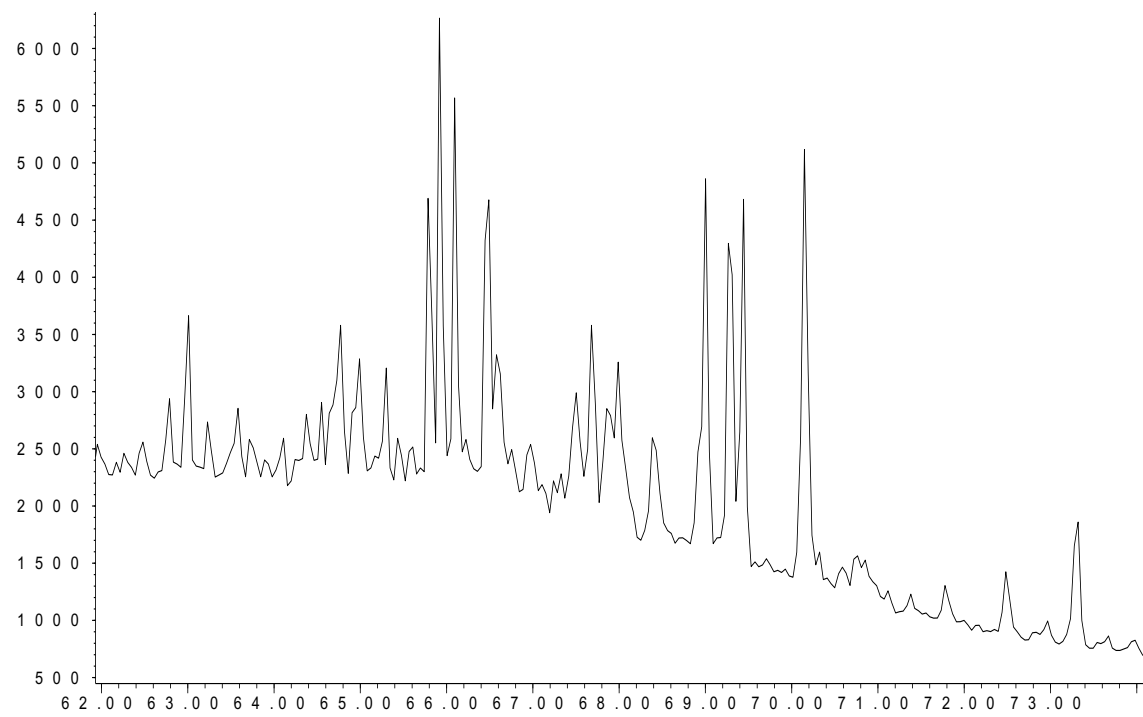
Woodford 45 Aromatics – m/z 133.3 + 134.3 (70-120 min.)



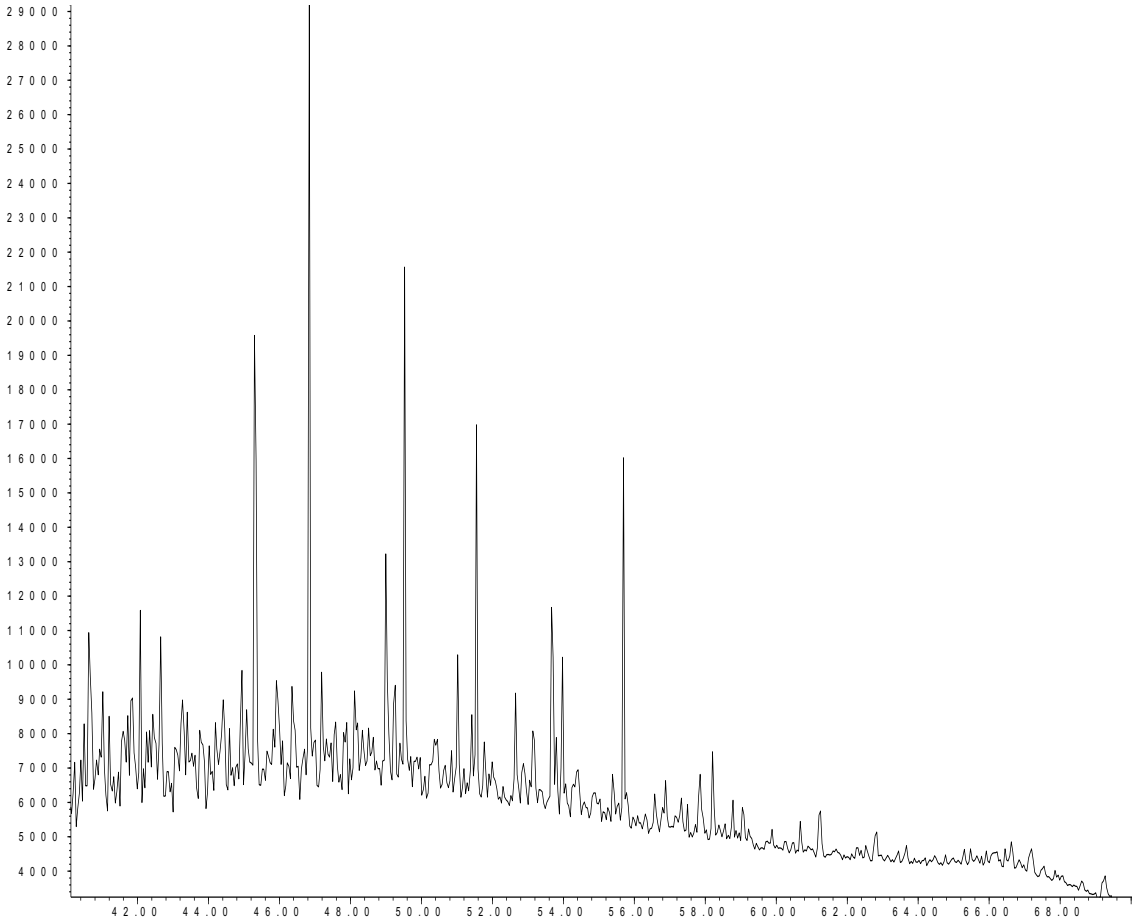
Woodford 50 Aliphatics – m/z 191.3



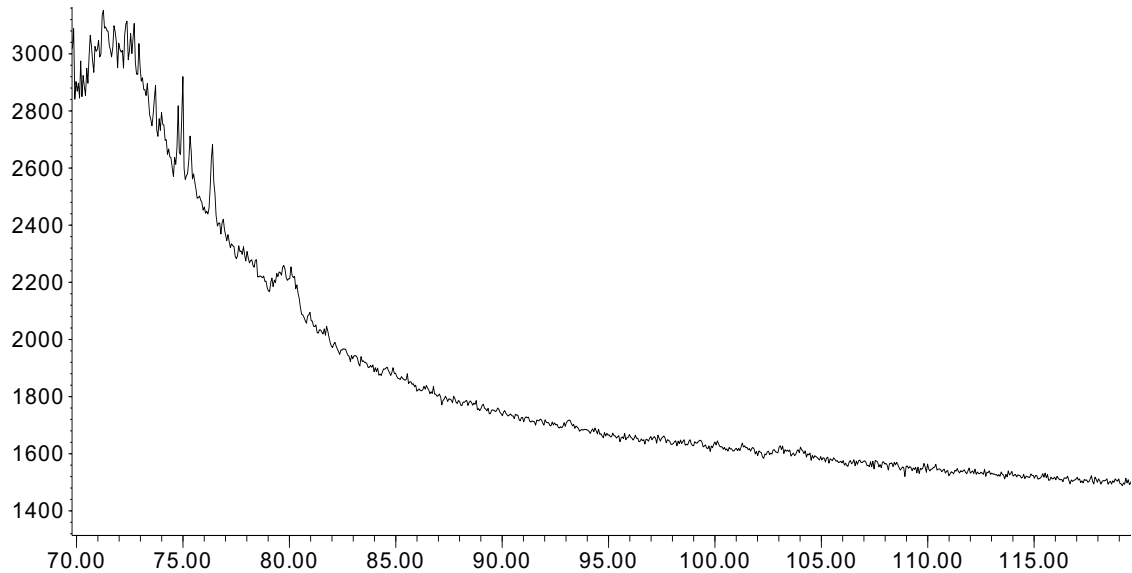
Woodford 50 Aliphatics – m/z 217.3



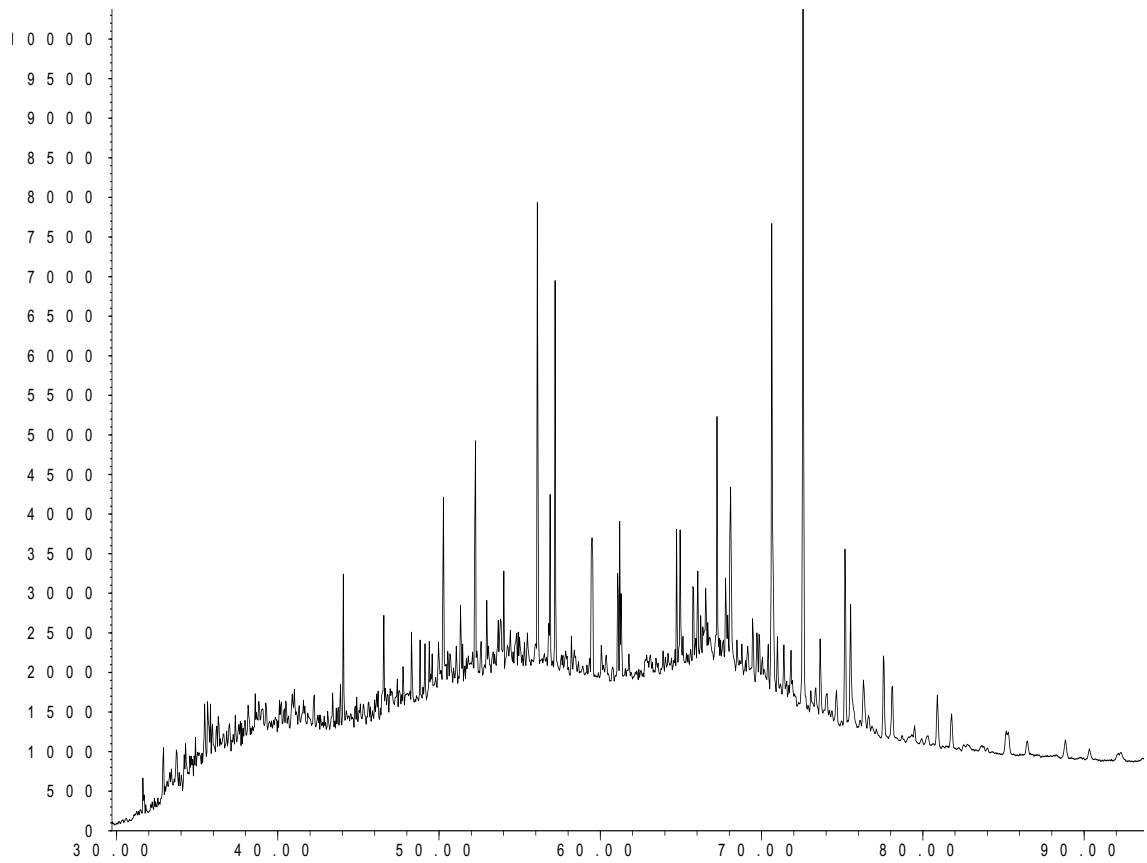
Woodford 50 Aliphatics – m/z 133.3 + 134.3 (40-70 min.)



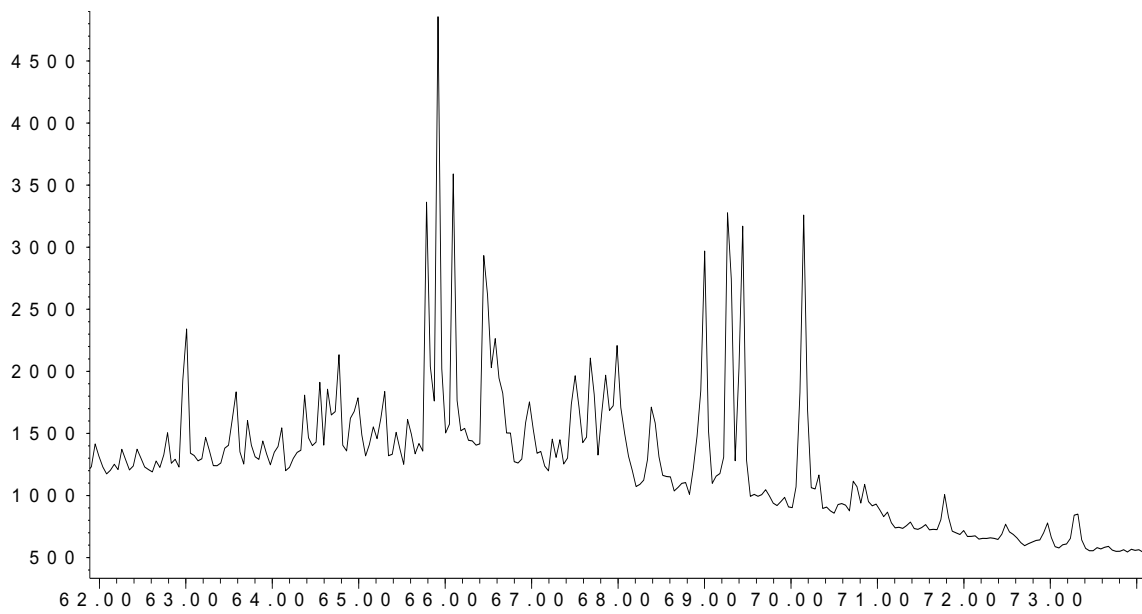
Woodford 50 Aromatics – m/z 133.3 + 134.3 (70-120 min.)



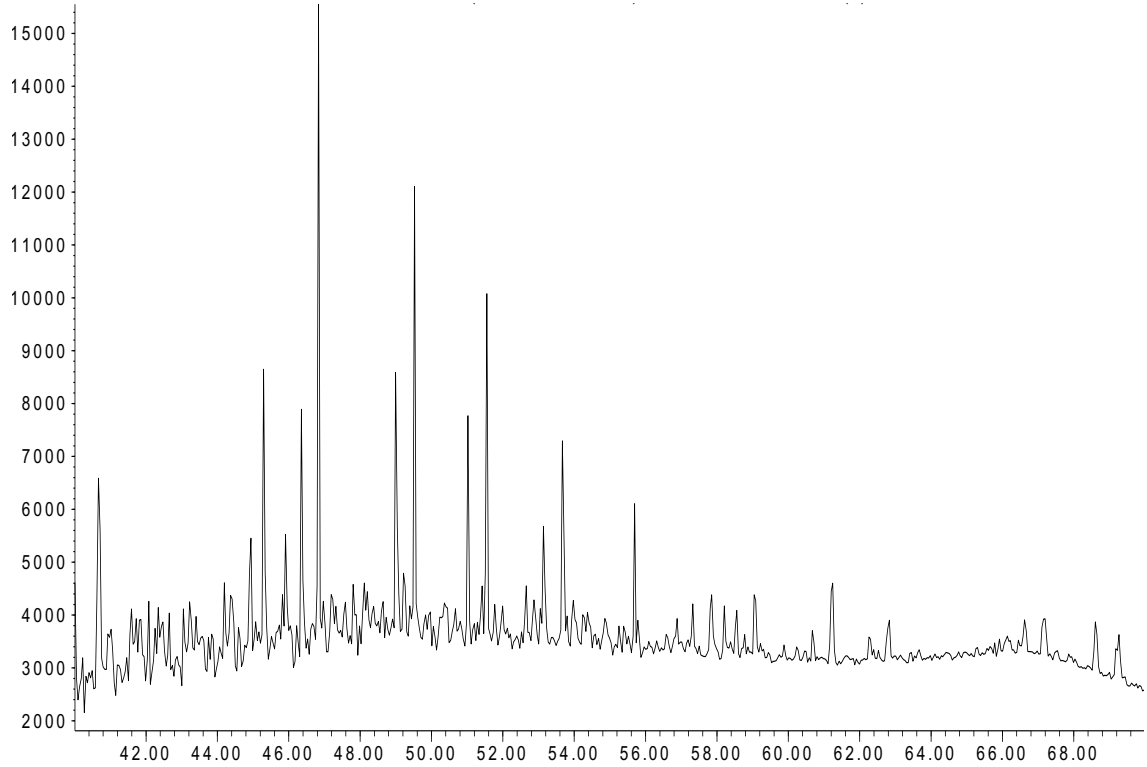
Woodford 65 Aliphatics – m/z 191.3



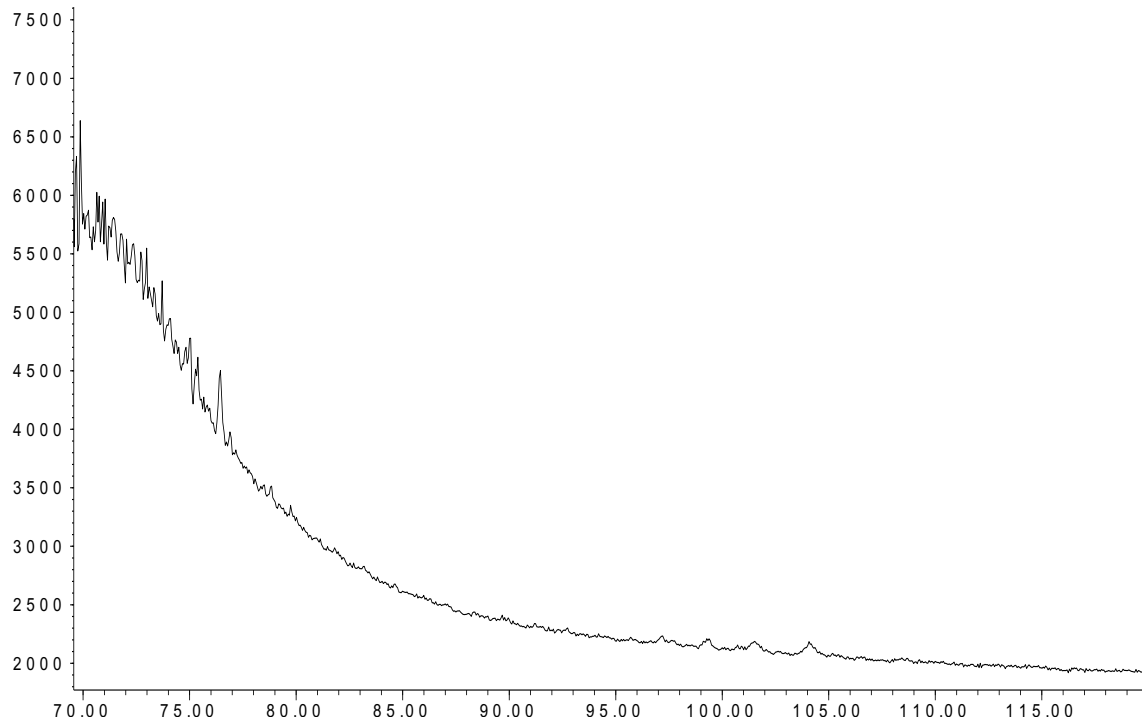
Woodford 65 Aliphatics – m/z 217.3



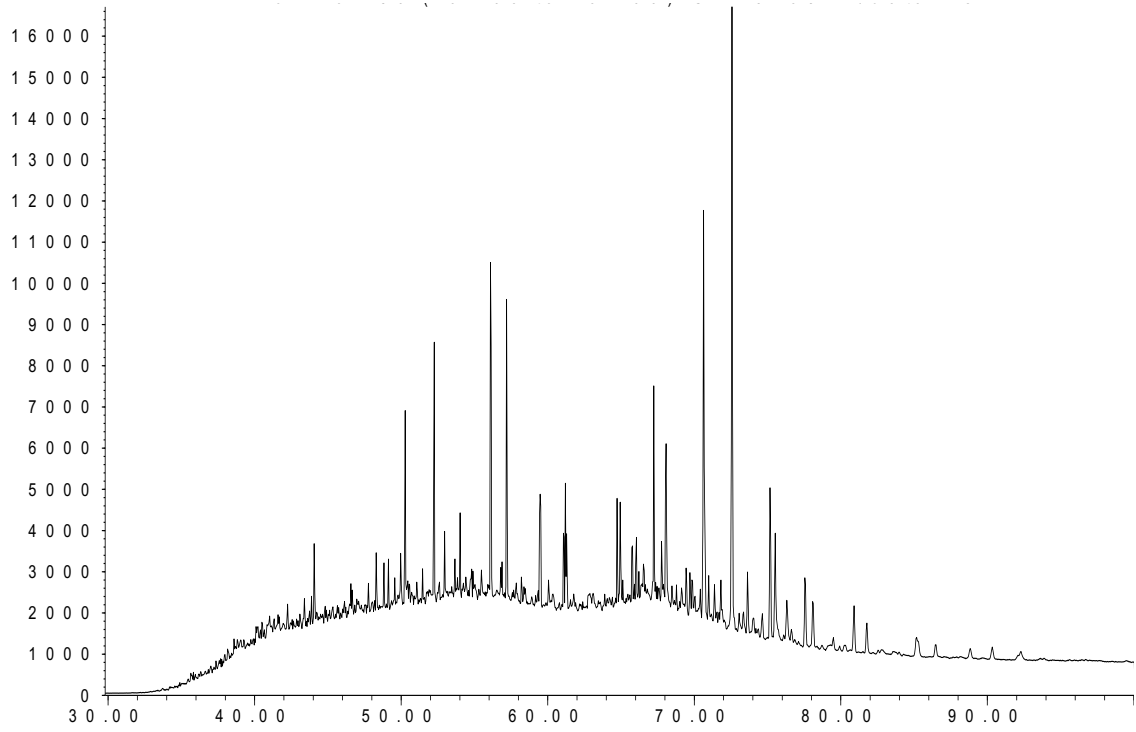
Woodford 65 Aliphatics – m/z 133.3 + 134.2 (40-70 min.)



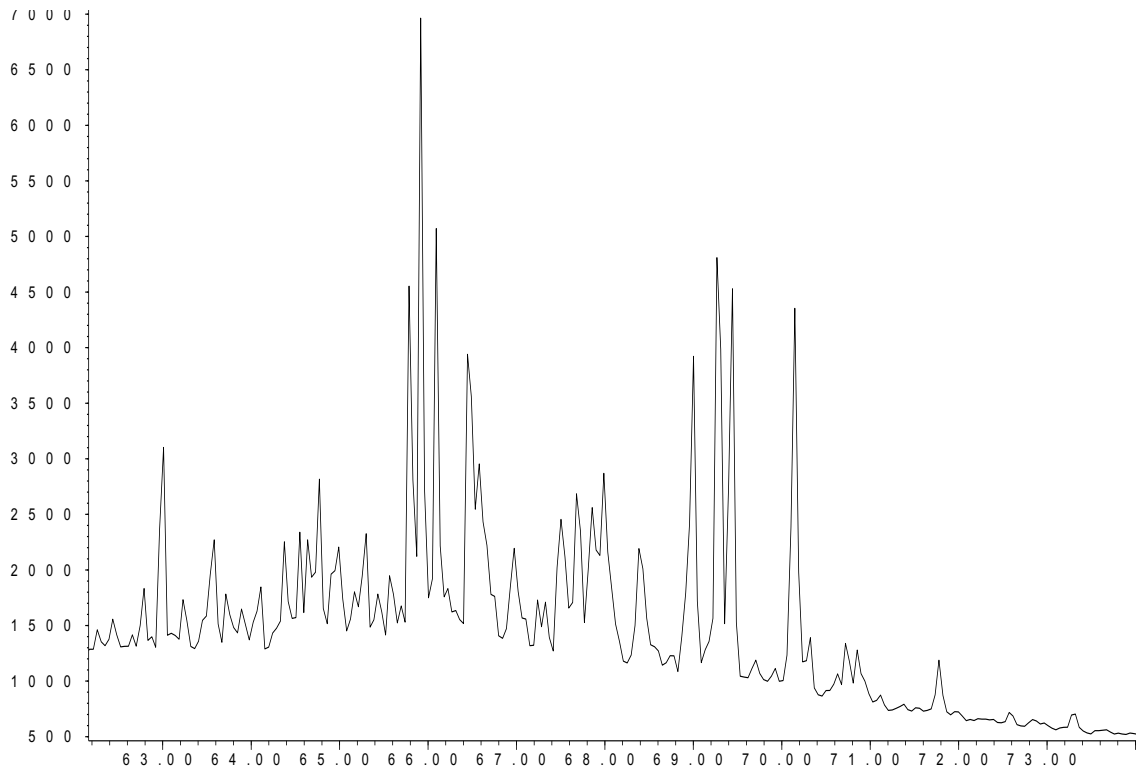
Woodford 65 Aromatics – m/z 133.3 + 134.2 (70-120 min.)



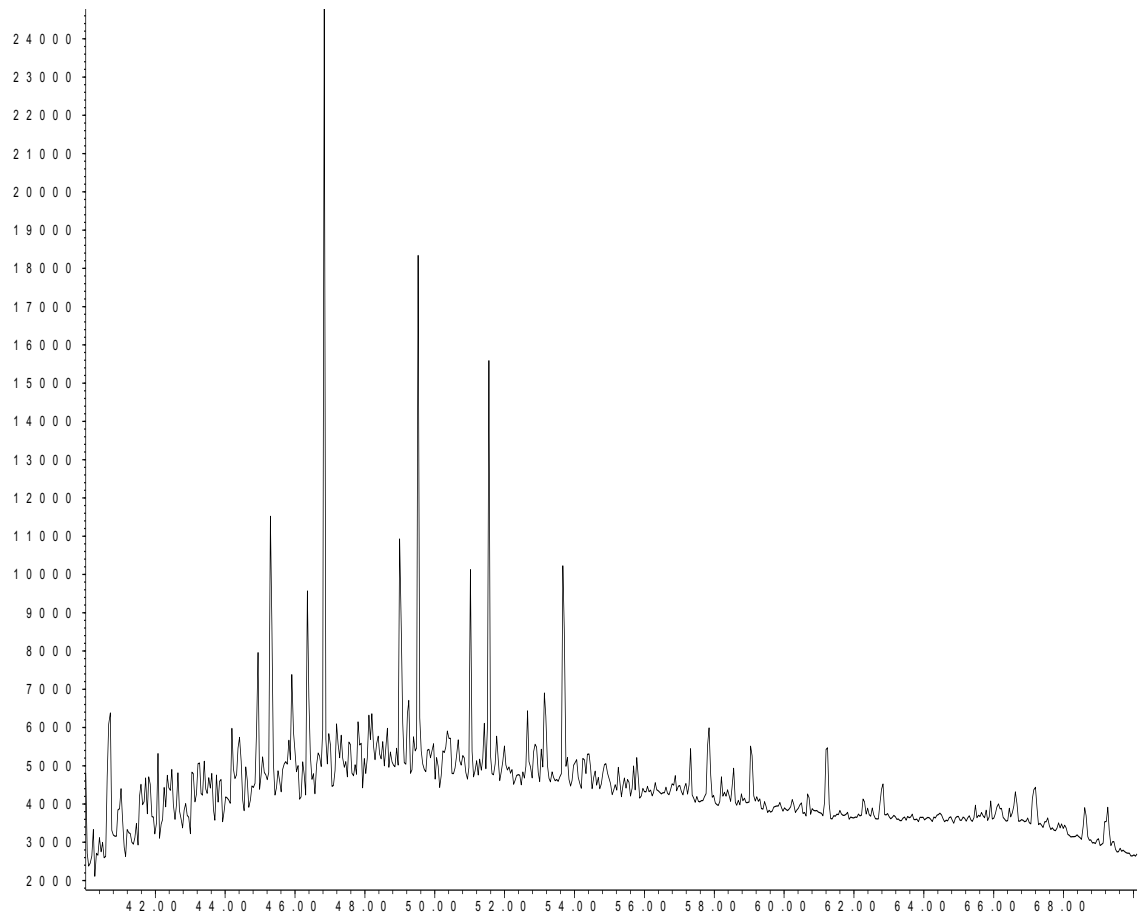
Woodford 70 Aliphatics – m/z 191.3



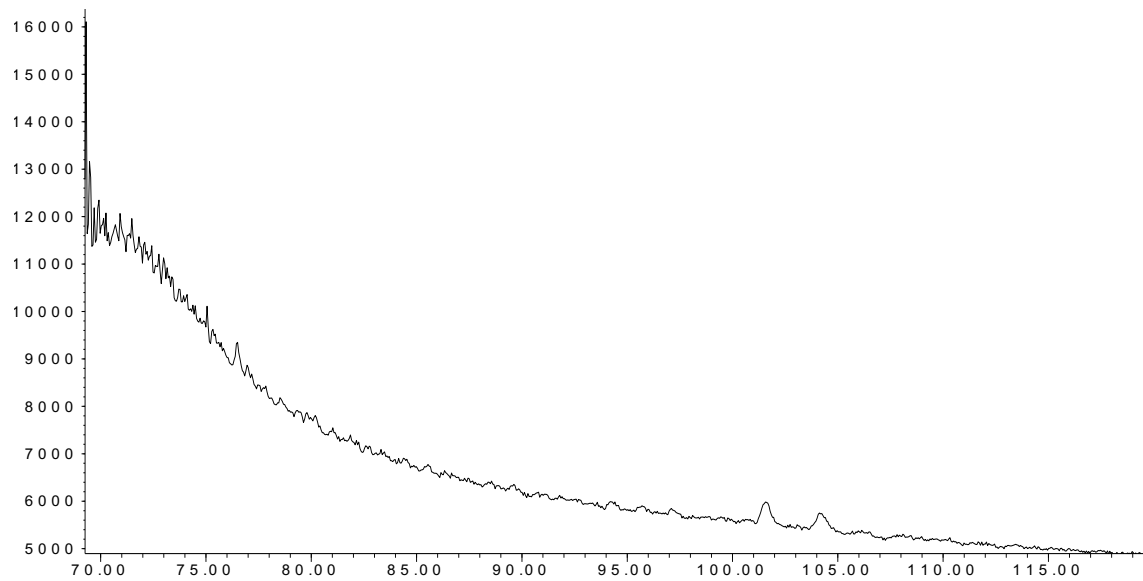
Woodford 70 Aliphatics – m/z 217.3



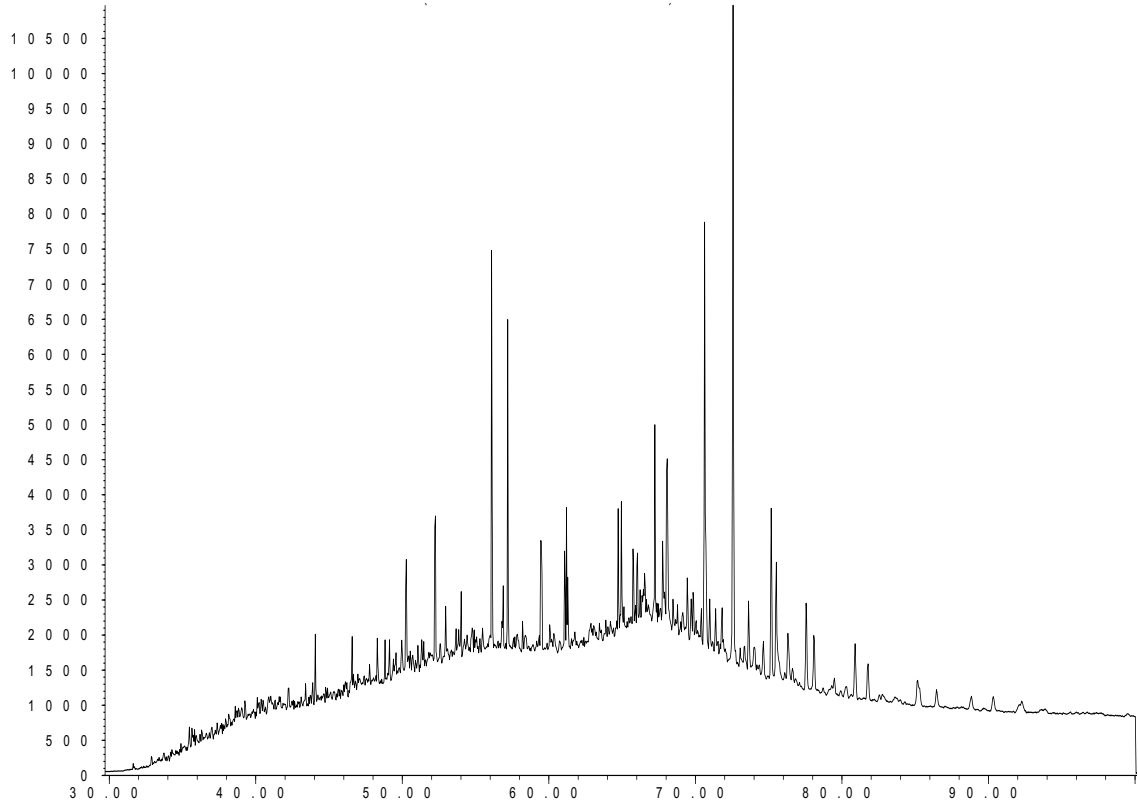
Woodford 70 Aliphatics – m/z 133.3+134.3 (40-70 min.)



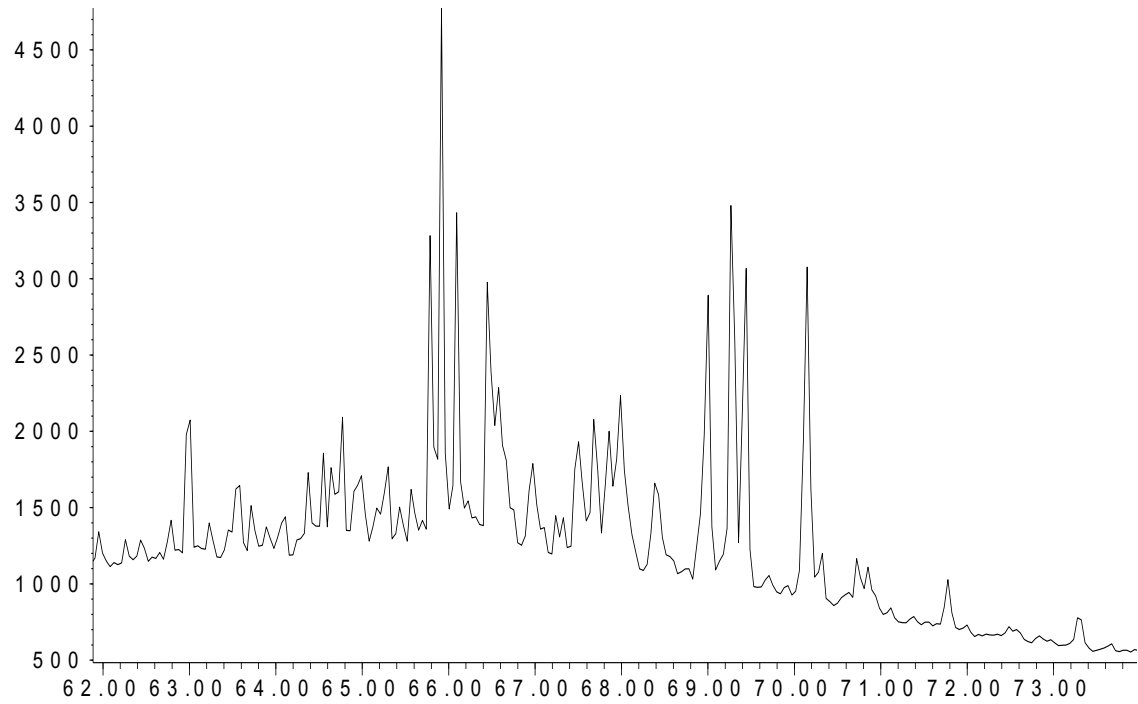
Woodford 70 Aromatics – m/z 133.3+134.3 (70-120 min.)



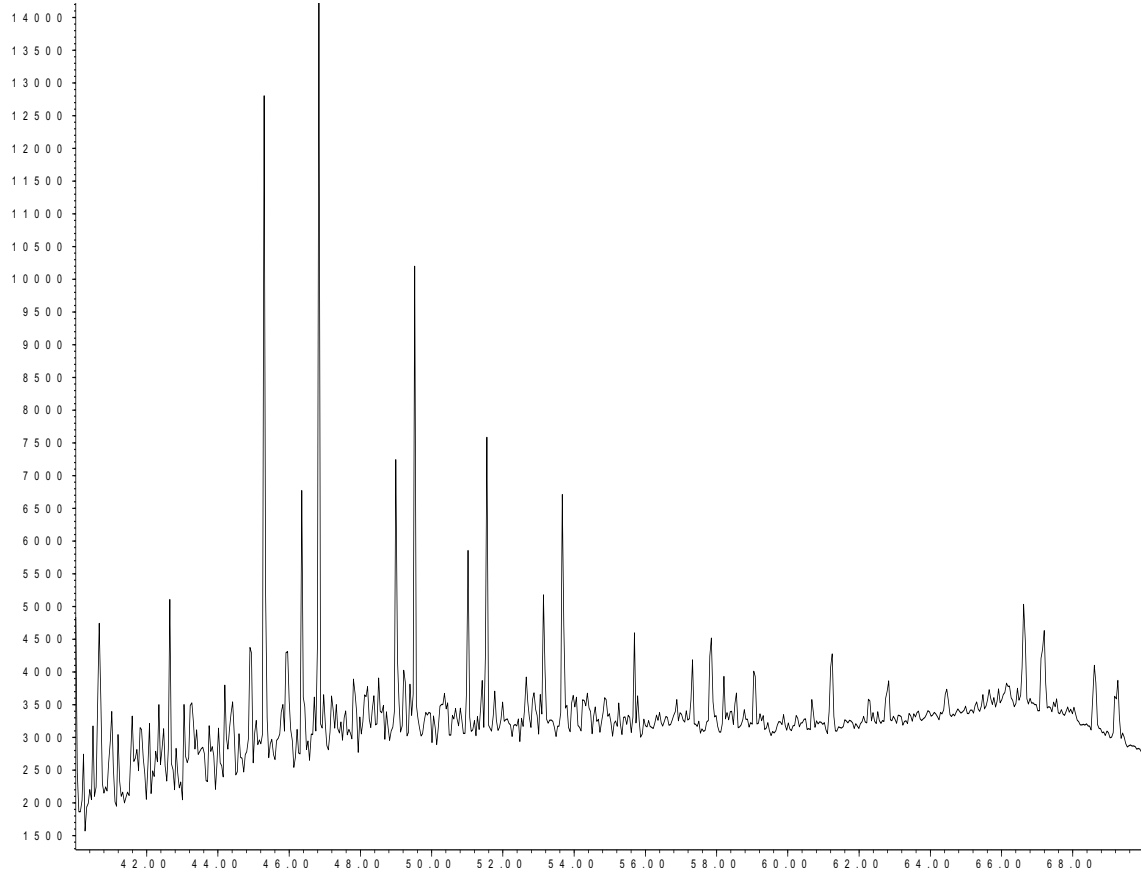
Woodford 75 Aliphatics – m/z 191.3



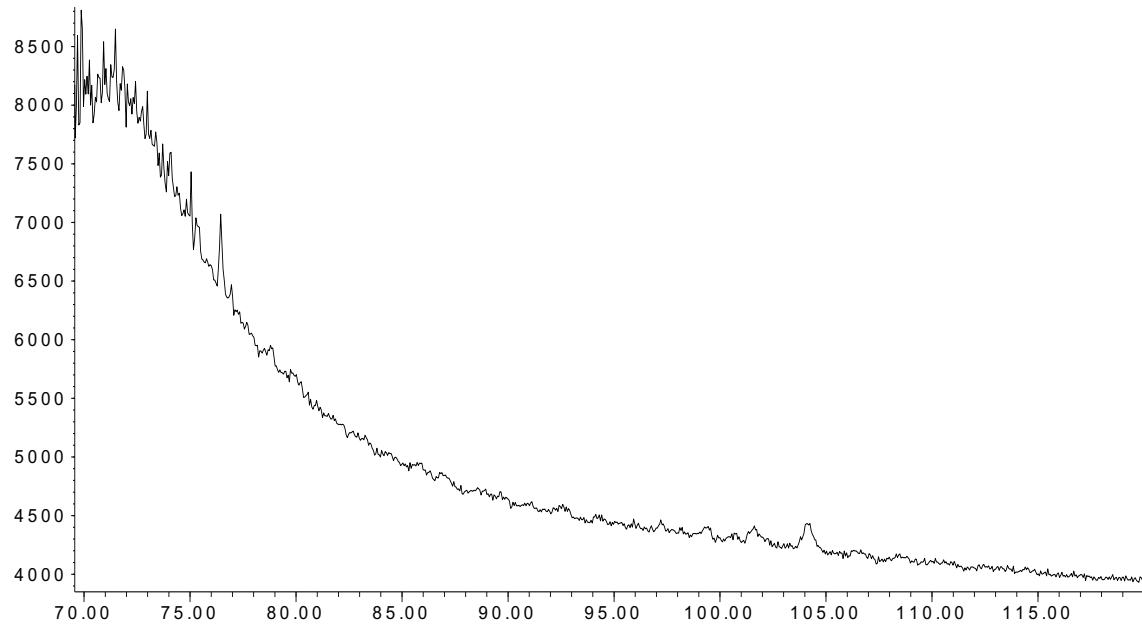
Woodford 75 Aliphatics – m/z 217.3



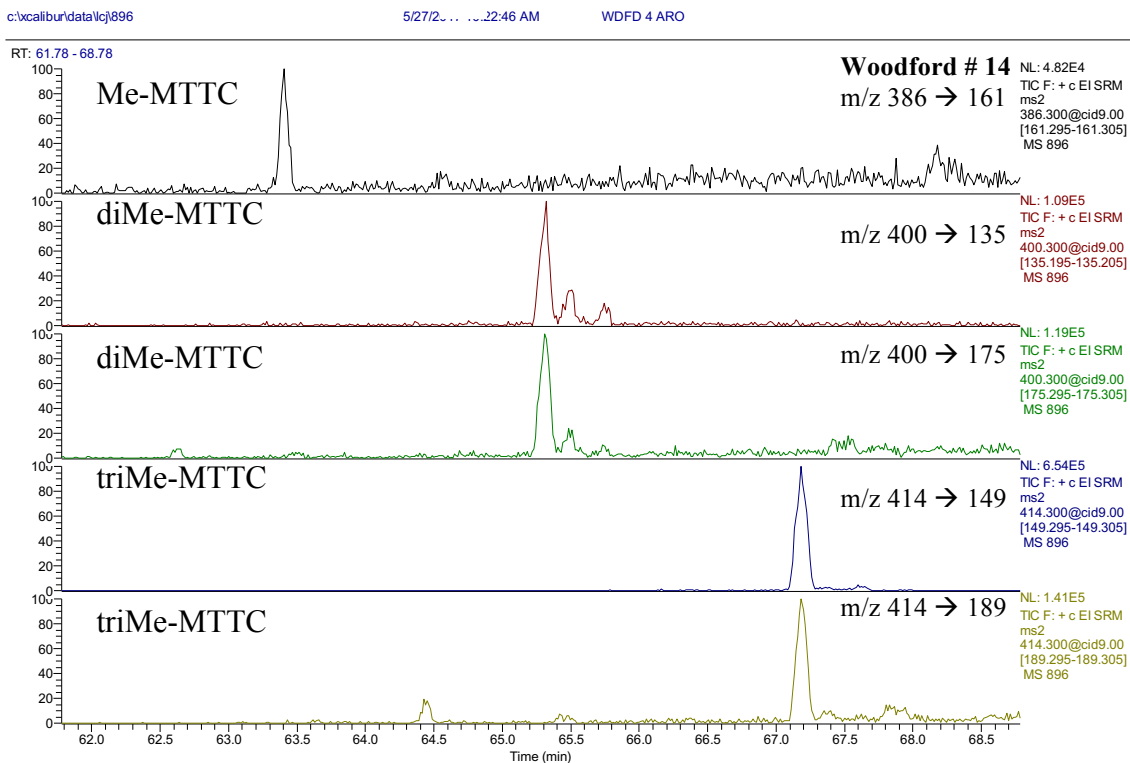
Woodford 75 Aliphatics – m/z 133.3 + 134.3 (40-70 min.)



Woodford 75 Aromatics – m/z 133.3 + 134.3 (70-120 min.)



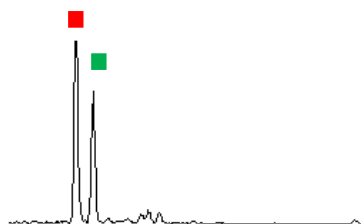
Appendix D: Selected GC/MS/MS Identifications



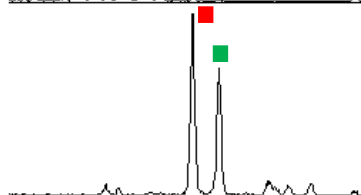
GC/MS/MS identification of Me-MTTC, diMe-MTTC, triMe-MTTC.

Woodford #14
Aromatics

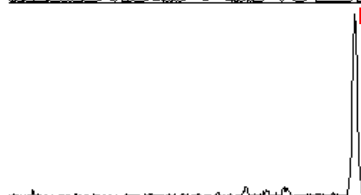
C₃₁ Homohopane
426→191



C₃₂ Homohopane
440→191



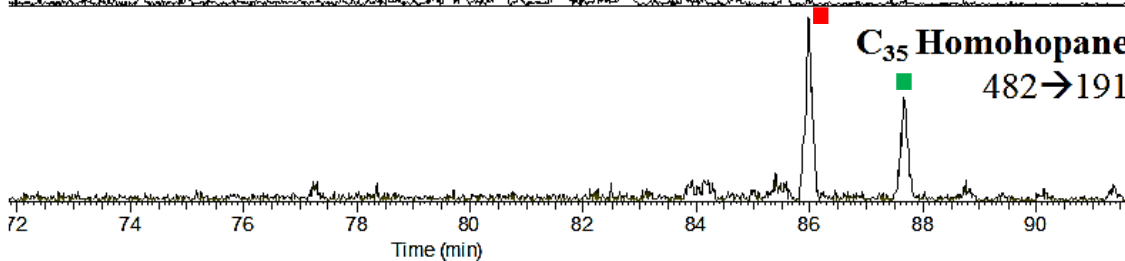
C₃₃ Homohopane
454→191



C₃₄ Homohopane
486→191



C₃₅ Homohopane
482→191



GC/MS/MS identification of C₃₁ – C₃₅ homohopanes.

- C-22 S epimer
- C-22 R epimer

Appendix E: Conodont Biostratigraphy Information (Over, 1992).

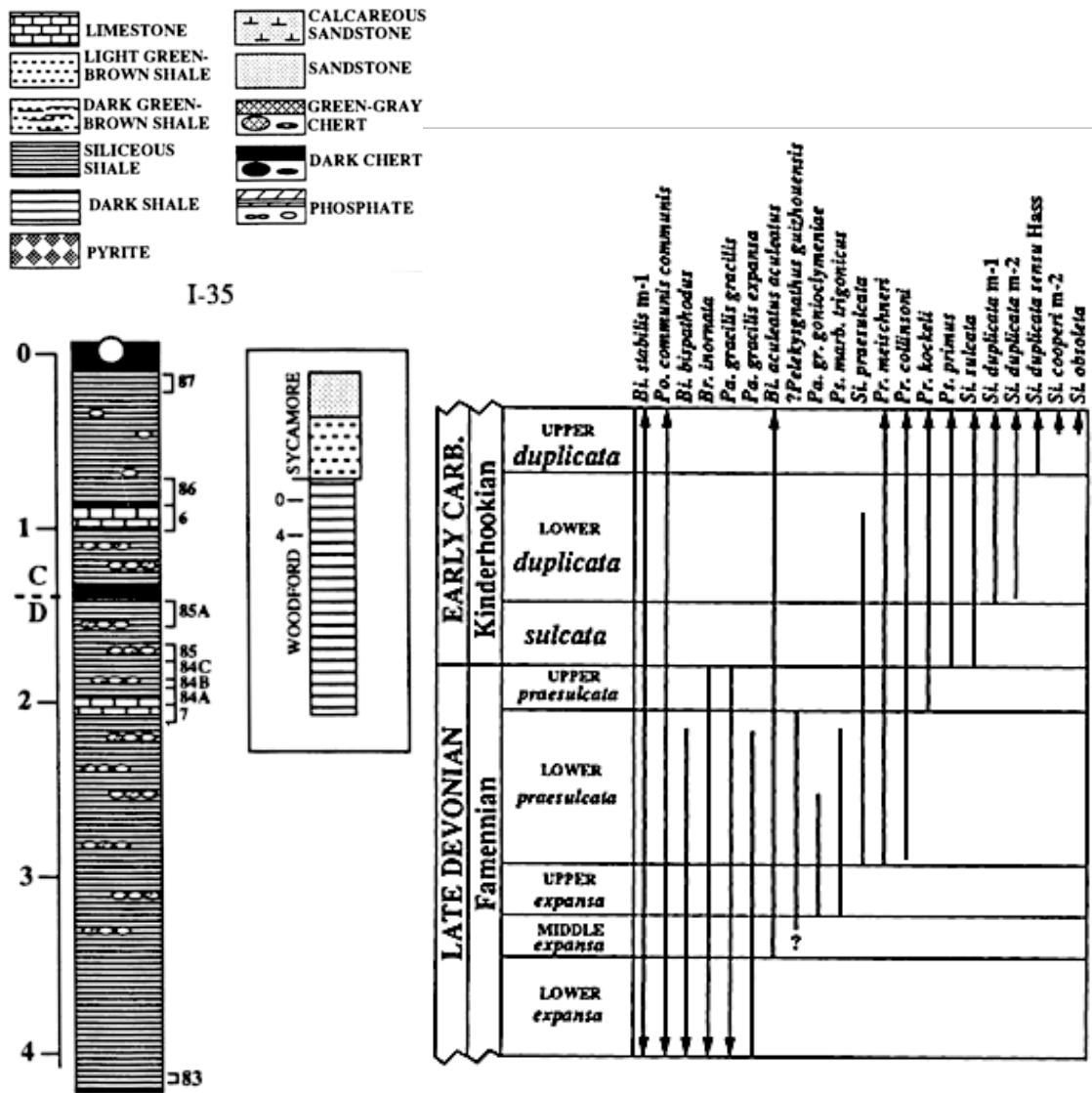


TABLE 2—Distribution and abundance of conodont species represented by Pa and all elements of *Conchodontus* from the uppermost Woodford Shale, I-35 roadcut section, southern Arbuckle Mountains. Sample weights represent amount of material processed. See Figure 2.2 for sample intervals on stratigraphic section. () indicates conform elements of *?Pelekysgnathus*; X indicates species present but not counted; ? indicates questionable identification.

Species	Sample weight (kg) Sample	0.6 83	1.0 7	0.5 84A	0.5 84B	0.5 84C	0.5 85	0.5 85A	3.0 6	0.5 86	0.5 87
<i>Bispathodus stabilis</i> morphotype 1		X	6	1	—	—	—	3	—	—	—
<i>Pseudopolygnathus marburgensis</i> trigonicus		X	—	—	—	—	—	—	—	—	—
<i>Palmatolepis gracilis</i> gracilis		X	—	—	1?	—	—	1	—	—	—
<i>Branmehla inornata</i>		X	4	3	—	1?	—	3	—	—	—
<i>?Pelekysgnathus guizhouensis</i>		—	(1)	—	(2)	—	—	—	—	—	—
<i>Polygnathus symmetricus</i>		—	5	3	2	1	—	7	—	—	—
<i>Conchodontus ziegleri</i>		—	—	1	—	—	—	50	—	—	—
<i>Palmatolepis gracilis</i> ssp.		—	—	1	—	—	—	—	—	—	—
<i>Siphonodella praesulcata</i>		—	—	1?	—	—	—	—	—	—	—
<i>Siphonodella duplicata</i> morphotype 1		—	—	—	—	—	—	—	1	—	—
<i>Siphonodella duplicata</i> morphotype 2		—	—	—	—	—	—	—	—	X	—
<i>Siphonodella obsoleta</i>		—	—	—	—	—	—	—	—	X	—